CHARGE TRANSFER PROCESSES IN ELECTROACTIVE POLYMER FILMS

by

Steven Holdcroft

B.Sc. (Honours), University of Salford, U.K., 1983

A THESIS SUBMITTED IN PARTIAL FULFILLMENT

OF THE REQUIREMENT FOR THE DEGREE OF

DOCTOR OF PHILOSOPHY

in the Department

of

Chemistry

Simon Fraser University

June 1987

APPROVAL

Name: Steven Holdcroft

Degree: Doctor of Philosophy

Title of Thesis: Charge Transfer Processes in Electroactive Polymer Films

Examining Committee:

Chairman: Dr. F. W. B. Einstein

Dr. B. L. Funt
Senior Supervisor

Dr. S. R. Morrison

Dr. T. N. Bell

Dr. R. J. Cushley

Dr. R. N. O'Brien
External Examiner
Professor,
Department of Chemistry,
University of Victoria

Date of approval: 17th June 1987

PARTIAL COPYRIGHT LICENSE

I hereby grant to Simon Fraser University the right to lend my thesis, project or extended essay (the title of which is shown below) to users of the Simon Fraser University Library, and to make partial or single copies only for such users or in response to a request from the library of any other university, or other educational institution, on its own behalf or for one of its users. I further agree that permission for multiple copying of this work for scholarly purposes may be granted by me or the Dean of Graduate Studies. It is understood that copying or publication of this work for financial gain shall not be allowed without my written permission.

Title of Thesis/Project/Extended Essay

CHARGE TRANSFER PROCESSES IN ELECTROACTIVE POLYMER FILMS

Author:

(signature)

S. HOLDCROFT

(name)

23rd JUNE 1987

(date)

ABSTRACT

Polymer modified electrodes have potential applications in energy conversion and storage systems, sensors, displays, chemical synthesis and microelectronic devices. This work investigates the charge transfer processes accompanying electrochemical reactions at polymer modified electrodes.

Thin films of poly-[(9,10 anthraquinone-2-carbonyl)styrene-co-styrene (PAQ) were deposited on Pt electrodes and their electrochemical properties investigated. PAQ films were electrocatalytic towards O_2 reduction in non-aqueous media. The kinetic parameters were investigated and the current densities associated with permeation of O_2, charge propagation and rate of cross reaction were determined. Theoretical plots of catalytic efficiency vs. film thickness were developed. The experimental data are consistent with such plots and indicate that the catalytic efficiency is insensitive to film thickness.

The protection of silicon semiconductors by PAQ films and the transfer of conduction band carriers through PAQ to oxidising agents in solution were investigated. PAQ coated Si electrodes exhibited superior stability for the reduction of O_2 over bare Si in the presence and absence of AQ in solution.

Films of polypyrrole (PP) were electrodeposited on electrodes. PP coated electrodes, in conjunction with PAQ coated electrodes, were employed as cathodes in simple electrochemical rechargeable cells. The charge storage capabilities of these cells were determined. Photo-assisted rechargeable cells were devised using PAQ coated semiconductor anodes and PP coated cathodes.

The energetics of electron transfer at the Si/PP interface were studied using a.c. impedance techniques, voltammetry and open circuit voltage

measurements. The data are interpreted on the basis of facile electron transfer between silicon semiconductor surface states and the polypyrrole film.

The conductive nature of PP prompted the fabrication and investigation of PP films containing Pt particles for electrocatalytic purposes. The distribution of Pt, as clarified by Auger electron spectroscopy, can be made homogeneous through the film, or localised at specified regions by a number of film forming techniques. PP/Pt films electrocatalyse O_2 reduction within a narrow potential window.

Rotating disk electrode studies, using films of various thickness and Pt loading, indicate that the catalytic current obtained for films containing homogeneously dispersed Pt is strongly dependent on the rate of O_2 permeation.

TO MY MOTHER AND FATHER

ACKNOWLEDGEMENTS

My thanks go to:

Dr. B. L. Funt for his steady support and supervision.

Dr. S. R. Morrison and the Energy Research Institute for helpful comments and discussions.

Dr. P. P. M. Hoang and Messrs. S. V. Lowen, F. Orfino, G. H. Fritzke and E. M. Peters for assistance in experimental tasks.

Members and fellow graduate workers of the Department of Chemistry for friendship and useful discussions.

I would like to express my gratitude to Drs. B. L. Funt and S. R. Morrison, the Department of Chemistry, and Simon Fraser University for financial assistance.

Last, but not least, I thank my wife, Amanda, for her patience and encouragement while preparing this thesis.

LIST OF ABBREVIATIONS

A	Electrode area
A	Substrate
A/B	Substrate couple
AES	Auger electron spectroscopy
AQ	Anthraquinone
bpy	2,2'-bipyridine
BQ	Benzoquinone
C	Capacitance
C-V	Capacitance-voltage
$(CH)_x$	Polyacetylene
CH_3CN	Acetonitrile
$(C_4H_3N)_x$	Polypyrrole
C_0 & C_R	Bulk concentration of oxidised and reduced species
C_0^e & C_R^e	Concentration of oxidised and reduced species at the electrode surface
C_{SC}	Space charge capacitance
d	Film thickness
D_{film} & D	Diffusion coefficient of substrate in the film and solution
D_E	Electron diffusion coefficient
D_0 & D_R	Diffusion coefficient of species O & R
DMSO	Dimethyl sulphoxide
E	Kinetic control by diffusion of electrons in the film
E_{CB}	Conduction band energy
E_B	Barrier height
ED	Energy density
ESD	Electricity storage density
E_{pa}	Potential of anodic peak

E_{pc}	Potential of cathodic peak
E_{PP}	Electrochemical potential of polypyrrole
E_{VB}	Valence band energy
$E^{0'}$	Formal potential of redox couple
$E_{1/2}$	Half wave potential
E_1	Rest potential of polypyrrole film
F	Faraday
GC	Glassy carbon
i_A	Levich current
i_E	Current density associated with charge propagation through the film
i_K	Current density associated with rate of cross reaction
i_L	Limiting current
i_p	Peak current
i_S	Current density associated with permeation of substrate in the polymer film
i-V	Current-voltage
i_1	Current density associated with the interplay of i_E, i_S, i_K and i_A
K	Equilibrium constant
k	Rate constant for cross reaction between the substrate and mediator
k^0	Standard heterogeneous electron transfer rate constant
n	Number of electrons involved in reaction
n_A	Concentration (AES)
P	Oxidised form of catalyst
PAQ	Poly[p-(9,10 anthraquinone-2-carbonyl)styrene]-co-styrene
PEC	Photoelectrochemical cell
PP	Polypyrrole
P/Q	Mediator couple
Q	Reduced form of catalyst

Q_{form}	Charge associated with PP formation
Q_{red}	Charge required to reduce a polypyrrole film
Q_{ox}	Charge associated with electrochemical doping of PP
Q_{tot}	Total charge passed during polymerisation
R	Gas constant
R	Kinetic control by the cross exchange reaction
RDE	Rotating disk electrode
RRDE	Rotating ring-disk electrode
S	Kinetic control by the diffusion of the substrate in the film
SC	Semiconductor
SCE	Saturated calomel electrode
T	Temperature
TEAP	Tetraethylammonium perchlorate
V_{FB}	Flat band potential
V_{oc}	Open circuit voltage
V_{ph}	Open circuit photovoltage
δ	Diffusion layer
δ_p	Peak width at half height
Γ	Surface coverage of attached electroactive material
Γ_{Appl}	Quantity of material applied to the electrode
Γ_{obs}	Observed surface coverage of electroactive material
Γ_P	Surface coverage of catalyst P
Γ_T	Total coverage of attached electroactive material
κ	Partition coefficient
ρ	Density
λ_M	Inelastic mean free path of Auger electrons
ν_k	Kinematic viscosity of solution
ω	Angular velocity (rad/s)

TABLE OF CONTENTS

APPROVAL	ii
ABSTRACT	iii
DEDICATION	v
ACKNOWLEDGEMENTS	vi
LIST OF ABBREVIATIONS	vii
TABLE OF CONTENTS	x
LIST OF TABLES	xiv
LIST OF FIGURES	xv
GENERAL INTRODUCTION	1
I. THEORETICAL ASPECTS	5
I.1. ANALYTICAL TECHNIQUES	5
I.1.1. ELECTROANALYTICAL TECHNIQUES	5
1. CYCLIC VOLTAMMETRY	5
2. CHRONOAMPEROMETRY	9
3. ROTATING DISK VOLTAMMETRY	10
I.1.2. ELECTROANALTYTICAL TECHNIQUES APPLIED TO POLYMER FILMS	14
1. THEORY OF VOLTAMMETRY AND CHARGE TRANSPORT	14
2. THEORY OF ELECTROCATALYSIS BY REDOX POLYMER FILMS	19
I.1.3. SPECTRAL TECHNIQUES	24
1. ABSORPTION SPECTROPHOTOMETRY	24
2. AUGER ELECTRON SPECTROSCOPY (AES)	26
I.2. SEMICONDUCTOR ELECTROCHEMISTRY	31
I.2.1. THE ELECTRICAL DOUBLE LAYER MODEL	31
I.2.2. THE SEMICONDUCTOR SPACE CHARGE LAYER	33
I.2.3. BAND EDGE UNPINNING	34
I.2.4. THE CONDUCTION AND VALENCE BAND ENERGY	37

II. **ELECTROCHEMICAL STUDIES OF ANTHRAQUINONE REDOX POLYMER FILMS ON CONDUCTIVE AND SEMICONDUCTIVE SUBSTRATES** 40

II.1. INTRODUCTION 40

II.1.1. TYPES OF REDOX POLYMER FILM 41

II.1.2. VOLTAMMETRY 43

II.1.3. CHARGE TRANSPORT 44

II.1.4. ELECTROCATALYSIS 46

II.1.5. SEMICONDUCTOR ELECTRODES MODIFIED BY REDOX POLYMER FILMS 47

II.2. EXPERIMENTAL 49

II.2.1. CHEMICALS 49

II.2.2. FILM PREPARATION 49

II.2.3. ELECTROCHEMISTRY 50

II.3. RESULTS AND DISCUSSION 54

II.3.1. VOLTAMMETRY AND CHARGE TRANSPORT 54

II.3.2. ELECTROCATALYSIS OF O_2 64

II.3.3. THE ELECTROCHEMICAL BEHAVIOUR OF Si ELECTRODES MODIFIED BY FILMS OF PAQ 84

II.4. CONCLUSION 99

III. **CHARGE STORAGE PROPERTIES OF PAQ AND POLYPYRROLE FILMS** 101

III.1. INTRODUCTION 101

III.1.1. ELECTROCHEMICAL PROPERTIES OF POLYPYRROLE 102

III.1.2. PRINCIPLES OF CHARGE STORAGE TECHNOLOGY 104

III.1.3. RECHARGEABLE STORAGE CELLS BASED ON ORGANIC CONDUCTING POLYMERS 105

III.2. EXPERIMENTAL 108

III.2.1. CHEMICALS 108

III.2.2. FILM PREPARATION 108

III.2.3. ELECTROCHEMISTRY 109

1. CHRONOCOULOMETRY 110

2. CYCLIC VOLTAMMETRY 110

3. DISCHARGE CHARACTERISTICS 110

III.3. RESULTS AND DISCUSSION 111

III.3.1. ELECTROCHEMISTRY OF PAQ AND PP COATED ELECTRODES 111

III.3.2. Pt/PAQ//PP/Pt RECHARGEABLE CELLS 115

III.3.3. p-SEMICONDUCTOR/PAQ//PP/Pt RECHARGEABLE CELLS 123

III.4. CONCLUSION 129

IV. THE ENERGETICS OF ELECTRON TRANSFER AT THE POLYPYRROLE/SILICON INTERFACE 130

IV.1. INTRODUCTION 130

IV.1.1. ELECTROCHEMISTRY WITH SILICON ELECTRODES 130

IV.1.2. POLYPYRROLE COATED SILICON ELECTRODES 131

IV.2. EXPERIMENTAL 133

IV.2.1. CHEMICALS 133

IV.2.2. FILM PREPARATION 133

IV.2.3. ELECTROCHEMISTRY 133

IV.3. RESULTS AND DISCUSSION 135

IV.4. CONCLUSION 157

V. ELECTROCATALYTIC ACTIVITY OF POLYPYRROLE FILMS INCORPORATING Pt MICROPARTICLES 158

V.1. INTRODUCTION 158

V.2. EXPERIMENTAL 162

V.2.1. CHEMICALS 162

V.2.2. PREPARATION OF POLYMER FILMS 162

V.2.3. AUGER ELECTRON SPECTROSCOPY 164

V.2.4. ELECTROCHEMISTRY 165

V.3. RESULTS AND DISCUSSION 167

V.3.1. CHARACTERISATION OF PP/Pt FILMS 167

1. PP FILM THICKNESS 167

2. COULOMETRY AND SPECTROPHOTOMETRY 167

3. AES 169

V.3.2. ELECTROCATALYTIC PROPERTIES OF PP/Pt FILMS 178

1. EFFECT OF pH 178

2. EFFECT OF Pt LOADING AND FILM THICKNESS 182

V.4. CONCLUSION 190

REFERENCES 191

LIST OF TABLES

Table 1. Voltammetric characteristics of PAQ films 52

Table 2. Effect of Cation Size and AQ Loading on D_E 62

Table 3. Variations of i_E, i_S and i_K with film thickness 78

Table 4. Open circuit potentials of Pt/PAQ//PP/Pt cells 120

Table 5. Open circuit potentials of p-Si/PAQ//PP/Pt cells 127

Table 6. Open circuit potentials of p-InP/PAQ//PP/Pt cells 127

Table 7. V_{oc} values for p-Si electrodes in contact with various redox couples 131

Table 8. Coulombic assay of PP films 167

Table 9. Cathodic Peak Potential for O_2 reduction 180

Table 10. % H_2O_2 Produced at GC and PP/Pt electrodes 180

LIST OF FIGURES

Figure 1. Scheme for electrochemical reduction of a surface confined redox species. 1

Figure 2. Scheme for mediated electrocatalysis. 3

Figure 3. Scheme for electron transfer at an n-type semiconductor electrode coated with a redox polymer film. 4

Figure 4. Cyclic voltammogram for a reversible redox couple. 7

Figure 5. The rotating disk electrode (RDE) 11

Figure 6. The variation of i_L with $\omega^{1/2}$. 13

Figure 7. RDE voltammmetry. 15

Figure 8. The rotating ring-disk electrode (RRDE). 16

Figure 9. Cyclic voltammogram of a reversible monolayer. 18

Figure 10. The differing kinetic situations that may arise for catalytic reactions at polymer films. 25

Figure 11. The energy level model for silicon indicating a $L_{2,3}VV$ Auger process. 28

Figure 12. Classification of PEC cells. 32

Figure 13. Energy profiles of n- and p-type semiconductors in equilibrium with a redox couple, and the corresponding photocurrent-voltage curves. 35

Figure 14. Equivalent circuit corresponding to the semiconductor and Helmholtz layer. 36

Figure 15. Variations in the semiconductor-electrolyte interface in the presence of redox couples with differing E_{redox}. 38

Figure 16. Electrochemical cell. 51

Figure 17. Photoelectrochemical cell. 53

Figure 18. Cyclic voltammetry of PAQ films in various solvents. 55

Figure 19. Cyclic voltammetry of PAQ films of various thickness. 58

Figure 20. Effect of scan rate on the peak current for films of various thickness. 60

Figure 21. The i-t decay response and the corresponding Cottrell plot for a 1000 Å film. 61

Figure 22. Proposed model of structure for PAQ films (d>100 Å) in DMSO. 65

Figure 23. Voltammetry of a saturated O_2 solution at various scan rates. 66

Figure 24. Nernstian plots for the reduction of O_2 at a) bare Pt, b) PAQ Coated Pt (100 Å). 68

Figure 25. RDE voltammetry of saturated O_2 solution: a) Bare Pt, b) PAQ film (10 Å), c) PAQ film (50 Å). 69

Figure 26. Levich plots for the reduction of O_2: a) Bare Pt, b) PAQ film (10 Å). 70

Figure 27. Inverse-Levich plots for the reduction of O_2: a) Bare Pt, b) PAQ film (10 Å). 71

Figure 28. Voltammetry of BQ (1 mM) in 0.1 M TEAP/DMSO: a) Bare Pt, b) PAQ film (100 Å) in the absence of BQ, c) as (a) but with BQ present. 73

Figure 29. Voltammetry of BQ (1 mM) in 0.1 M TEAP/H_2O: a) Bare Pt, b) PAQ film (100 Å). 74

Figure 30. Levich plots for the reduction of BQ (2.1 mM): a) Bare Pt, b) PAQ film (1000 Å). 75

Figure 31. Inverse-Levich plots for the reduction of BQ (2.1 mM): a) Bare Pt, b) PAQ film (1000 Å). 76

Figure 32. Concentration profiles of A and Q for the electrocatalytic reduction of oxygen at PAQ films. A = O_2, Q = $AQ^{\cdot-}$. 81

Figure 33. Theoretical plots of i_1/i_A vs. log (rotation rate), (rpm). 83

Figure 34. Mott-Schottky plot for n-Si in 0.1 M TEAP/DMSO. 85

Figure 35. Cyclic voltammetry of PAQ coated n-Si electrodes. 86

Figure 36. Cyclic voltammetry of PAQ coated n-Si: (A) Steady state, (B) see text. 87

Figure 37. Cyclic voltammetry of AQ (1 mM) at n-Si. 89

Figure 38. Cyclic voltammetry of PAQ film (A) and 1 mM AQ (B) at p-Si. 90

Figure 39. Schematic representation for the mediated reduction of oxygen at PAQ coated silicon electrodes. 91

Figure 40. Cyclic voltammetry of O_2 at n-Si. 93

Figure 41. Cyclic voltametry of O_2 at illuminated p-Si. 94

Figure 42. Chronoamperometry of O_2 reduction at illuminated p-Si electrodes. 95

Figure 43. Schematic representation of the semiconductor/electrolyte interface in the absence, (A), and presence, (B), of a surface oxide film and accompanying interface states. 96

Figure 44. Proposed mechanism for electropolymerisation of heterocyclic monomers. For pyrrole, X=NH. 103

Figure 45. Cyclic voltammetry of PAQ films: a) three electrode system, b) two electrode system (counter electrode = PP film). 112

Figure 46. Cyclic voltammetry of PP films. 113

Figure 47. Chronocoulometric determination of the storage capacity of PP as a function of applied potential. 114

Figure 48. Free standing potential of PP as a function of ClO_4^- dopant concentration. 116

Figure 49. Schematic representation of the Pt/PAQ//PP/Pt cell. 118

Figure 50. Voltage-time discharge curves for Pt/PAQ//PP/Pt 121

Figure 51. Energy level diagram for p-SC/PAQ//PP/Pt cells. 124

Figure 52. Cyclic voltammetry of: a) PAQ coated p-Si, b) PAQ coated p-InP, c) p-Si/PAQ//PP/Pt cell, d) p-InP/PAQ//PP/Pt cell. 126

Figure 53. Voltage-time discharge curves for p-SC/PAQ//PP/Pt cells: a) SC = Si, b) SC = InP. 128

Figure 54. C-V plots for n-Si electrodes. 136

Figure 55. C-V plots for p-Si electrodes. 137

Figure 56. Mott-Schottky plots for Si electrodes in 0.1 M TEAP/CH_3CN. 138

Figure 57. Cyclic voltammetry of PP coated Pt and Si electrodes. 139

Figure 58. Mott-Schottky plots for Si/PP electrodes with varying E_{pp}. 140

Figure 59. Correlation between the Si flat band potential and the electrochemical potential of PP. 141

Figure 60. Photovoltage-E_{pp} plot for Si/PP electrodes. 143

Figure 61. Effect of the illumination intensity on the p-Si/PP photovoltage. 144

Figure 62. Plot of E_{pp} as a function of the electrochemical potential of solution. 145

Figure 63. Photovoltage-$E_{solution}$ plots for: a) n-Si, b) n-Si/PP, c) p-Si, d) p-Si/PP electrodes. 147

Figure 64. Cyclic voltammetry of ferrocene (10 mM) at Pt and Si electrodes. 148

Figure 65. Cyclic voltammetry of ferrocene (10 mM) at p-Si electrodes under chopped light. 149

Figure 66. Mott-Schottky plots for n-Si (a&b) and n-Si/PP (c&d) electrodes in the presence of ferrocene/ferrocenium (10 mM). 151

Figure 67. Schematic representation of band edge unpinning at Si/PP interfaces. 153

Figure 68. Cyclic voltammetry of Si/PP and Si/Pt/PP electrodes. 155

Figure 69. Mott-Schottky plots for Si/Pt electrodes in 0.1 M TEAP/CH_3CN. 156

Figure 70. Schematic illustration of mediated O_2 reduction at PP/Pt films. 161

Figure 71. Absorption spectra of PP films (0.16 μm) in deionised water: A) Electrochemically oxidised, B) Electrochemically reduced, C) After (B) has been immersed in 1mM K_2PtCl_6 for several min. 168

Figure 72. Surface coverage of $Fe(CN)_6^{3-}$ incorporated in PP vs. number of coulombs passed during polymerisation. 170

Figure 73. AES elemental survey of electrode III(0.16)13.3 before and after sputtering. 171

Figure 74. Depth profile analyses and composition of electrodes: VI, VII and VIII. 173

Figure 75. Depth profile analysis of electrode II(0.16)13.1. 174

Figure 76. Depth profile analyses of PP/Pt electrodes: III(0.8)13.0, III(0.16)13.3 and III(0.16)5.4. 175

Figure 77. Depth profile analyses of PP/Pt electrodes: III(0.16) 2.8, V(0.16)2.3., and IV(0.16)1.7 176

Figure 78. Schematic illustration of the various catalytic films prepared 177

Figure 79. Cyclic voltammetry of PP films (0.16 μm): A) PP only in 0.1 M KCl, B) Electrode III(0.16)13.3 in 0.1 M KCl, C)PP only in KOH solution. 179

Figure 80. Cyclic voltammetry of PP & PP/Pt electrodes in O_2 saturated solutions of varying pH: 181

Figure 81. Illustration of how i_L is obtained from the rising plateau of a RDE voltammogram. 183

Figure 82. RDE voltammograms of electrodes I, II, III and IV: constant film thickness, varying Pt loading. 184

Figure 83. Levich plots for electrodes I, II and III: constant film thickness (0.16 μm), varying Pt loading. 185

Figure 84. RDE voltammograms and corresponding Levich plots for electrodes III: constant film thickness (0.8 μm), varying Pt loading. 187

Figure 85. RDE voltammograms and corresponding Levich plots for electrodes II and III: constant Pt loading ($\approx$13 $\mu g/cm^2$), varying film thickness. 188

GENERAL INTRODUCTION

Over recent years surface synthetic procedures have been developed for immobilising monomolecular and multimolecular layers on electrode surfaces [1-5]. The motive behind deliberately immobilising a chemical on an electrode surface is that the electrode then exhibits chemical, electrochemical and other properties of the confined species. Selection of the immobilised chemical is therefore based on the known properties of the reagent and the desired use of the electrode. The most studied immobilised chemicals are those which are electrochemically reactive. A surface confined electroactive species can undergo electron transfer processes with the electrode corresponding to electrochemical redox reactions (Figure 1). No conventional mass transfer of reactant and product is required as is the case for electroactive redox species in solution.

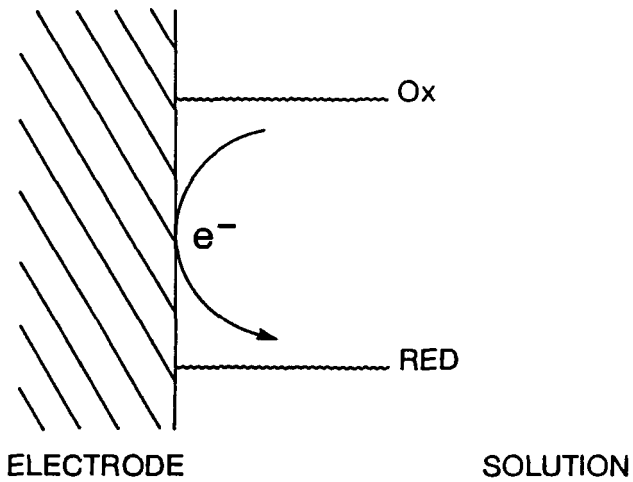

Figure 1. Electrochemical reduction of a surface confined redox species.

The techniques for retaining electroactive groups at the electrode surface fall into three categories: chemisorption, covalent derivatisation and polymer film deposition. Chemisorption refers to irreversible adsorption of the electroactive substance on the surface of the electrode. Lane and

Hubbard were the first to demonstrate deliberate modification by this technique when they found that olefinic compounds adsorbed strongly on a platinum surface when the metal was soaked in a solution of the organic compound. By using olefins with different terminal groups, a variety of surface functional groups was obtained[6,7]. In 1975, Murray and coworkers developed the general strategy of covalent derivatisation[8]. The technique utilises hydroxy groups, produced by delicate procedures, on metal oxide and some conductive substrate surfaces. The -OH groups are reactive towards chloro- or alkoxy silanes, producing covalent bonds between the substrate and the silane. Electroactive functional groups, if not present before silanisation, can be attached by a succeeding reaction.

The study of immobilised chemical species changed direction when the electroactivity of redox polymer films was reported[9-14]. Polymer films, while being more stable than monolayers, are technically easier to prepare and the number of immobilised electroactive centres can be controlled by regulating the film thickness. Furthermore, multilayers of electroactive sites have a number of special features, including the processes by which multilayers exchange electrons with the electrode and with oxidising and reducing agents in solution.

In addition to the group of electroactive macromolecules known as redox polymers, there are the electrically conducting organic polymers formed from the electrochemical oxidation of aromatic heterocyclic, benzenoid and non-benzenoid molecules[15-19]. Thin films of these polymers can be electrochemically cycled between the oxidised, conducting state, and the neutral, insulating state. Thick films can be peeled off the electrode surface to yield free standing electrically conducting films.

An important application of redox polymer modified electrodes is the catalysed oxidation or reduction of solution substrates by the immobilised

redox couple[20-21]. For the coating to be catalytic, the rate of electrochemical reaction between the film and the substrate must be greater than that between the bare electrode and substrate. Mediated electrocatalysis is represented in Figure 2.

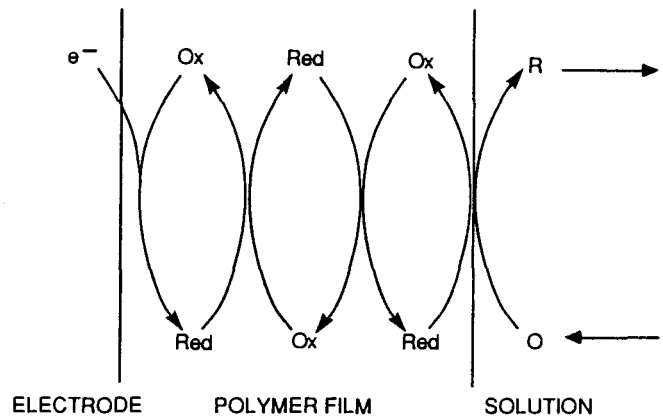

Figure 2. Scheme for mediated electrocatalysis.

Polymer films may be coated on virtually any surface. When coated on semiconductor electrodes they can relay photogenerated charge away from the surface to substrates in solution (Figure 3). Such films can contribute to the protection of the semiconductor lattice and enhance the overall rate of photoelectrochemical reaction[22-25].

Polymer films may be spatially positioned on electrodes to facilitate investigation of polymer film properties and provide novel devices. This topic is being actively persued because of potential microelectronic applications. Bilayer electrodes[26,27], polymer films with particulates[28-30], sandwich electrodes[31], ion gates[32] and electrochemical transistors[33] are examples of spatially modified electrodes. Such electrodes have potential use in electro-optical devices[34], electro-analysis of trace oxidants or reductants[34], signal amplification[33] and ion permselective membranes[35].

Many of the potential applications and novel devices are based on the

doping-undoping phenomena associated with the electrochemical behaviour of conducting polymers. In this vein, conducting polymer films have been used for battery materials[36,37], hosts for the controlled release of drugs to specific targets[38,39], materials for the deionisation of water[40] and pH modulators[41].

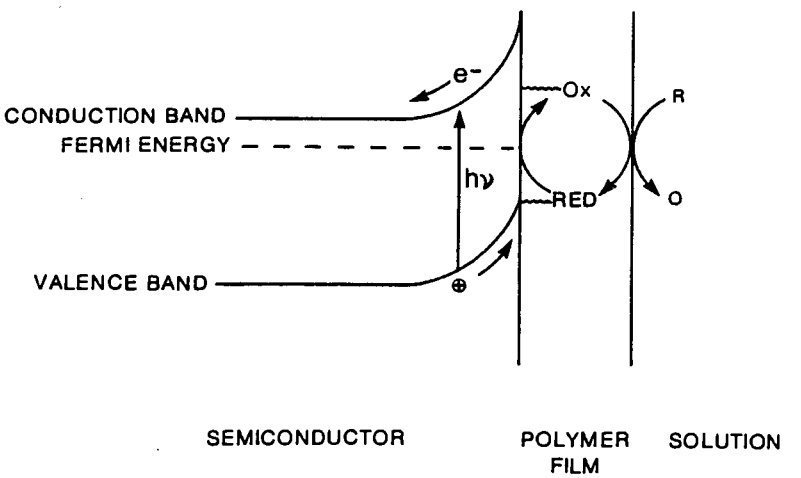

Figure 3. Scheme for electron transfer at an n-type semiconductor electrode coated with a redox polymer film.

This theses is concerned with the mass and charge transfer processes accompanying electrochemical reaction of polymer films. Such processes collectively determine the rate at which thermodynamically favoured reactions proceed and are thus, of fundamental importance when designing modified electrodes for specific purposes. In Chapter I, the theoretical aspects associated with polymer films and their characterisation are set forth. Chapter II describes the elucidation of various mass and charge transfer components associated with electrocatalysis by redox polymer films coated on conductive and semiconductor substrates[42,43]. Chapter III highlights the charge storage properties of redox and electrically conductive polymer films while Chapter IV deals with the semiconductor/ conductive polymer interface. The last Chapter is concerned with electrocatalysis and the use of conductive polymer films containing dispersed catalyst.

CHAPTER I

THEORETICAL ASPECTS

I.1. ANALYTICAL TECHNIQUES

Analytical studies of electroactive polymer films generally involve some type of electrochemical measurement to establish the thermodynamic and kinetic parameters of electron transfer. Additional information on the integrity of surface films can be obtained through spectroscopic techniques such as XPS, AES, absorption spectrophotometry, reflectance spectroscopy, scanning electron microscopy, and secondary-ion mass spectroscopy. Several electroanalytical and spectral methods have been employed in this research and thus, a brief description of these techniques is presented.

I.1.1. ELECTROANALYTICAL TECHNIQUES

I.1.1.1. CYCLIC VOLTAMMETRY

In this technique[44], the potential of the electrode in quiescent electrolyte is changed linearly with time in a saw tooth manner. During the potential cycle the current required to oxidise and reduce redox centres is measured. The combination of increased electrochemical rate constant, as the potential is increased, and the decrease in the concentration of unreacted redox centres leads to a current maximum. When the potential is decreased to the original value a second current maximum is observed due to the reverse process.

Consider the reversible electrochemical reaction of species O and R in

solution:

$$O + ne^- \rightleftharpoons R \qquad (1)$$

The Nernst equation[45] gives the relation between the electrode potential, E, and the solution composition in the vicinity of the electrode surface:

$$E = E^{0'} + (RT/nF)\ \ln(C_O^e/C_R^e) \qquad (2)$$

$E^{0'}$ is the formal potential of the redox couple, R is the gas constant, T is the temperature, n is the number of electrons involved in reaction, F is the Faraday and C_O^e & C_R^e are the concentration of O and R at the electrode surface. At 25 °C reaction (2) can be written as:

$$E = E^{0'} + 0.059\ \log(C_O^e/C_R^e) \qquad (3)$$

Figure 4 shows a typical cyclic voltammogram for a reversible redox system. The current obtained depends on two processes: mass transfer of electroactive material to the electrode surface and the electron transfer process. The rate of electron transfer varies with potential according to the expression:

$$k_f = k^0 \exp[(-\alpha nF/RT)(E-E^{0'})] \qquad (4)$$

k^0 is the standard heterogeneous electron transfer rate constant and α is the transfer coefficient, arising from the fact that only a fraction of the input energy lowers the activation energy barrier.

The steep rise in current near $E^{0'}$ is due to the exponential dependence of k_f on applied potential. As electrolysis proceeds the reactant is depleted near the electrode surface and diffusion becomes the principal means of moving reactant to the surface. The average distance reactant molecules must travel to reach the electrode surface increases and therefore the rate of mass transport decreases. Eventually, with the increasing rate of electron transfer, mass transport becomes rate determining and a current

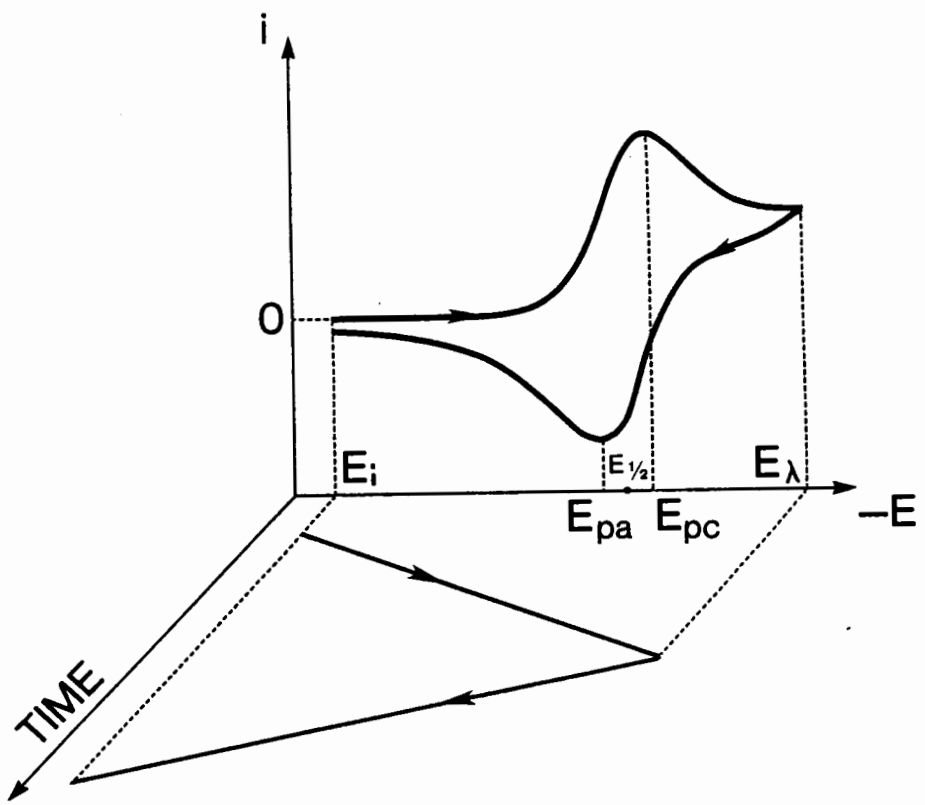

Figure 4. Cyclic voltammogram for a reversible redox couple.

maximum is observed. Beyond the peak, the current is time dependent and independent of potential. On the reverse scan, the product formed is reoxidised and the anodic peak is observed.

Several important parameters are obtained from cyclic voltammetry, including the cathodic (i_{pc}) and anodic (i_{pa}) peak currents, and the potential at which these peaks (E_{pc} & E_{pa}) occur. The magnitude of the peak current is given by the Randles-Sevcik equation[46]:

$$i_p = 2.69 \times 10^5 n^{3/2} A D_0^{1/2} C_0 \nu^{1/2} \qquad (5)$$

A is the electrode area, C_0 and D_0 are the bulk concentration and diffusion coefficient of species O respectively. ν is the potential scan rate.

The value of $E^{0'}$ can be obtained by cyclic voltammetry through the parameter $E_{1/2}$. $E_{1/2}$ is the half wave potential which corresponds to a value on a polarographic curve when the current is one half of the limiting value:

$$E_{1/2} = E^{0'} + 0.059 \log(D_R/D_0)^{1/2} \qquad (6)$$

D_R and D_0 are the diffusion coefficients of O and R respectively. Usually $D_R \approx D_0$ and therefore, $E_{1/2} \approx E^{0'}$. $E_{1/2}$ is obtained from the position of the cathodic and anodic peaks using the expressions derived by Nicholson and Shain[47].

$$E_{pc} = E_{1/2} - 28.5/n \quad mV \qquad (7)$$

$$E_{pc} = E_{1/2} + 28.5/n \quad mV \qquad (8)$$

The above equations indicate that the peak separations for reversible processes are 59/n mV, peak currents are proportional to $\nu^{1/2}$, peak potentials are independent of scan rate and the ratio of anodic and cathodic peak currents is unity. This simple picture assumes that the sweep rate is sufficiently slow and the kinetics of electron transfer sufficiently fast for

mass transfer processes to dominate the i-v behavior. In cases of slow electron exchange relative to the experimental time scale, the ratio of concentrations of O and R differs significantly from that calculated using the Nernst equation. As a consequence, smaller peak currents are obtained and, as scan rate is increased, larger peak separations are observed than those predicted. Expressions pertaining to such quasi-reversible and irreversible systems are well established and kinetic parameters are calculable[44].

I.1.1.2. CHRONOAMPEROMETRY

Chronoamperometry utilises the fact that at applied potentials substantially beyond the redox formal potential, the current is limited by the rate at which reactant is supplied to the electrode surface. If the experimental conditions are so arranged that the reactant is transported to the surface by means of linear diffusion (i.e. quiescent solution, flat electrode geometry) an expression originally derived by Cottrell[48] can be used to calculate the current that flows at any time following a potential step:

$$i = nFAC_0(D_0/\pi t)^{1/2} \qquad (9)$$

where t is the time passed following the potential step. The current is actually composed of two components: the Cottrell current given by equation (9) and the capacitance charging current, i_c, present with all electrode /electrolyte interfaces. The charging current can be observed by applying a potential step in the absence of a redox species. Subtraction of the charging current from the i-t decay behaviour yields the Cottrell current component. Plots of i vs. $t^{1/2}$ should be linear with gradients proportional

to $D_0^{1/2}$ and C_0.

I.1.1.3. ROTATING DISK VOLTAMMETRY

The previous two electrochemical techniques decribed rely on the linear diffusion of redox species to the electrode surface. However, much more information can be obtained using forced convection electrolysis. In these systems, one determines the dependence of the limiting current on hydrodynamic parameters.

The rotating disk electrode (RDE) is the most practical form of electrode for which the hydrodynamic properties of solution can be controlled[49]. The electrode consists of a flat disk set into an insulating cylinder. As the electrode rotates the thin layer of liquid adjacent to the electrode surface acquires rotational momentum and spins out radially from the centre of the disk. The liquid at the surface is replenished by upward axial flow (Figure 5).

As shown by Levich[50], the current flux at the electrode surface is controlled by mass and charge transfer according to the relation:

$$i = \frac{nFAD_0C_0}{\delta + D_0/k_f} \qquad (10)$$

δ is the thin diffusion layer which exists at the vicinity of the electrode surface. In this region, the solution is motionless and mass transport across the film is by diffusion only. The thickness of the diffusion layer was derived by Levich from hydrodynamic theory:

$$\delta = 1.61D^{1/3}\nu_k^{1/6}\omega^{-1/2} \qquad (11)$$

ω is the angular velocity of the disk (rad/s) and ν_k is the kinematic

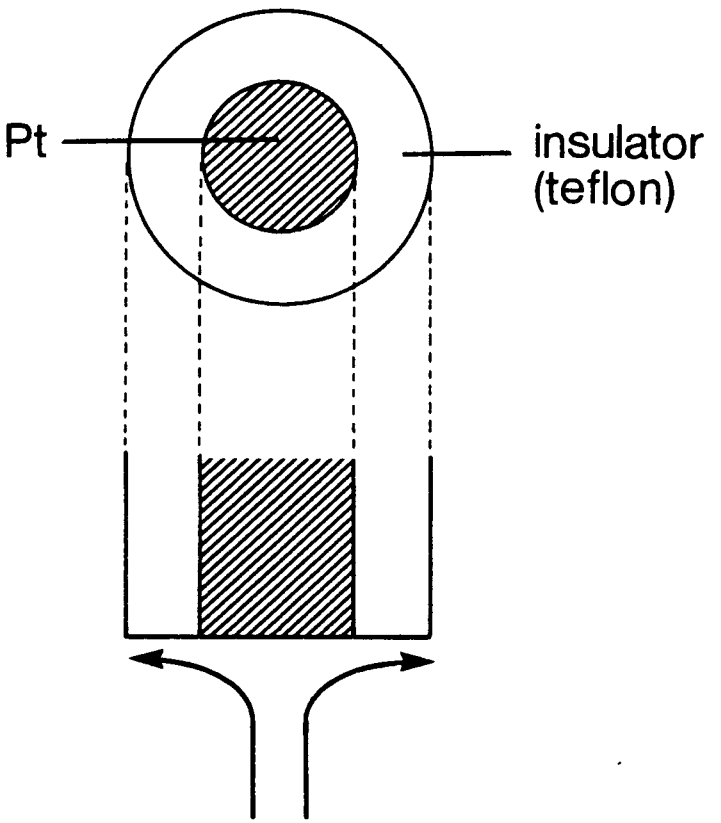

Figure 5. The rotating disk electrode (RDE)

viscosity of the solution (i.e. the ratio of solution viscosity and density).

Substition and simplification yields the useful relationship:

$$1/i_L = 1/i_A + 1/i_k \tag{12}$$

where i_L is the observed limiting current, i_A is known as the Levich current and is given by:

$$i_A = 0.62nFAC_0D^{2/3}\nu_k^{-1/6}\omega^{1/2} \tag{13}$$

and i_k is the kinetic contribution to current given by:

$$i_k = nFC_0k^0\exp[(-\alpha nF/RT)(E-E^{0'})] \tag{14}$$

The relative values of i_A and i_k define the two extreme cases in which mass transfer alone and charge transfer alone are current limiting. When the value of E, and therefore k_f is sufficiently large, the term $1/i_k$ may be neglected and the limiting current corresponding to mass transfer is obtained (i.e. $i_L=i_A$). Conversly, if the potential is such that i_k is small compared to i_A then $i_L=i_k$, corresponding to charge transfer control. In the latter case i_L is independent of ω.

The variation of i_L with $\omega^{1/2}$ is shown in Figure 6. In this illustration potential $E_1<E_2<E_3$. At potential E_1, i_L is independent of ω and is controlled by charge transfer only. At higher potentials, E_3, i_L is controlled by mass transfer and is proportional to $\omega^{1/2}$. At the intermediate potential, E_2, the current is successively controlled by mass and charge transfer.

RDE voltammmetry can be used to determine the thermodynamic quantity $E_{1/2}$. For a reversible system, combination of equation (3) and (13) with the relation:

$$C_0 = C_0^e + C_R^e \tag{15}$$

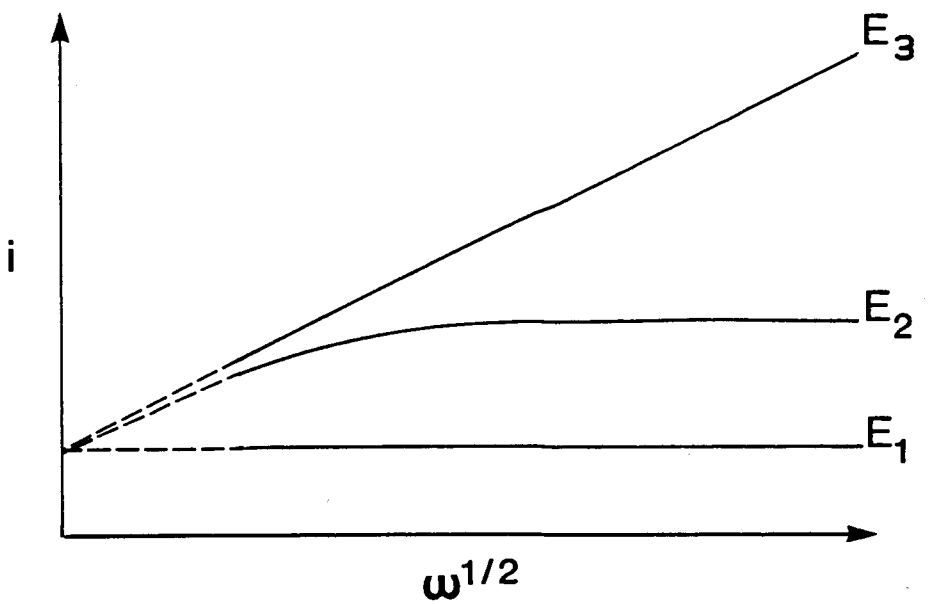

Figure 6. The variation of i_L with $\omega^{1/2}$.

yields

$$E = E_{1/2} - (0.059/n)\log[(i_L - i)/i] \quad (16)$$

$E_{1/2}$ is the potential where the current is one half of the limiting value. A plot of E vs. $\log[(i_L - i)/i]$ yields a straight line of gradient -0.059/n and an intercept equal to $E_{1/2}$. A typical RDE voltammogram is shown in figure 7. Two features are evident: the half wave potential and the transition between the charge and mass controlling processes.

A modification of the RDE is the rotating ring-disk electrode (RRDE) as shown in Figure 8. These electrodes are useful electroanalytical tools for providing mechanistic information. The RRDE consists of two spatially separated electrode surfaces, the inner disk and the outer ring. The electrodes are connected to provide two voltammetric circuits. The potential of the disk is ramped as with conventional sweep voltammetry while the potential of the ring is kept constant. In this way, electroactive species produced at the disk can be electrochemically detected when they are swept radially over the ring.

I.1.2. ELECTROANALTYTICAL TECHNIQUES APPLIED TO POLYMER FILMS

I.1.2.1. THEORY OF VOLTAMMETRY AND CHARGE TRANSPORT

Cyclic potential scanning or cyclic voltammetry is perhaps the most widely used electroanalytical technique for studying redox polymer films. The simplest case to consider is a monolayer of immobilised redox sites. If the electrochemical reaction shows Nernstian behavior then the voltammetric current is related to the electrode potential by[6,51]

$$i = \frac{n^2F^2A\Gamma_T \exp(E-E^{0'})\nu}{RT[1+(E-E^{0'})]^2} \quad (17)$$

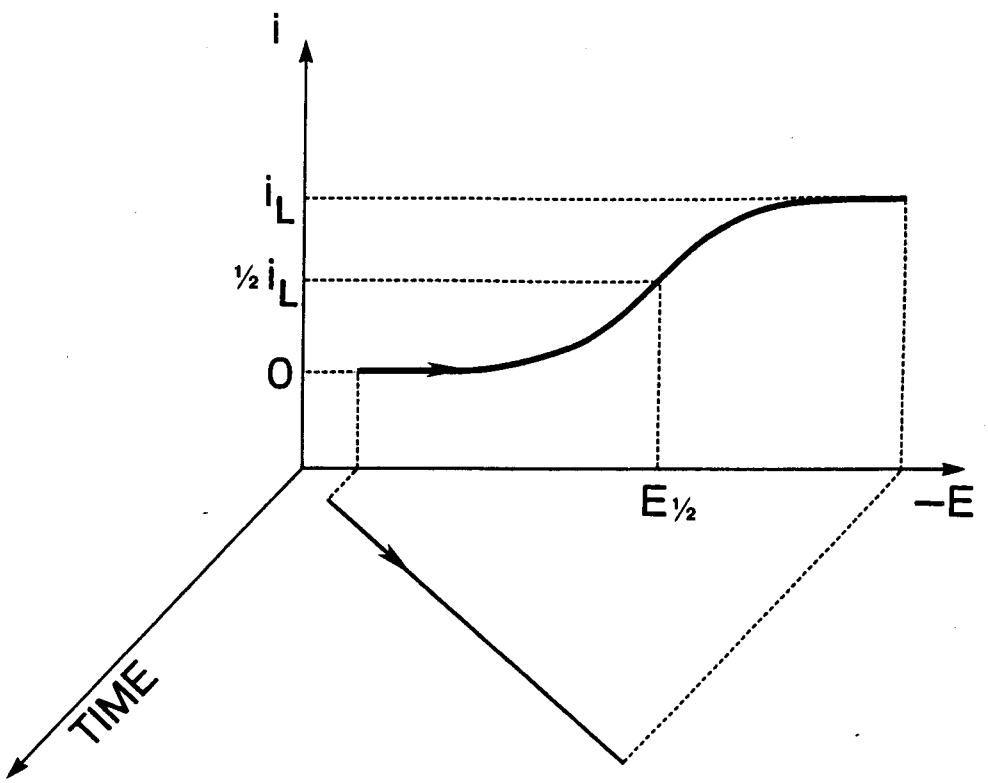

Figure 7. RDE voltammmetry.

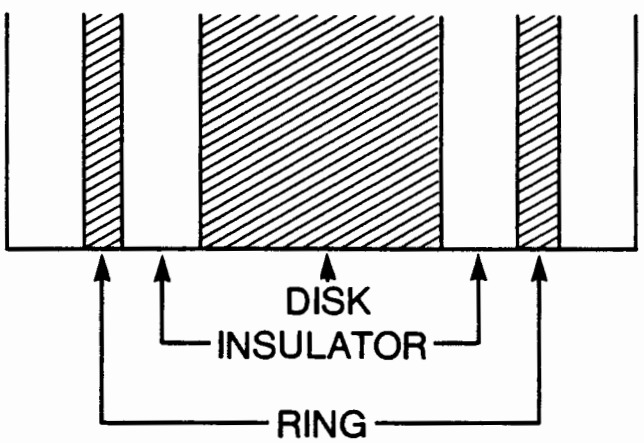

Figure 8. The rotating ring-disk electrode (RRDE).

and the cathodic and anodic peak currents are given by

$$i_p = \frac{n^2 F^2 A \Gamma_T \nu}{4RT} \qquad (18)$$

The important properties derived from these expressions are: i_p is directly proportional to potential sweep rate (cf. $\nu^{1/2}$ dependence for species in solution), the peak potentials and wave shapes for the forward and reverse sweeps are identical with $E_{pc} = E_{pa} = E^{0\prime}$, the peak width at half maximum, δ_p, is 90.6 mV (for n=1 at 25 °C), and the area under the curve gives the total quantity of attached electroactive material, Γ_T. These properties are illustrated in Figure 9.

The voltammetry of multimolecular polymeric films is more complex than the monolayer case. Electrochemical reaction of a polymer film requires a mechanism of electron propagation through the bulk of the film since redox sites in the outer regions are not in direct contact with the electrode surface. The propagation process includes self exchange reactions, segmental motions of the polymer, diffusion of redox species (in the case of ion exchange polymer films) and the motion of charge compensating counter ions.

Kaufman was the first to propose electron self exchange reactions between neighbour sites of different oxidation state as being the mechanism of charge transport through redox polymer films[52]. Theoretical treatments have shown that the electron hopping process follows simple diffusion laws for which the rate can be expressed as an electron diffusion coefficient, D_E[53-56]. The rate of charge transport through a polymer film of thickness d relative to the experimental time scale determines the time and potential dependent concentration profiles of O and R in the film. If charge transport is substantially faster than the experimental time scale then the ratio Γ_O/Γ_R will be uniform through the film and in thermodynamic equilibrium with the

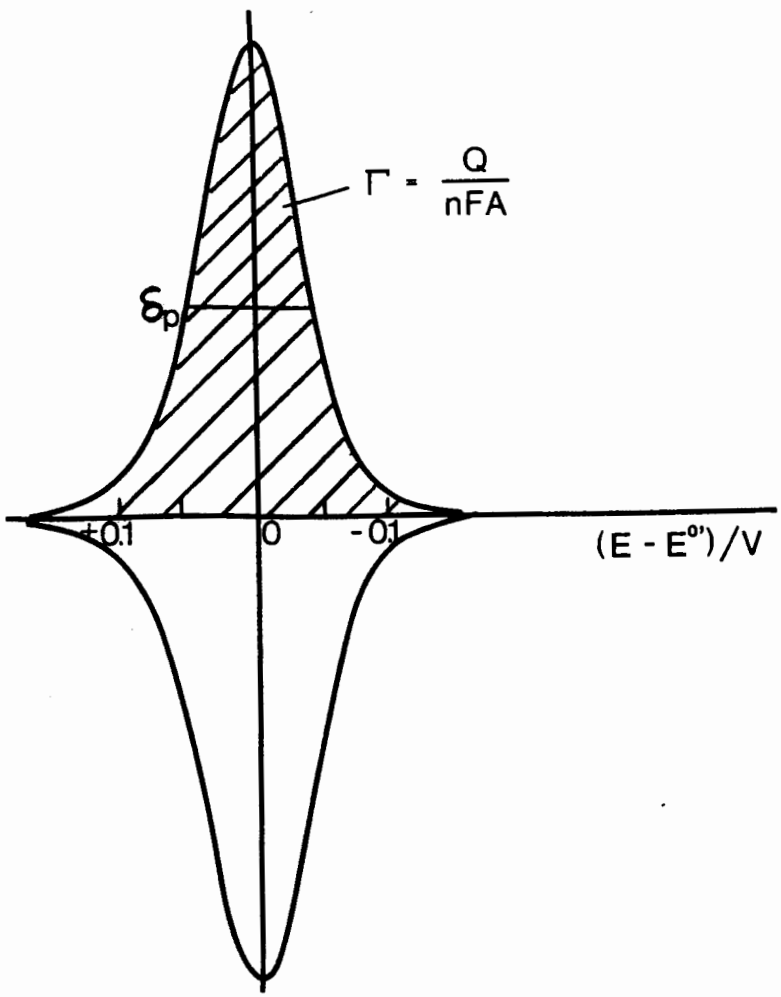

Figure 9. Cyclic voltammogram of a reversible monolayer.

applied electrode potential. In this case, cyclic voltammetric waveshapes will be symmetric like that for immobilised monolayers. Alternatively, if D_E is small or d is large such that the diffusion layer at time t, given by $(2D_E t)^{1/2}$ [57], is less than the film thickness then voltammetric and chronoamperometric data will be quantitatively the same as for redox species in solution. The voltammetric reponse of redox polymers therefore shows two extremes depending on the parameter $2D_E t/d^2$: symmetrical behaviour predicted by equation (17) and diffusive behaviour predicted by the Randles-Sevcik equation (5).

The condition $(2D_E t)^{1/2} < d$ is obtained for a short interval of time following a potential step beyond the formal potential of the couple. In this time interval the i-t decay conforms to the Cottrell equation (9):

$$i = nFAC(D_E/\pi t)^{1/2} \qquad (19)$$

where C is the concentration of active sites in the film. D_E is obtained from the gradient of a i vs. $t^{-1/2}$ plot.

I.1.2.2. THEORY OF ELECTROCATALYSIS BY REDOX POLYMER FILMS

The mediated electron transfer to a substrate in solution by a redox couple attached to an electrode surface can be considered as

$$P + e^- \rightleftharpoons Q \qquad (20)$$

$$A + Q \underset{k_{-1}}{\overset{k}{\rightleftharpoons}} B + P \qquad (21)$$

where P/Q is the mediator couple and A/B is the substrate couple. The cross reaction equilibrium constant can be determined from

$$\Delta G^0 = -RT\ln K = -nF(E_{AB} - E_{PQ}) \qquad (22)$$

where K is the equilibrium constant and E_{AB} and E_{PQ} are the formal electrochemical potentials of the redox couples.

The plateau current for the reduction of a substrate at a polymer coated rotating disk electrode (RDE) containing the P/Q couple is influenced by four rate limiting factors, which can be expressed in terms of their respective characteristic current densities: permeation of the substrate in the polymer film i_S, charge propagation through the film i_E, rate of cross reaction i_K, and rate of supply of the substrate to the film-solution interface i_A.

$$i_E = nFC_P{}^0 D_E/d = nF\Gamma_P D_E/d^2 \quad (23)$$

$$i_S = nFC_A \kappa D_{film}/d \quad (24)$$

$$i_K = nFC_A \kappa k C_P d = nFC_A \kappa k \Gamma_P \quad (25)$$

$$i_A = 0.62\ nFC_A D^{2/3} \nu_k{}^{1/6} \omega^{1/2} \quad (26)$$

where C_A is the bulk concentration of substrate, Γ_P and $C_P{}^0$ are the surface coverage and concentration of mediator in the film, κ is the partition coefficient of the substrate between the solution and the film, d is the film thickness, D_{film} and D are the diffusion coefficients of the substrate in the film and solution respectively, D_E is the diffusion coefficient of charge propagation through the film, and k is the rate of cross reaction between the substrate and mediator.

Several papers have shown that when one or two of these factors are dominant relatively simple equations can be employed to express the plateau current[5,20,58-62].

Classically, the plateau current for redox reactions occurring at a RDE is given by $1/i_L = 1/i_A + 1/i_k$ (Section I.1.1.3.). For polymer modified electrodes, i_k is replaced by i_1, an overall current density associated with the interplay of the four rate limiting factors shown above. The value of i_1 can usually be obtained from the intercept of a $1/i_L$ vs. $\omega^{-1/2}$ plot (inverse Levich plot) i.e. i_1 is the limiting current at infinite rotation rate. The

interactions of i_S, i_E, i_K, and i_A giving rise to the overall kinetic current density i_L, have been defined using differential equations derived from linear diffusion laws.

The limiting cases are designated with the letters R, S, E and combinations thereof. These letters indicate the nature of the rate limiting processes: R, kinetic control by the cross exchange reaction; S, kinetic control by the diffusion of the substrate in the film; E, kinetic control by diffusion of electrons in the film.

When the diffusion of electrons and substrate in the film is faster than the rate of cross reaction (i.e. i_E, $i_S \gg i_K$, i_A) then the plateau current is controlled by the rate of the catalytic reaction and substrate diffusion in solution. This is the "R" case and the derived equation determining the limiting current density is given by:

$$1/i_1 = 1/i_A + 1/i_K \tag{27}$$

If a second current wave is observed then:

$$1/(i_1+i_2) = 1/i_A + 1/i_S \tag{28}$$

The reaction occurs throughout the film and the concentrations of A & Q are uniform.

If diffusion of electrons is faster than the permeation of the substrate ($i_E \gg i_A$ & $i_K \gg i_S$) then the "SR" case is reached corresponding to simultaneous control of reaction kinetics by the catalytic reaction and substrate diffusion in the film. This leads to a thin reaction layer close to the film/electrolyte interface. The appropiate equations are:

$$1/i_1 = 1/i_A + 1/(i_K i_S)^{1/2} \tag{29}$$

and

$$i_2 = 0 \tag{30}$$

Under conditions where $i_E >> i_A$ and $i_K \dashrightarrow i_S$, the "R+S" situation is obtained. As in the "R" and "SR" cases, the concentration of Q is uniform through the film and the reciprocal of the rate limiting current at infinite rotation rate is given:

$$1/i_1 = 1/i_A + 1/ [(i_K i_S)^{1/2} \tanh(i_K i_S)^{1/2}] \quad (31)$$

$$1/(i_1+i_2) = 1/i_A + [\tanh(i_K i_S)^{1/2}/(i_K i_S)^{1/2}] \quad (32)$$

Depending on the relative magnitudes of i_S, i_E, i_K, and i_A, electron transfer may occur in the bulk of the film but the majority of charge will be transfered at the film/electrolyte interface.

Another kinetic situation is reached when i_E is only slightly greater than i_A and $i_K >> i_S$. This situation is termed "SR+E". The transition from the "SR" case to "SR+E" results from a decrease in i_E or an increase in i_A. Under these conditions:

$$1/i_1 = 1/i_A + \left\{\frac{(i_E)^{1/2}}{(i_K i_S)^{1/2}}\right\} \frac{i_E - i_1(1-K^{-1})}{i_E - i_1} \quad (33)$$

$$i_2 = 0 \quad (34)$$

In examining cases where film diffusion of the substrate is faster than diffusion of electrons, it is useful to use the "R" case as a reference point (i_E, $i_S >> i_K$, i_A). If i_E decreases such that $i_K >> i_E$ and $i_S >> i_A$ then the "ER" situation exists, and the current density is given by:

$$1/i_1 = (1/i_A)(1-K^{-1}) + \left\{\frac{i_A - (1-K^{-1})i_1}{i_A - i_1}\right\}^2 \frac{i_1}{i_E i_K} \quad (35)$$

$$1/(i_1+i_2) = 1/i_A + 1/i_S \quad (36)$$

The concentration of A is uniform while Q is localised in a thin region at

the electrode/film interface.

When $i_S \dashrightarrow i_A$ and $i_K \gg i_E$ then C_A is no longer uniform through the film, although Q is still confined to a narrow region at the electrode surface. This situation is termed "ER+S" and the corresponding equations are

$$1/i_1 = \left\{\frac{1}{i_A} + \frac{1}{i_S}\ (1-K^{-1})\right\} + \frac{i_E\, i_K}{i_1} \left\{\frac{1}{i_1} - \frac{1}{i_A} - \frac{1}{i_S}\right\}^2 \tag{37}$$

$$1/(i_1+i_2) = 1/i_A + 1/i_S \tag{38}$$

Another kinetic situation is reached when $i_S \gg i_A$ and $i_K \dashrightarrow i_E$. In this case, designated "R+E", C_A is uniform through the film while the concentration profile of Q extends from the electrode film interface, where C_Q is greatest, to film/electrolyte interface, where C_Q is least. Under these conditions:

$$1/i_1 = (1/i_A)(1-K^{-1}) + \left\{\frac{i_A-(1-K^{-1})i_1}{i_A-i_1}\right\}^2 \frac{i_1}{i_E\, i_K\, \tanh^2\left[\left(\frac{i_K}{i_E\, i_A}\right)[i_A-(1-K^{-1})i_1]\right]^{1/2}} \tag{39}$$

$$1/(i_1+i_2) = 1/i_A + 1/i_S \tag{40}$$

Consider the situation where $i_K \gg i_S$ and $i_A \gg i_E$. This is known as the "E" case. the kinetic reaction is controlled solely by electron diffusion in the film and the substrate is not considered to significantly penetrate the film. Thus, the kinetic current density is given by:

$$1/i_1 = 1/i_E \tag{41}$$

When $i_K \gg i_E$ and $i_A \gg i_S$, the "S" case is reached. This is the same situation as for direct reduction of the substrate at an electrode surface coated with a non-catalytic membrane:

$$1/i_1 = 1/i_A + 1/i_S \tag{42}$$

Consider now the situation when electron diffusion and film diffusion of the substrate have comparable rates. As previously defined, the "R" case exists when i_E, $i_S \gg i_K$, i_A. However, if i_K, $i_A \gg i_E$, i_S then the kinetics are governed by electron and substrate diffusion in the film. This is the "S+E" case where

$$1/i_1 = 1/i_E + 1/i_S \qquad (43)$$

In this kinetic situation a thin reaction layer exists in the film. If the i_S/i_E ratio increases then the reaction layer moves towards the electrode/film interface, tending towards the "S" situation. Conversly, if the i_S/i_E ratio decreases, the reaction layer moves towards the film/solution interface to the limit where the "E" case is reached.

A final situation which may arise when the catalytic reaction, electron diffusion and film diffusion of the substrate have similar rates. This kinetic situation is termed (R+S+E).

Figure 10 displays the differing kinetic situations in terms of steady state concentrations of catalyst sites and substrate in the polymer film and in solution. To date, relatively few of these cases have been experimentally observed and thus, more data are required to verify the general theory.

I.1.3. SPECTRAL TECHNIQUES

I.1.3.1. ABSORPTION SPECTROPHOTOMETRY

When chromophores are present in the polymer film then the film may be studied on an optically transparent electrode, such as SnO_2 coated glass, using visible or uv spectroscopy[63,64]. The simplest characterisation using this technique is to measure the total amount of chromophore in the film:

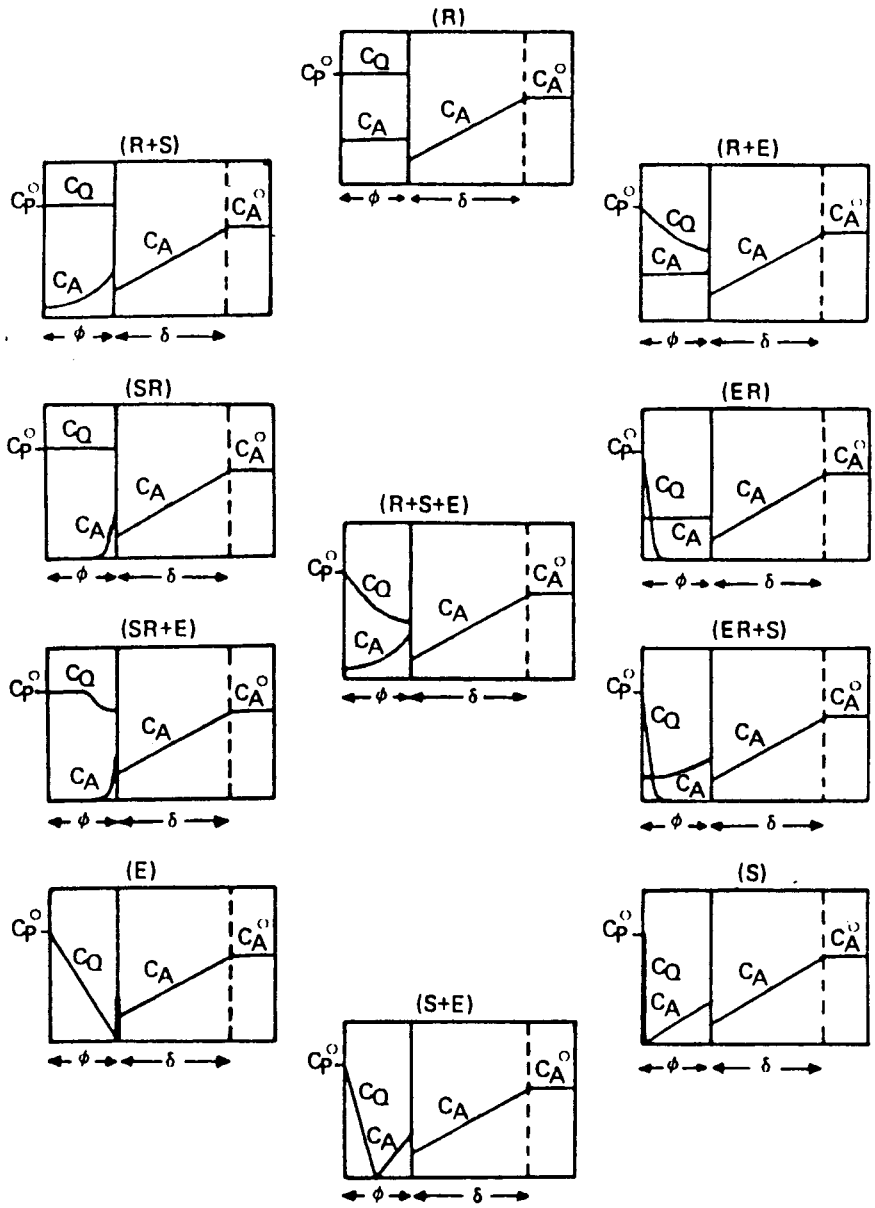

Figure 10. The differing kinetic situations that may arise for catalytic reactions at polymer films. C_P^0 is the concentration of catalyst in the polymer film; C_Q is the space-dependent concentration of the reduced form of the catalyst; C_A^0 is the bulk concentration of the substrate; C_A is the space-dependent concentration of the substrate.

$$\log(I_0/I) = 10^3 \epsilon \Gamma_T \qquad (44)$$

where I_0 and I are the intensities of radiant energy striking and emerging from the sample repectively. ϵ is the molar extinction coefficient of the chromophore.

When the chromophore is the electroactive component then changes in oxidation state produce changes in the spectral response. Thus, absorbance-time or absorbance-potential measurements can be used with such electrodes to observe changes in oxidation state of the redox couple. The relationship between the electrode potential and absorbance has been derived from thin layer spectroelectrochemistry and is given by[65]:

$$E = E_{1/2} + 0.059 \log \frac{A_{red}-A}{A-A_{ox}} \qquad (45)$$

where A_{red} and A_{ox} are the absorbances of the film in the completely reduced and completely oxidised state respectively.

I.1.3.2. AUGER ELECTRON SPECTROSCOPY (AES)

Auger electron spectroscopy is part of the broader field of secondary electron spectroscopy dealing with the analysis of the entire secondary electron spectrum. Data obtained from AES comes from the top five atomic layers and allows identification of each element in this region. Trace elements down to concentrations of 10^{12} atoms/cm^3 may be detected for well prepared samples. This method therefore, has great capabilities for analysing solid surfaces[66,67].

The mechanism of Auger electron ejection is one of internal conversion. When an atom is bombarded with an electron of sufficient energy, an inner electron is emitted, ionising the atom in the process. The vacancy is filled

by a higher orbital electron and energy is released. The energy may be released as a x-ray photon, leading to well established x-ray emission techniques, or the energy may be transfered to a nearby electron, ejecting it in the process. The ejected electron is known as the Auger electron, the energy of which is characteristic of the emitting element and independent of the incident electron beam energy.

The process may be illustrated using the silicon atom model (Figure 11). The K, L inner core electrons are shown with their corresponding energy levels for single ionisation. The valence band level, VB, is shown as a continuous band, representing the condition occurring in the solid when the atoms are brought together. The density of states within the level is illustrated by the shaded area. The diagram shows ionisation of the $L_{2,3}$ by a primary electron. The hole created is filled by internal cascade. The energy may be sufficient to eject a nearby electron from the surface. The figure indicates emission of an electron from the V_1 level although any other electron from within the band may have been ejected. The energy of the released electron is given by:

$$E = E_{L2,3} - E_{V1} - E_{V1'} \qquad (46)$$

where $E_{V1'}$ is the energy needed to escape from the surface. It has been proposed that $E_{V1'}$ is the ionisation energy for the V_1 level after the primary excitation step.

The Auger electron energy is characteristic of a given element and allows elemental identification[68]. The Auger electron current on the other hand yields quantitative information. If one wants to extract quantitative information then an understanding of the Auger signal is required: The magnitude of an Auger signal is given by

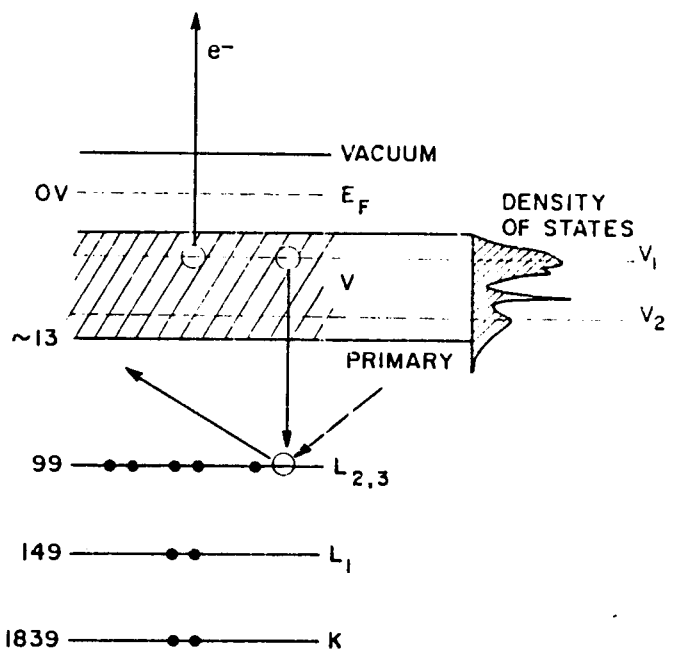

Figure 11. The energy level model for silicon indicating a $L_{2,3}VV$ Auger process.

$$S_A = S_0 . \sigma_A(E_p) . [1+r_x(E_A)] . T(E_A) . D(E_A) . n_X . \lambda_M . \text{Cos } \theta \qquad (47)$$

where S_0 is the primary electron beam current, $\sigma_A(E_p)$ is the ionisation cross section of electrons of energy (E_p), $[1+r_x(E_A)]$ is a factor which takes into account the back scattering of Auger electrons of energy E_A, from element X in matrix M, $T(E_A)$ and $D(E_A)$ are the transmission and electron detector efficiences, n_A is the atom distribution in the depth sampled, λ_M is the inelastic mean free path of Auger electrons in the matrix, and θ is the angle of Auger emission to the surface normal.

The number of unknowns can be reduced by considering the ratio of signal intensities of element X in the sample matrix M_S and of the element X in pure form, M_X. Thus:

$$\frac{S_{Ms}}{S_{Mx}} = \frac{[1+r_{Ms}(E_A)] . n_{Ms} . \lambda_{Ms}}{[1+r_{Mx}(E_A)] . n_{Mx} . \lambda_{Mx}} \qquad (48)$$

The back scattering factor $[1+r_X(E_A)]$ is obtained fom the empirical relation[69,70]

$$[1+r_X(E_A)] = 1 + 2.8[1-0.9(E_A/E_p)]\eta \qquad (49)$$

where $\eta = 0.0254 + 0.016Z - 1.86 \times 10^{-4}Z^2 + 8.3 \times 10^{-7}Z^3$. Z is the average atomic number of the matrix. For PP, Z=5.14 and η=0.052.

The inelastic mean free path, λ, is also obtained by an empirical relation:

$$\lambda_M = \frac{A_M}{E_A^2} + B_M E_A^{1/2} \qquad (50)$$

where A and B are 143 & 0.054 respectively for elements and 31 & 0.087 for organic compounds.

Calculation of the variables and substitution into equation (48) allows

determination of the elemental concentration in the sample matrix, n_{Ms}.

Information on the elemental dispersion in the sample matrix can be obtained by sputtering away surface layers by Ar^+ ions while simultaneously recording the elemental Auger signal. This method is destructive to the sample in the region under investigation and one must be careful that sputtering does not substantially change the elemental distribution.

I.2. SEMICONDUCTOR ELECTROCHEMISTRY

Tremendous interest has developed in the use of photoelectrochemical (PEC) systems for conversion and storage of solar energy. It is now well established that semiconductor based PEC cells are among the most efficient of man made solar conversion systems. They can be divided into two categories: Those in which the Gibb's free energy change in the electrolyte is zero (photovoltaic), and those in which the free energy change in the electrolyte is non-zero (photo-electrosynthetic). The general classifications are shown in Figure 12.

In trying to improve quantum efficiency, the semiconductor-electrolyte interface has come under close scrutiny[71-75]. The important principles related to this thesis are presented.

I.2.1. THE ELECTRICAL DOUBLE LAYER MODEL

Immersion of a semiconductor into an electrolyte results in the formation of electrical double layers. It is these double layers that control the physical, chemical and electrical properties of the semiconductor in contact with solution. According to the conventional model, two double layers are of major importance. These are the space charge region in the semiconductor and the Helmholtz double layer between the solid and the outer Helmholtz plane - the distance of closest approach of non-adsorbed ions.

There are three regions of excess charge in this model. In the space charge region charge may be present due to mobile electrons or holes at the surface, trapped holes or trapped electrons, or uncompensated impurities. Two other forms of charge exist on the two sides of the Helmholtz region: On the semiconductor side charge is in the form of surface states or adsorbed

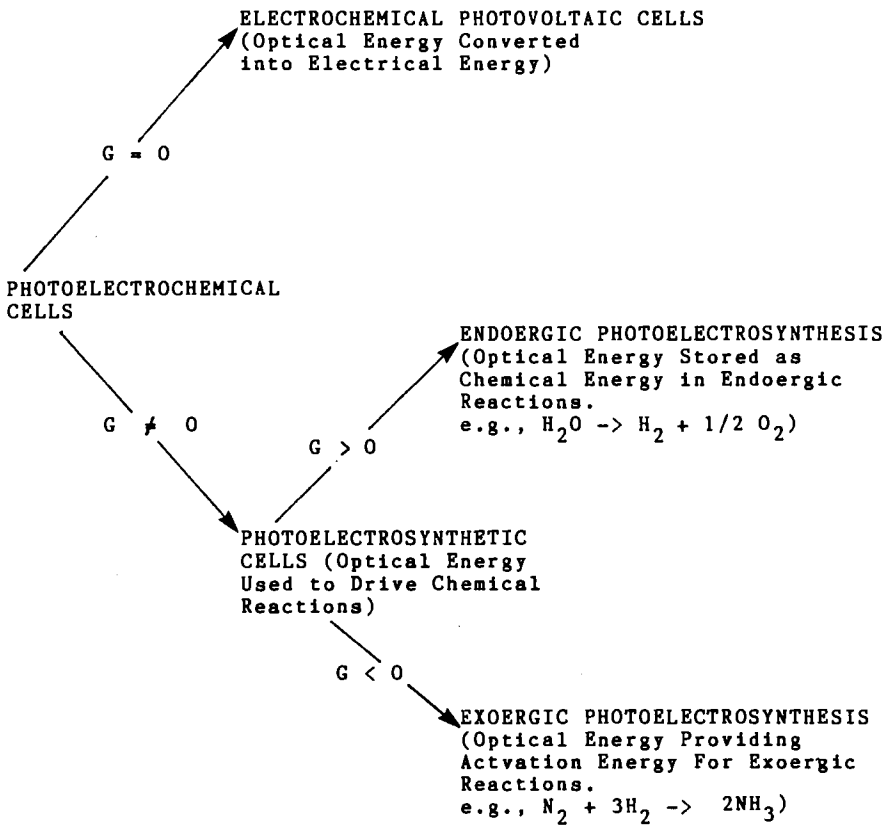

Figure 12. Classification of PEC cells.

ions, while charge on the outer Helmholtz plane arises from ions in solution attracted to the semiconductor by surface charges.

I.2.2. THE SEMICONDUCTOR SPACE CHARGE LAYER

A space charge develops in a semiconductor upon immersion into an electrolyte when ions in solution can extract electrons from, or inject electrons into, the semiconductor, or a change in surface state occupancy occurs. A further change may be induced by applying an external voltage between two electrodes. When majority carriers are extracted from the surface a depletion layer exists at the semiconductor surface. Under these conditions photogenerated carriers diffuse to the surface under the influence of the electric field and electrochemical reactions can essentially be driven uphill. When majority carriers are injected into the semiconductor from solution, or an external voltage is supplied to generate majority carriers at the surface, an accumulation layer exists. If the Fermi energy is forced into the band, then the semiconductor is said to be degenerate and will show metallic behavior. Another space charge condition arises when majority carriers are extracted from the minority carrier band such that the surface charge has inverted: n-type is converted to p-type and p-type inverted to n-type.

The formation of the depletion layer in the semiconductor is essential to the development of viable systems for PEC energy conversion. The depletion region gives rise to a Schottky barrier providing a mechanism for preventing the recombination of photochemical charge carriers, e^- & h^+, with each other or with products obtained from the initial transfer of photo-generated carrier. The energy profiles of n- and p-type semiconductors in equilibrium with a redox couple, with a formal potential in the band gap

region, is shown in figure 13. A large barrier height, E_B, gives rise to a large photovoltage and a large quantum yield for electron flow. Also shown in Figure 13 are the corresponding photocurrent-voltage curves obtained when the equilibrium condition is perturbed by an external voltage. The important feature is that the onset potential for cathodic current is shifted positively for p-type semiconductor electrodes and the onset of anodic current is shifted negatively for n-type electrodes relative the reversible electrode.

I.2.3. BAND EDGE UNPINNING

The semiconductor-electrolyte interface can be considered as comprising of a number of resistive and capactive components which can be simplified by describing an equivalent circuit. For simplicity, consider the equivalent circuit corresponding to the semiconductor and Helmholtz layer only (Figure 14)[88]. In the absence of semiconductor surface states, the overall impedance of the circuit, Z, is given by:

$$Z = (R_{SC} + 1/j\omega C_{SC}) + (R_H + 1/j\omega C_H) \quad (51)$$

or

$$Z = Z_{SC} + Z_H \quad (52)$$

When a semiconductor depletion layer is present, $Z_{SC} >> Z_H$ and any potential difference present between the semiconductor and the electrolyte occurs across the space charge layer. In the case of an accumulation or inversion layer, Z_{SC} can be comparable to, or smaller than, Z_H, and any potential difference present occurs across the Helmholtz layer[76].

A common explanation of movement of band edges relative to a fixed reference is Fermi level pinning[71,77,78]. Fermi level pinning refers to a

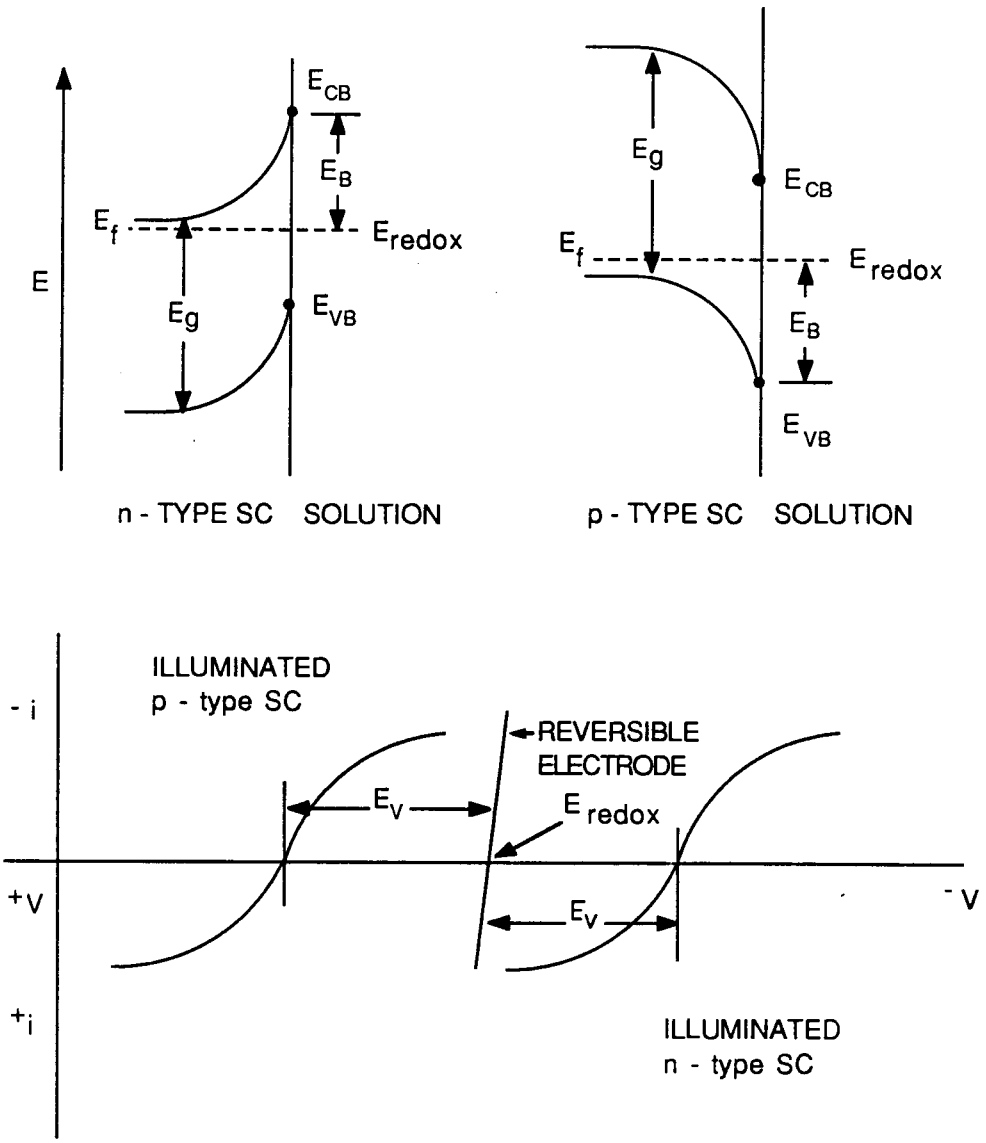

Figure 13. Energy profiles of n- and p-type semiconductors in equilibrium with a redox couple, and the corresponding photocurrent-voltage curves.

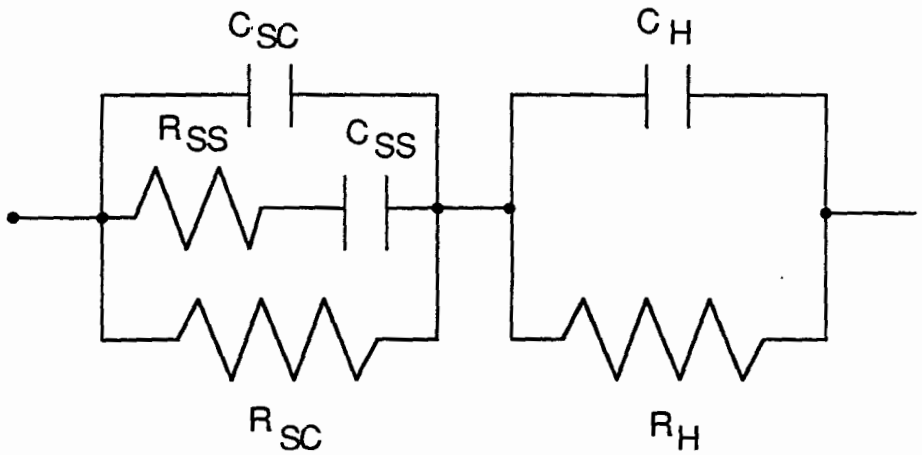

Figure 14. Equivalent circuit corresponding to the semiconductor and Helmholtz layer.

situation where band bending in the semiconductor space charge layer is essentially independent of the redox couple in solution. Additional changes in potential difference occur across the Helmholtz layer. This phenomena is brought about by a small quantity of surfaces states ($10^{12}/cm^2$).

Variations of the semiconductor-electrolyte interface in the presence of redox couples with differing E_{redox} are shown in Figure 15 for the accumulation and inversion layer case (top), and the Fermi level pinning case (bottom). In the former case, the band edges are fixed when E_{redox} lies within the bandgap region, and are unpinned when E_{redox} lies above or below the conduction or the valence band energy level respectively. In the Fermi level pinning case, the position of the band edges are strongly determined by the redox species in solution, irrespective of whether E_{redox} is above, below, or between the band edges.

I.2.4. THE CONDUCTION AND VALENCE BAND ENERGY

The energy of the conduction and valence band in relation to E_{redox} determines the probability of electron transfer. A knowledge of E_{CB} and E_{VB} is therefore esssential before proceeding to analyse electrochemical reactions at semiconductor electrodes. E_{CB} and E_{VB} are most readily obtained from the expressions:

$$E_{CB} = V_{fb} + kT \ln (N_D/N_{CB}) \qquad \text{(n-type)} \qquad (53)$$

$$E_{VB} = V_{fb} + kT \ln (N_{VB}/N_A) \qquad \text{(p-type)} \qquad (54)$$

where N_D and N_A are the donor and accepter densities in the semiconductor and N_{CB} and N_{VB} are the effective density of states in the CB and VB respectively. V_{FB} is the potential at which the semiconductor energy bands are flat.

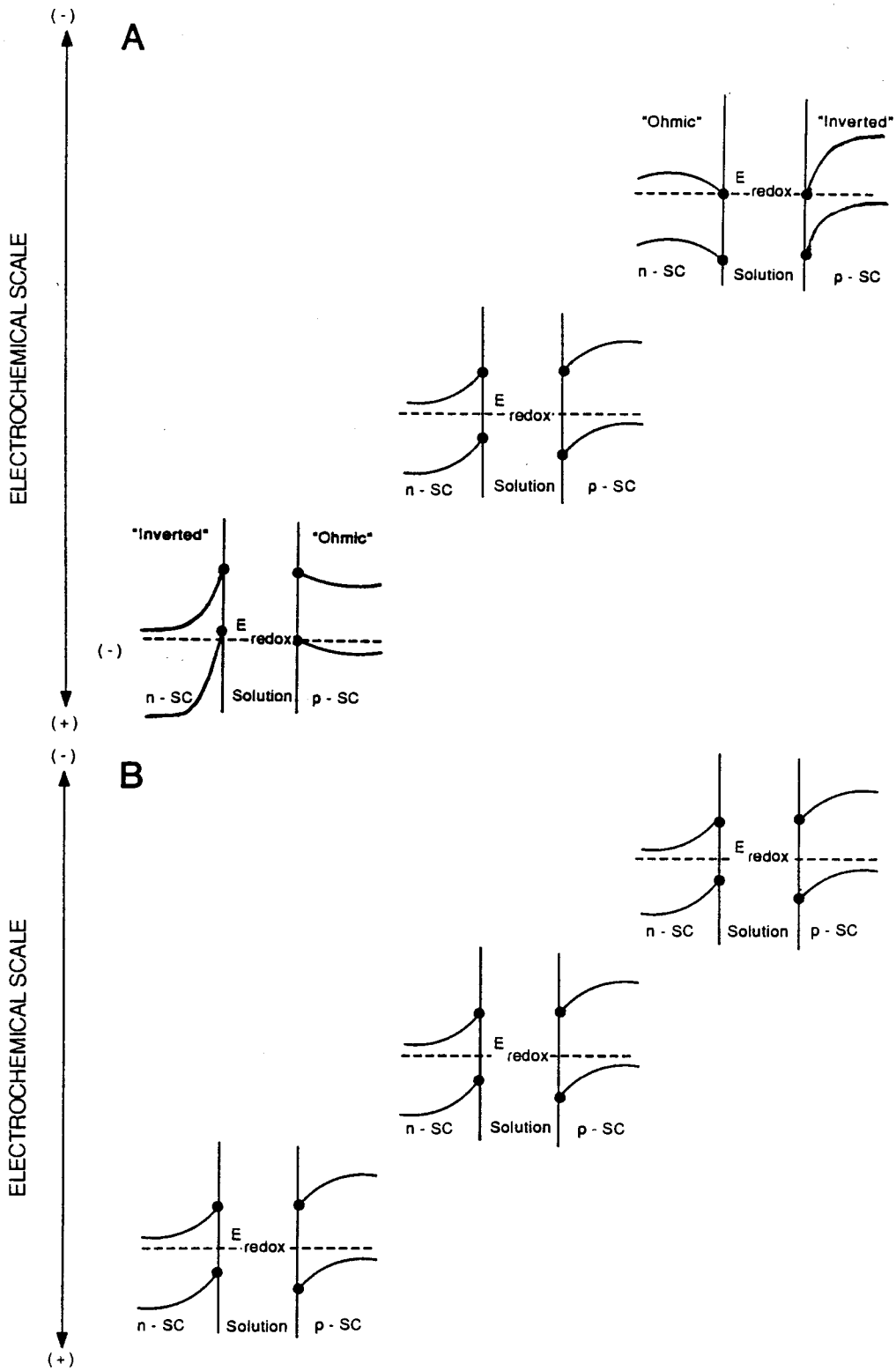

Figure 15. Variations in the semiconductor-electrolyte interface in the presence of redox couples with differing E_{redox}: a) for the accumulation and inversion layer case (top), b) for the Fermi level pinning case (bottom).

The classical method of determining V_{FB} is based on the Mott-Schottky equation:

$$1/C_{SC} = (2/qN_D \kappa \epsilon_o A)(V_M - V_{FB} - kT/q) \quad (55)$$

where C_{SC} is the space charge capacitance, q the charge on the electron, κ the dielectric constant, ϵ_o the permittivity of free space, A the electrode area, V_M the electrode potential and k the Boltzman constant.

The method involves measuring the differential capacitance of the semiconductor electrode as function of applied voltage V_M by a.c. impedance techniques. For an ideal system, a plot of $1/C^2$ against V_M (Mott-Schottky plot) yields a straight line with an intercept approximately equal to V_{FB} and a slope related to the carrier density.

CHAPTER II

ELECTROCHEMICAL STUDIES OF ANTHRAQUINONE REDOX POLYMER FILMS ON CONDUCTIVE AND SEMICONDUCTIVE SUBSTRATES

I.1. INTRODUCTION

A theoretical treatment of the electrochemical behaviour of polymer films has been outlined in Chapter I. Experimental data are important for verifying present theory although, very often, interesting and important information can be extracted from unpredicted behaviour. The research described in this chapter was motivated by the requirement for further information on the charge and mass transfer processes that occur during electrochemical reaction at polymer films, particularly in the area of electrocatalysis and photoelectrochemistry. A greater number of electrocatalytic studies would be beneficial in verifying present electrocatalytic theory, while studies of electron transfer between polymer films and semiconductor substrates would prove useful in the designing of PEC cells employing polymer films.

For these studies, a polyanthraquinone redox polymer was synthesised and the electrochemistry of thin films investigated on platinum and silicon semiconductor electrodes. The charge and mass transfer processes accompanying electrocatalytic reaction at these films was investigated using dissolved oxygen as the catalysed substrate.

Since these studies were initiated a number of reports and several comprehensive reviews[1-5] concerning polymer modified electrodes have appeared. A brief summary is presented here.

II.1.1. TYPES OF REDOX POLYMER FILM

The drive for creating novel and useful polymer modified electrodes has led to the synthesis of new electroactive polymers and the refining of film forming methods.

The most direct approach of redox polymer films is to synthesise the desired polymer and apply it to the electrode surface by one of a number of film forming techniques. One method of obtaining preformed polymers is to polymerise the appropriate electroactive monomer. Another is to chemically attach an electroactive functionality to an electro-inactive polymer. Polymer films prepared by these methods have a number of advantages over other film forming techniques since the isolated polymer may be readily purified and analytically characterised.

Methods employed for applying films of polymers include droplet evaporation, dip coating, spin coating, oxidative or reductive deposition and the binding of polymer to reactive monolayer sites. Droplet evaporation simply requires the spreading and evaporation of a polymer solution on an electrode. In this manner the quantity of polymer applied is immediately known[79,80]. Dip coating, first reported by Miller and Van de Mark, is accomplished by immersing the electrode into a dilute solution of the polymer[81]. Spin coating of preformed redox polymers is simply a droplet evaporation technique performed on a spinning substrate[52,82,83]. Redox deposition depends on the change in polymer solubility induced by oxidation or reduction and has been utilised to deposit polyvinylferrocene from CH_2Cl_2 solutions[9]. The binding of polymers to reactive monolayers has been demonstrated by Itaya and Bard[84]. The procedure involved the functionalisation of an electrode with a monolayer of silane sites, reaction between the silane and an electro-inactive polymer, and chemical attachment

of the electroactive group.

An elegant technique leading to redox polymer films utilises the ion-exchange properties of polycations and polyanions[85]. Ion-exchanging polymer films are prepared from preformed polymers and coated on electrodes by one of the above film forming techniques. Films bear fixed ionic groups, as with sulphonated polystyrene[86], Nafion[87] and ionic redox polymers[88] or film ionicity may be induced by exposure to acid or base, as with poly-(vinylpyridine) and poly(acrylic acid)[14]. The electroactive ion is incorporated or in-partitioned by immersing the polyionic film into a solution of the redox ion. The film is then transfered to fresh solution for electroactive study. Leaching of the retained ions, and thus lifetime of the electrode, is governed by the ion exchange partition coefficient and poorly understood out-partitioning kinetics.

Another route to obtaining polymeric films is the direct coupling of monomers at the electrode surface. Into these categories fall organosilanisation using di- and tri-functional silanes, plasma polymerisation, in which monomer vapours are exposed to a radio frequency plasma discharge[89], and electrochemical polymerisation. Electropolymerisation is an electro-initiated polymerisation process. During electrolysis, precipitated polymer adsorbs and accumulates at the electrode surface and the film retains electrochemical activity for sustained polymerisation. By this route redox polymeric films containing monomeric sites of ferrocene[90], thionine[91], metalloporphyrins[92], naphthoquinone[93] and Ru, Os and Fe metal complexes[94,95] can be obtained. The electro-chemical oxidation of certain aromatic organic molecules leading to the formation of the so called conducting polymers will be dealt with in another chapter.

II.1.2. VOLTAMMETRY

The simplest reversible voltammetric waveshape occurs for a homogeneous film with non-interacting sites. When the kinetics of electron transport are facile, the film is in equilibrium with the applied potential and the waveshape is the same as for an ideal monolayer: peak separations are zero, peak shapes are identical and the peak width at half height, δ_p, is 90.6 mV. In most cases, the voltammetric behaviour differs from ideal. The most common deviation is that δ_p is greater than, or less than, 90.6 mV. These phenomenon are usually observed even when $E_{peak} \approx 0$ and peak shapes are identical. This has been explained by activity effects[96]. Negative interaction parameters yield broadened voltammetric peaks, while positive interactions produce narrowed peaks, often in the form of current spikes[9,82,97]. In other systems, the cathodic and anodic waves have different shapes. These effects are often observed when one of the oxidation states of the polymer is electrically neutral. In electrically neutral polymers, permeability to electrolyte ions and solvent is decreased[98,99].

Another explanation of peak broadening is that not all sites exhibit the same formal potential. A narrow gaussian distribution of $E^{0'}$ yields a broadening of peak shape while E_{peak} remains at zero[91]. Slight variations in $E^{0'}$ might be induced by local variations in polymer crystallinity, crosslinking, packing, or some other physical parameter. In extreme cases electrochemically non-equivalent sites can produce multiple waveshape voltammograms even though the film consists of only one type of redox centre. Such behaviour has been reported for polyvinylferrocene films[55], poly(p-nitrostyrene)[10] and polyvinylpyridine films incorporating $Ru^{III}EDTA$[95,100].

Electrochemical behaviour is also largely governed by the nature of the solvent. Polymer contracts in "poor" solvent, and electrolyte cannot readily

permeate into the film. The defficiency of electrolyte at the electrode interface results in a high resistance to charge transfer and renders the redox polymer electrochemically inactive in that solvent[101,102].

The above variations in voltammetric waveform have been discussed on a thermodynamic basis corresponding to situations where the experimental time scale is large so that the film is in equilibrium with the applied potential. When the time scale is much smaller, or the film thickness is much larger, then the voltammetric response shows evidence of the finite rate of charge propagation through the film. In these situations, peak separations are much greater than zero and i_p is not proportional to scan rate. In the limit, E_p --> 59/n mV and i_p is proportional to $\nu^{1/2}$.

II.1.3. CHARGE TRANSPORT

The rate of propagation of electrochemical charge through a redox polymer film determines the maximum film thickness which can be employed when such electrodes are integrated into useful devices. For this reason, charge transport in polymer films is one of the most actively studied topics in the area of polymer modified electrodes. The main issues concern: the mechanism of electron transport in polymer films; the rate determining step for the transport of electrons; the dependency of the physical characteristics of the polymer on the rate of transport.

The general consensus is that transmission of electrons through the film occurs by an electron hopping mechanism, wherein self exchange reactions take place between neighbouring oxidised and reduced sites. Fortunately, the transport mechanism follows Fick's laws of diffusion for which the rate of charge propagation can be expressed as a diffusion coefficient D_E (Section I.1.1.2.). The magnitude of D_E, and the rate determining step, varies from

system to system. Possible rate determining steps can be conceived to be: The chemical rate of electron transfer between neighbour redox sites upon collision; the rate of segmental motion of polymer chains required for site-site collision; the rate of counter ion permeation necessary to maintain electroneutrality. Separating these processes can be difficult. The dominant process depends on the system under investigation, each rate determining step having been identified[12,82,101].

Consideration can be given to the concentration of electroactive centres in cases where counter ion transport is not controlling. The electron hopping mechanism implies that an increase in concentration of active sites will facilitate electron exchange and enhance the rate of charge propagation. An increase in D_E was observed for vinylferrocene-siloxane copolymers with increasing concentration of sites[103], although no change was observed for $Ru(bpy)_3$-Nafion films[104-106]. It is possible that, for a given polymer system, the concentation dependence of charge transport may vary with the concentration of active sites. In this aspect, the D_E of certain Ru and Os containing copolymers was constant at moderate concentrations but increased with concentration in the high and low concentration regions[107].

The study of ionic redox polymer films are further complicated by the fact that active redox groups may diffuse to the electrode surface and undergo electrochemical reaction. Thus, D_E is the sum of the diffusional motion of redox groups and the diffusional motion of electrons. In some cases, D_E is dominated by the former, in others it is the latter and in others still diffusional rates of redox groups and electrons are comparable[103,104].

II.1.4. ELECTROCATALYSIS

It is now well established that the acceleration or mediation of slow electrode reactions can frequently be achieved by employing chemically modified electrodes. Numerous examples have been reported including: The oxidation of ascorbic acid by ferrocene[102], hydroxy phenyl[108], ferrocyanide [109], benzidine[110] and pentachloroiridate[111] containing polymers; the reduction of organo halides by polynitostyrene[98,112] and metallotetraphenylporhpyrins[113]; the oxidation of NADH by polymer bound dopamines[114]; the oxidation of Cl^- [115], isopropanol, xylene[116] and metal ions[117] by polypyridyl complexes of ruthenium; the reduction and oxidation of metal complexes by redox sites electrostatically held in ionic polymer films[96,118-127].

One of the most intriguing electrochemical reactions is the reduction of O_2. A good catalytic electrode would be invaluable for fuel cells, for electrochemical sensors and for the electrochemical production of hydrogen. Numerous reports concerning O_2 reduction at chemically modified electrodes have appeared. Most are based on metalloporphyrin or phthalocyanine films with iron or cobalt centres[128-135]. The RRDE has been used extensively to determine whether O_2 is reduced to H_2O_2 by the $2e^-$ pathway or to H_2O by the $4e^-$ pathway. In general, Co centres produce H_2O_2 while Fe tends to produce water. Remarkable electrocatalytic effects have been found with dicobalt face-to-face porphyrins[136-138]. In these studies the yield of H_2O_2 was measured as a function of the separation of redox centres. The reaction pathway was found to be strongly dependent on the distance between redox centres.

Dihydroanthraquinone species have been employed for many years as catalysts for the large scale production of H_2O_2 from oxygen in aqueous solution[139]. Surface molecular forms based on the quinone structure have

also been investigated for this purpose and promising results have been obtained[93,140-142]. Other derivatised electrodes which have been used for O_2 catalysis include modifying agents such as poly(viologen)-poly(sulphonate) complexes[143], prussian blue[144], cobalt(II) acetate[145] and fungal laccase[146].

In accordance with the electrocatalytic theory of polymer films described in section (I.1.2.2.), a variety of kinetic situations have been observed and identified. When the current densities associated with the rate of cross reaction, i_K, and diffusion of electrons through the film, i_E, are large compared to that corresponding to permeation of the substrate, i_S, then substrate is consumed exclusively by a few monolayers of catalyst sites at the polymer/electrolyte interface[93,96,109,111,113,114,119,120,123,124,126,127]. Alternatively, when i_K is small and i_E & i_S are large, all the catalytic sites in the film are utilised[119,147,148]. The majority of cases fall into these two categories and only a handful of other limiting and mixed rate control cases have been reported[118,135].

II.1.5. SEMICONDUCTOR ELECTRODES MODIFIED BY REDOX POLYMER FILMS

Since the photooxidation of water at TiO_2 semiconductor electrodes was demonstrated[149], there has been intense interest in developing semiconductor based PEC cells for solar energy conversion. However, large band gap semiconductors, such as TiO_2 and SnO_2, capture only a small section of the solar spectrum. Narrow band gap materials, such as Si, Ge and GaAs, are of more interest for practical solar energy conversion but undergo rapid photocorrosion and passivation due to competitive reactions yielding surface oxides. Wrighton and coworkers developed the idea of attaching a redox couple to the semiconductor to relay photogenerated charge away from the

surface. They showed that n-type silicon electrodes coated with various organosilane ferrocene polymers were more resistant to passification [22,150,151]. The ferrocene functions by capturing the photogenerated hole which, in the absence of the polymer film, can oxidise the surface lattice. The oxidised ferrocene molecule subsequently transfers charge to reducing agents in solution.

Another filming technique leading to stabilised narrow band gap n-type semiconductors utilises the electrostatic binding properties of ionic redox polymers. In this instance, viologen based polymer films on n-type Si electrodes have been found to increase electrode stability, as compared to naked Si anodes, for the sustained photooxidation of ferrocyanide ions in solution[152]. There are numerous examples illustrating the suppression of photocorrosion of semiconductors by employing films of electrically conducting polymers but they are not discussed in this section (see Section VI.1.2.)

Narrow band gap p-type semiconductors do not readily undergo oxidative decomposition reactions when majority carriers are prohibited from reaching the surface. However, the kinetics of electron transfer between the conduction band electrons and oxidising agents in solution can be poor. Redox polymer films have been employed to enhance reaction kinetics. The rate of H_2 evolution at p-type silicon photocathodes has been shown to increase when polyviologen films, incorporating Pt and Pd microparticles, are present[29,30,153]. Polyviologen, films in the absence of metal particulates, have unfavourable heterogeneous kinetics for proton reduction. The metal particulates act as catalysts, relaying photogenerated charge to H^+ ions, via the redox polymer film.

II.2. EXPERIMENTAL

II.2.1. CHEMICALS

Dimethyl sulfoxide (DMSO) (BDH, analytical grade) and acetonitrile (ACN) (BDH, analytical grade) were fractionally distilled, dried over activated alumina (type WN-6, Sigma) and stored under N_2 in the presence of molecular sieve 4A. Toluene and isopropyl alcohol (BDH, analytical grade) were used without further purification. Tetraethylammonium perchlorate (TEAP) (Aldrich) was recrystallised twice from distilled water and dried under vacuum for several days. Benzoquinone (BQ) and 9,10 anthraquinone (AQ) (Matheson, Coleman & Bell) were used as received.

II.2.2. FILM PREPARATION

Poly[p-(9,10 anthraquinone-2-carbonyl)styrene]-co-styrene (PAQ) was synthesised by Dr. P. P. M. Hoang according to the following method[154,155]. Polystyrene and 2-anthraquinone carbonyl chloride were allowed to react in dry nitrobenzene, in the presence of aluminum chloride at room temperature for three days.

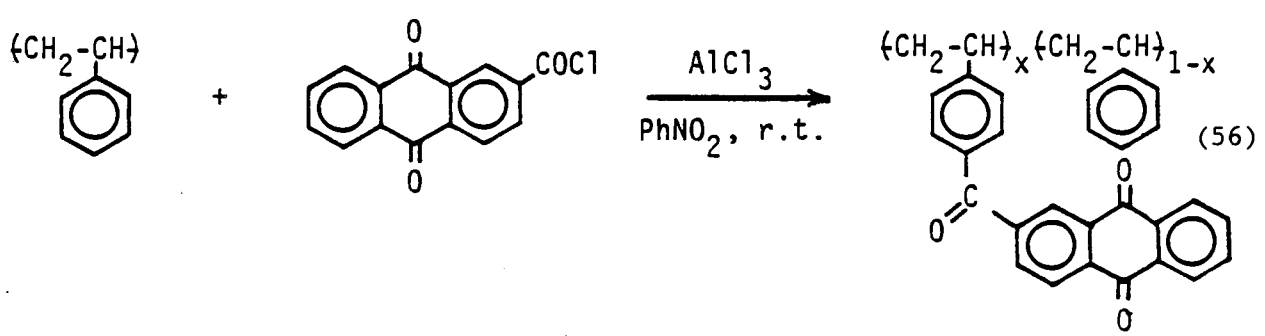

The product was purified by repeated precipitation from methanol and finally freeze dried under vacuum. Copolymer compositions were characterised by ir spectroscopy, elemental analysis and gel permeation chromatography.

The sample utilised in this thesis possessed an anthraquinone content of 28.0 mol%, contained 2170 repeating units in the chain (unless otherwise stated) and its molecular weight was 3.69×10^5 daltons. Polymers of different AQ loading were prepared by varying the concentration ratio of the reactants.

Films of PAQ were prepared by placing a measured volume of polymer solution in toluene (0.05-1.0 w/v%) on the surface of the working electrode and allowing the solvent to slowly evaporate. The electrode was subsequently dried under vacuum for 5 minutes. The film thickness was estimated from the quantity of material applied, assuming a density of 1.0 g/cm^3. Films prepared for study in DMSO were crosslinked by irradiating coated electrodes in isopropyl alcohol with uv light from a 100 W mercury lamp (Engelhard Hanovia). Crosslinked films were finally dried under vacuum for 10 minutes.

II.2.3. ELECTROCHEMISTRY

A three compartment cell, as illustrated in Figure 16, was used for studying PAQ films on platinum. The areas of the Pt electrodes were 0.18 cm^2 (Beckman), for cyclic voltammetric studies, and 0.46 cm^2, for RDE studies. Pt electrodes were polished successively with SiC 600, 3 μm and 1 μm diamond paste, and subsequently sonicated in distilled water for 10 minutes. Between experimental runs, the electrode was polished with 1 μm diamond paste, sonicated in distilled water and dried under vacuum.

A Pt wire counter electrode and a SCE reference electrode were used. The counter and reference electrodes were separated from solution by a salt bridge. All potentials are reported relative to the SCE. Solutions were flushed with argon and an argon atmosphere was maintained during the course of the experiments. For electrocatalytic studies, solutions were maintained at 25 °C and flushed with O_2 for 30 minutes. The concentration of O_2 was taken

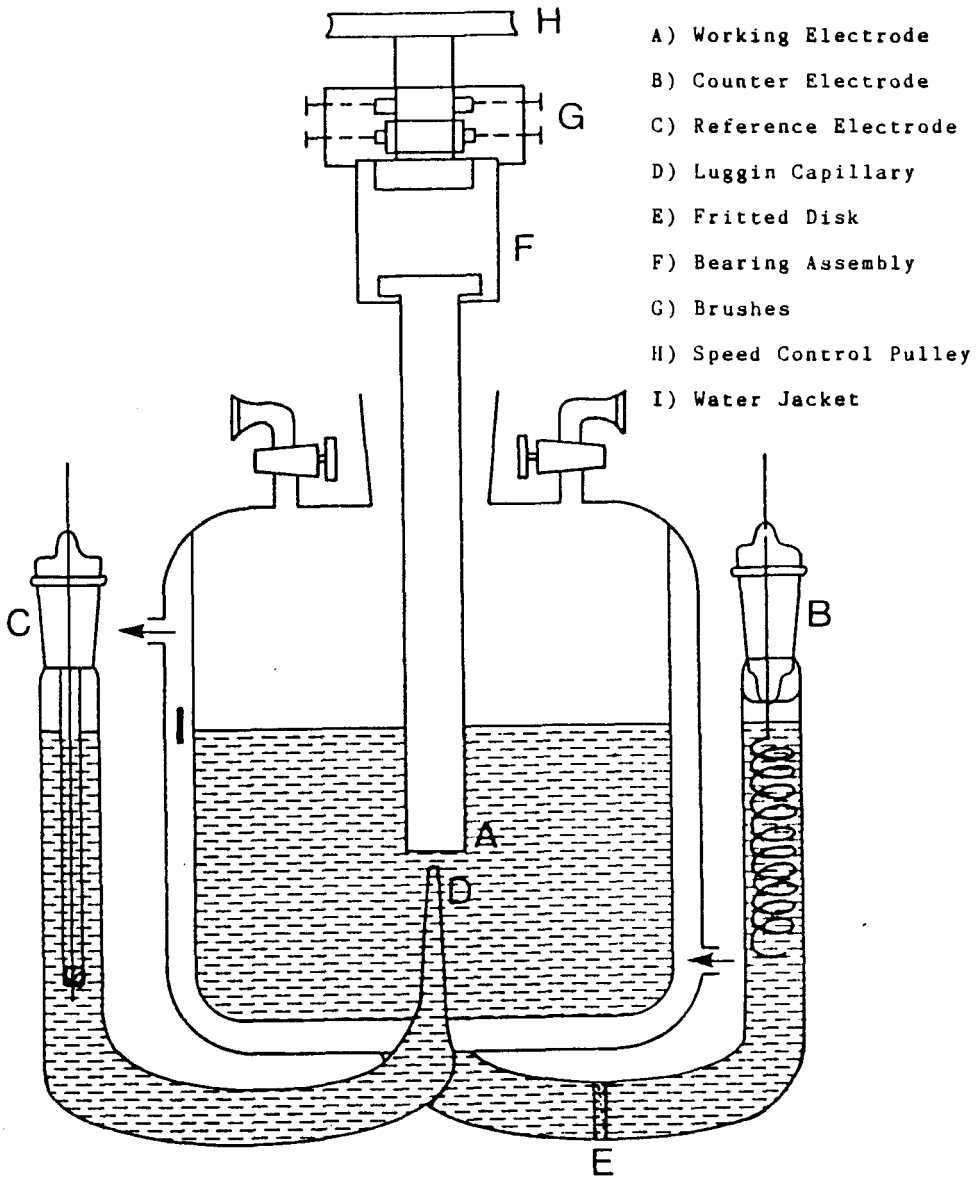

Figure 16. Electrochemical cell.

as 2.1 mM [156].

Voltammetric experiments were performed using a PAR 170 Electrochemistry System or a model RDE 4 bipotentiostat (Pine). Electrode rotation was obtained with an ASR 415 analytical rotator (Pine). An Apple II microcomputer based data aquisition system was employed for chronoamperometric measurements. Gradients of linear plots were obtained from the average of the sum of the maximum and minimum gradients that could be drawn through data points.

Studies of PAQ films on semiconductor materials were performed using silicon crystals (100 face) obtained from Ameteck Inc.. n- and p-type samples were phosphorus and Boron doped respectively ($\approx 10^{15}$ cm^{-3}). Si samples were planar etched (75% v/v conc. HNO_3, 17% conc. CH_3COOH & 8% conc. HF) and mounted on glass with silicone adhesive. Electrodes were etched in 10% HF for 15s prior to use. Ohmic contacts were made with a gallium-indium eutectic. Electrode areas were: n-type ≈ 0.25 cm^2, p-type ≈ 0.12 cm^2.

Films of PAQ on silicon electrodes were prepared as described above and crosslinked with uv light. The film thickness, estimated from the amount of polymer deposited, was ≈500Å.

A three compartment electrochemical cell incorporating a quartz window was used in conjunction with a Pt counter electrode and a SCE reference electrode (Figure 17). The electrolyte was 0.1 M TEAP in DMSO. The effect of solution resistance was minimised by a Luggin capillary placed close to the working electrode. Impedance measurements were performed by superimposing a 2 mV sine wave (HP 239A oscillator) on a d.c. voltage ramp (HP 3310B function generator). In-phase and out-of-phase components were measured with a lock-in amplifier (EG&G, model 128). Voltammetric measurements were performed with a RDE4 potentiostat (Pine Instruments) and monitored on a HP Z046B X-Y recorder. Band gap illumination was provided by a 200 W tungsten lamp (Thorn Lighting). All photoelectrochemical experiments were performed in a light tight box.

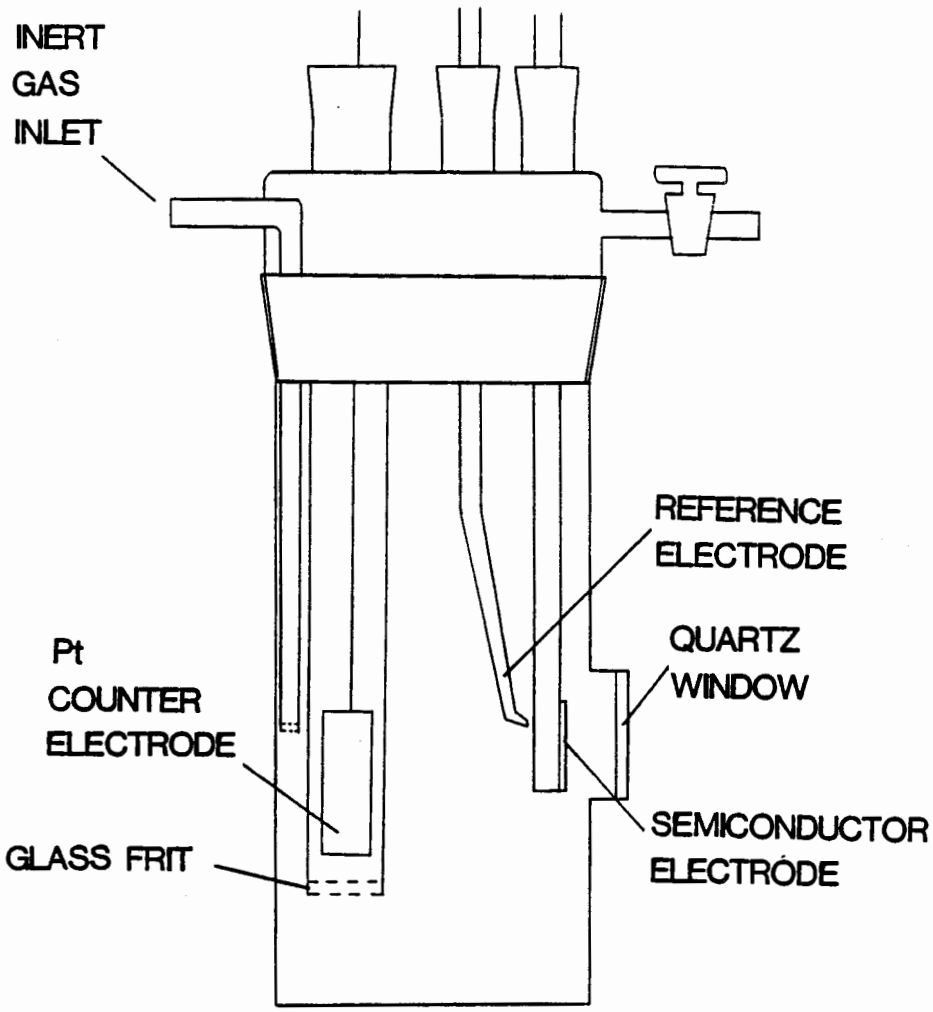

Figure 17. Photoelectrochemical cell.

II.3. RESULTS AND DISCUSSION

II.3.1. VOLTAMMETRY AND CHARGE TRANSPORT

The voltammetry of anthraquinone in aqueous and non-aqueous solutions has been well documented[157]. Two reduction peaks are usually observed in non-aqueous electrolytes corresponding to the formation of $AQ^{\cdot}$ and $AQ^{2\cdot}$ ions. On the reverse scan two oxidative peaks are observed corresponding to the reoxidation of these species. In aqueous solution a single reduction peak is observed due to the formation of the dihydroanthraquinone species, AQH_2. This species is reoxidised during the reverse cycle.

The voltammetry of PAQ films in various solvents is shown in Figure 18. Electroactivity of PAQ films is observed in CH_3CN and DMSO, whereas the film is virtually electroinactive in aqueous solution. In CH_3CN, the reduction of the neutral film produces a sharp cathodic spike (Figure 18B). The peak potential of this spike shifts with scan rate and the peak current does not vary linearly with scan rate. In contrast, the second reduction peak, and the two oxidation peaks obtained on the reverse scan, varied little with scan rate and the peak currents were proportional to scan rate. In DMSO, the PAQ film produced two reductive peaks and two oxidative peaks which decreased in magnitude upon further cycling due to desorption of the polymer (Figure 18C). PAQ films in DMSO were stabilised by the crosslinking of polymer chains upon exposure to uv irradiation[156] (Figure 18D).

The variations in electrochemical response of PAQ films in different solvents can be attributed to a change in counter ion permeability arising from changes in chain conformation. The polystyrene backbone in PAQ induces hydrophobicity. In aqueous solution, PAQ films are sufficiently compact so as to inhibit permeation of electrolyte. In addition, the polymer chains may

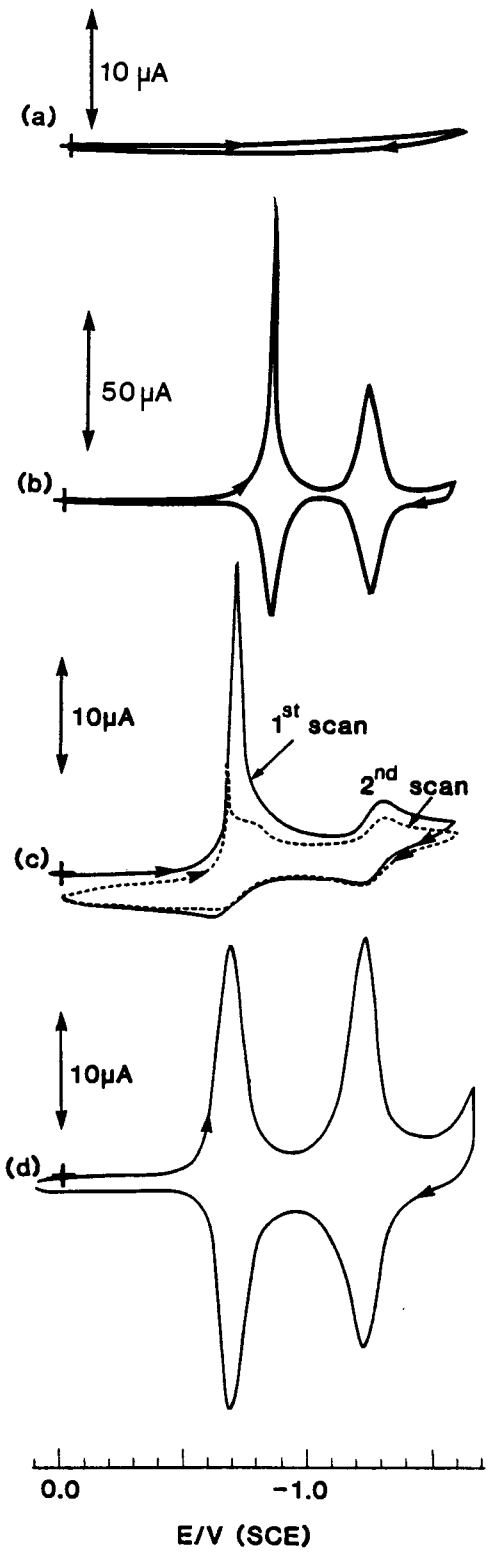

Figure 18. Cyclic voltammetry of PAQ films in various solvents: a) 0.1 M TEAP/H_2O, b) 0.1 M TEAP/CH_3CN, c) 0.1 M TEAP/DMSO, d) 0.1 M TEAP/DMSO after crosslinking. Film thickness, 100 Å; scan rate, 50 mV/s; electrode area, 0.18 cm^2.

lack the flexibility required for site-site collisions. These properties render PAQ films electroinactive in aqueous solution.

The electrochemical behaviour of PAQ films in CH_3CN may be explained by swelling/deswelling processes occurring during the redox cycle. A neutral film is poorly swollen in this solvent and electrolyte permeability is low. The lack of electrolyte at the electrode/polymer interface results in poor electron transfer kinetics. Thus, the peak current is not proportional to scan rate and the peak potential varies significantly with scan rate. In the reduced or charged state the polymer matrix swells due to repulsive interactions. A more open structure allows facile penetration of electrolyte. Consequently, the second reduction peak and the two reoxidation processes follow ideal behaviour. After a complete cycle the film is again neutral and hence, voltammograms obtained for successive scans are similar to the initial voltammogram.

In DMSO, the polymer swells to a greater extent, with respect to H_2O and CH_3CN. Solvation occurs so readily that polymer chains are desorbed when charged. Sufficient insolubilisation of the polymer is obtained by crosslinking with uv irradiation. Crosslinked films still show a large degree of swelling, allowing easy access for counter ions and associated solvent.

The effect of film thickness on the electrochemical response of PAQ films in 0.1 M TEAP/DMSO is summarised in Table 1. The data pertains to the first reduction peak. The typical voltammograms for films of three different thicknesses are illustrated on Figure 19. For a 100 Å film, the cathodic and anodic peaks are symmetrical as theoretically predicted for an ideal reversible adsorbed reactant. No diffusional tailing is observed at slow scan rates and the peak width at half height is 98 mV, in close agreement with the theoretical value, 90.6 mV. The surface coverage of electroactive material is 78% of the quantity of AQ units applied, suggesting that some

Table 1. Voltammetric characteristics of PAQ films

Thickness (10^3 Å)	E (mV)	δ_p (mV)	i_{pc} (mA/cm^2)	Γ_{obs} (nmol/cm^2)	$\Gamma_{obs}/\Gamma_{tot}$ (%)
0.1	0	98	0.045	1.3	79.0
0.5	0	110	0.067	1.9	22.6
1.0	16	112	0.102	2.7	16.4
5.0	16	112	0.400	9.7	11.8
10.0	16	112	0.611	14.9	9.0
15.0	20	112	0.866	21.0	8.3
20.0	25	116	0.966	23.4	7.1
30.0	32	112	1.022	24.8	5.0

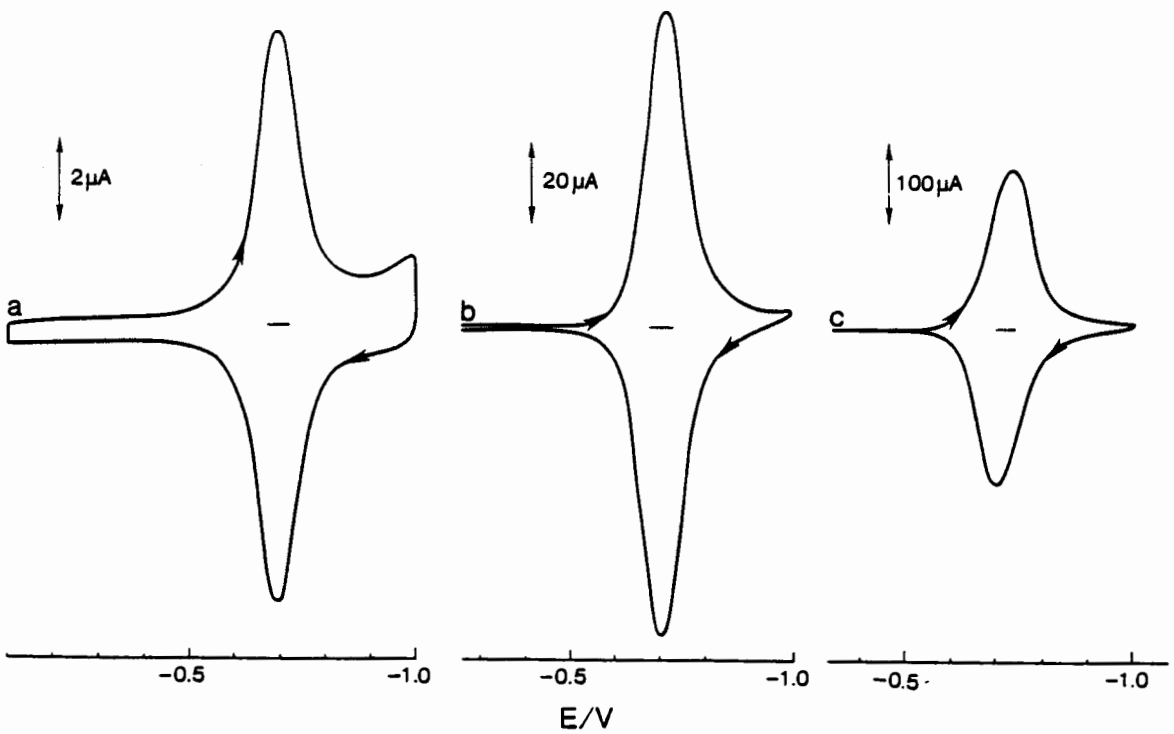

Figure 19. Cyclic voltammetry of PAQ films of various thickness: a) 100 Å, b) $5x10^3$ Å, c) $3x10^4$. Electrolyte, 0.1 M TEAP/DMSO; scan rate, 50 mV/s; electrode area, 0.18 cm^2.

electroactive centres have been destroyed by the cross linking process. A several hundred fold increase in film thickness does not produce major deviations of curve shape. However, the ratio $\Gamma_{observed}$ /$\Gamma_{applied}$ decreased sharply with increasing thickness.

The effect of scan rate on the peak current for films of various thickness is shown in Figure 20. For films <1000 Å thick, a linear relationship is observed whereas films of thickness >1000 Å deviate from linearity.

Crosslinked PAQ films in DMSO are extremely stable. 50 potential cycles between 0.0 and -1.6 V (SCE) results in less than a 1% loss in electrochemical activity. The electrode could be maintained in the test solution for several days without loss of activity.

Chronoamperometry was employed to determine the parameter D_E. The technique is described in Section I.1.1.2.. The electrode potential was stepped from -0.2 to -0.9 V and the time dependent current decay observed. The i-t decay response and the corresponding Cottrell plot for a 1000 Å film are shown in Figure 21. The current initially decreased linearly with $t^{-1/2}$ indicative of an electron propagation mechanism which follows semi-infinite diffusion laws. At longer times the depletion layer reaches the film/electrolyte interface and the Cottrell slope deviates from linearity. The electron diffusion coefficient, D_E, was evaluated as $(5.1 \pm 0.8)\times10^{-11}$ cm^2/s from the slope of the Cottrell plot. The slope and corresponding errors of uncertainty were estimated from the maximum and minimum gradients that could be drawn through the data points. The concentration of AQ groups in the film may be smaller than estimated due to crosslinking and swelling of the polymer. In effect, D_E may be slightly larger than calculated. The value D_E for the reoxidation process was obtained using a potential step of -0.9 to -0.2 V. For this oxidation process D_E is $(1.0 \pm 0.1)\times10^{-10}$ cm^2/s, the larger value indicating a more facile electron transfer process.

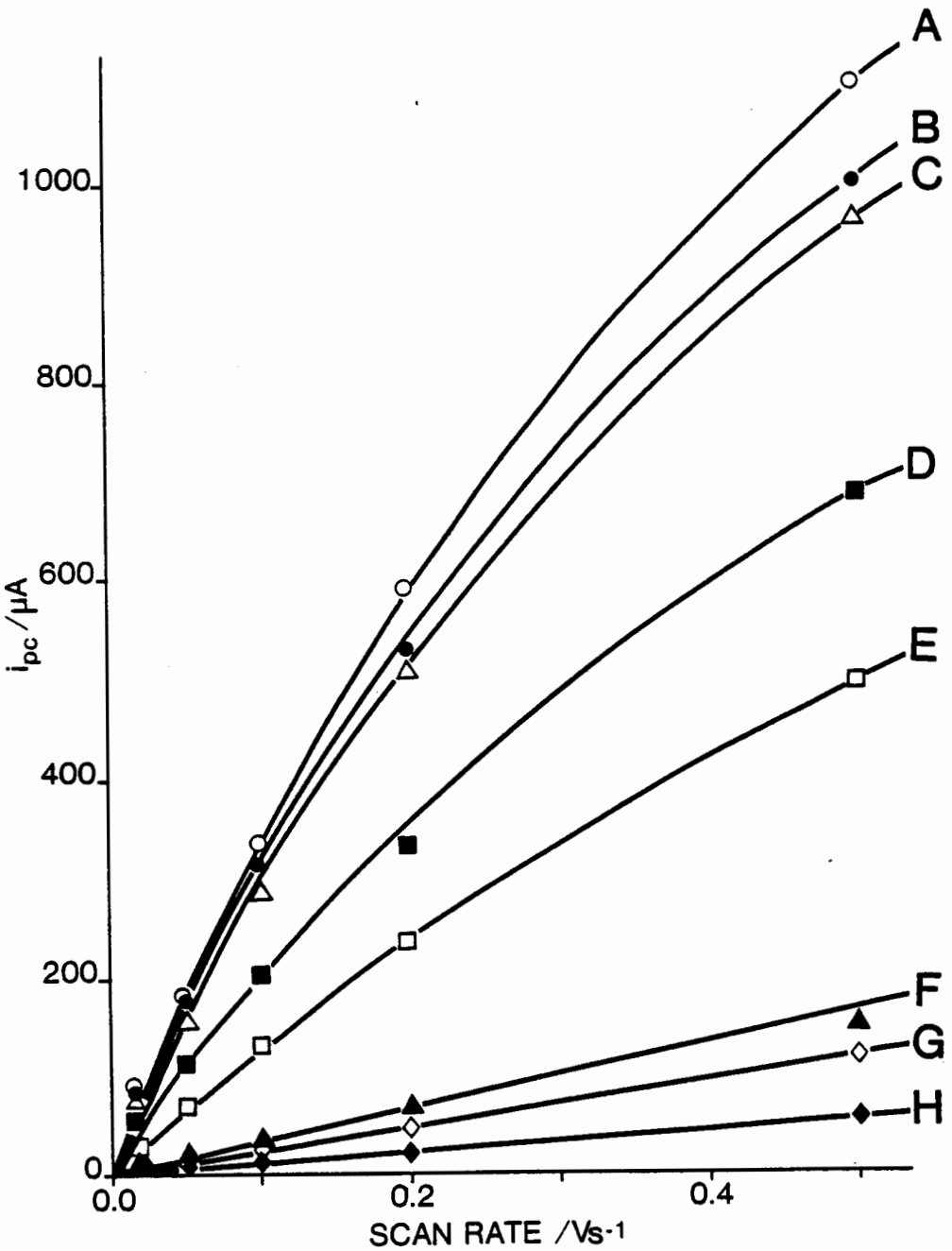

Figure 20. Effect of scan rate on the peak current for films of various thickness (Å): a) $3x10^4$, b) $2x10^4$, c) $1.5x10^4$, d) $1x10^4$, e) $5x10^3$, f) $1x10^3$, g) $5x10^2$, h) $1x10^2$. Electrolyte, 0.1 M TEAP/DMSO; scan rate, 50 mV/s; electrode area, 0.18 cm^2.

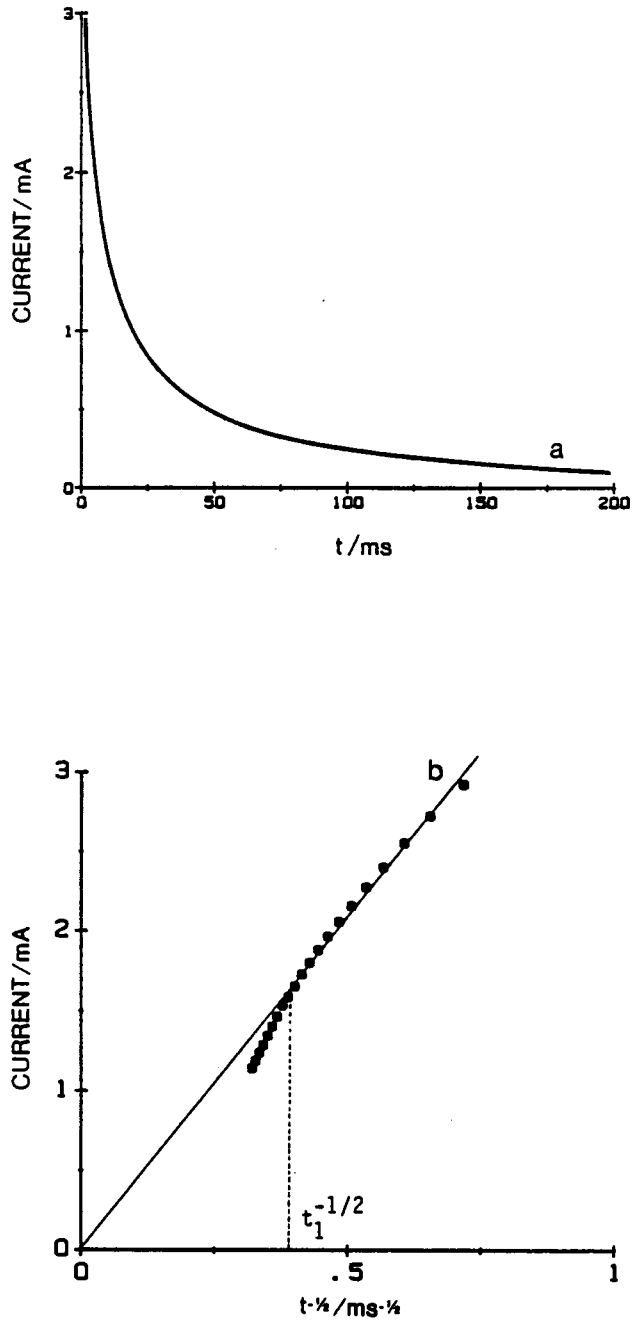

Figure 21. The i-t decay response and the corresponding Cottrell plot for a 1000 Å film. Potential step, -0.2 -> -0.9 V; electrolyte, 0.1 M TEAP/DMSO; electrode area, 0.18 cm^2.

Charge transport coefficients reported for a number of polymer films vary over several orders of magnitude (10^{-7}-10^{-13} cm^2/s). Smaller values are observed when the active group is attached covalently to the polymer backbone. This is consistent with the value obtained for PAQ films.

The value of D_E can be used to calculate the thickness of the diffusion layer, δ, at time t, using the following equation[57].

$$\delta = (2D_E t)^{1/2} \qquad (57)$$

When t_1 is the time at which the i-$t^{1/2}$ plot deviates from linearity, δ corresponds to the thickness, beyond which, reducible AQ groups are no longer uniformily distributed in the film. From Figure 21, t_1 was estimated as 6.5 ms, from which, δ was calculated to be 86 Å.

The effect of the volume concentration of electroactive sites and the effect of counter ion size on the magnitude of D_E was investigated using PAQ films of higher AQ loadings and cations of differing size. The data are summarised in Table 2.

Table 2. Effect of cation size and AQ loading on D_E

AQ%	Supporting Electrolyte 0.1 M/DMSO	$D_E \times 10^{11}$ cm^2/s
19.5	TEAP	6.8 ± 2.1
28.0	TEAP	5.1 ± 0.8
28.0	$KClO_4$	3.6 ± 0.7
47.4	TEAP	5.4 ± 0.5

A charge transport process limited by the permeation of counter ions would be greatly affected by a change of cation size: a decrease in cation

size producing a significant increase in D_E. In changing the cation from a large $(C_2H_6)_4N^+$ ion to a relatively small K^+ ion, D_E is virtually unchanged. One can conclude that the rate of charge propagation is not counter ion limited.

In the absence of a counter ion limiting process, the effect of the volume concentration of electroactive sites can be studied. D_E is essentially insensitive to AQ content indicating that a closer spacing of redox groups does not facilitate electron propagation in the film. The interpretation however, may be an oversimplification since a number of negative effects might be imposed when the polymer composition is changed. While an increase in AQ concentration may facilitate the number of site-site collisions, the former reduces polymer solubility and thus, decreases chain flexibility. In addition, uv irradiation may induce greater crosslinking at higher AQ loadings, again decreasing polymer chain mobility. It has been suggested by Murray that,for these studies, changes in concentration should be performed on polymers in which the active site is diluted by the process of replacing them with inactive sites of comparable size, polarity and solubility[103]. In such cases, one is certain that changes in distance between active groups, and not changes in chain conformation, are being studied.

PAQ films in DMSO exhibit almost ideal voltammetric behaviour and are essentially in equilibrium with the applied potential in the time scale of these experiments. However, the percentage of electroactive groups falls dramatically with increasing film thickness. For a 1000 Å film, only 16.4% of the total number of AQ units are electroactive. Chronoamperometric results for a 1000 Å film indicate that only the first 100 Å or so contain homogeneously dispersed reducible AQ groups. It is suggested therefore, that for thicker films, the polymer chains are oriented so that AQ groups within

the first 100 Å are all reducible, beyond this, reducible AQ groups are found only in preferred channels. The proposed structure is shown in Figure 22. The model is consistent with the observation that films of larger thickness yield voltammetric peaks which are not proportional to the total AQ loading, while the voltammetric waveshape indicates Nernstian behaviour.

II.3.2. ELECTROCATALYSIS OF O_2

The cyclic voltammetry of oxygen dissolved in 0.1 M TEAP/ DMSO is shown in Figure 23. The multiple voltammograms correspond to increasing scan rates. At naked Pt, O_2 is reduced by a one electron transfer mechanism to the superoxide ion, $O_2^{\cdot}$. The peak separation for electrochemical redox reactions of dissolved species is ideally 59/n mV, this is observed for O_2 reduction at slow scan rates. When scan rate is increased peak separations become larger than 59 mV indicating a relatively slow rate of electron transfer between Pt and O_2.

With an electrode coated with a PAQ film, the positions of the anodic and cathodic peaks for the O_2 reaction are insensitive to scan rate. The PAQ film in the absence of O_2, produced an insignificant current in this range of potential. The voltammograms are explained by considering a mediated electron transfer process. The constant peak separation with varying scan rate is indicative of a facile electron transfer process. One can conclude that the combined rate of electron transfer between the Pt electrode and PAQ, and between $P(AQ^{\cdot})$ and O_2, is much faster than that between Pt and O_2. The mechanism for the mediated reduction of O_2 is given below.

$$PAQ \xrightarrow{e^-} P(AQ^{\cdot}) \qquad (58)$$

$$P(AQ^{\cdot}) + O_2 \longrightarrow PAQ + O_2^{\cdot} \qquad (59)$$

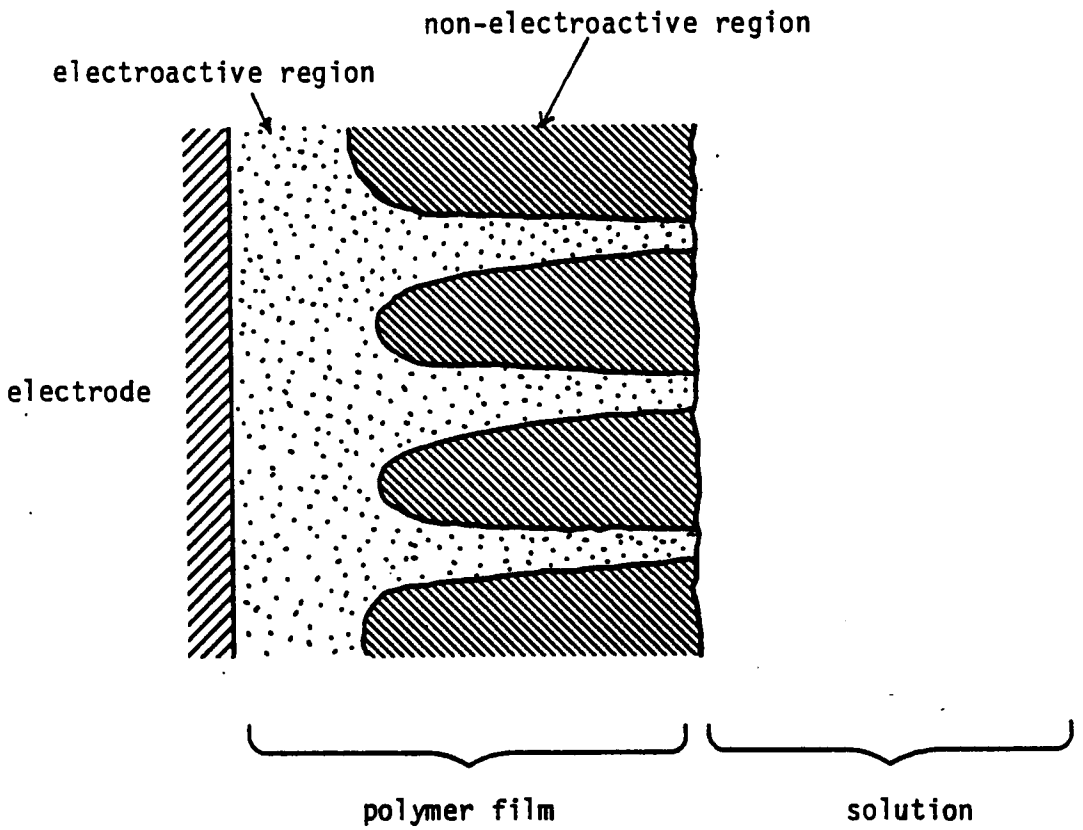

Figure 22. Proposed model of structure for PAQ films (d>100 Å) in DMSO.

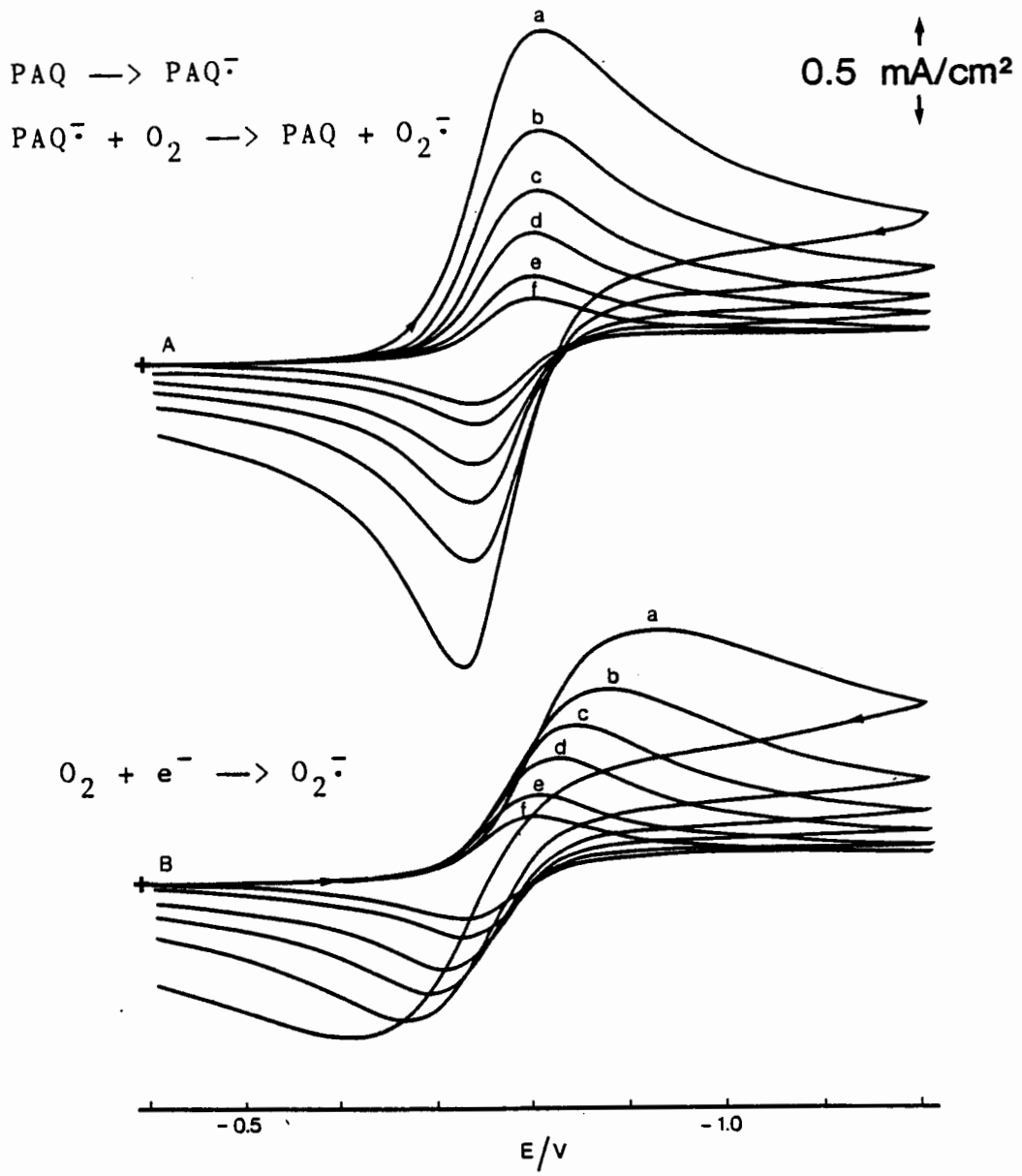

Figure 23. Voltammetry of a saturated O_2 solution at various scan rates: A) PAQ Coated Pt (100 Å), B) Bare Pt. Scan rate (mV/s): a) 500 b) 200 c) 100 d) 50 e) 20 f) 10. Electrolyte, 0.1 M TEAP/DMSO.

The polymer film caused a sharpening of RDE voltammograms for O_2 reduction. As rotation rate was increased, $E_{1/2}$ values shifted more negatively for naked electrodes, but remained constant for coated electrodes. Plots of $[E-E_{1/2}]$ vs. $\log[(i_l-i)/i]$ are linear for both coated and uncoated electrodes (Figure 24). However, the slopes of the plots are significantly different, 63 ±3 mV and 128 ±15 mV respectively. The slope for an Nernstian system is 59 mV, indicating that the former process is more reversible.

The electrocatalytic reduction was studied in detail with the RDE using films of approximate thickness 10, 50, 100 and 1000 Å. The RDE voltammogram for O_2 reduction at a 10 Å film did not show as steep a rise found for thicker films. Two limiting currents are apparent, the second of which is identical to that of O_2 reduction at bare Pt. These are shown in Figure 25 in conjunction with the voltammograms for a 50 Å PAQ film and a bare Pt electrode.

The Levich and inverse-Levich plots for 10 Å films are shown in Figures 26 and 27 respectively. From the latter i_1 was determined as 15.62 mA/cm^2. RDE voltammograms for films of 50, 100 and 1000 Å indicate that two current plateau regions exist. However, the first plateau was indistinct and it was not possible to derive meaningful experimental results for these films.

The current density associated with diffusion of charge through the film may be determined for any thickness of film since $i_E = nFT_pD_E/d^2$. D_E has been previously evaluated as 5.1×10^{-11} cm^2/s from chronoamperometric experiments.

The difference between the limiting currents in the polymer film and the Levich current is relatively small. A precise determination of i_s due to substrate diffusion through the film cannot be made directly. In order to determine i_s, and to investigate the possibility of pinholes being present in the film, the reduction of benzoquinone (BQ) to its radical anion was

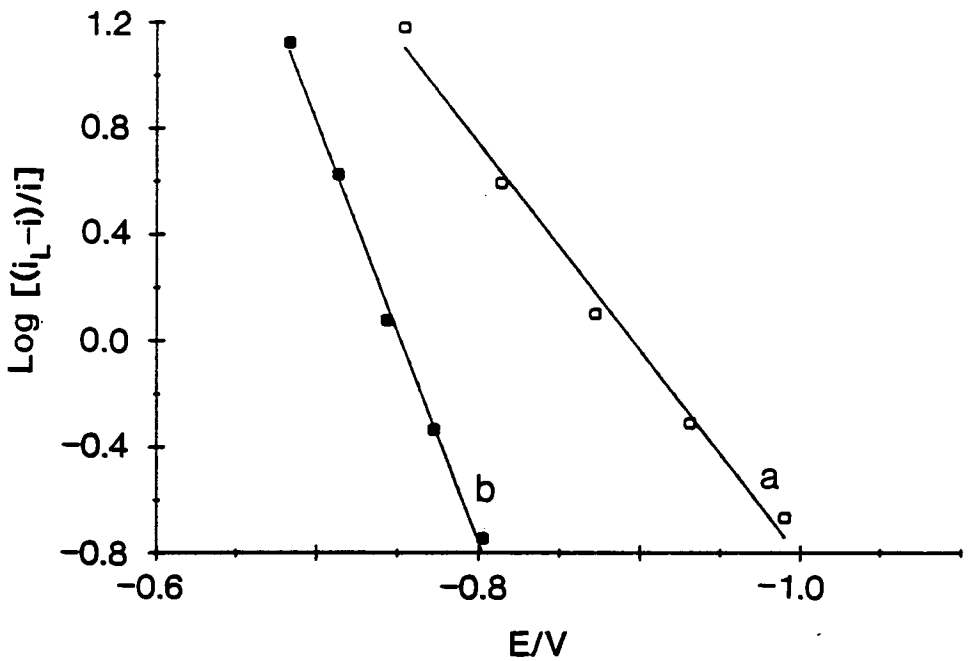

Figure 24. Nernstian plots for the reduction of O_2 at a) bare Pt, b) PAQ Coated Pt (100 Å). Electrolyte, 0.1 M TEAP/DMSO; scan rate, 50 mV/s; rotation rate, 1500 rpm.

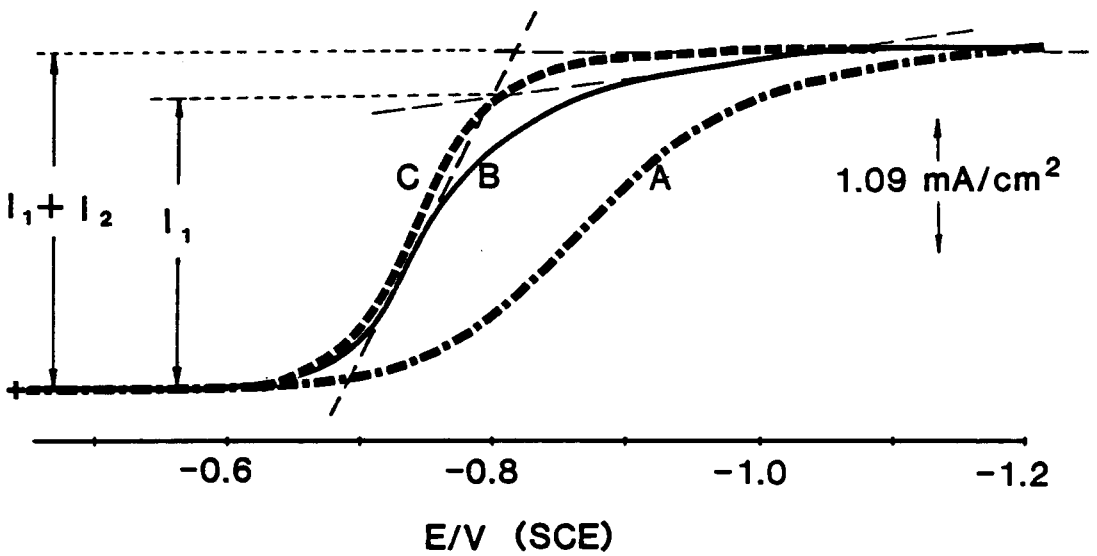

Figure 25. RDE voltammetry of saturated O_2 solution: a) Bare Pt, b) PAQ film (10 Å), c) PAQ film (50 Å). Electrolyte, 0.1 M TEAP/DMSO; scan rate, 50 mV/s; rotation rate, 2000 rpm.

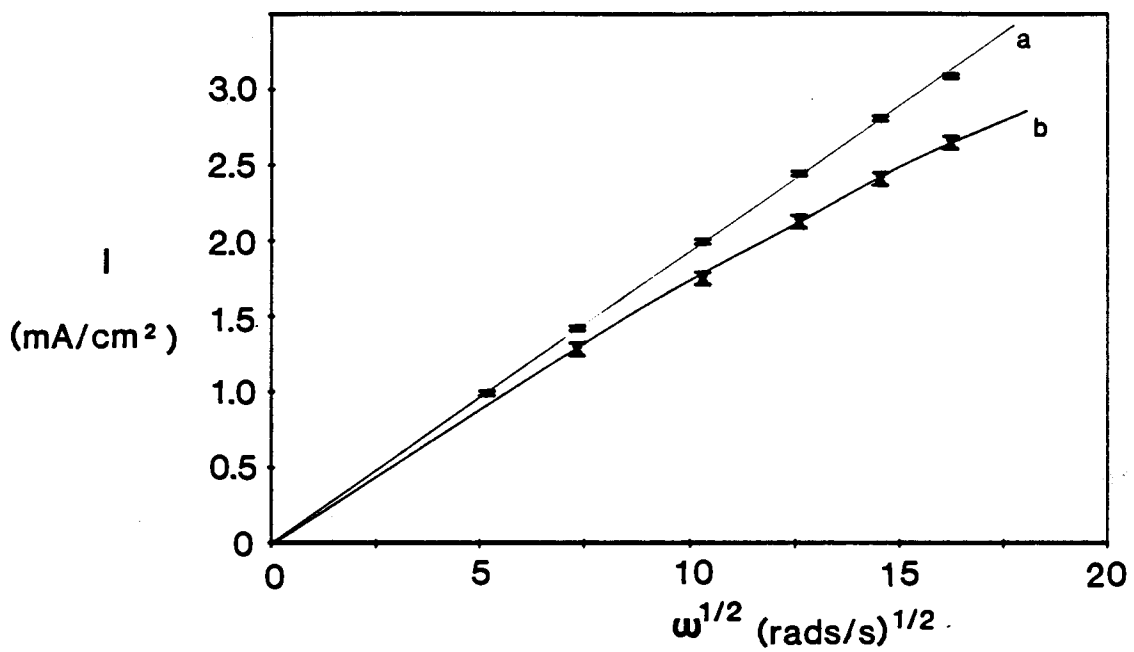

Figure 26. Levich plots for the reduction of O_2: a) Bare Pt, b) PAQ film (10 Å). Electrolyte, 0.1 M TEAP/DMSO; scan rate, 50 mV/s.

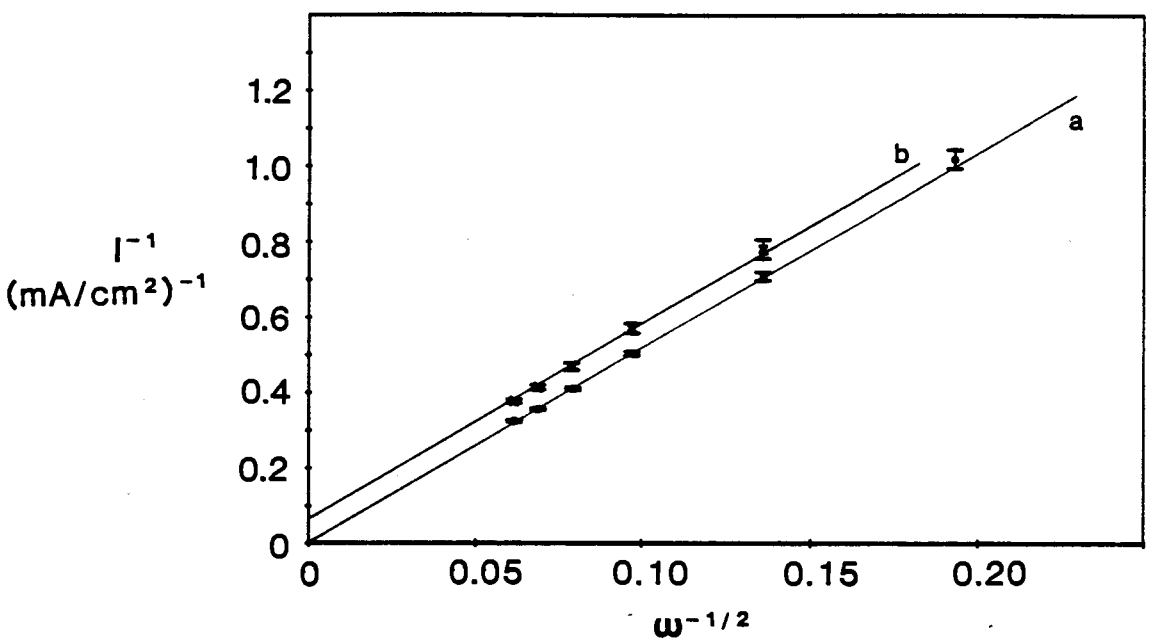

Figure 27. Inverse-Levich plots for the reduction of O_2: a) Bare Pt, b) PAQ film (10 Å). Electrolyte, 0.1 M TEAP/DMSO; scan rate, 50 mV/s.

examined at PAQ films. The reduction of BQ occurs 300 mV more positive than the formal potential of PAQ and is therefore not mediated by the polymer film.

The voltammetry of BQ in DMSO at bare and PAQ coated electrodes is shown in Figure 28. The presence of the PAQ film did not significantly affect the electrode reaction. The reduction of BQ occurred at the same potentials with similar current magnitudes as observed at the naked electrode. Similar results were obtained for films of much greater thickness. The porous nature of PAQ films in this solvent allows relatively easy access for BQ to reach the electrode and undergo reaction. When the same electrode is transfered into an aqueous solution of BQ, the reduction of the latter is greatly impeded (Figure 29). The substantial decrease in electroactivity implies that BQ cannot reach the electrode surface and, more important, it is evidence that PAQ films do not possess gross pinholes. The presence of large pinholes cannot be simply accounted for in the electrocatalytic theory without detailed computation.

The magnitude of the cathodic current due to reduction of BQ at stationary PAQ coated electrodes in DMSO is similar to that obtained at bare electrodes. However, at rotated electrodes the cathodic current can differ significantly due to the finite rate of diffusion of BQ through the film, $D_{BQ\text{-}film}$. This phenomenon allows determination of $D_{BQ\text{-}film}$ and subsequent evaluation of i_s. The Levich and inverse-Levich plots for BQ reduction at 1000 Å PAQ electrodes in 0.1 M TEAP/DMSO are shown in Figures 30 and 31. From the intercept of the inverse-Levich plot, i_s = 2.06 mA/cm^2 and $D_{BQ\text{-}film}$ = 1.06x10^{-7} cm^2/s. At equal concentrations, the ratio of the inverse Levich slopes for O_2 reduction and BQ reduction on bare Pt is equivalent to the ratio D_{O2}/D_{BQ}. This ratio was found experimentally to be 25.52. The D_{O2} in solution was taken as 3.23x10^{-5} cm^2/s [156] and thus, D_{BQ} in solution was

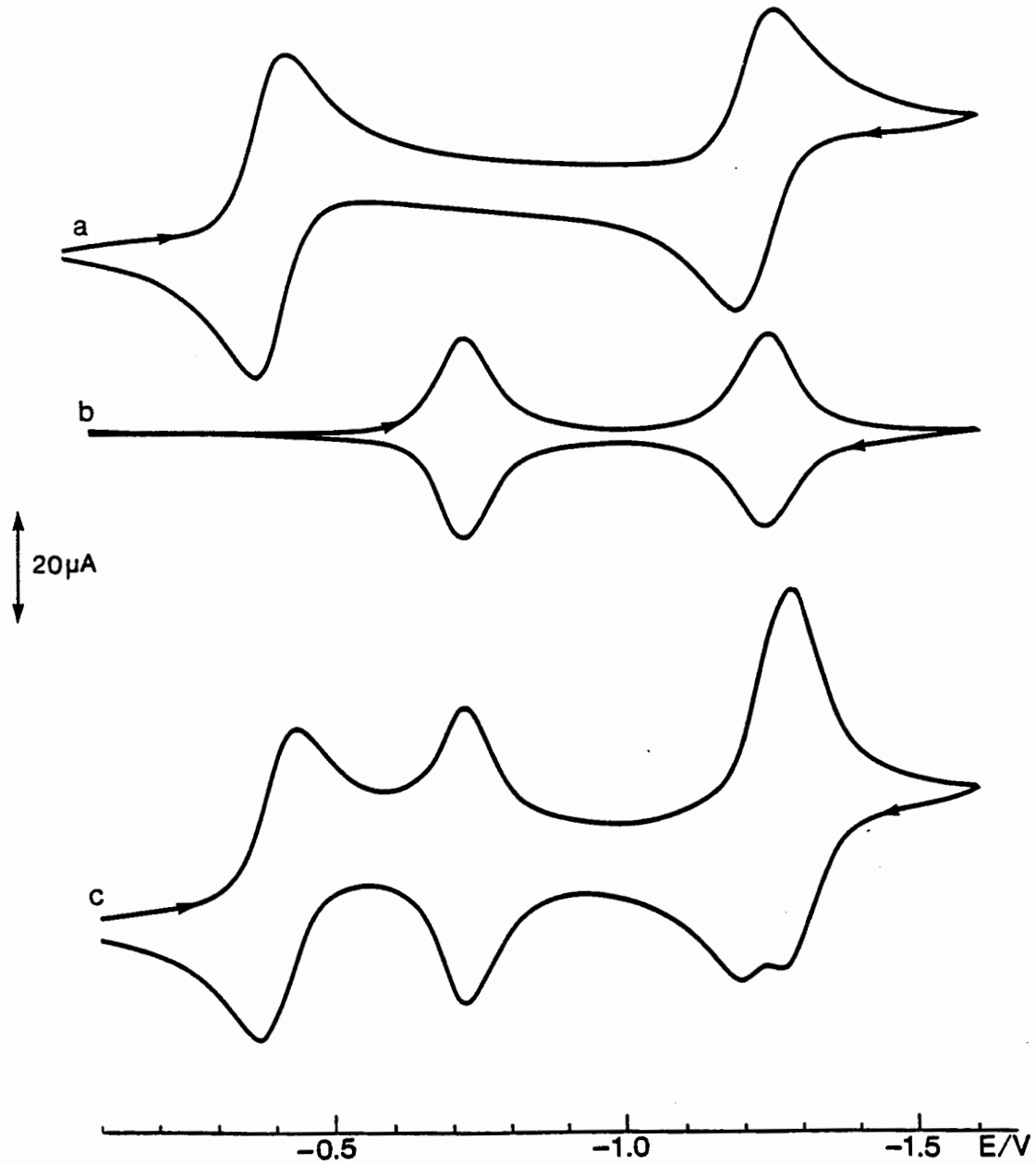

Figure 28. Voltammetry of BQ (1 mM) in 0.1 M TEAP/DMSO: a) Bare Pt, b) PAQ film (100 Å) in the absence of BQ, c) as (a) but with BQ present. Scan rate, 50 mV/s; electrode area, 0.18 cm^2.

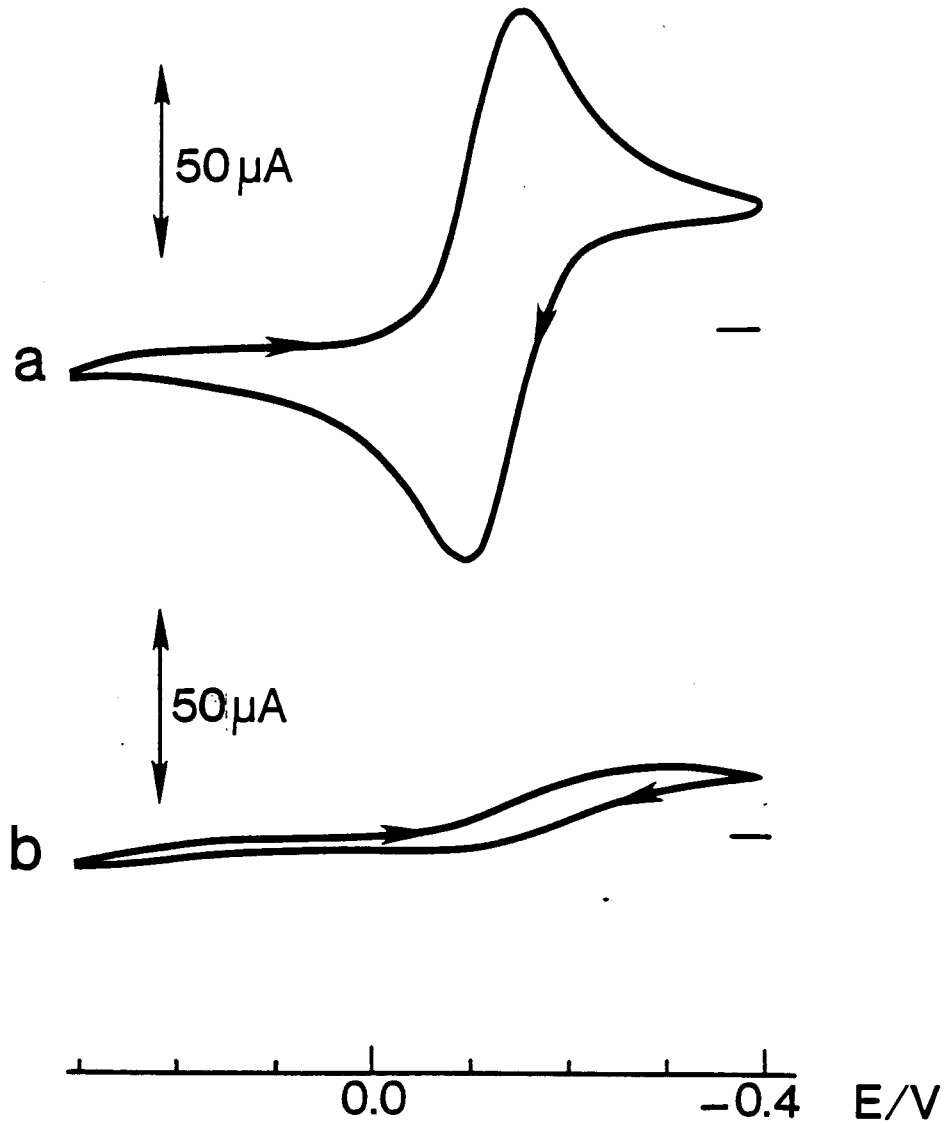

Figure 29. Voltammetry of BQ (1 mM) in 0.1 M TEAP/H_2O: a) Bare Pt, b) PAQ film (100 Å). Scan rate, 50 mV/s; electrode area, 0.18 cm^2.

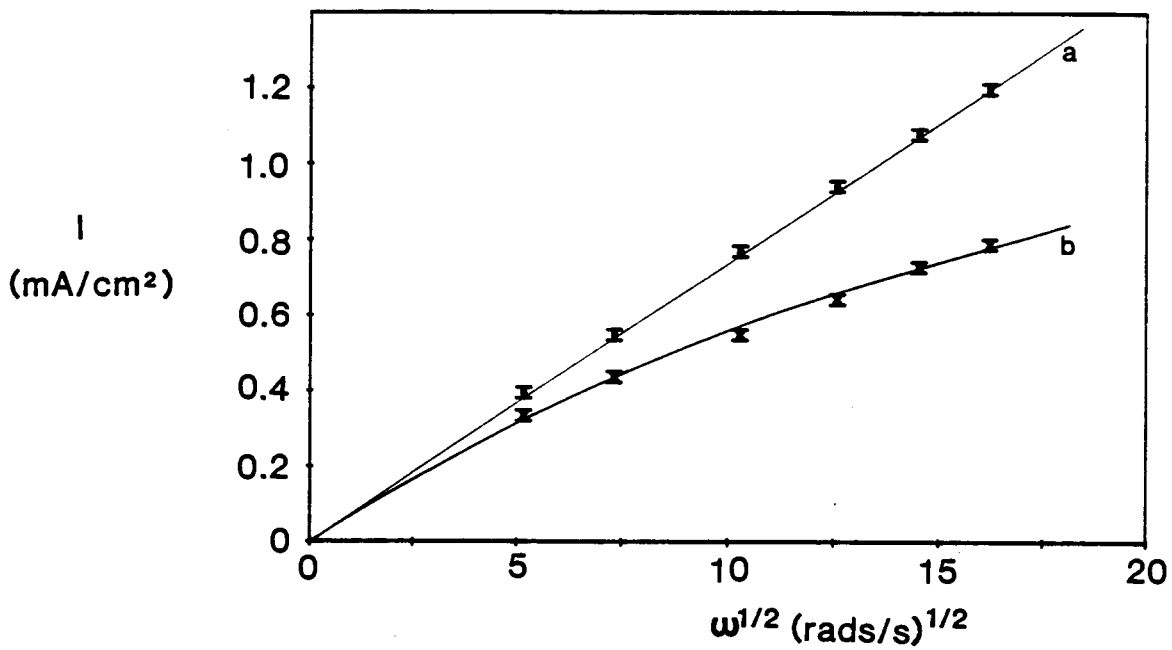

Figure 30. Levich plots for the reduction of BQ (2.1 mM): a) Bare Pt, b) PAQ film (1000 Å). Electrolyte, 0.1 M TEAP/DMSO; scan rate, 50 mV/s.

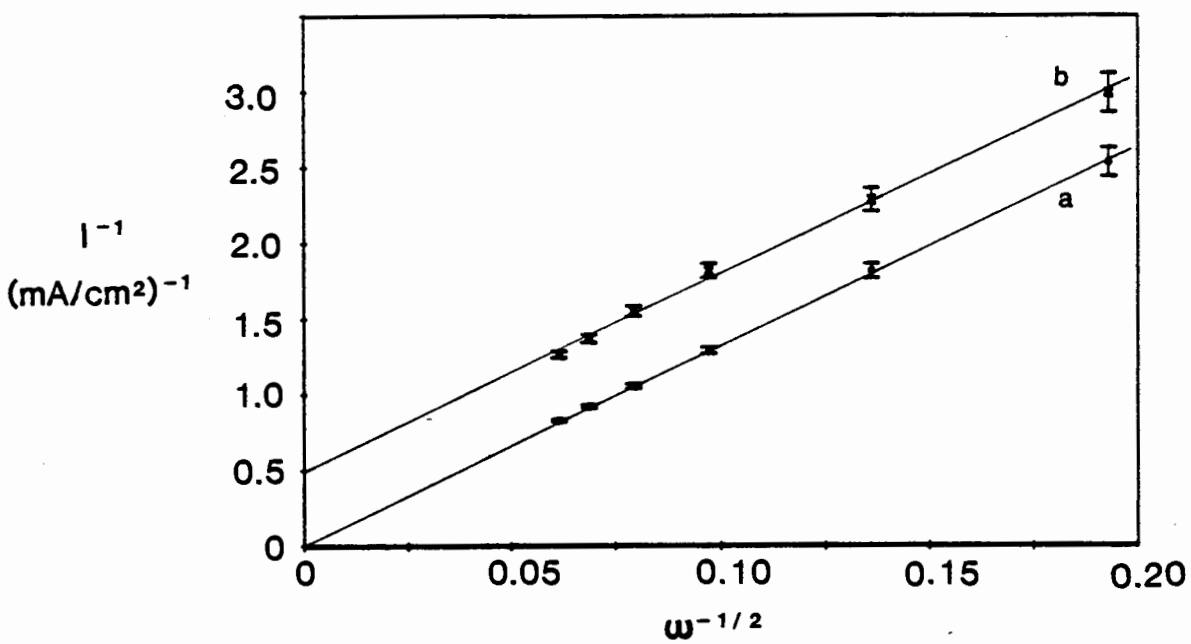

Figure 31. Inverse-Levich plots for the reduction of BQ (2.1 mM): a) Bare Pt, b) PAQ film (1000 Å). Electrolyte, 0.1 M TEAP/DMSO; scan rate, 50 mV/s.

1.26×10^{-6} cm^2/s. This compares with 9.65×10^{-6} cm^2/s for BQ in DMF[158], a solvent with a lower kinematic viscosity.

We may assume that D_{BQ}/D_{O2} changes proportionately in going from bulk electrolyte to film. This assumption is justified because the polymer's permeability is adequate to rule out size exclusion effects. Charge effects, caused by the electrostatic interaction between polymer and substrate are absent due to the neutral state of BQ and O_2. Substituting the appropriate values into $D_{O2\text{-}film}/D_{O2} = D_{BQ\text{-}film}/D_{BQ}$ gives $D_{O2\text{-}film} = 2.59 \times 10^{-6}$ cm^2/s from which, values of i_s were determined for various film thicknesses. The value of $D_{O2\text{-}film}$ may be even greater than calculated since $D_{BQ\text{-}film}$ is determined by permeation through neutral film whereas O_2 diffuses through reduced and swollen polymer. However, the kinetic designations are not affected by such small changes in diffusion coefficient. The only situation where changes in $D_{O2\text{-}film}$ could affect the kinetic process is for films of 1000 Å. In this case, 84% of the polymer remains in the neutral state at maximum reduction and thus, $D_{O2\text{-}film}$, as calculated from the permeability of BQ through the neutral film, is a reasonable estimation.

An estimate of i_K was made using Savéant's model[60]. It can be seen from Table 3 that i_E and i_S for a 10 Å PAQ film had values of 73.3 and 5250 mA/cm^2 respectively. Since $i_S \gg i_E \gg i_A$, the possible mechanisms that might apply are those labelled "R", "R+E" and "ER" using the terminology of the Savéant treatment. The "R" case represents a uniform concentration of $AQ^{\cdot}$ groups throughout the film. This kinetic situation is often observed for thin films or monolayers. In the "R+E" case there is a continuous decline in $[AQ^{\cdot}]$ but the concentration of substrate, O_2, is uniform throughout the film. This situation is found experimentally in thicker films where diffusion of charge is slow compared to the rate of cross reaction and substrate diffusion in the film. The (ER) case often occurs for very thick films or films with very low

Table 3 . Variations of I_E, i_S and i_K with film thickness

Γ_{Appl}	a Γ_{OBS}	b d	c i_A	d i_E	f i_S	h i_K	j Kinetic Situation
$\frac{nmol}{cm^2}$	$\frac{nmol}{cm^2}$	(Å)	$\frac{mA}{cm^2}$	$\frac{mA}{cm^2}$	$\frac{mA}{cm^2}$	$\frac{mA}{cm^2}$	
0.165	0.15	10	3.08	73.3	5250	15.6[i]	R
0.825	0.64	50	3.08	14.3	1050	67.2	R+E
1.65	1.3	100	3.08	7.2	525	136.4	ER
16.5	2.7	1000	3.08	4.9[e]	52.5[g]	283.4	ER/ER+S

a) Obtained from coulometric assay.
b) Calculated from data in Column II.
c) Levich current for maximum rotation rate employed (2500 rpm)
d) Calculated from equation 23.
e) Calculated using d = 164 Å.
f) Calculated from equation 24.
g) Calculated using d = 1000 Å.
h) Calculated from equation 25.
i) From Figure 27.
j) From references 58 & 60.

charge diffusion coefficients. The electroactive groups are confined to a thin layer very near the electrode, but the substrate concentration is still maintained at a constant value through the film.

Figure 27 shows a linear plot of reciprocal current vs. $\omega^{-1/2}$. This rules out "R+E" and "ER" since these models give inherently non-linear inverse-Levich plots. Thus, the kinetic situation applying to the reduction of O_2 at a 10 Å PAQ coated electrode can be classified as "R". This is not surprising since $\Gamma_{OBS} = 1.49 \times 10^{-10}$ mol/cm^2: this is close to monolayer coverage. The reciprocal current $1/i_1$ for such a system is $1/i_A + 1/i_K$. From this, $i_K = 15.6$ mA/cm^2 and $k = 5.2 \times 10^8$ cm^3 mol^{-1} s^{-1} are obtained.

From these values the data in Table III were assembled for various film thicknesses. The assignment of the "R" case for the 10 Å film has already been outlined. For the 50 Å film, the data indicate that diffusion of the substrate in the film is fast relative to charge diffusion, catalytic reaction rate and diffusion of the substrate in solution. Hence the catalytic current is determined by the latter three parameters. These conditons satisfy the "R+E" case. However, i_K and i_E are so large that no data can be obtained from the plateau currents at the rotation rates employed.

Two limiting situations are found for the "R+E" case for extreme values of the ratio i_K/i_E. When this ratio --> 0 the catalytic current is controlled solely by the rate of reaction and substrate diffusion in solution. This is termed the "R" case. The other limiting situation occurs when i_K/i_E --> ∞. The result is a thin reaction layer at the electrode/film interface. This is designated the "ER" case. In the reduction of O_2 at a 100 Å PAQ coated electrode $i_S \gg i_A$ and $i_K > i_E$ by a factor of 20. When $i_K \gg i_E$ the limiting "ER" case applies. With a ratio of 20 the intermediate situations "R+E" and "ER" may apply.

For the 1000 Å films, i_E was calculated using d = 164 Å. It was previously observed that the electroactive layer of such a thick PAQ film is confined to the electrode film interface and that only 16.4% of the AQ units in such a film are electroactive. This suggests that the activity resides in a layer of about 164 Å close to the electrode film-interface. The calculation of i_S, however, requires the total thickness of the film to be taken into account, active and non-active, since the substrate must diffuse through the entire film to reach the electrode surface. Increasing the thickness of the film causes i_K to increase and i_S to decrease such that $i_K >> i_E$ and $i_S \dashrightarrow i_A$. This is the case for the 1000 Å PAQ film although I_S is still somewhat greater than i_A. The kinetic situation can be considered as being intermediate of the "ER" and "ER+S" cases.

The steady state concentration profiles of the catalyst and substrate, and the corresponding limiting current kinetics are clearly dependent upon the film thickness employed. The kinetic cases, as termed by Savéant, change in the following manner with increase in film thickness: "R" --> "R+E" --> "ER" --> "ER+S". The Schematic representations of the models pertaining to this study are show in Figure 32.

The relationship among the various rate limiting factors also affect the half wave potentials for the i-V curves[60]. The simplest relation is that of the "R" case where

$$E_{1/2} = E^0_{AQ/AQ^{\cdot}} + (RT/nF)\ \ln K = E^0_{O_2/O_2^{\cdot}} \qquad (60)$$

Using slow scan rates at a bare Pt electrode $E^0_{O_2/O_2^{\cdot}}$ was determined to be -0.746 V (SCE) by cyclic voltammetry. $E_{1/2}$ determined experimentally with the PAQ coated RDE was -0.74 V, in good agreement with theoretical predictions.

The theoretical catalytic efficiency[86], i_1/i_A, for the various film

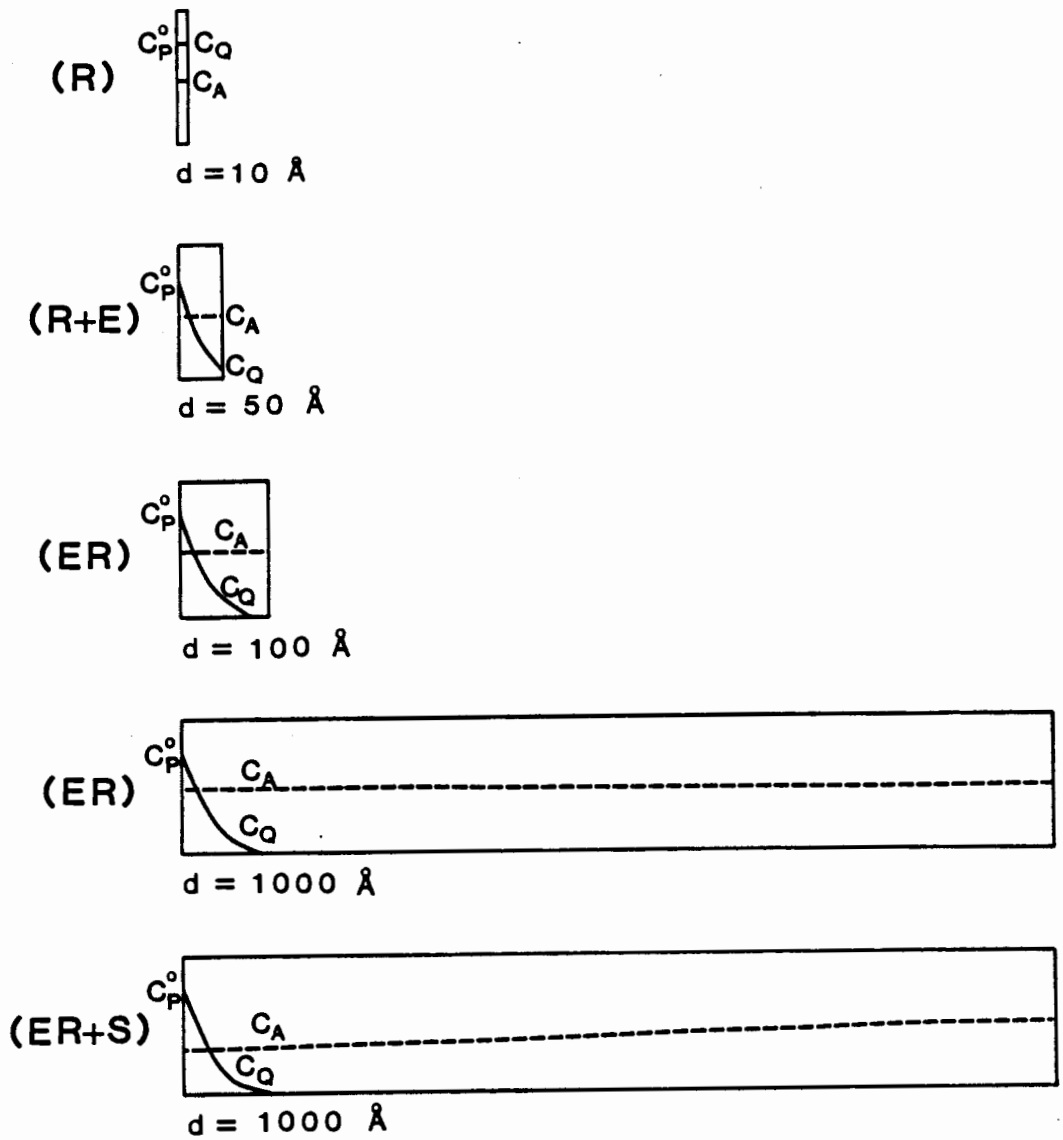

Figure 32. Concentration profiles of A and Q for the electrocatalytic reduction of oxygen at PAQ films. A = O_2, Q = $AQ^{\cdot}$.

thicknesses can be calculated using the assigned kinetic models. The calculated values of i_1/i_A are shown in Figure 33 as a function of electrode rotation rate. Plot 33A is derived from the "R" situation corresponding to a 10 Å film, where $i_1/i_A = i_K/(i_K + i_A)$. Theoretical plots shown in Figure 33B and 33C were obtained for "ER" situation where

$$1/i_1 = (1/i_A)(1-K^{-1}) + \left\{\frac{i_A-(1-K^{-1})i_1}{i_A-i_1}\right\}^2 \frac{i_1}{i_E i_K} \qquad (35)$$

The "ER" condition is assigned to the 100 Å and 1000 Å films, the difference being in the values of $(i_E . i_K)$. As can be observed from plot 33, films of 10, 100 and 1000 Å yield similar catalytic efficiencies. Thus, the experimental observation of two current plateaus for O_2 reduction at these films is justified. The lack of definition of the plateau regions for films of 50 Å and greater may be due to the electrochemical response of the polymer itself.

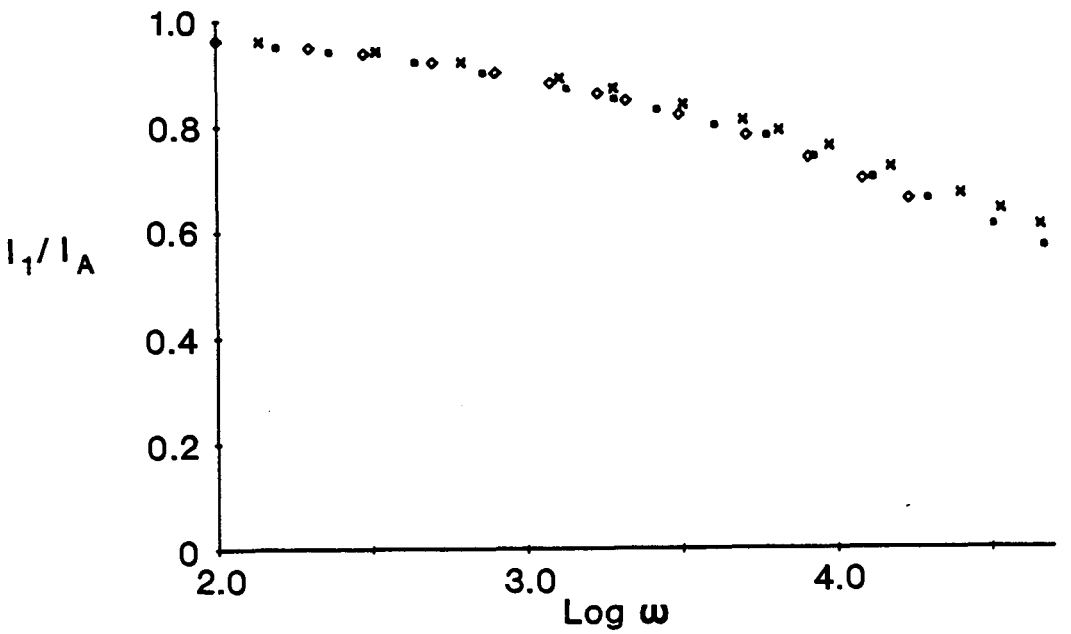

Figure 33. Theoretical plots of i_1/i_A vs. log (rotation rate), (rpm):
a) 10 Å film, ◊, (R) case,
b) 100 Å film, □, (ER) case.
c) 1000 Å film, x, (ER) case.

II.3.3. THE ELECTROCHEMICAL BEHAVIOUR OF Si ELECTRODES MODIFIED BY FILMS OF PAQ

The flat band potential and energy levels of Si in 0.1 M TEAP/DMSO were assigned using a Mott-Schottky treatment of impedance data. A plot of $1/C^2$ against V_M for a n-Si electrode is shown in Figure 34. The flat band potential, V_{fb}, obtained from the voltage intercept is -0.22V vs. SCE and is in the range of values found for n-Si in non-aqueous media[159-161]. The band edges of n-type samples were thus: E_{CB} = -0.46 V (SCE) and, since E_g = 1.1 eV, E_{VB} = +0.64 V. Similar measurements on p-Si showed the flat band potential to be +0.15 V. This is comparable to previous reports [159-165] and led to the assignment of the following energy levels for p-Si in DMSO: E_{CB}= -0.71 V, E_{VB}=+0.39 V. It is assumed that the energy levels of the redox couples AQ, PAQ and O_2 correspond to the $E_{1/2}$ value measured by cyclic voltammetry at a Pt electrode. These were -0.77, -0.71 and -0.75 V respectively for the first reduction process.

The cyclic voltammetry of PAQ coated n-Si electrodes in the dark is shown in Figure 35. The behaviour during the first scan is shown as the solid curve. On continuous cycling (dotted line), the peak separation increases and the anodic wave becomes more obscure. The data indicate that the semiconductor/electrolyte interface has changed from ohmic to partially rectifying. A much more positive voltage is required to oxidise the reduced PAQ, as shown in the steady state curves of Figure 36A.

The sample was potentiostated at -0.8 V and illuminated. A large anodic current was observed (not shown) which decreased rapidly. Illumination was stopped and the potential cycle continued in a positive direction to +0.1 V as shown by the initial part of the solid curve in Figure 36B. No significant anodic current was observed. This indicates that the $AQ^{\cdot}$ was

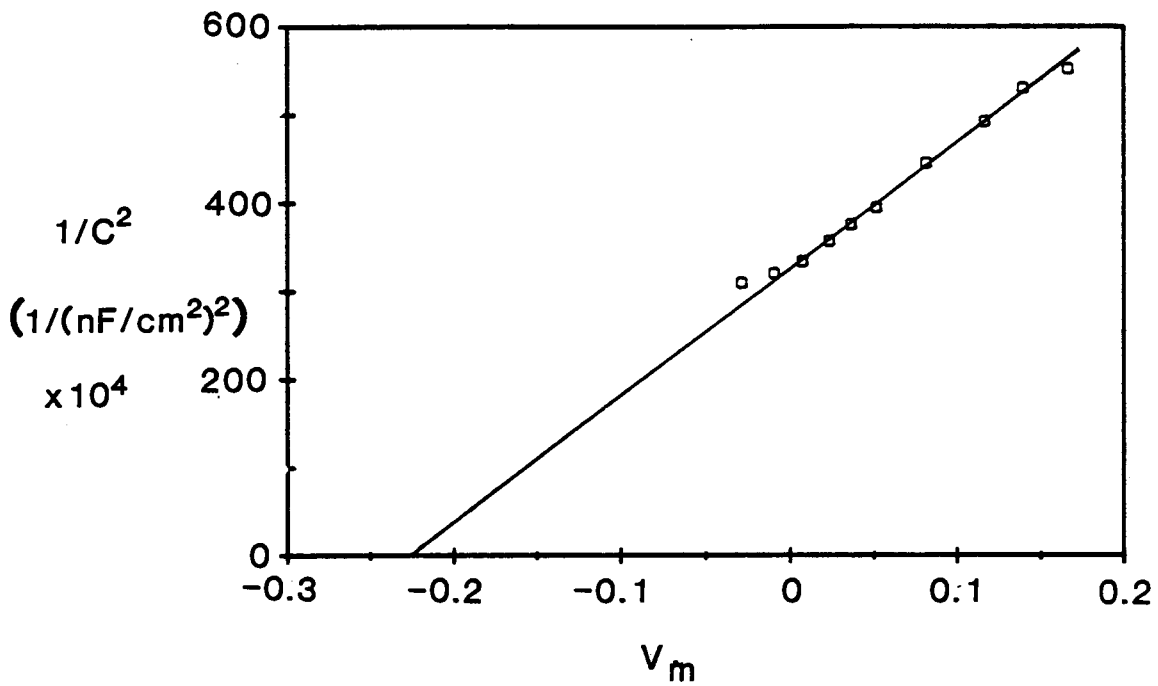

Figure 34. Mott-Schottky plot for n-Si in 0.1 M TEAP/DMSO. Frequency = 5 KHz.

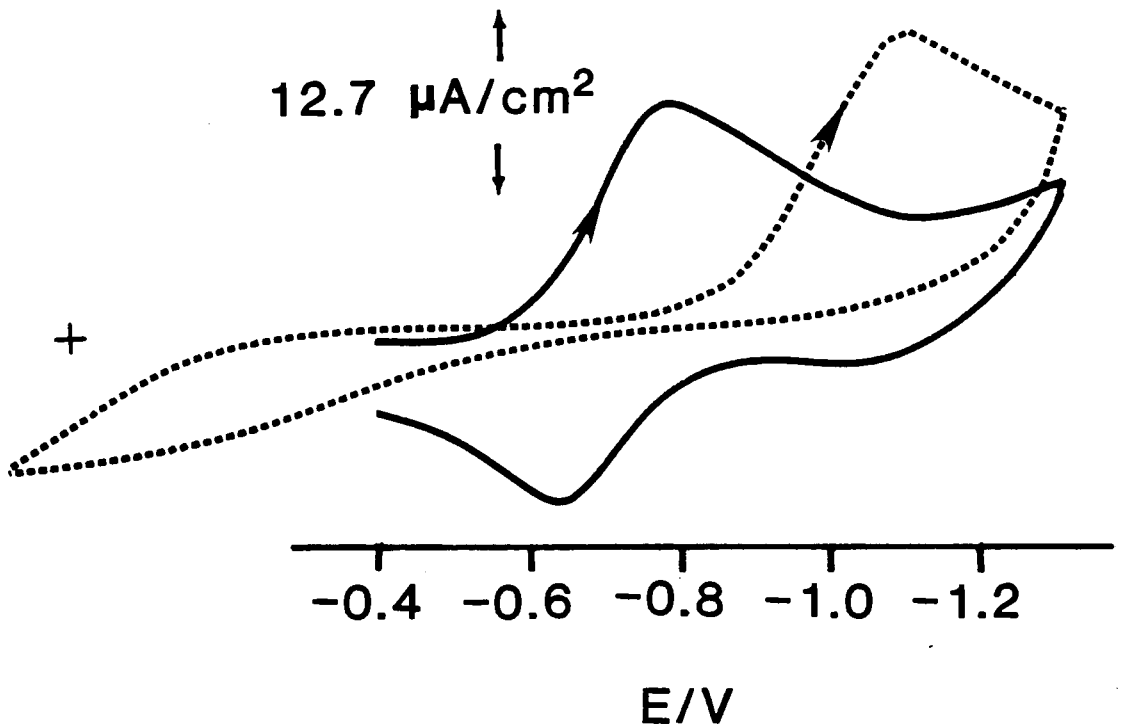

Figure 35. Cyclic voltammetry of PAQ coated n-Si electrodes: (—) first scan, (----) after 30 minutes of continuous cycling. Electrolyte, 0.1M TEAP/DMSO; scan rate, 50 mV/s.

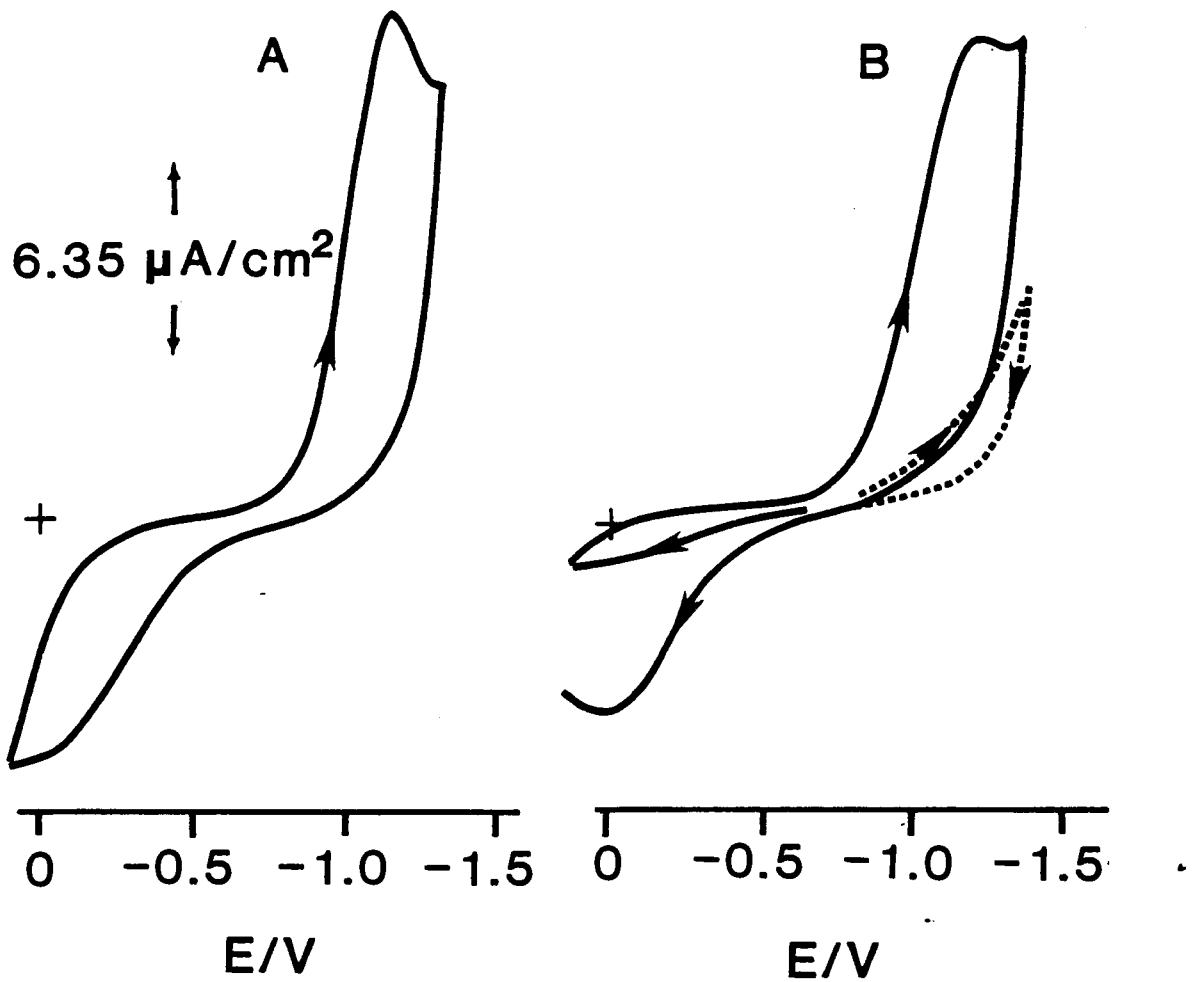

Figure 36. Cyclic voltammetry of PAQ coated n-Si: (A) Steady State, (B) see text.

already oxidised by holes during the illumination. A subsequent sweep of potential between +0.1 and -1.3 V (solid curve of Figure 36B), where AQ was reduced during the cathodic sweep, resulted in the restoration of the original voltammogram.

In order to compare AQ in solution with AQ in the polymer, n-Si, with no surface film, was immersed in a solution containing AQ and the cyclic voltammogram recorded. This is shown in Figure 37. Rectifying behaviour up to high voltages is exhibited immediatly in this case (Figure 37A) and it is evident that photogenerated holes are required to oxidise $AQ^{\cdot-}$ (Figure 37B). The potential of the cathodic peaks remained constant for many potential cycles.

An analogous study with p-Si, instead of n-Si, comparing again the behaviour of AQ in solution and in polymeric films (PAQ) is shown in Figure 38. No cathodic dark current occurs within the potential limits employed (dashed curves), as could be expected with essentially no conduction band electrons. Band gap illumination generates conduction band electrons, and permits the reduction of the redox couple (dotted and solid curves). By comparing the observed first to third cycle it appears that the PAQ sample is much more stable than the bare silicon where AQ is in solution. In both cases the reduction peaks shift: the peaks only shift from -0.75 to -0.85 V for the coated electrode but shift from -0.81 to -1.27 V for the bare electrode with AQ in solution.

There is current interest in the use of polymer films for transporting current to a solution species while protecting the electrode. In the previous section the electrocatalytic activity of PAQ films on Pt electrodes towards the O_2 reduction reaction was described. An analogous investigation of the homogeneous mediation of O_2 by AQ vs. the polymer coated semiconductor was undertaken in the present study. The behaviour expected for the mediated reduction of O_2 by conduction band electrons is shown schematically in Figure

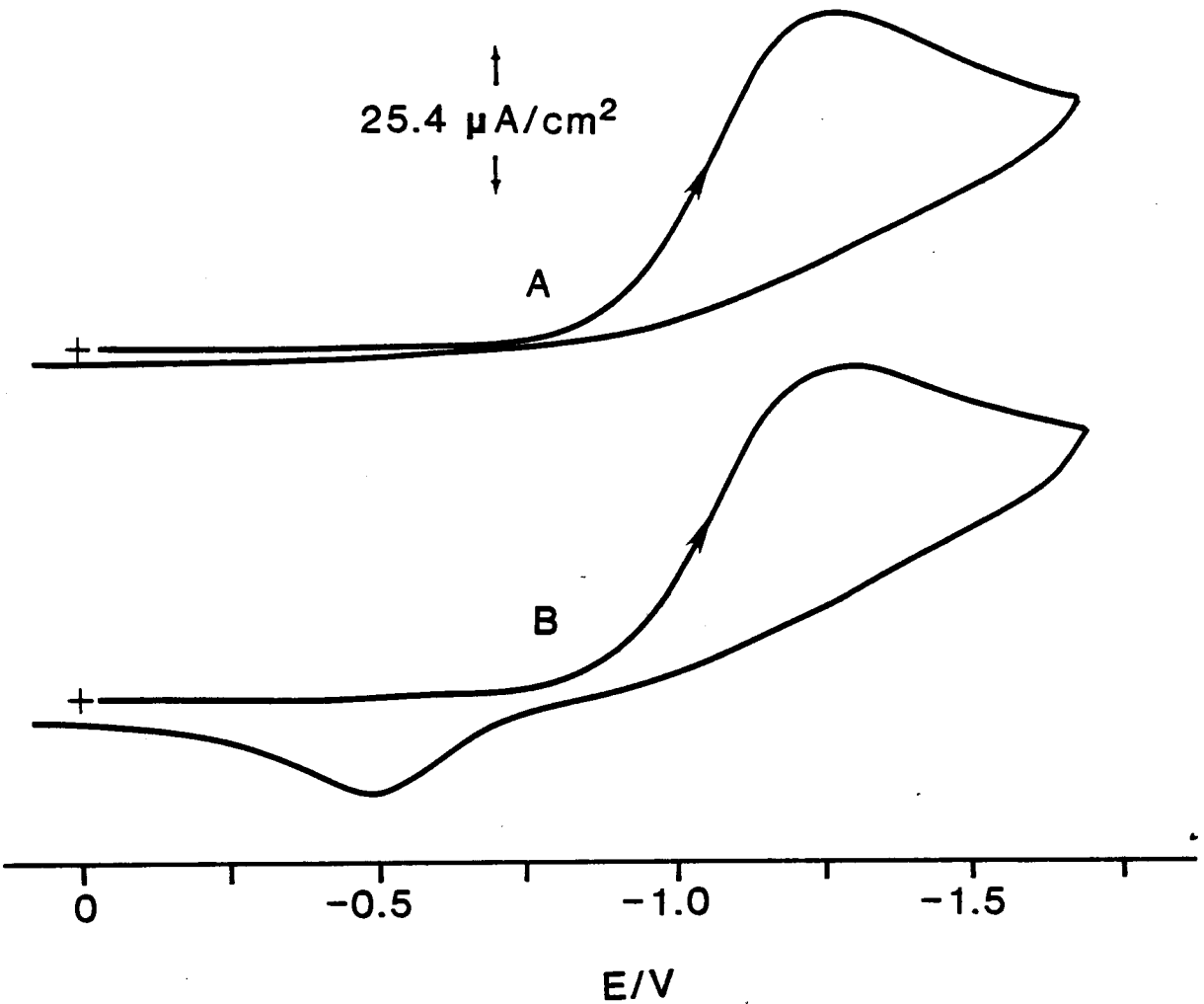

Figure 37. Cyclic voltammetry of AQ (1 mM) at n-Si (first cycle): (A) dark, (B) under illumination. Electrolyte, 0.1 M TEAP/DMSO, scan rate, 50 mV/s.

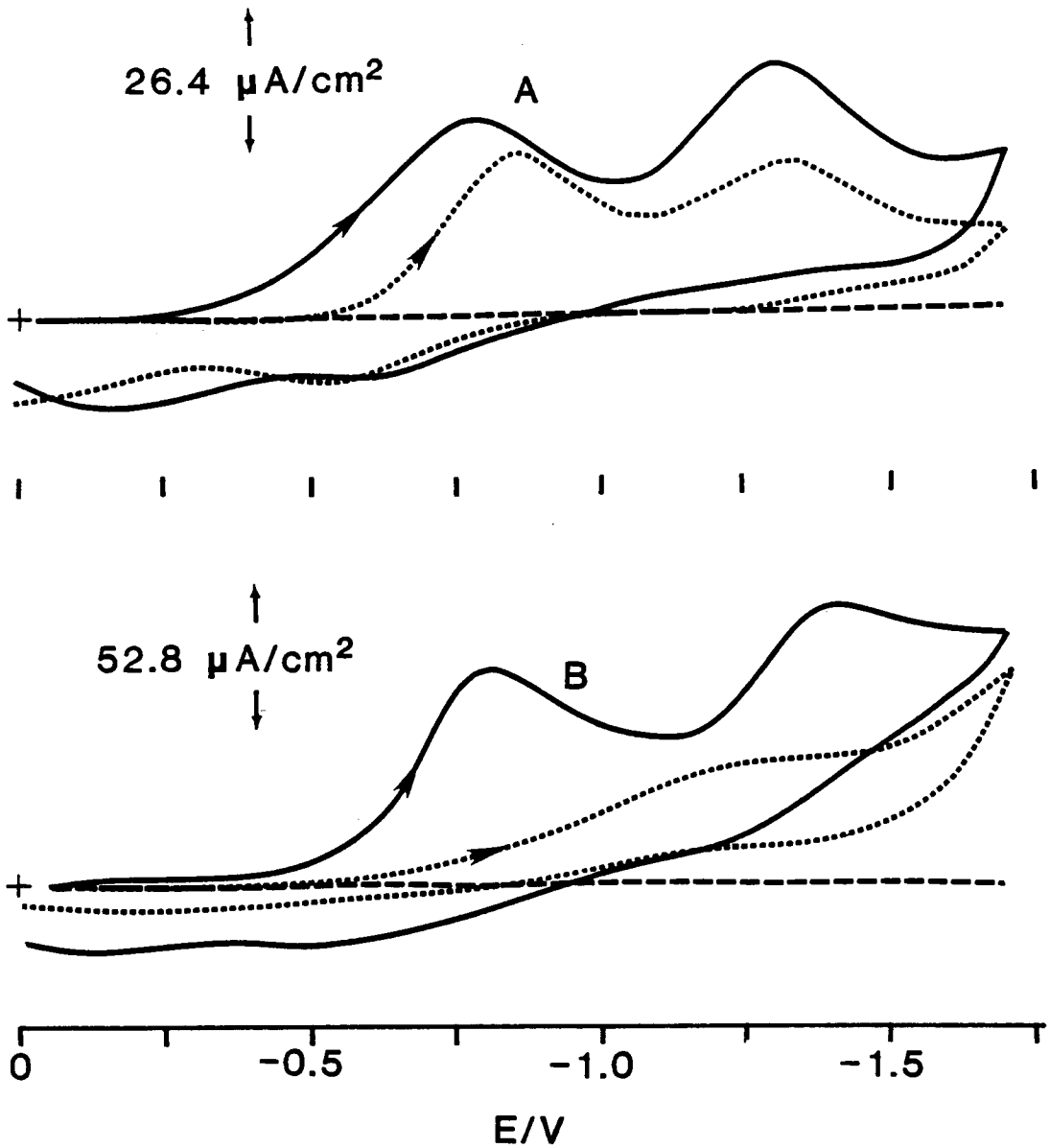

Figure 38. Cyclic voltammetry of PAQ film (A) and 1 mM AQ (B) at p-Si: (----) dark, (——) and (••••) under illumination, 1st and 3rd cycle respectively. Electrolyte, 0.1 M TEAP/DMSO; scan rate, 50 mV/s.

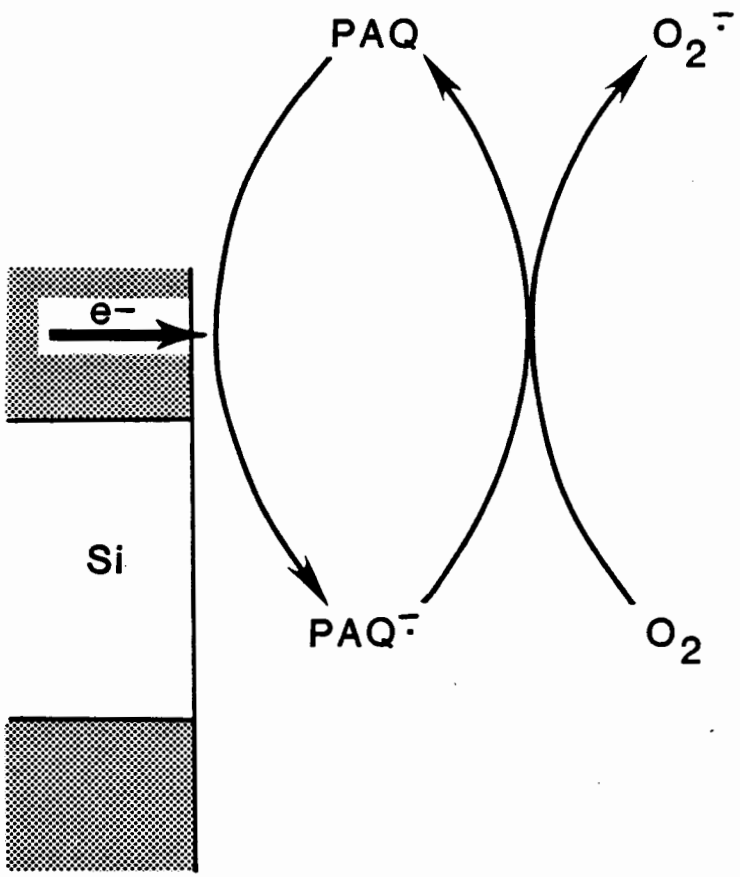

Figure 39. Schematic representation for the mediated reduction of oxygen at PAQ coated silicon electrodes.

39.

The reduction of O_2 to O_2^- at bare n-Si, shown in Figure 40A, is found to require a large overpotential compared to the reduction at Pt. Furthermore, the reduction requires increasingly negative potentials upon further cycling. The voltammetry of O_2 reduction in the presence of AQ in solution is shown in Figure 40B. The high current in the first cycle indicates that the AQ acts as an electron mediator for oxygen reduction. However, the shift in the dashed curve indicates that again the electrode stability is poor. The polymer coated electrode (Figure 40C) is more stable, although it also shows a slight negative shift in the cathodic peak potential with successive cycles.

Similar effects are found with p-Si electrodes (Fig 41). Since p-type electrodes normally have no conduction band electrons, they must be illuminated with band gap light to produce them for reduction. The first scans indicate that AQ, in solution and in the PAQ polymer films, is an efficient mediator for oxygen reduction. However, on subsequent cycles the superior stability of PAQ coated electrodes is evident. This is also indicated by the chronoamperometry of these systems as shown in Figure 42.

The behaviour of AQ and PAQ, in the absence of oxygen, at the n-Si/solution interface is directly explicable by assuming the slow growth of a thin oxide layer or some other insulating film at the silicon surface (Figure 43). The accompanying interface states result in a fixed potential drop across the semiconductor and a variable potential drop across the Helmholtz layer. Initially the AQ energy level should be above the conduction band energy level, as determined by the V_{fb} measurement. In this case, the electrode should act metallic as indicated by Figure 43A, and indeed it does (Figure 36A). After a few cycles it begins to rectify, indicating the AQ level has moved below the conduction band edge (Figure 43B). This must arise

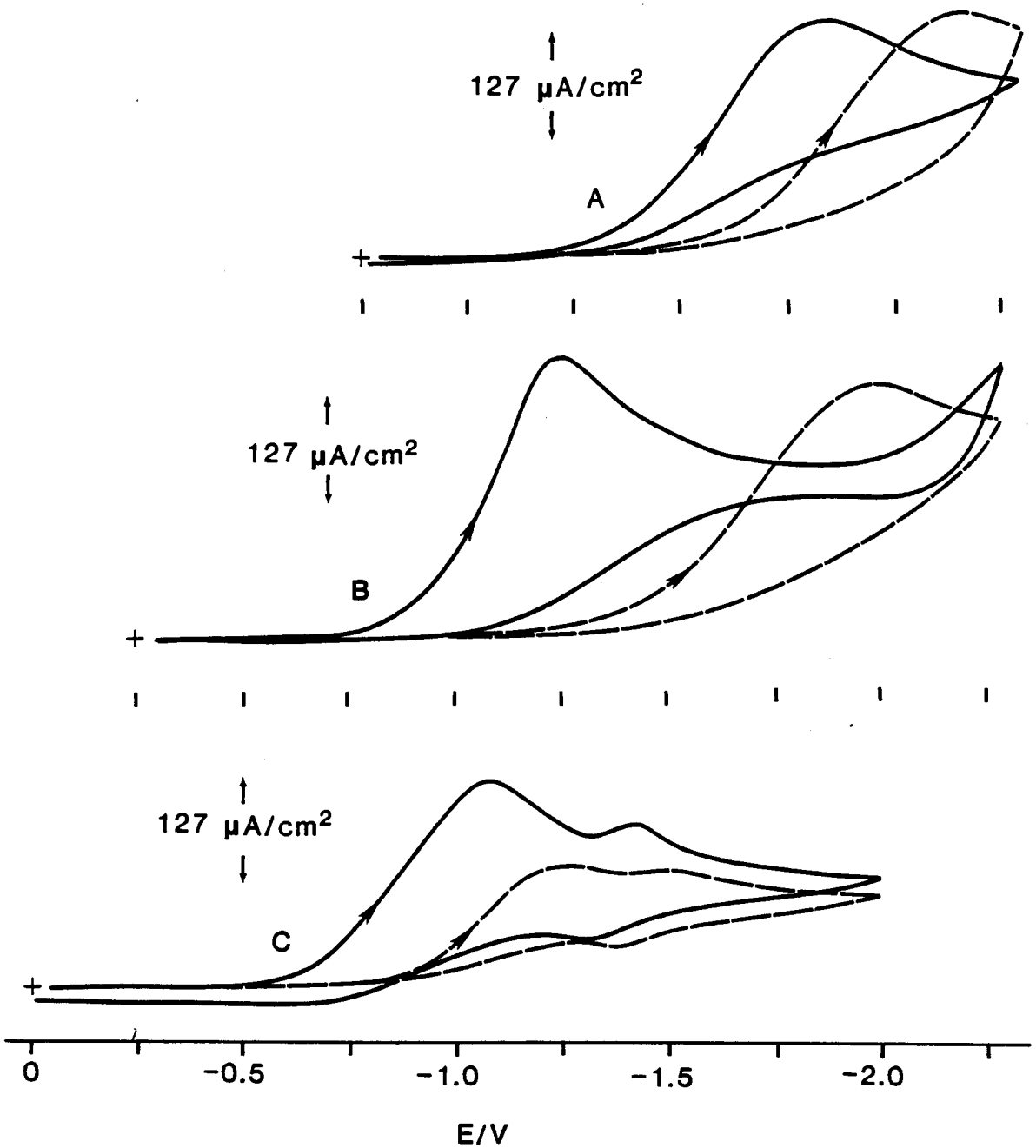

Figure 40. Cyclic voltammetry of O_2 at n-Si: A) bare electrode, B) bare electrode in the presence of AQ (1 mM), C) PAQ coated electrode. (——) 1st scan, (----) 3rd scan. Electrolyte, 0.1 M TEAP/DMSO; scan rate, 50 mV/s.

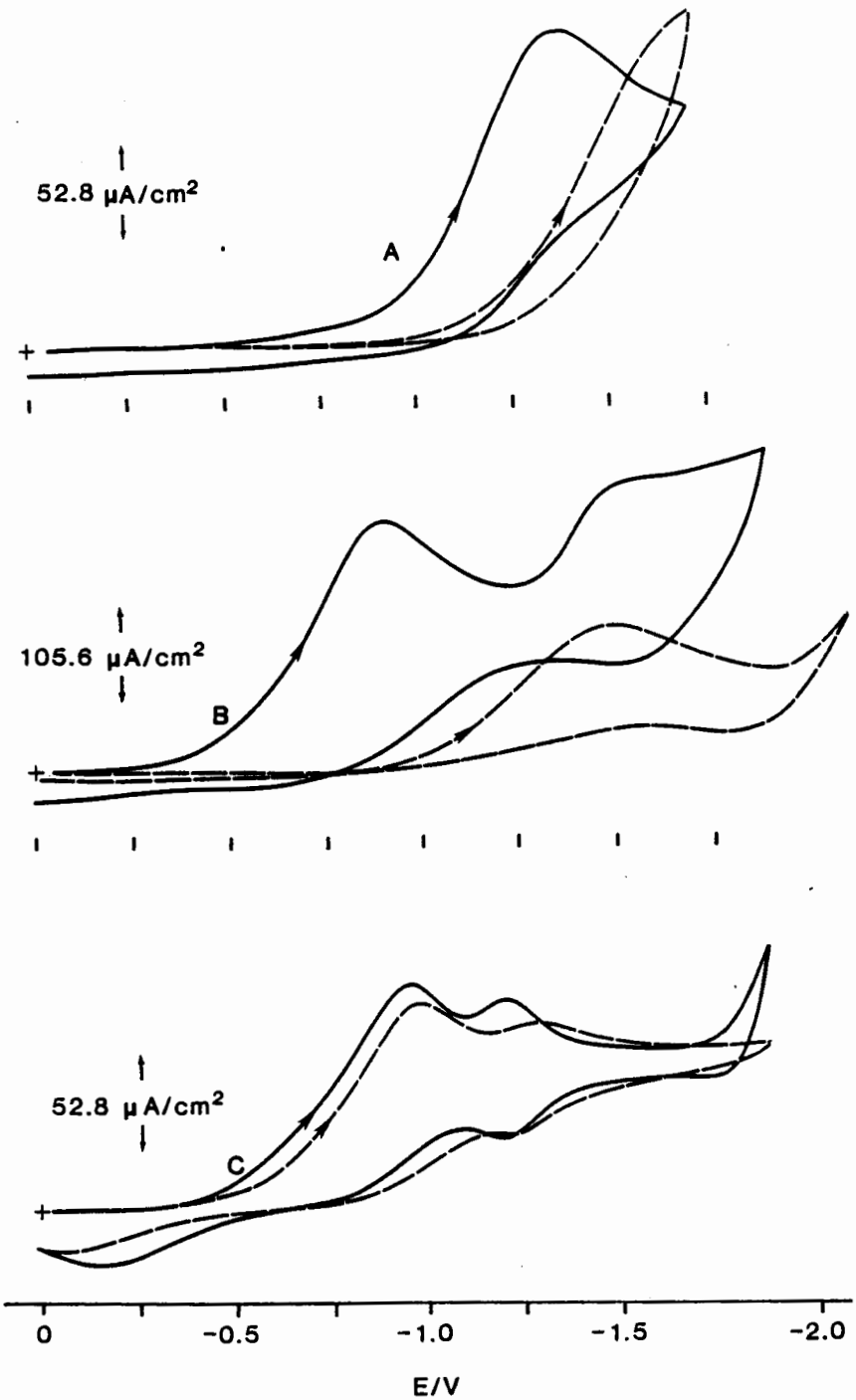

Figure 41. Cyclic voltametry of O_2 at illuminated p-Si: A) bare electrode, B) bare electrode in the presence of AQ (1 mM), C) PAQ coated electrode. (——) 1st scan, (----) 3rd scan. Electrolyte, 0.1 M TEAP/DMSO, scan rate, 50 mV/s.

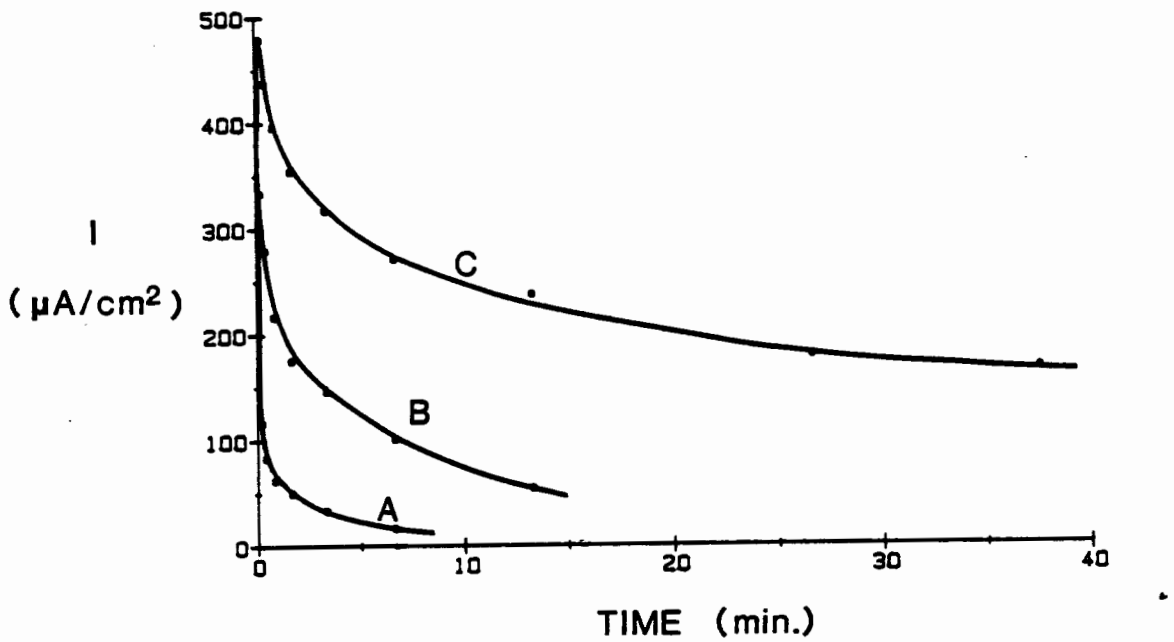

Figure 42. Chronoamperometry of O_2 reduction at illuminated p-Si: A) bare electrode, B) bare electrode in the presence of AQ (1 mM), C) PAQ coated electrode. Electrolyte, 0.1 M TEAP/DMSO; Potential, -1.0 V (SCE); stirred solution.

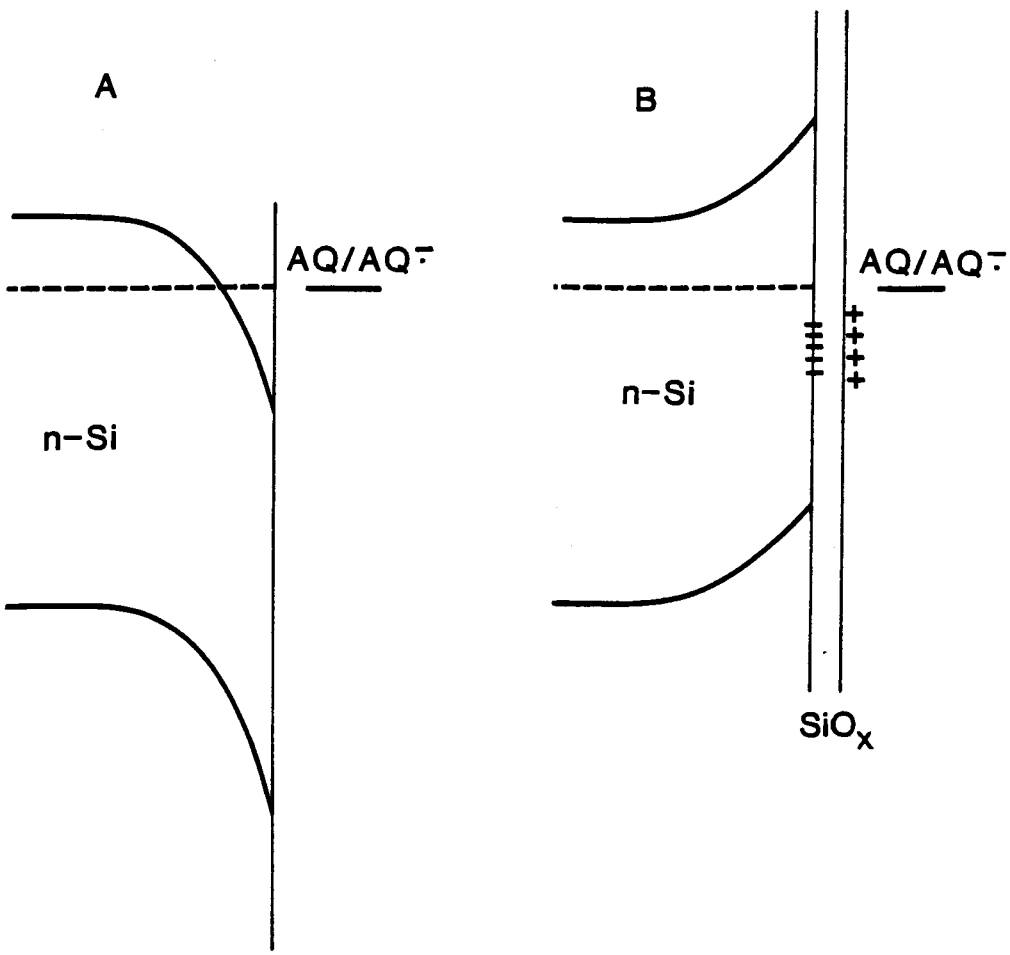

Figure 43. Schematic representation of the semiconductor/electrolyte interface in the absence, (A), and presence, (B), of a surface oxide film and accompanying interface states.

from a double layer as shown in the sketch. Interface states will become negatively charged by electron capture from $AQ^{\cdot}$, and the potential between the charged interface states and the redox couple raises the band edge so that the redox energy level is within the band gap. Thus, minimal anodic current will flow in the dark because electrons can no longer be injected into the conduction band: a rectifying junction exists. With AQ alone, the surface deteriorates rapidly and insufficient stability is exhibited for comparative measurements to be made. The PAQ effectively reduces the rate of formation of the insulating layer and thereby the rate of formation of the interface states.

Other groups have investigated the electrochemistry of AQ dissolved in non-aqueous media at Si electrodes[160-163,166]. In agreement with the above studies, a rectifying interface is observed even though the energy level of the redox couple, in relation to E_{CB} and E_{VB} of the semiconductor, suggests that an ohmic interface should be present. Studies, in which trace water is rigorously excluded, show that AQ in solution initially forms an ohmic junction at the n-Si interface prior to the formation of a rectifying interface[160,166]. Such behavior has also been attributed to the evolution of an oxide film, and accompanying interface states.

In the reduction of O_2 in an aprotic solvent, the superoxide ion $O_2^{\cdot}$ is relatively stable[156,167] but it is postulated that O_2 can react with the Si semiconductor. However, when PAQ is employed as a mediator the location of electron transfer is within the polymeric film rather than at the solid interface. The electron transfer through the film, the rate of cross reaction and the rate of diffusion determine the region at which O_2 reduction occurs[60], and in this instance it is generally distant from the silicon surface. Thus, the polymer film effectively insulates the semiconductor from the superoxide ion and prevents chemical reaction and deterioration. With a

bare silicon surface, of course, with and without AQ in solution, $O_2^{\cdot}$ is formed at the silicon surface and can induce oxidation.

II.4. CONCLUSION

Electron hopping is the proposed mechanism of electron transport in PAQ films. A number of factors constitute the rate controlling event including permeation of counter ions and segmental motion of polymer chains. The nature of the solvent thus, greatly influences the electrochemical response. This is evident from the electrochemical study of PAQ films in various solvents.

PAQ films in DMSO exhibit almost ideal voltammetric waveshapes. However, the ratio $\Gamma_{obs}/\Gamma_{app}$ decreases sharply with increase in film thickness. Chronamperometric measurements yield results which are consistent with this observation. It is postulated that the polymer chains are oriented such that the total number of AQ units present in a thin region next to the electrode surface are reducible, beyond this, reducible AQ groups are found only in preferred channels.

The mediation of electrochemical reactions by electroactive polymer modified electrodes requires several mass and charge transfer processes. The relative importance of charge transfer through the film, diffusion of substrate, and electron transfer between substrate and redox groups changes with film thickness. The interplay of these various factors has been described quantitatively in a model proposed by Savéant and coworkers[60]. The results obtained with PAQ are fully compatible with this approach, and the various limiting cases have been described in this context.

In extremely thin films, the rate of cross reaction between substrate and redox groups determines the limiting current. With increase in thickness, the rate of charge propagation through the film increases in relative importance. This is manifested in a smaller proportion of total redox groups being reduced in thicker films. Thus, it was also found that increase in

film thickness, with the accompanying increase in available redox groups, does not substantially affect the catalytic efficiency. Thick and thin films are equally effective in the mediated reduction of O_2.

The transfer of electrons from the silicon conduction band to polymeric films containing AQ groups, and to AQ in solution proceeds essentially by the same mechanism. The gradual formation of an oxide layer, or some other insulating layer, at the Si surface, results in the formation of a rectifying junction as opposed to the ohmic junction anticipated based on energy level models. The rate of formation of this insulating layer is decreased when the PAQ film is present. This is possibly due to the hydrophobic nature of PAQ and the exclusion of trace H_2O from the Si surface. In photoelectrochemical reactions of solution species, the presence of the polymer film retards reactive, passivating agents or products from reaching the semiconductor surface, while maintaining facile electron transfer to oxidising agents in solution. Thus, semiconductor electrodes coated with catalytic polymer films exhibit superior stability over naked semiconductor electrodes employing homogeneous catalysts.

CHAPTER III

CHARGE STORAGE PROPERTIES OF PAQ AND POLYPYRROLE FILMS

III.1. INTRODUCTION

During the late seventies it was discovered that polyacetylene, $(CH)_x$, could be partially oxidised or reduced to yield highly conductive materials. It was also found that films of $(CH)_x$ on electrode substrates can be electrochemically cycled between the charged, conductive state and the neutral, insulating state. It has since been realised that these materials have potential use as electricity storage media. These initial studies have led to the discovery of a number of organic conducting polymers, a few of which, have been examined as rechargeable storage media.

Polyacetylene has a storage capacity (on a mass basis) superior to other organic conducting polymers due to the low molecular weight of the repeating CH unit. However, $(CH)_x$ can only be oxidised or reduced to the $(CH^{0.10+})_x$ and $(CH^{0.18-})_x$ states respectively. Low molecular weight polymeric materials, which can be charged to a greater degree, should exhibit superior capacitative properties over $(CH)_x$ films. Such qualities may possibly be found in redox polymer films. To date, no charge storage cells based on redox polymer films have been reported.

This chapter reports the results obtained from a study of the charge storage properties of cells employing PAQ coated anodes and polypyrrole coated cathodes. Polypyrrole is a member of the organic conducting polymer family, and is of current commmercial and academic interest. A novel device, in which the charging cycle is photoassisted, was investigated using PAQ coated p-type semiconductor anodes. The results are discussed in terms of an

energy level model.

The electrochemical properties of polypyrrole; the basic principles and terminology of charge storage; and the recent advances in polymeric based charge storage cells are described below to aid discussion.

III.1.1. ELECTROCHEMICAL PROPERTIES OF POLYPYRROLE

The examination of organic conducting polymers has been active for several years[168-170]. Increasing attention is being devoted to those polymers derived from hetetrocyclic monomers, especially polypyrrole[171-175]. Polypyrrole (PP) typifies the general properties of heterocyclic conducting polymers: They are formed by electropolymerisation of the monomer to yield oxidised conductive films; thin films may be electrochemically cycled between the oxidised, conductive state and the reduced, insulating state; oxidised films represent charged polycations, whereby charge is stabilised by the incorporation of anions; oxidised and reduced states differ significantly in optical absorbance.

The electropolymerisation proceeds with electrochemical stoichiometry and allows characterisation of the reaction. Between 2 and 2.4 electrons per monomer are involved in the polymerisation reaction: 2 electrons are used in forming the film, and that charge in excess of 2.0 is consumed by the accompanying electrooxidation of the film. The proposed mechanism of polymerisation for simple heterocycles is given in Figure 44[176].

The electrochemical potential required to induce polymerisation varies depending on the ionisation potential of the heterocycle. The voltage required to form PP films is generally lower (less positive) than that required for other heterocycles. Similarly, the redox potential associated with the switching between conductive and insulating states, and that

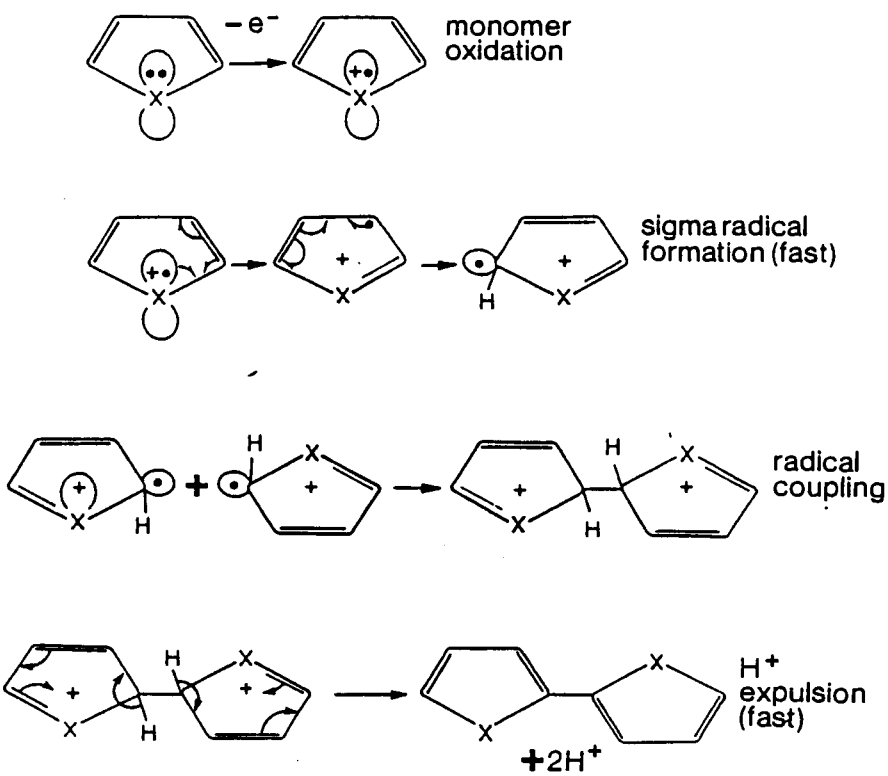

Figure 44. Proposed mechanism for electropolymerisation of heterocyclic monomers. For pyrrole, X=NH.

potential associated with irreversible oxidative processes, also occurs at less positive potentials compared to other conducting polymers. The irreversible oxidative process, found with all conductive polymers, leads to a dramatic change in polymer properties. PP therefore, has a characteristic workable potential window, as do all heterocyclic conducting polymers.

III.1.2. PRINCIPLES OF CHARGE STORAGE TECHNOLOGY

An electrochemical reaction at an anode, or at a cathode, will proceed spontaneously if there is a decrease in energy of the system, i.e. when ΔG is negative. ΔG can be calculated from electrochemical data using the Nernst equation (2) and the relation $\Delta G = -nFE$.

When two half cells are brought together the cell potential is determined by the two half cell electrode potentials:

$$E_{cell} = E_{cathode} - E_{anode} \qquad (61)$$

By definition, the anode and cathode are the electrodes where electrochemical oxidation and reduction occur respectively.

In dealing with charge storage systems, there are several important properties which should be defined[177]: The electricity storage density (ESD) is a measure of the maximum quantity of electricity which can be drawn from a unit mass of substance. The theoretical value is given by $nF/[3.6(M.Wt.)]$ Ahr/kg, while the experimental value is obtained by dividing the number of coulombs passed during discharge by the mass of electroactive material. The overall ESD takes the masses of both the anode and cathode into account. The energy density (ED) describes the energy which may be extracted from a given mass of substance. The ED of individual electrodes is given by ESD x V_e, where V_e is the reversible electrode potential and the ED of the cell is

given by ESD x V_{cell} , where V_{cell} is the cell potential. The energy density is governed by electrode kinetics and thus, the rate at which the cell is discharged. The power density describes the rate at which the cell can release energy. The power density is the product of the cell potential and the current density. The term coulombic efficiency describes the ratio of the charge output to the charge input.

III.1.3. RECHARGEABLE STORAGE CELLS BASED ON ORGANIC CONDUCTING POLYMERS

MacDiarmid, Heeger and coworkers were the first to report polymer based rechargeable cells[36,178-180]. Their original studies utilised a polyacetylene cathode and a Li/Li^+ anode in a cell containing $LiClO_4$ /propylene carbonate. A $(CH)_x$ film, of dimension 1.0 x 0.5 x 0.01 cm, provided an open circuit voltage of 3.7 V, an energy density of 176 Whr/kg and power densities in excess of 30 kW/kg, based on the mass of $[(CH)^{0.06+}(ClO_4^-)_{0.06}]_x$ initially employed and the mass of Li consumed.

In later experiments, the Li/Li^+ half cell was replaced by cationically and anionically doped $(CH)_x$ films. In all cases, electron flow occurs from the lower oxidised state to the higher oxidised state. The net result, after complete discharge, is two electrodes of the same composition. Open circuit voltages generated by $[(CH)^{y+}(ClO_4^-)_y]_x$ and $[(CH)^{y-}(Bu^nN^+)_y]_x$ anodes were reasonably high (2.5 V) while voltages generated by $[(CH)^{y+}(ClO_4^-)_y]_x$ cathodes and $[(CH)^{z+}(ClO_4^-)_z]_x$ anodes were much lower ($\approx$0.6 V). Recently, a cell utilising a polymeric solid electrolyte sandwiched between a $(CH)_x$ anode and cathode, was constructed[181]. The "all plastic" battery produced an open circuit voltage of 3.4 V, and delivered a short circuit current of 10 mA for

films of dimension 1.0 x 2.0 x 0.007 cm.

The initial studies of $(CH)_x$ films have prompted the investigation into other organic conductive polymers. Poly(p-phenylene) (C_6H_4) is highly conductive when doped to yield n- and p-type materials. These samples have been employed as anodes and cathodes in rechargeable cells[182,183]. Cells constructed with Li anodes and $[(C_6H_4)^{0.4+}(AsF_6^-)_{0.4}]_x$ cathodes produced a V_{oc} of 4.4 V and a theoretical energy density of 285 Whr/kg. Cells based on n- and p-type $(C_6H_4)_x$ electrodes produced a V_{oc} of 3.3 V and a theoretical energy density of 150 Whr/kg.

Polyaniline has been of considerable interest[184] since it is stated to have a comparable energy density to polyacetylene and may be electrochemically cycled in aqueous or non-aqueous solution.

A number of studies have been performed on polythiophene (C_4H_2S) based cells[185-187]. In one study, the experimental cell consisted of two 0.75 μm thick polythiophene films (2.0 cm^2), one cationically and the other anionically doped, in $Bu^n{}_4N^+BF_4^-/CH_3CN$. The electricity storage density and energy density, based upon 24% dopant, were 24 Ahr/kg and 63 Whr/kg respectively. The maximum power density, as determined through a 100 Ω resistance, was 61 kW/kg.

To increase the energy density of a system one has to consider the oxidative or reductive capacity, and the rest potential of the polymer. Polypyrrole has a larger oxidative capacity than other conductive polymers, although the maximum oxidation state is, at best, one positive charge delocalised over 3 pyrrole rings. Redox polymers, on the other hand, can maintain one, two, or three charges per repeat unit although this can be offset by the higher molecular weight of the unit. Both polypyrrole and redox polymers have potential use as reversible cathode materials and thus, a study was warranted. The charge storage properties of polypyrrole, but not

redox polymers, have since been investigated and exploited by other groups[188-190]

A comparison between the charge storage properties of polymers and conventional materials is difficult and often misleading since the reported values of ESD and ED for commercial cells include the masses of electrode materials, electrolyte, casing, contacts, etc.. In addition, the efficiency of a particular cell generally increases as technology advances. However, energy densities for a number of active components in commercial cells have been reported and can be tentatively used for comparison:
PbO_2-H_2SO_4-Pb, theoretical ED = 180 Whr/kg, experimental ED = 20 Whr/kg;
NiO(OH)-KOH-Cd, theoretical ED = 220 Whr/kg, experimental ED = 40 Whr/kg;
Ag_2O_2-KOH-Zn, theoretical ED = 440 Whr/kg, experimental ED = 110 Whr/kg[191].

III.2. EXPERIMENTAL

III.2.1. CHEMICALS

Acetonitrile and TEAP were purified as described in Section II.2.1.. The synthesis of poly[p-(9,10 anthraquinone-2-carbonyl styrene]-co-styrene has been previously described in Section II.2.2.. The PAQ sample used in this study contained 47 mol% AQ. Pyrrole was distilled under reduced pressure in a spinning band column and stored over molecular sieve, type 4A.

III.2.2. FILM PREPARATION

PAQ films on Pt, p-Si and p-InP, were prepared by placing an aliquot of 0.5 wt% PAQ solution in pyridine on the electrode substrate and allowing the solvent to evaporate. The electrode was subsequently dried under vacuum for 5 minutes. The quantity of polymer deposited was 1.09×10^{-6} mol /cm^2.

PP films were electropolymerised on Pt electrodes (0.18 cm^2) from 0.1 M pyrrole in 0.1 M TEAP/CH_3CN. Films were grown using a constant current density of 71.2 mA/cm^2. Electrolysis was continued until 662 mC/cm^2 of anodic charge had passed.

The thickness of the film was estimated from

$$d = \frac{M.Wt \times Q_{form}}{n \times 96485 \times \rho \times A} \qquad (62)$$

where M.Wt is the molecular weight of a repeating pyrrole unit (plus dopant); n is the number of electrons associated with polymer formation (in the absence of doping) and is equal to 2; ρ is the estimated density of the film (1.5 g/cm^3)[174,175]; A is the electrode area; and Q_{form} is the charge

associated with formation of the polymer. Q_{form} is determined from $Q_{form} = Q_{tot} - Q_{ox}$. Q_{tot} is simply the total charge passed during electrolysis and Q_{ox} is the charge associated with electrochemical doping of the polymer. Q_{ox} is obtained by measuring the number of coulombs required to completely reduce a freshly formed film.

II.2.3. ELECTROCHEMISTRY

The treatment of Pt and p-type silicon working electrodes has been described in Section II.2.3.. Samples of p-type InP (100 face) were purchased from Varian, Palo Alto, California, and mounted on glass with silicone adhesive. Ohmic contacts were prepared by placing Ga-In eutectic on the back of the sample and heating to 450 °C for two hours under vacuum. The heat treatment reduced the resistance of the contact from ≈10 KΩ to 8 Ω. InP electrodes were etched with 5% Br_2/methanol for 30-60s prior to use.

A single compartment cell (40 ml.) incorporating a quartz window was employed in conjunction with a Pt counter electrode and a Ag/AgCl reference electrode. All potentials are reported with respect to the SCE. The electrolyte used for these studies was 0.1 M TEAP/CH_3CN. Solutions were flushed with N_2 or Ar prior to use and an inert atmosphere maintained throughout the experiments. Leaching of water into the electrolyte was prevented by separating the reference electrode from the main compartment by an agar salt bridge saturated with NaCl. The reference electrode was further isolated by placing the salt bridge in an ancillary compartment containing 0.1 M TEAP/CH_3CN. The ancillary compartment was immersed in the electrolyte and electrical contact achieved through a glass frit. The effect of trace water already present in solution was diminished by the addition of activated alumina (type WN-6, Sigma) (≈5g)

III.2.3.1 CHRONOCOULOMETRY

Chronocoulometry of PP coated electrodes was performed by measuring the charge passed following a potential step from an initial value of -0.55 V to more positive values. The charge was recorded when the current had dropped to < 10 $\mu A/cm^2$ (1-10 min). The charge associated with background processes was subtracted from the recorded value. The open circuit voltage of the oxidised PP coated electrode was recorded immediatly following the anodic potential step using a high impedance electrometer (Keithley).

III.2.3.2. CYCLIC VOLTAMMETRY

Cyclic voltammetry was performed on two and three electrode systems using the equipment described in Section II.2.3.. The two electrode system was employed for rechargeable cell studies. Here, the working electrode terminal of the potentiostat was connected to one electrode (PAQ coated) and the counter and reference electrode terminals attached to the second electrode (PP coated). Prior to voltammetry, the PP film was electrochemically oxidised, such that the free standing potential of the film was +0.05 V (SCE). Voltammetry at semiconductor electrodes was assisted by illumination from a 150 W tungsten lamp (Spectro). The illumination intensity was 40 mW/cm^2 at the electrode surface.

III.2.3.3. DISCHARGE CHARACTERISTICS

The discharge characteristics of rechargeable cells were analysed by short circuiting charged PAQ coated anodes and PP coated cathodes through a variable resistance.

III.3. RESULTS AND DISCUSSION

II.3.1. ELECTROCHEMISTRY OF PAQ AND PP COATED ELECTRODES

The electrochemical properties of thin PAQ films in 0.1 M TEAP/CH_3CN have been described in the previous chapter. The solubility of PAQ in CH_3CN is poor and thus, crosslinking is not required to stabilise the film. The cyclic voltammogram of a thick PAQ film (5 μm) is shown in Figure 45a. The electrochemically derived surface coverage of AQ units was 2.0×10^{-7} mol/cm^2, while that calculated from the quantity of material applied was 1.09×10^{-6} mol/cm^2. The ratio, $\Gamma_{obs}/\Gamma_{Appl}$, is therefore, 0.18. Low $\Gamma_{obs}/\Gamma_{Appl}$ ratios have been previously observed in DMSO. It is again suggested that the low mobility of polymer chains prevents the required orientation for complete electron propagation through the film. It is highly probable, based on the results obtained in DMSO, that electroactivity is confined to a thin region close to the electrode surface.

The cyclic voltammetry of a PP coated electrode is shown in Figure 46. The voltammogram shows broad current peaks centered at +0.15 V (SCE). The broad waveshape is the result of the doping-undoping process which occurs concurrently with changes in applied potential.

Potential step chronocoulometry was performed on PP films in order to determine the relationship between the dopant (ClO_4^-) concentration and the free standing potential of PP films. The charge storage capacity of PP, as a function of applied potential, is shown in Figure 47. At less positive potentials (<-0.25 V), the film is neutral and the charge storage capacity is negligible. As the applied potential is made more positive, PP is oxidised to greater extents. The charge storage capacity is linearly dependent on applied potential above -0.2 V. Oxidation of PP is slightly irreversible

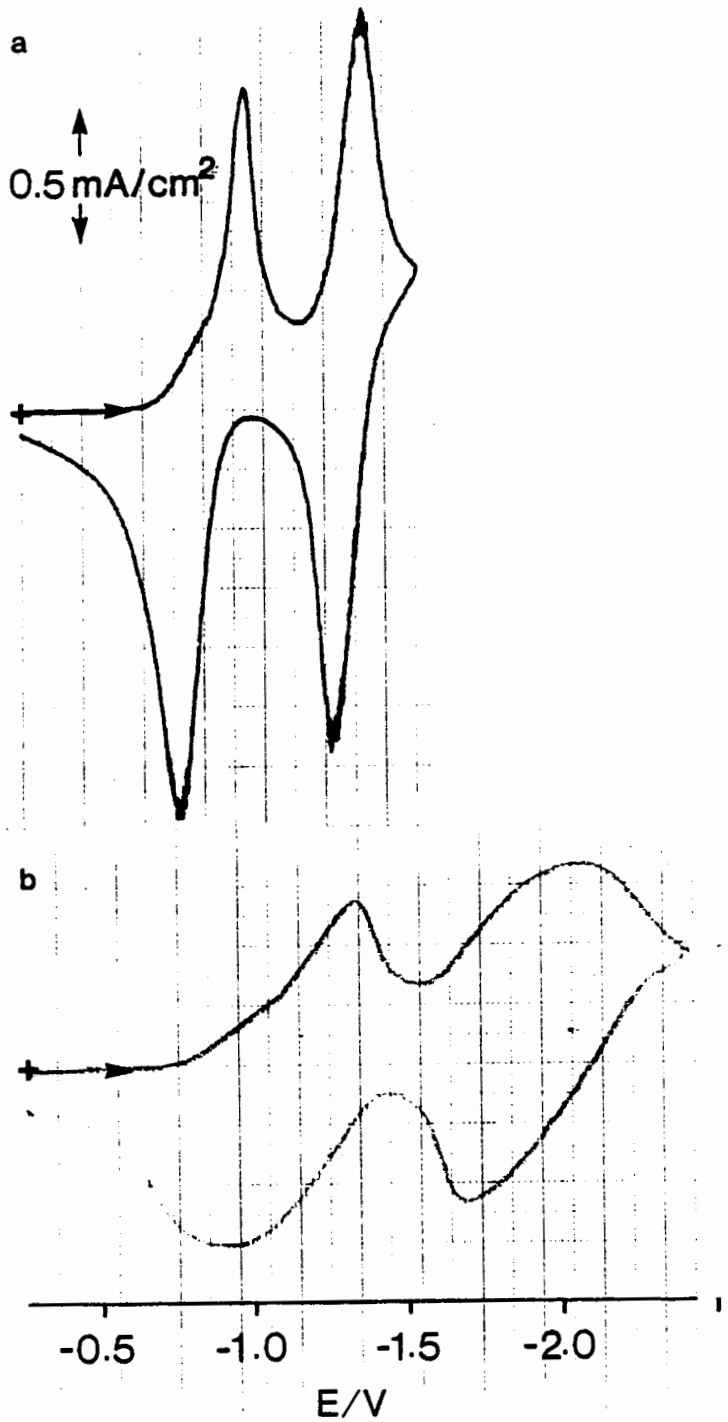

Figure 45. Cyclic voltammetry of PAQ films: a) three electrode system, b) two electrode system (counter electrode = PP film). Electrolyte, 0.1 M TEAP/CH_3CN; scan rate, 20 mV/s; initial oxidation state of PP, 0.005+.

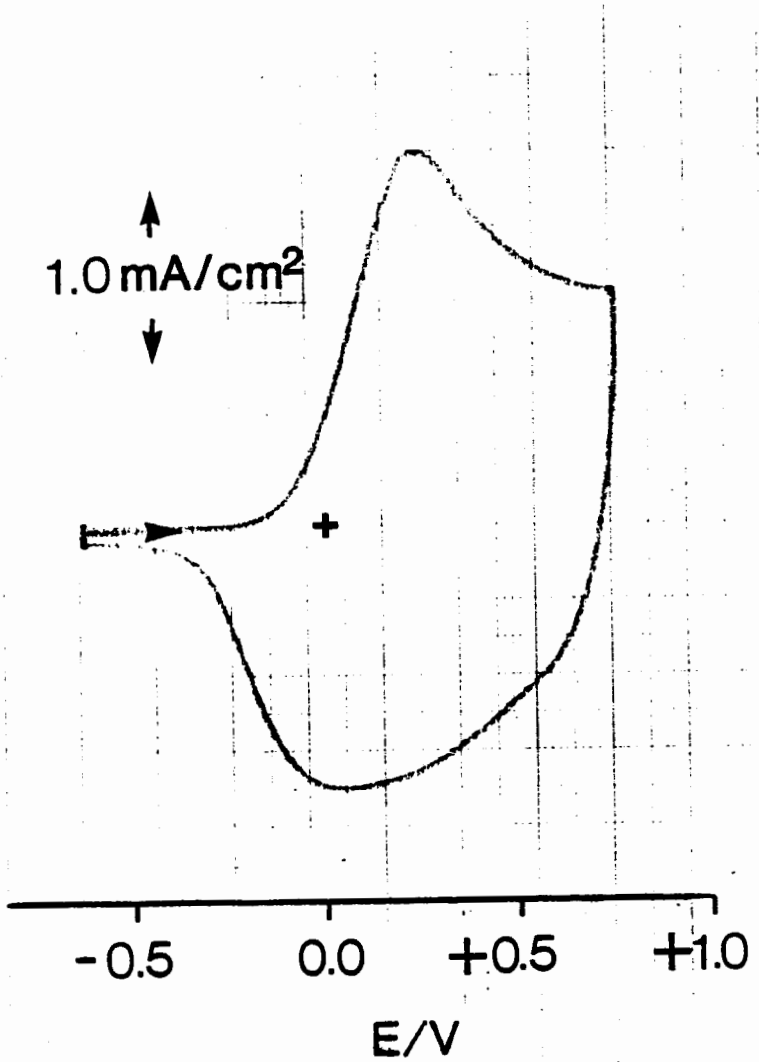

Figure 46. Cyclic voltammetry of PP films. Electrolyte, 0.1 M TEAP/CH_3CN; scan rate, 50 mV/s.

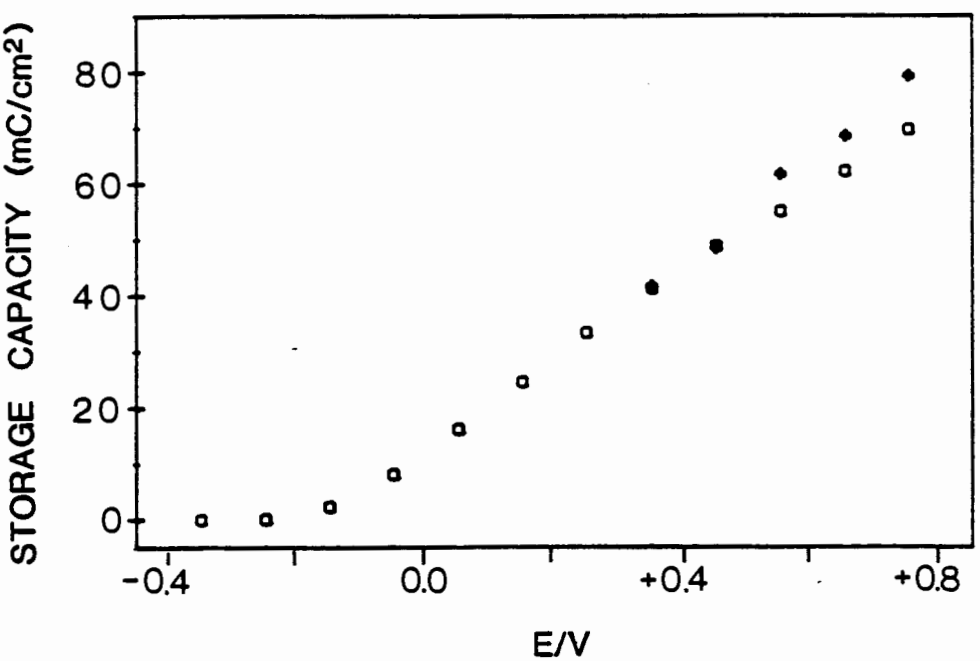

Figure 47. Chronocoulometric determination of the storage capacity of PP as a function of applied potential: □) single electrode used for all data points, +) fresh film used for each data point. Electrolyte, 0.1 M TEAP/CH_3CN; initial potential, -0.55 V.

above +0.5 V as observed by the data obtained from a single PP film. Here, the same film was used for all chronocoulometric measurements, beginning with the smallest potential step and continuing with increasingly larger potential steps. When freshly prepared PP films were used to obtain each data point a linear relationship was observed.

PP films possess excellent charge memory characteristics: When the external voltage is removed, the film exhibits a free standing potential equivalent to that initially applied. The memory effect lasts for extremely long periods and is attributed to the stability of oxidised PP films.

The chronocoulometric data were used to calculate the mass of PP deposited and the concentration of dopant at any given potential. PP films prepared using the conditions described in the experimental section developed a free standing potential of +0.59 $\pm$0.015 V (SCE). The cathodic charge required to completely reduce a freshly formed film, Q_{ox}, was 62.2 mC/cm^2. The surface coverage of PP, estimated from $\Gamma = Q_{form}/2F$, was 3.11x10^{-6} mol/cm^2, based on the pyrrole unit. Tentatively assigning a PP density of 1.5 g/cm^3 gives an approximate film thickness of 1.8 μm. Q_{ox}, which is 62.2 mC/cm^2, is equivalent to 6.4x10^{-7} mol/cm^2 of ClO_4^-. Combining Γ_{pp} and $\Gamma_{perchlorate}$ yields a doping level of 21 mol%. In a similar manner, the dopant concentrations were calculated at various potentials and correlated to the free standing potential of PP films (Figure 48).

III.3.2. Pt/PAQ//PP/Pt RECHARGEABLE CELLS

In conventional three electrode voltammetry, AQ groups in PAQ films can be reversibly reduced to form radical anions, $AQ^{\cdot}$, and dianions, AQ^{2-}, with concurrent oxidation of the solvent at the counter electrode. When a two electrode system is employed, in which the second electrode is a PP film,

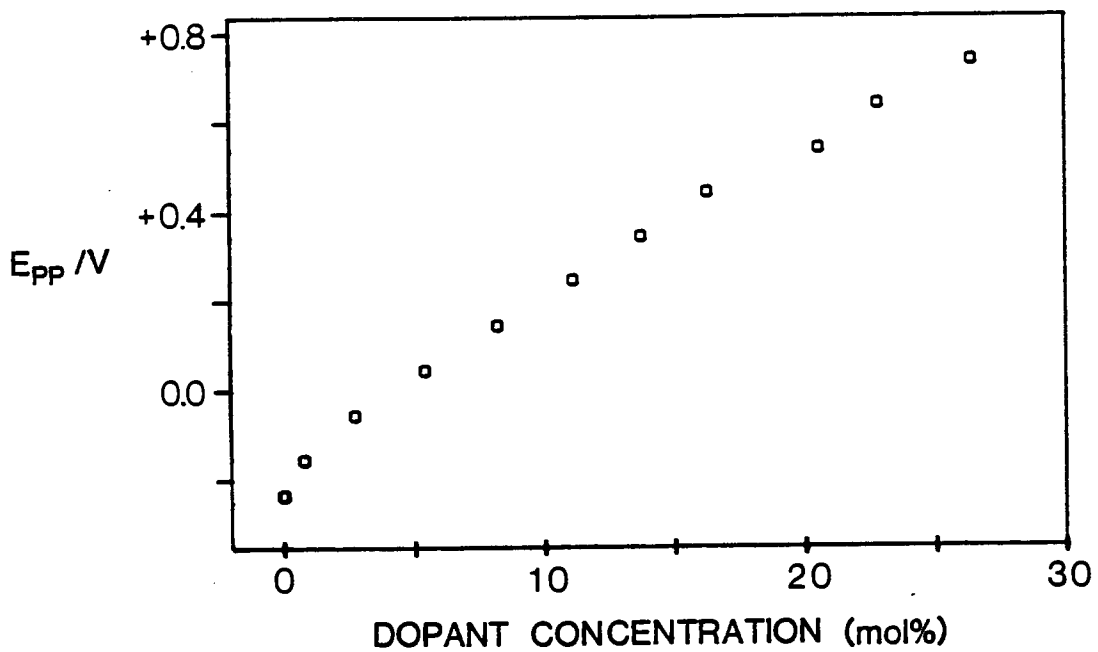

Figure 48. Free standing potential of PP as a function of ClO_4^- dopant concentration.

reduction of PAQ is accompanied by simultaneous oxidation of PP. Figure 49 shows a schematic representation of a cell constructed with PAQ and PP coated electrodes. The cell notation is given by Pt/PAQ//PP/Pt. The cyclic voltammetry of this cell is shown in Figure 45b. The shift in peak potentials and smoothing of peaks associated with the reduction of PAQ is a result of the simultaneous change in oxidation state of PP. The free standing potential of the PP film increases from the initial value of +0.05 V (= 5% doping) to +0.31 V (= 13% doping) when PAQ is reduced to the $P(AQ^{\cdot})$ state, and to +0.68 V (= 24% doping) when reduced to the $P(AQ^{2\cdot})$ state.

The simultaneous reduction of PAQ and oxidation of PP can be considered as the charging cycle in a rechargeable cell. These electrodes release the stored energy and revert back to their original forms when short circuited. The stoichiometry of the electrochemical discharge reactions are given below, where $(AQ)_x$ = PAQ and $(C_4H_3N)_x$ = PP.

When PAQ is charged to the $P(AQ^{\cdot})$ state, the anodic discharge reaction is:

$$(y-0.05)[(AQ^{\cdot})Et_4N^{+}]_x \text{ ---> } (y-0.05)(AQ)_x + x(y-0.05)Et_4N^{+} + x(y-0.05)e^{-} \quad (63)$$

and the cathodic discharge reaction is:

$$[(C_4H_3N)^{y+}(ClO_4^{-})_y]_x + x(y-0.05)e^{-} \text{ ---> } [(C_4H_3N)^{0.05+}(ClO_4^{-})_{0.05}]_x + x(y-0.05)ClO_4^{-} \quad (64)$$

The net discharge reaction is:

$$(y-0.05)[(AQ^{\cdot})Et_4N^{+}]_x + [(C_4H_3N)^{y+}(ClO_4^{-})_y]_x \text{ ---> } (y-0.05)(AQ)_x + [(C_4H_3N)^{0.05+}(ClO_4^{-})_{0.05}]_x + x(y-0.05)Et_4NClO_4 \quad (65)$$

When PAQ is charged to the $P(AQ^{2\cdot})$ state, the discharge cycle occurs via two, one-electron steps. The first discharge process is associated with the

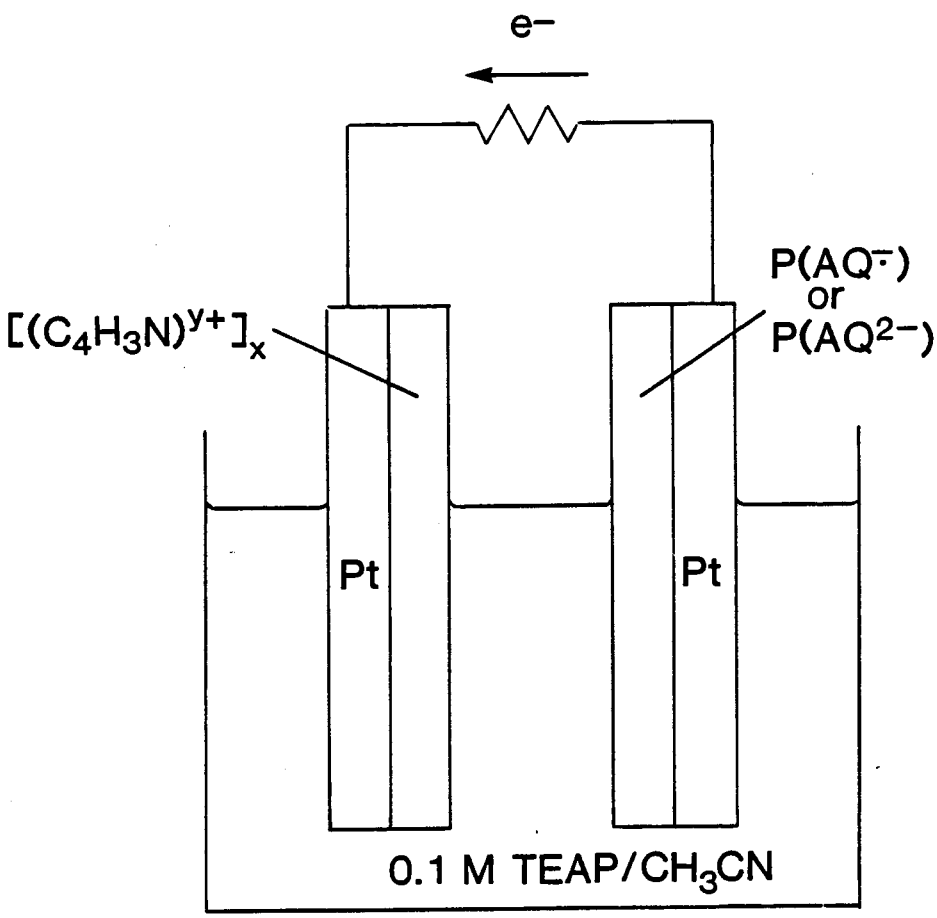

Figure 49. Schematic representation of the Pt/PAQ//PP/Pt cell.

oxidation of $P(AQ^{2\cdot})$ to $P(AQ^{\cdot})$ and the accompanying change in doping level of PP. At the anode:

$$(y-z)[(AQ^{2\cdot})(Et_4N^+)_2]_x \text{ ---> } (y-z)[(AQ^{\cdot})Et_4N^+]_x + x(y-z)Et_4N^+ + x(y-z)e^- \quad (66)$$

At the cathode:

$$[(C_4H_3N)^{y+}(ClO_4^-)_y]_x + x(y-z)e^- \text{ ---> } [(C_4H_3N)^{z+}(ClO_4^-)_z]_x + x(y-z)ClO_4^- \quad (67)$$

The overall discharge reaction (first step) is:

$$(y-z)[(AQ^{2\cdot})(Et_4N^+)_2]_x + [(C_4H_3N)^{y+}(ClO_4^-)_y]_x \quad (68)$$
$$\text{---> } (y-z)[(AQ^{\cdot})Et_4N^+]_x + [(C_4H_3N)^{z+}(ClO_4^-)_z]_x + x(y-z)Et_4NClO_4$$

The second discharge process is associated with the oxidation of $P(AQ^{\cdot})$ to PAQ. At the anode:

$$(y-z)[(AQ^{\cdot})Et_4N^+]_x \text{ ---> } (y-z)(AQ)_x + x(y-z)Et_4N^+ + x(y-z)e^- \quad (69)$$

At the cathode:

$$[(C_4H_3N)^{z+}(ClO_4^-)_z]_x + x(z-0.05)e^- \text{ ---> } [(C_4H_3N)^{0.05+}(ClO_4^-)_{0.05}]_x + x(z-0.05)ClO_4^- \quad (70)$$

Since $(y-z) = (z-0.05)$, the overall discharge reaction for the second discharge cycle is given by:

$$(y-z)[(AQ^{\cdot})Et_4N^+]_x + [(C_4H_3N)^{z+}(ClO_4^-)_z]_x \quad (71)$$
$$\text{---> } (y-z)(AQ)_x + [(C_4H_3N)^{0.05+}(ClO_4^-)_{0.05}]_x + x(y-z)Et_4NClO_4$$

The Pt/PAQ//PP/Pt cell was charged to varying degrees by an external source. The open circuit potentials of the cell, V_{oc}, and of the individual electrodes are shown in Table 4.

Table 4. Open circuit potentials of Pt/PAQ//PP/Pt cells

$E_{external}$ V	V_{oc} (PAQ/Pt) V	V_{oc} (PP/Pt) V	Y	V_{oc} (cell) V
1.3	-0.86	+0.31	0.13	1.17
2.1	-1.35	+0.68	0.24	2.03

The voltage-time curves obtained when these cells are discharged through a given resistance are shown in Figure 50 The curves associated with the discharge of P($AQ^{\cdot}$) are shown in Figure 50a. The coulombic efficiences for the charge/ discharge cycle are 90.5, 96.7 and 95.5% for discharge through resistances of 100, 50 and 25 kΩ respectively. The curve 50b illustrates the discharge behaviour when the anode is charged to P($AQ^{2\cdot}$) state. A double plateau is obtained, evidence of the two one-electron discharge process. The coulombic efficiency is 89% when discharged through a 100 kΩ resistance. The cells were found to be stable for long periods of time. 25 charge/discharge cycles did not affect the charge storage capabilities of the cell. Since the PAQ film is stable for extremely long periods of time, any loss of storage is expected to arise from irreversible oxidation of PP.

The theoretical electricity storage densities of PAQ, based on the molecular weight of the repeat unit and on the mass of the charge balancing counter ion, are 46 and 75 Ahr/kg when reduced to P($AQ^{\cdot}$) and P($AQ^{2\cdot}$) respectively. The ESD derived from experimental data is significantly lower, 10 and 12 Ahr/kg. The ESD of $[(C_4H_3N)^{y+}(ClO_4^{-})_y]_x$ is a function of the extent of doping y. y was estimated as 0.13 and 0.24 (Table 4) when PAQ is reduced to P($AQ^{\cdot}$) and P($AQ^{2\cdot}$) respectively. These values yield electricity storage densities of 45 and 70 Ahr/kg for the PP film.

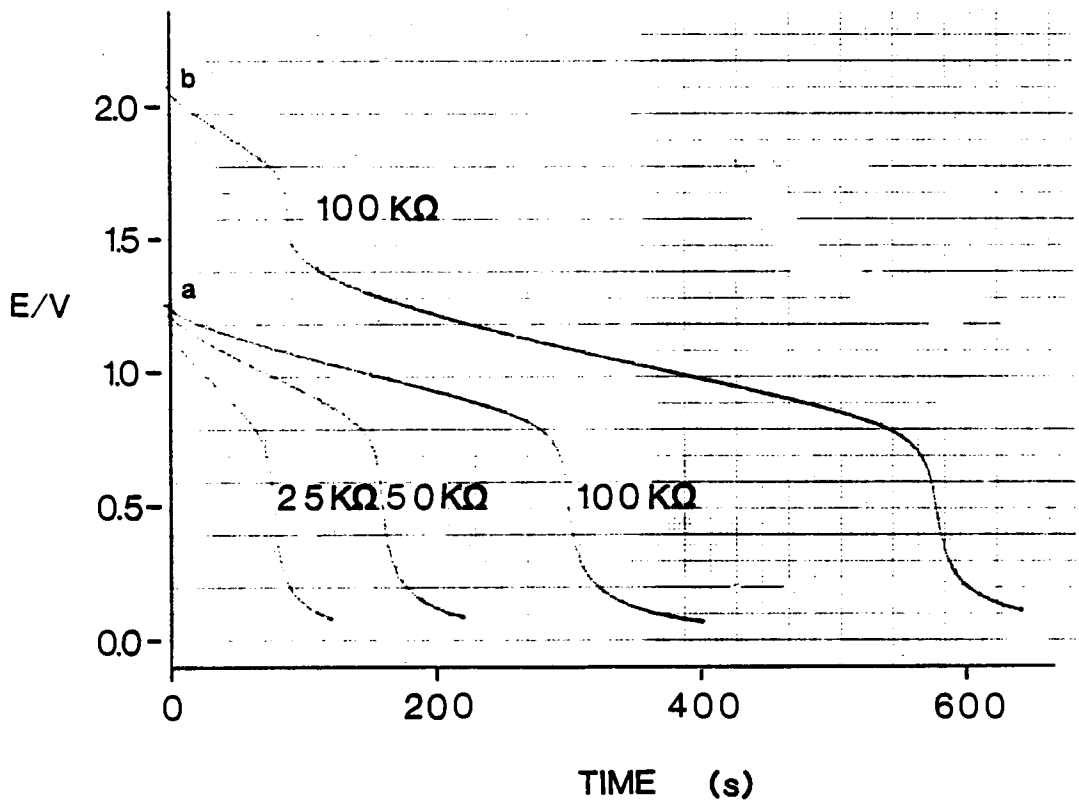

Figure 50. Voltage-time discharge curves for Pt/PAQ//PP/Pt cells: a) $P(AQ^{\cdot})/PP^{y+}$, b) $P(AQ^{2\cdot})/PP^{y+}$. The external resistance of the cell is given in bold type. Electrolyte, 0.1 M TEAP/CH_3CN; electrode areas, 0.18 cm^2.

The experimental ESD of the cell includes the masses of both polymer films. ESD_{cell} values are 7 and 14 Ahr/kg, from which, energy densities of 8.4 and 28 Whr/kg were calculated. The experimental ESD and ED values for the cell are very much lower than those reported for other polymer based systems (Section III.1.3.). This is a consequence of poor electron propagation through thick PAQ films. As shown previously, only 18% of the PAQ film is electroactive. The magnitude of the ESD and ED can be dramatically increased by complete reduction of the PAQ film. The electricity storage density of the cell would theoretically increase to 58 and 78 Ahr/kg since an increase in the number of AQ groups reduced produces a corresponding increase in the oxidation state of the PP film. As a result, the energy density of the cell increases to theoretical values of 99 and 171 Whr/kg. The values are comparable to, or larger than, those values reported for cells based on other polymeric materials.

It is appropriate to use the condition of 100% reduction of the PAQ film to exemplify the charge storage properties of redox polymer films. PAQ is not a suitable material for the design of high energy storage cells due to the poor charge storage capacity. It is evident however, that with correct choice of redox polymer, a rechargeable cell of greater or comparable energy density to polyacetylene cells can be achieved. The advantage of redox polymer systems lies in the extensive choice of redox couple and polymer backbone, and in the diversity of film forming techniques.

The major problem with these systems is, at present, the limitation of film thickness and the consequent low storage capacity. In this aspect, conductive polymers are much superior to redox polymers. It is evident that the polymer chains in thick films lack flexibility for site-site collision. Electronic accessiblity of redox sites can be improved substantially by incorporating the electroactive unit into a conductive martrix. Bidan and

coworkers have recently reported the preparation of conducting PP films incorporating electroactive redox centres of Ru, ferrocene, paraquat, nitro-oxides and 9,10-anthraquinone[192,193]. These films have not yet been examined as charge storage media.

The volumetric energy density of all polymer based cells are obviously smaller than conventional battery systems since organic polymers are less dense than metallic or inorganic materials. On a mass basis however, energy densities may be comparable. In addition, the absence of mechanical changes (e.g. dissolution and redeposition processes) associated with conventional cells, is expected to promote longer life for polymer based cells.

III.3.3. p-SEMICONDUCTOR/PAQ//PP/Pt RECHARGEABLE CELLS

There is current interest in the conversion and storage of solar energy using semiconductor based PEC cells. With the correct matching of redox couple and semiconductor energy levels, it is possible to utilise solar radiation to drive electrochemical reactions thermodynamically "uphill". In this section the properties of a novel rechargeable cell using PAQ coated p-type semiconductor electrodes and PP coated Pt electrodes are reported. The difference between these and conventional PEC cells is that for the latter, photogenerated current ceases when the irradiating source is removed; unlike the former, in which dark current will flow in the reverse direction when the light source is removed.

For these studies, p-Si and p-InP semiconductors were used. The flat band potentials of p-Si and p-InP in 0.1 M TEAP/CH_3CN were estimated to be +0.05 V and -0.05 V from impedance measurements. Estimations of the redox energy levels of PAQ and the various oxidation states of PP allows construction of the schematic energy diagram shown in Figure 51. The energy

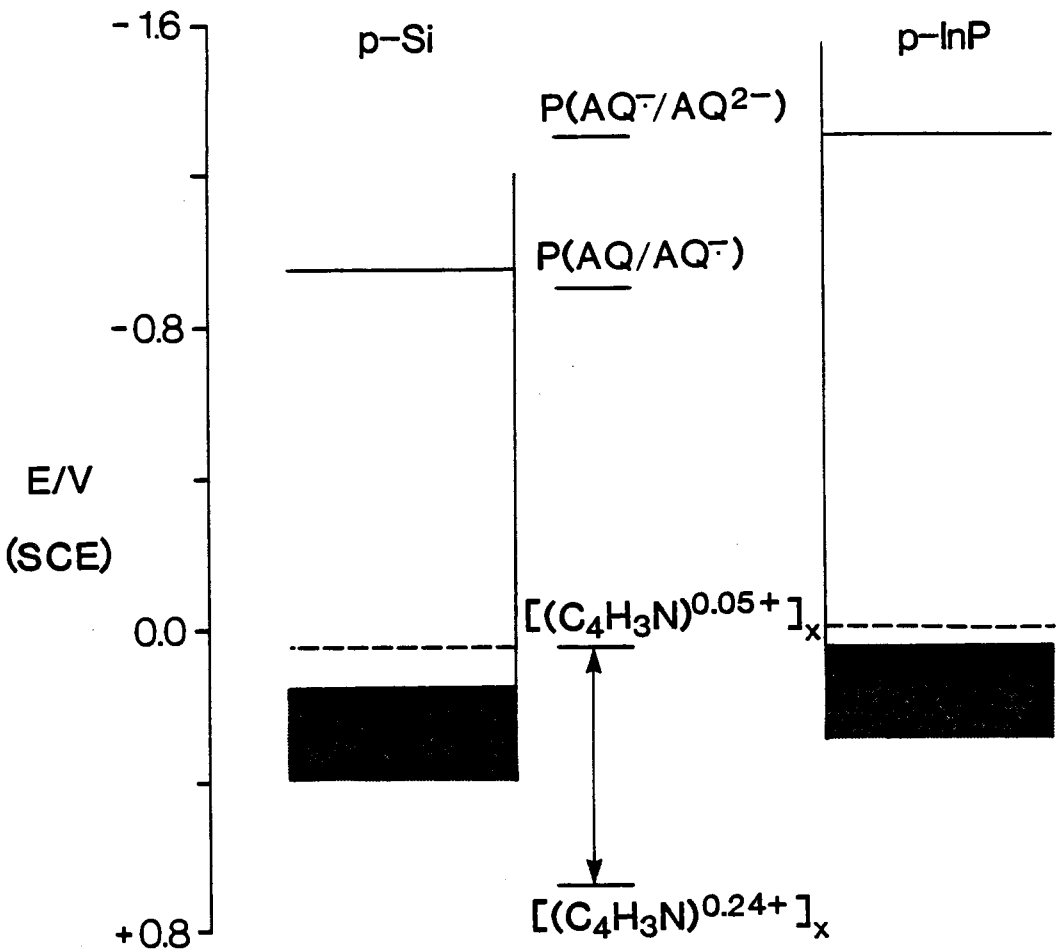

Figure 51. Energy level diagram for p-SC/PAQ//PP/Pt cells.

level of the P(AQ/AQ$^{\cdot}$) couple is similar to the conduction band energy level of p-Si and is below that of p-InP.

The cyclic voltammetry of PAQ films coated on p-Si and p-InP electrodes under illumination and using the conventional three electrode system are shown in Figures 52a and 52c respectively. In the absence of irradiation, negligible current flow was observed until extreme negative potentials are applied. The onset of cathodic photocurrent, associated with the reduction of PAQ at p-Si, occurs at -0.55 V (SCE) but the peak current is not observed until -1.1 V. This suggests that the redox energy level of PAQ is above the conduction band, and not within the band gap region as anticipated. The voltammetric waveshape remained constant for many potential cycles, in contrast to that obtained in DMSO. The stability of PAQ coated Si electrodes is attributed to the presence of activated alumina in solution which diminishes the effect of trace water. The onset and peak potential associated with the reduction of PAQ at illuminated p-InP electrodes are -0.5 V and -0.9 V respectively, indicative of a system in which the energy of redox couple lies within the band gap region.

The corresponding voltammograms obtained when the counter and reference electrode terminals of the potentiostat are attached to a PP coated Pt electrode are shown in Figure 52b and 52d.

The charging processes of the polymer films are essentially the same as that previously described except that reduction of PAQ occurs via conduction band electrons. The open circuit potential of the cell, and of the individual electrodes are shown in Table 5 and 6.

It is evident from Table 5, that the reduction of PAQ is not photoassisted by the illumination of p-Si electrodes. The reduction may however, be driven uphill by illumnated p-InP electrodes, albeit to a small degree. The photovoltage generated by the p-InP/PAQ electrode is much lower

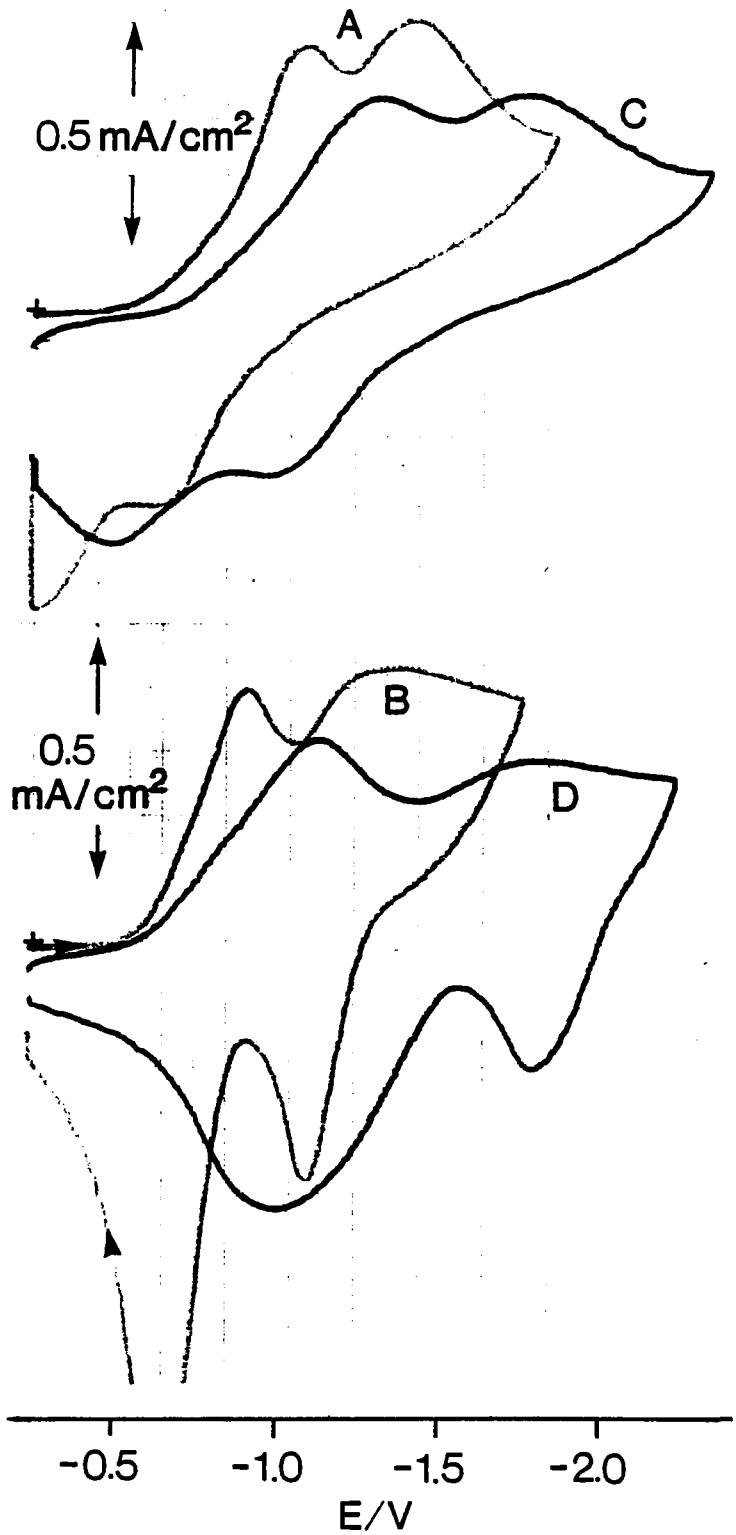

Figure 52. Cyclic voltammetry of: a) PAQ coated p-Si, b) PAQ coated p-InP, c) p-Si/PAQ//PP/Pt cell, d) p-InP/PAQ//PP/Pt cell. Electrolyte, 0.1 M TEAP/CH_3CN; scan rate, 20 mV/s. Electrode areas: p-Si = 0.139 cm^2, p-InP = 0.296 cm^2.

than that theoretically calculated by $|V_{fb}-V_{redox}|$, 0.85 V. The most likely reason for the low value is the injection of electrons from $P(AQ^{\cdot-})$ and $P(AQ^{2\cdot-})$ into InP surface states, leading to Fermi level pinning and constant band bending. This is supported by the fact that the generated photovoltage remains constant at ≈0.2 V.

Table 5. Open circuit potentials of p-Si/PAQ//PP/Pt cells

$E_{external}$ V	V_{oc} (PAQ/Si) V	V_{oc} (PP/Pt) V	Y	V_{oc} (cell) V
1.4	-1.02	+0.24	0.105	1.26
1.4 (25 cycles)	-0.95	+0.26	0.115	1.21
1.9	-1.17	+0.42	0.155	1.59

Table 6. Open circuit potentials of p-InP/PAQ//PP/Pt cells

$E_{external}$ V	V_{oc} (PAQ/InP) V	V_{oc} (PP/Pt) V	Y	V_{oc} (cell) V
0.95	-0.81	+0.36	0.145	1.17
1.3	-0.88	+0.50	0.165	1.38
1.3 (25 cycles)	-0.87	+0.59	0.21	1.46
1.55	-0.95	+0.64	0.22	1.59
1.9	-1.25	+0.84	0.31	2.09

The discharge curves for these cells through a 100 KΩ resistance are shown in Figure 53. Coulombic efficiencies were 80-88% for p-Si electrodes and 82-90% for p-InP electrodes.

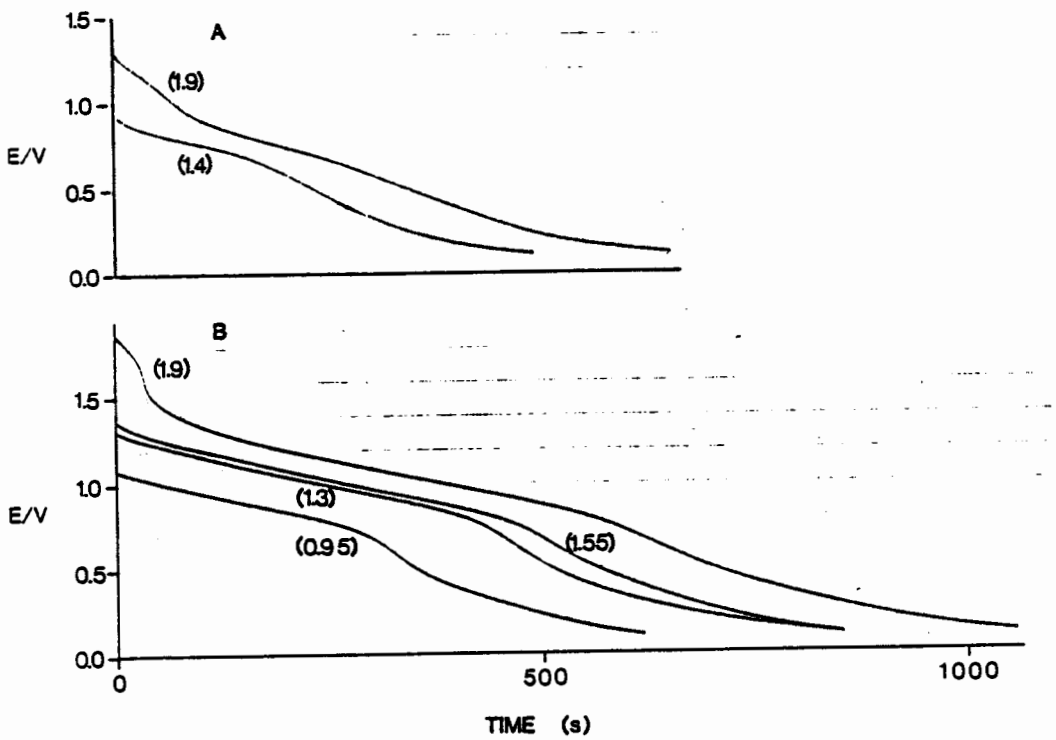

Figure 53. Voltage-time discharge curves for p-SC/PAQ//PP/Pt cells: a) SC = Si, b) SC = InP. The external voltages used for cell charging are given in brackets. Electrolyte, 0.1 M TEAP/CH_3CN. Electrode areas: p-Si = 0.139 cm^2, p-InP = 0.296 cm^2, Pt = 0.18 cm^2.

III.4. CONCLUSION

Electroactive redox polymers can conceivably store large quantities of electrical charge, which in favourable conditions, can be released to do useful work. The choice of redox couple determines the cell voltage, while the polymer backbone, solvent and electrolyte determine the stability of the films and the rate at which the energy can be released. The main problem lies in the limitation of film thickness and number of useful electroactive sites. Such problems may be overcome by incorporating the redox couple in a permeable conductive matrix.

Polypyrrole, unlike PAQ, exhibits a charge storage capacity which is linearly dependent on potential. When coupled with a redox polymer coated electrode, rechargeable cells of relatively high energy density may be obtained.

The charging cycle may be photoassisted by employing illuminated semiconductor electrodes. For maximum efficiency of solar conversion and storage, the energy level of the redox couple must be located just below the conduction band, or just above the valence band, for p- and n-type semiconductors respectively. The selection of suitable PEC systems is limited by the small number of available electroactive redox polymers. In this aspect, conductive polymeric films are promising, since their oxidation state or doping level changes as a function of potential and can therefore, be adjusted to suit the semiconductor energy levels.

CHAPTER IV

THE ENERGETICS OF ELECTRON TRANSFER AT THE POLYPYRROLE/SILICON INTERFACE

IV.1. INTRODUCTION

IV.1.1. ELECTROCHEMISTRY WITH SILICON ELECTRODES

Silicon is one of the most widely studied of semiconducting materials. It is used extensively in solid state voltaic cells and is attractive for use in PEC cells. However, in the presence of water, the Si electrode is rapidly corroded. The use of water-free organic solvents allow simple electrochemical processes to be investigated without the deleterious effects of oxide formation.

The flat band potential of p-type Si in CH_3CN, using a variety of supporting electrolytes, is consistently reported to be in the region +0.20 - +0.05 V (SCE)[159-165]. V_{fb} values for n-type Si are not so consistent. Reported values include -0.28, -0.11 and -0.9 V[159-161].

In the presence of redox couples, the band edges of Si become unpinned. A number of groups have observed constant V_{oc} values for p-Si electrodes in contact with redox couples which span a potential range much larger than the semiconductor band gap (Table 7)[194,195]. The data can be explained by Fermi level pinning[77].

Fermi level pinning of p-Si has been verified by the variation of V_{fb} in the presence of different redox couples[162]. Flat band potentials were determined using a Mott-Schottky analysis of capacitance-voltage data. Fermi level pinning of n-type Si has also been reported[160,166]. This group reports

that the barrier height (V_{redox}-V_{CB}) increases with time to values of ≈0.7 V (V_{oc}=0.5). Oxide formation yielding interface states and Fermi level pinning is the proposed mechanism.

Table 7. V_{oc} values for p-Si electrodes in contact with various redox couples

REDOX COUPLE	E^0 (SCE)	V_{oc} (V)
$AQ^{0/\cdot}$	-0.74	0.34
$AQ^{\cdot/2\cdot}$	-1.46	0.30
$PQ^{2+/+}$	-0.45	0.39
$PQ^{+/0}$	-0.85	0.42
$Ru(bpy)_3^{2+/+}$	-1.30	0.42
$Ru(bpy)_3^{+/0}$	-1.49	0.42
$Ru(bpy)_3^{0/\cdot}$	-1.73	0.38

Where PQ=N,N'-dimethyl-4,4'-bipyridium and bpy=2,2'-bipyridine.

IV.1.2. POLYPYRROLE COATED SILICON ELECTRODES

There has been active interest in coating silicon semiconductor electrodes with films of polypyrrole. Such films, on n-Si electrodes, have been shown to enhance the stability of the semiconductor in aqueous electrolytes[24,25,196-201]. PP films are porous to solvent and electrolyte and undergo electron transfer reactions with species in solution. However, the films are unstable to oxidative potentials above +0.6 V (SCE) in aqueous media[202]. Furthermore, PEC cells employing PP coated semiconductors exhibit photovoltages significantly lower than theoretically calculated.

There have been many reports concerning the enhanced lifetime of PP based PEC cells, but detailed studies on the PP/Si interface have escaped attention. The objective of this study was to determine the effect of PP films on the conduction and valence band edges of n- and p-type silicon electrodes. The influence of a redox couple in solution on the oxidation state of PP, and on the flat band potentials of Si and Si/PP electrodes, is also investigated. The effect of underlying layers of Pt between the semiconductor and PP film is discussed: Pt underlayers have been shown to increase the stability of PP based PEC cells[197,199,203].

IV.2. EXPERIMENTAL

IV.2.1. CHEMICALS

CH_3CN, TEAP and pyrrole were purified as described in Section III.2.1.. Ferrocene (Aldrich) was used as received.

IV.2.2. FILM PREPARATION

Polypyrrole films were electrodeposited from 0.5 M pyrrole in 0.1 M TEAP/CH_3CN using the following potentials: a) Pt, +0.95 V; b) p-Si, +0.95 V; c) n-Si + illumination, +0.5 V. Electrolysis was continued until ≈100 mC/cm^2 of anodic charge had passed.

The platinisation of semiconductors was acheived by the electrochemical reduction $PtCl_6^{2-}$ in 0.1 M KCl/1mM K_2Pt_6 (Johnson Matthey). Approximately 20 mC/cm^2 of cathodic charge was passed.

IV.2.3. ELECTROCHEMISTRY

The preparation of Pt and Si working electrodes has been described in Section II.2.3.. The electrolyte, electrochemical cell and equipment have been described in Section III.2.3.. The equipment employed for impedance measurements has been described in Section II.2.3..

The electrochemical potential of PP, E_{PP}, coated on Pt and Si semiconductors, was varied by the passage of cathodic or anodic charge, and evaluated by measuring the electrode Fermi energy against the SCE reference electrode with a Keithley 610C electrometer. The electrochemical potential of solutions containing ferrocene were varied by changing the [ferrocenium]

/[ferrocene] ratio. All potentials are reported relative to the SCE.

Illumination was provided by a 200 W mercury lamp (Illumination Industries Inc. Model LH371Q). UV irradiation was passed through a cut off filter (<550 nm cut off) and the intensity was controlled by neutral density filters (Oriel).

IV.3. RESULTS AND DISCUSSION

The capacitance-voltage curves for n- and p-type Si in 0.1 M TEAP/CH_3CN are shown in Figures 54 and 55 respectively. The corresponding Mott-Schottky plots are shown in Figure 56. The C-V data show a plateau for the n-type electrode, indicating the presence of surface or interface states. As expected, the effect of the surface states is pronounced at lower frequencies. Two flat band potentials can be extrapolated from the Mott-Schottky plot, -0.45 and -0.75 V ±0.05 V (SCE).

The C-V plot for p-Si does not show dual slope behaviour as found for n-Si electrodes. However, a strong frequency dependence on capacity is observed, which diminishes at higher frequency. This behaviour is again explained in terms of surface states. The lack of a plateau suggests that a broad distribution of surface states exists. The flat band potential of p-Si in 0.1 M TEAP/CH_3CN was estimated as +0.05 V from the Mott-Schottky plot.

The cyclic voltammetry of PP coated Pt, n-Si and p-Si electrodes are shown in Figure 57. The onset potential for oxidation of PP films at Si semiconductors occurs at a more positive value than anticipated based on the redox, conduction band and valence band energy levels. Similarly, the re-reduction of the oxidised film, which occurs on the reverse scan, also occurs at more positive potentials. These results can be explained by considering changes in the Si CB and VB energy levels accompanying changes in PP oxidation state. The apparent shift in V_{fb}, and thus, E_{CB} and E_{VB}, as a function of the electrochemical potential of PP is verified by C-V measurements on Si/PP electrodes (Figure 58). The correlation between V_{fb} and E_{pp} is illustrated in Figure 59.

The formation of a rectifying junction at the Si/PP interface was investigated by open circuit photovoltage measurements on Si/PP electrodes.

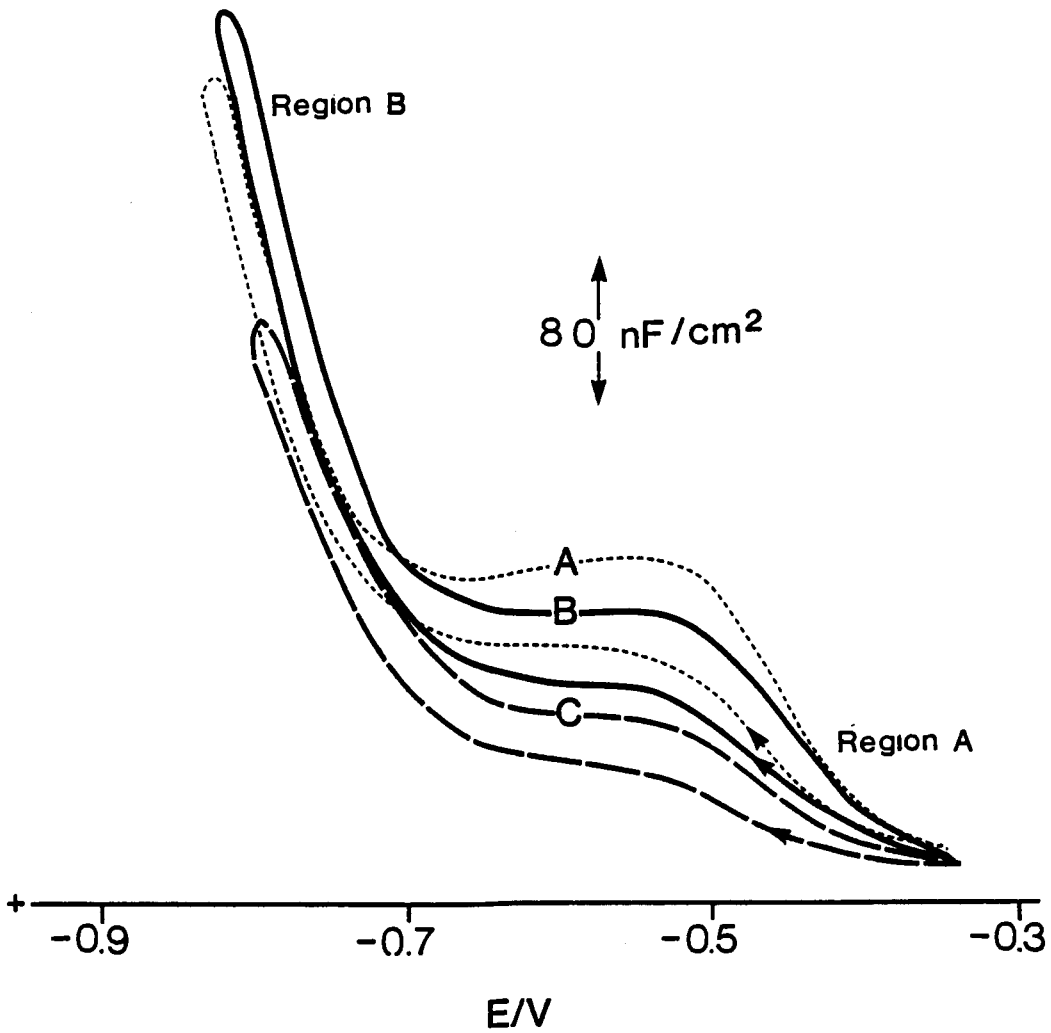

Figure 54. C-V plots for n-Si electrodes: a) 500 Hz, b) 1 KHz, c) 5 KHz. Electrolyte, 0.1 M TEAP/CH_3CN .

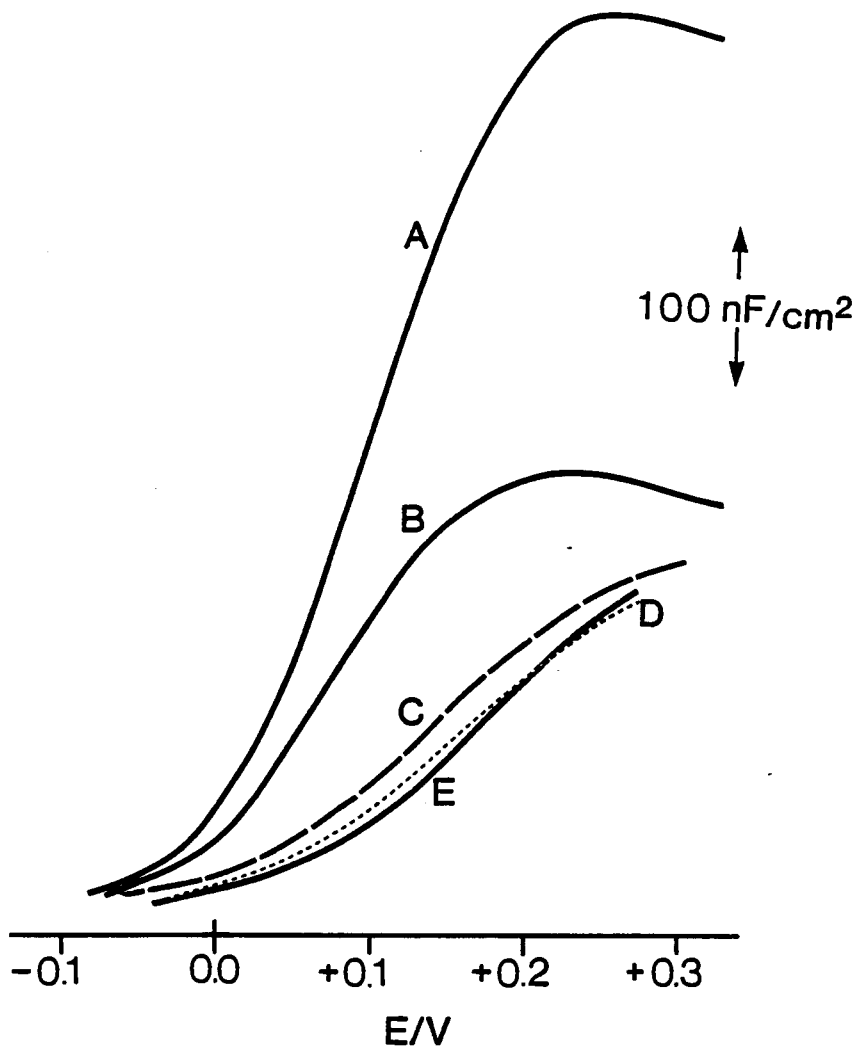

Figure 55. C-V plots for p-Si electrodes: a) 500 Hz, b) 1 KHz, c) 5 KHz, d) 8 KHz, e) 10 KHz. Electrolyte, 0.1 M TEAP/CH_3CN .

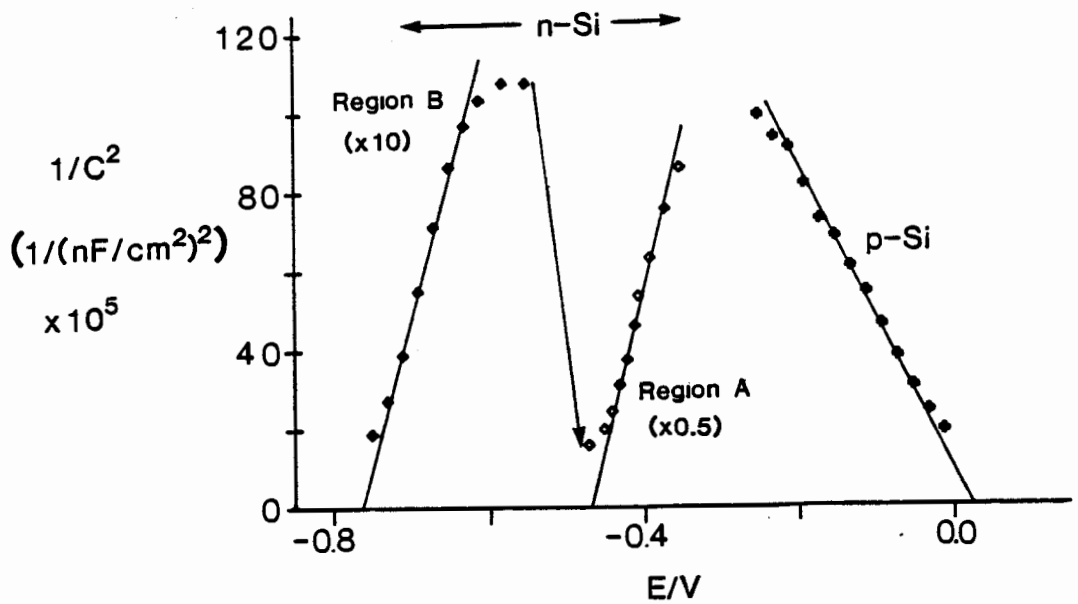

Figure 56. Mott-Schottky plots for Si electrodes in 0.1 M TEAP/CH_3CN. Frequency, 5 KHz.

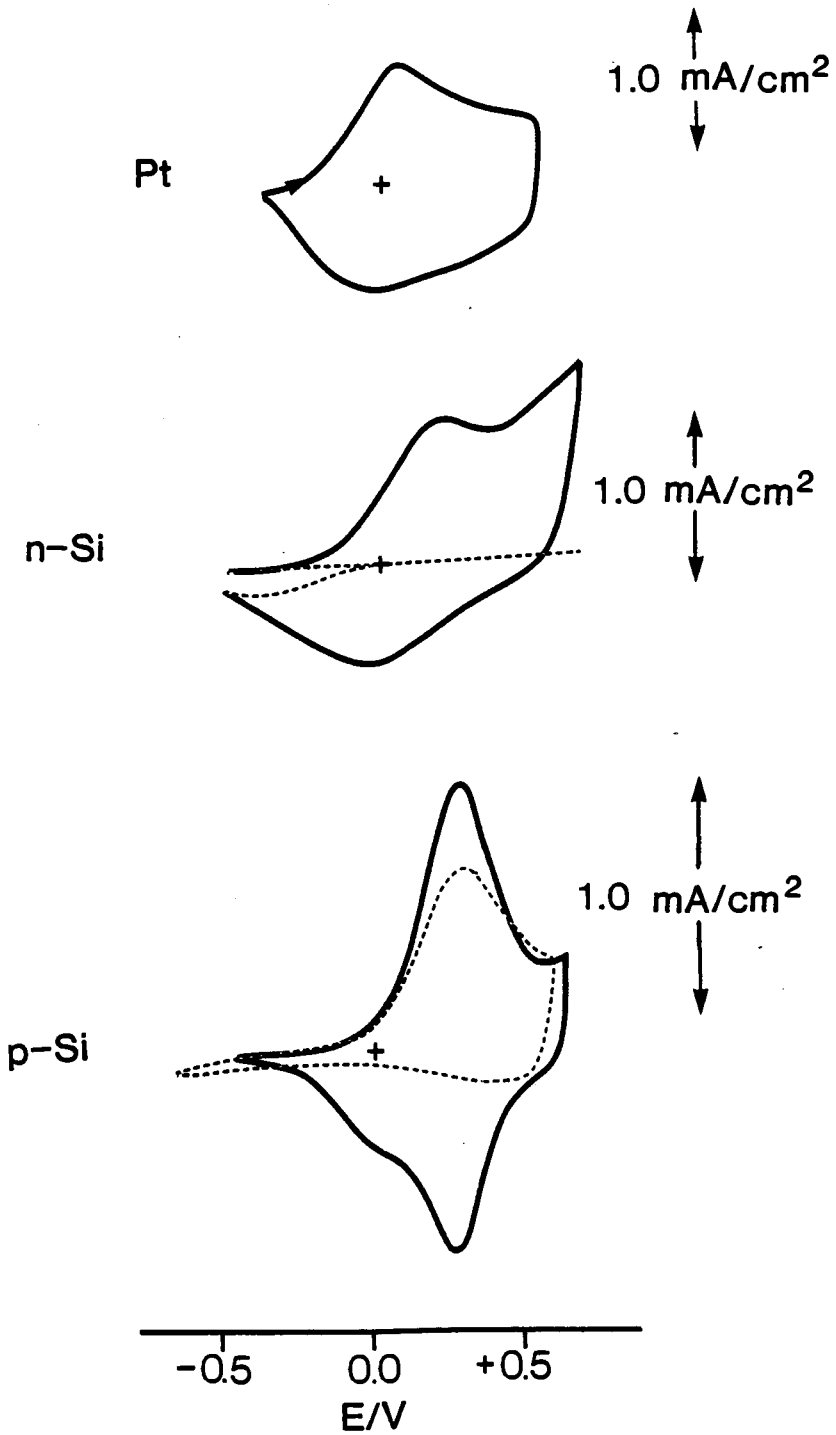

Figure 57. Cyclic voltammetry of PP coated Pt and Si electrodes: (——) illuminated electrode, (----) dark electrode. Electrolyte, 0.1 M TEAP/CH_3CN; scan rate, 50 mV/s.

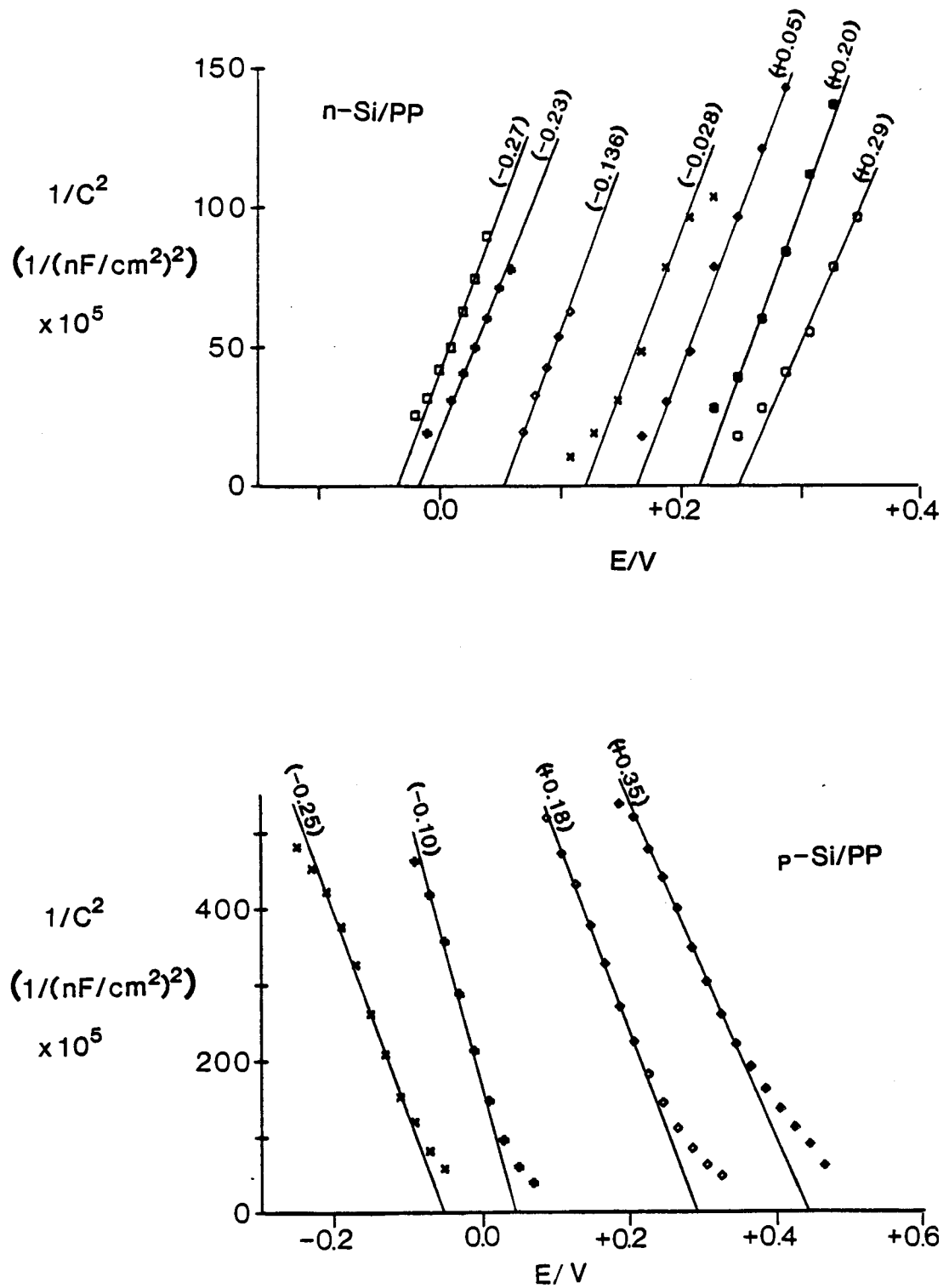

Figure 58. Mott-Schottky plots for Si/PP electrodes with varying E_{pp}: Top) n-Si/PP, Bottom) p-Si/PP. E_{pp} is given in brackets. Electrolyte, 0.1 M TEAP/CH_3CN; frequency, 5 KHz.

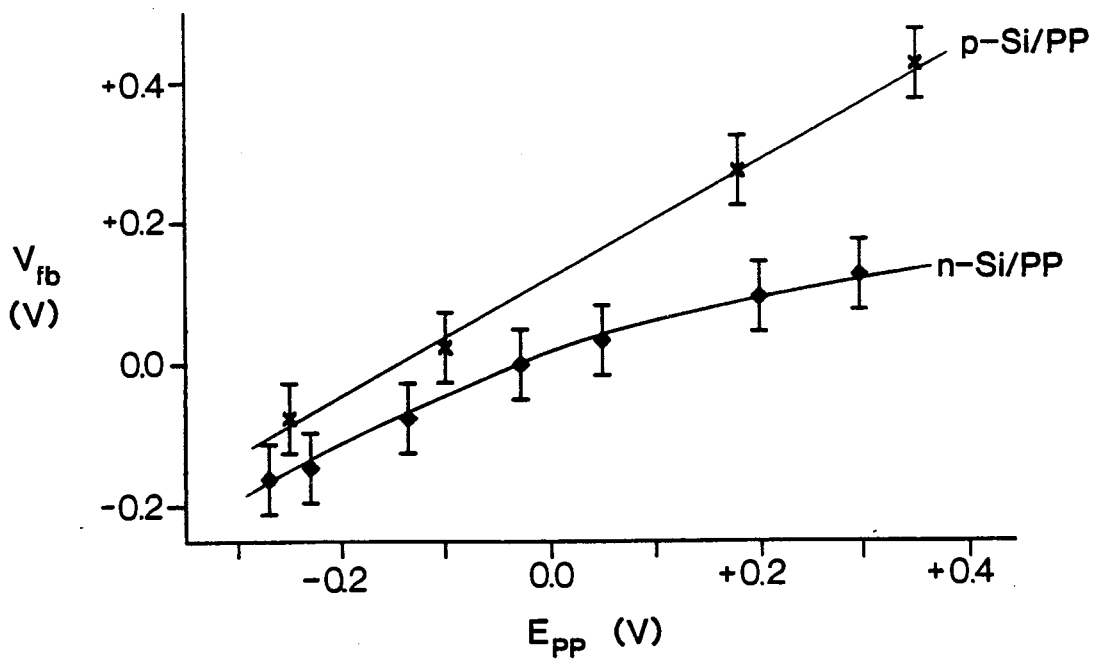

Figure 59. Correlation between the Si flat band potential and the electrochemical potential of PP.

Figure 60 shows a plot of the observed photovoltage as a function of the electrochemical potential of PP. For the n-Si/PP electrode, virtually no photovoltage is observed when E_{pp} is <+0.05 V, suggesting that E_{pp} is more negative than the flat band potential of n-Si. When E_{pp} is more positive than +0.5 V, a constant photovoltage of ≈100 mV is observed. The Fermi level of the semiconductor shifts negatively on the electrochemical scale upon illumination, indicating that a depletion layer was present in the semiconductor prior to illumination.

Semiconductor depletion layers are also evident for p-Si/PP electrodes even when E_{pp} is 500 mV more positive than the flat band potential of bare p-Si. A depletion layer is postulated in this case since the Fermi level of the p-semiconductor moves in a positive direction with respect to the SCE upon illumination.

One of the problems envisioned in these experiments is the varying absorptivity of polypyrrole as a function of oxidation state, and the subsequent effect on the measured photovoltage. This effect was investigated by varying the illumination intensity and measuring the photovoltage generated by p-Si/PP electrodes (Figure 61). The data indicate that with the illumination intensities employed, near-saturated photovoltages are produced.

The effect of redox species in solution on the electrochemical properties of Si and Si/PP electrodes were studied using the ferrocene redox couple ($E_{1/2}$=+0.35 SCE). The ratio of the oxidised and reduced forms determines the electrochemical potential of the solution. The equilibration of PP and the electroactive redox couple was observed by immersing a PP coated Pt electrode in the ferrocene/ferrocenium solution for a short period of time, and monitoring the electrochemical potential of the PP/Pt electrode in pure electrolyte. Figure 62 shows a plot of the E_{pp} versus the electrochemical potential of solution.

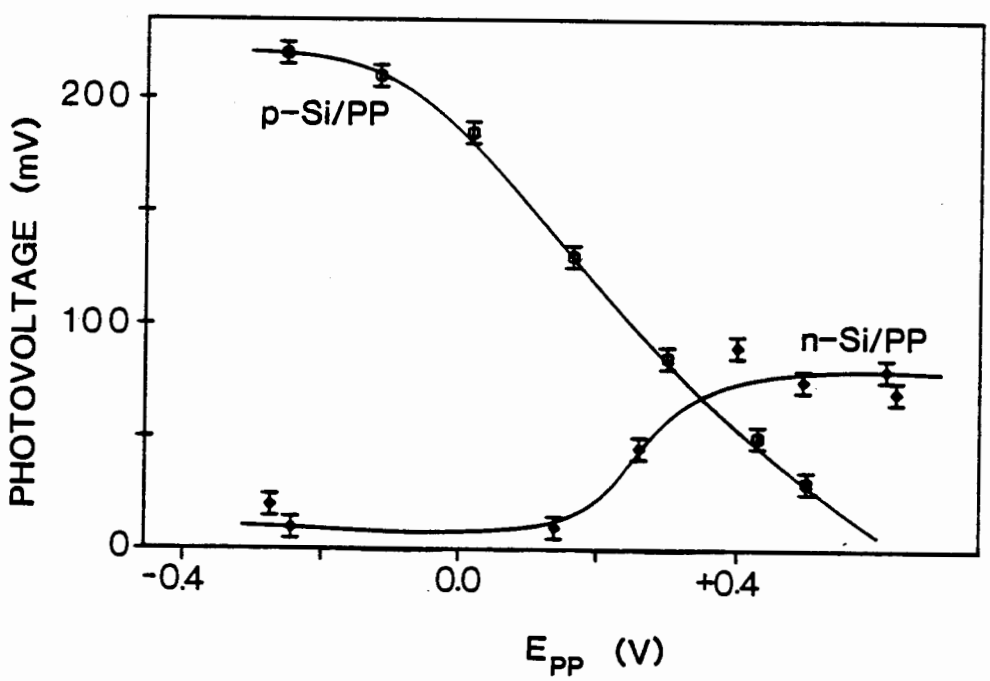

Figure 60. Photovoltage-E_{PP} plot for Si/PP electrodes. Electrolyte, 0.1 M TEAP/CH_3CN; illumination intensity, 80 mW/cm^2.

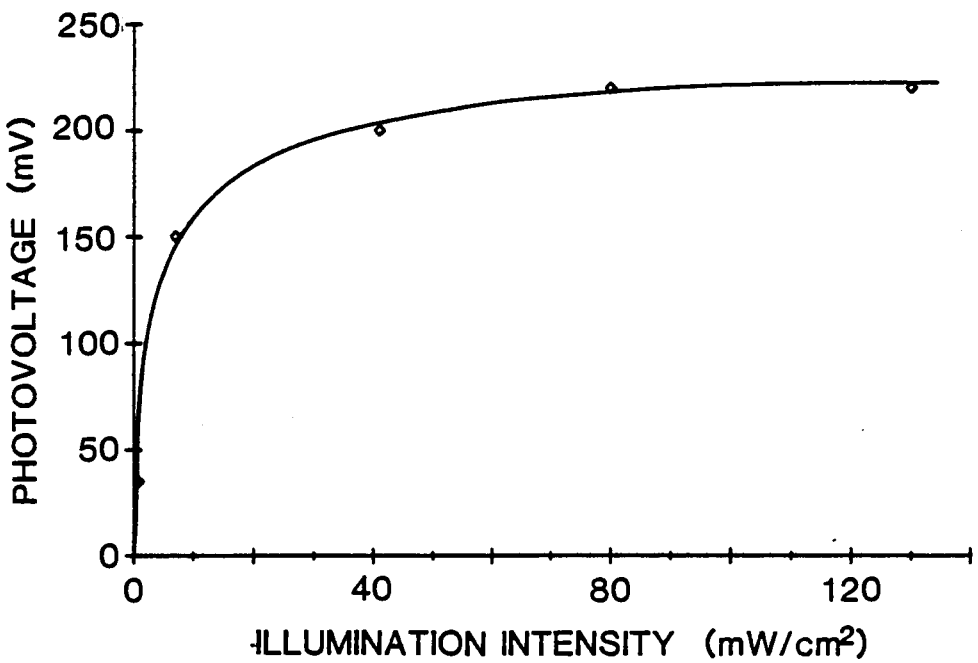

Figure 61. Effect of the illumination intensity on the p-Si/PP photovoltage. Electrolyte, 0.1 M TEAP/CH_3CN; E_{pp} = -0.25 V.

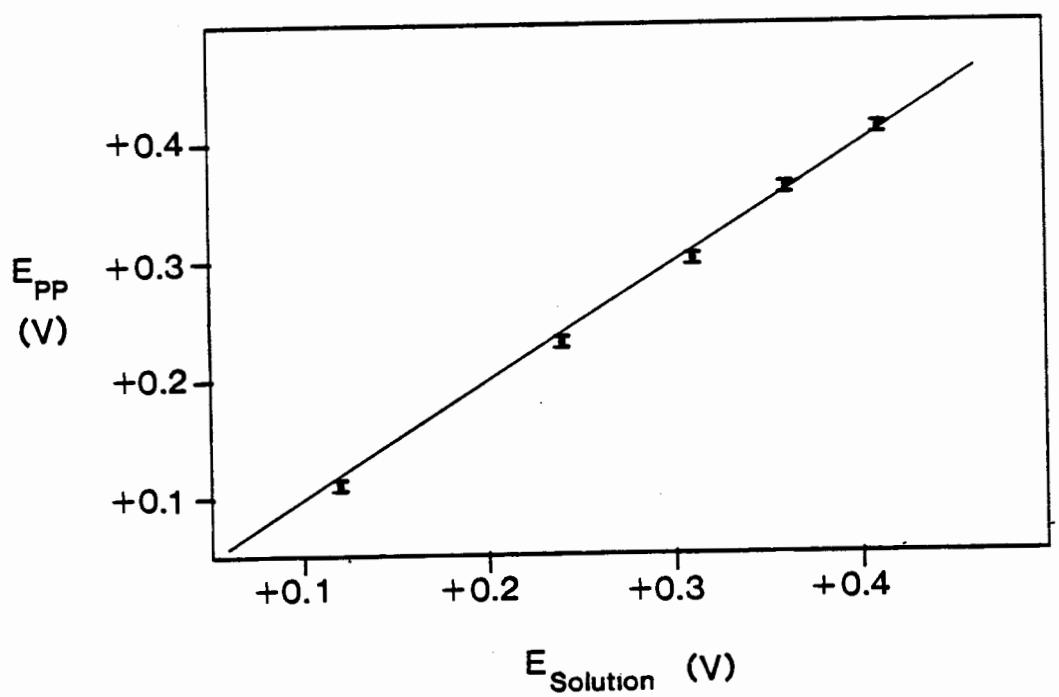

Figure 62. Plot of E_{pp} as a function of the electrochemical potential of solution. Electrolyte, 0.1 M TEAP/CH_3CN; redox couple, ferrocene/ferrocenium (10 mM).

The open circuit photovoltage, V_{ph}, generated by Si and Si/PP electrodes in the presence of ferrocene/ferrocenium are shown in Figure 63. The ratio of the oxidised and reduced forms was adjusted such that the electrochemical potential of the solution and thus, PP were varied. Illumination of n-Si electrodes, both in the presence and absence of a PP film, caused a negative shift of the semiconductor Fermi level (on the electrochemical scale), indicating that a depletion layer exists when the electrode is in the dark. For p-type electrodes, the Fermi level moves to more positive values upon illumination, also indicative of a depletion layer. The results are again explained by unpinning of the band edge energy levels.

Photovoltages were also monitored under pulsed light, in order to determine the instantaneous change in the semiconductor Fermi level. The results obtained by pulsed light experiments were identical to those obtained by equilibrium photovoltage measurements.

The cyclic voltammetry of ferrocene at Pt and Si electrodes are shown in Figure 64. At n-Si electrodes, a small photogenerated anodic current is observed at -0.55 V, with a larger anodic current occuring at an onset potential of $\approx$+0.05 V. The peak potential for ferrocene oxidation at n-Si is negative with respect to that obtained on bare Pt. With p-Si electrodes, anodic current is observed in the dark and under illumination. However, cathodic current is only produced upon illumination, indicating the existence of a rectifying junction.

A detailed study of the i-V characteristics was performed using periodic illumination during the potential cycle. Useful information can be obtained from such experiments by observing the transient anodic and cathodic currents. The voltammetry of ferrocene at p-Si electrodes under chopped light conditions is shown in Figure 65. During the anodic scan, the light pulse produces a transient cathodic current due to the reduction of

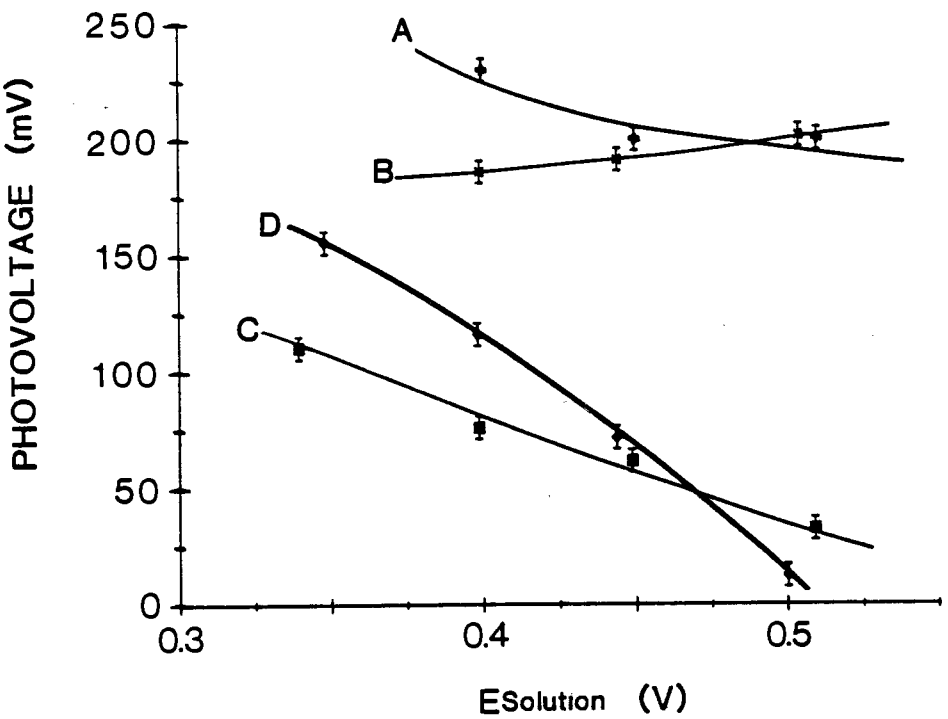

Figure 63. Photovoltage-$E_{solution}$ plots for: a) n-Si, b) n-Si/PP, c) p-Si, d) p-Si/PP electrodes. Electrolyte, 0.1 M TEAP/CH_3CN; illumination intensity, 80 mW/cm^2; redox couple, ferrocene/ferrocenium (10 mM).

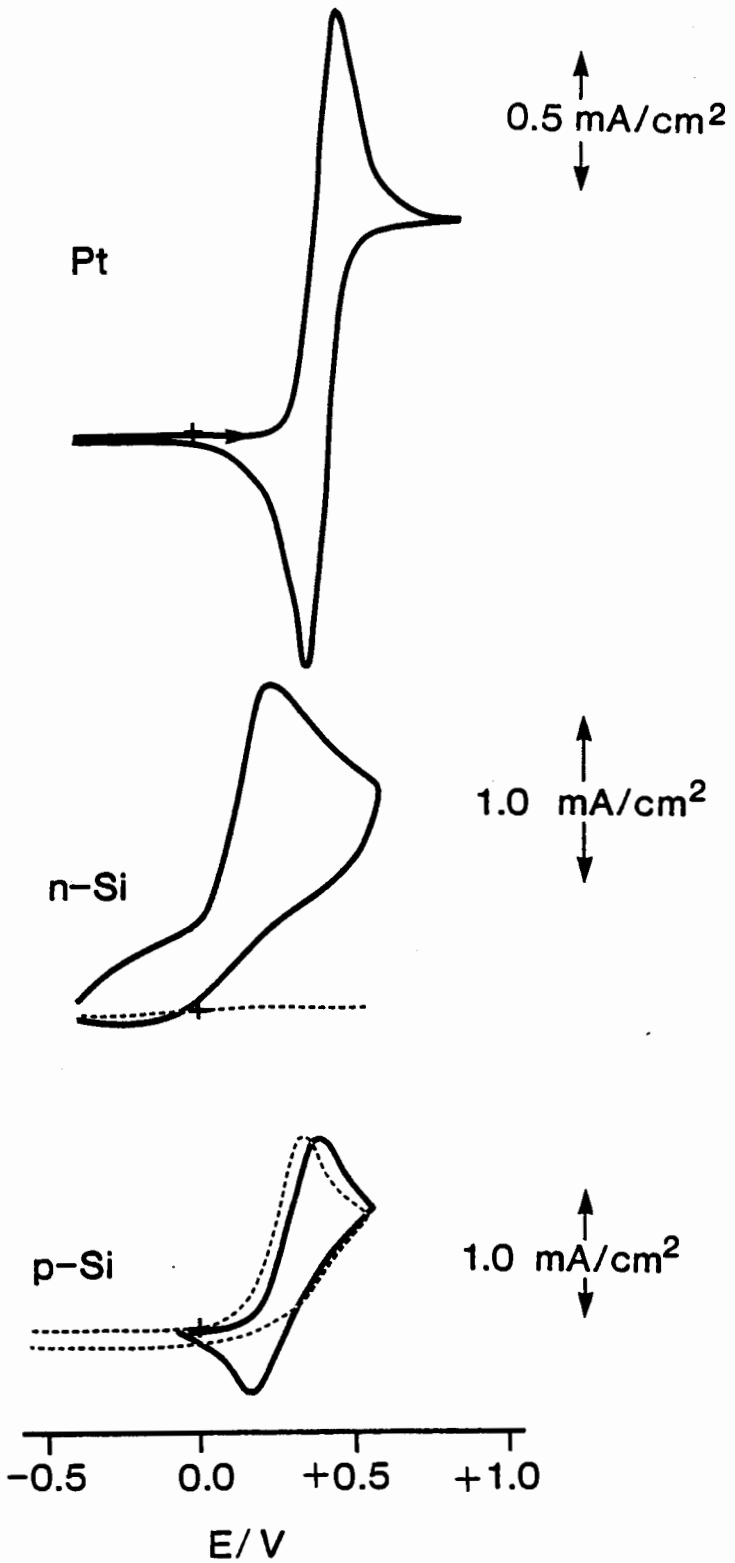

Figure 64. Cyclic voltammetry of ferrocene (10 mM) at Pt and Si electrodes: (——) illuminated electrode, (----) dark electrode. Electrolyte, 0.1 M TEAP/CH_3CN; scan rate, 50 mV/s.

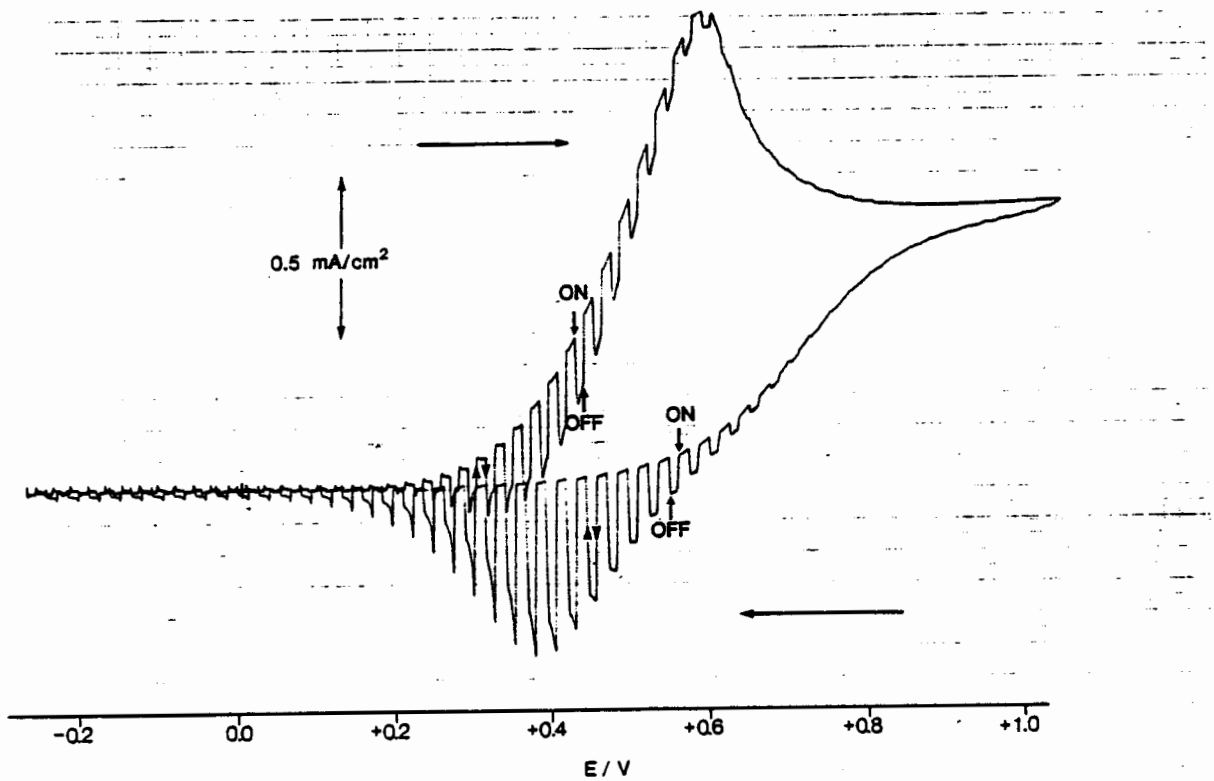

Figure 65. Cyclic voltammetry of ferrocene (10 mM) at p-Si electrodes under chopped light. Electrolyte, 0.1 M TEAP/CH_3CN; scan rate, 50 mV/s.

ferrocenium. The cathodic current spike decays during the period of illumination because of the decrease in concentration of ferrocenium near the electrode surface and the increase in the anodic back reaction as the surface concentration of ferrocene increases. When the light pulse is turned off, a small anodic spike is observed (at potentials <+0.45 V) on a large, and rising, anodic current background, representing the oxidation of photo-electrochemically generated ferrocene. At potentials positive of +0.60 V, photogenerated cathodic current is not observed. At this point an accumulation layer is formed, preventing photogenerated carriers traversing the barrier at the semiconductor surface. The potential at which this occurs is an indication of the flat band potential. Clearly, the flat band potential of p-Si is significantly different in the presence and absence of the redox couple. A similar photoeffect is observed on the reverse scan. Photogenerated cathodic current is observed 300 mV more positive than E_{redox}, indicating that a rectifying junction, and not an ohmic contact, exists.

Capacitance-voltage measurements were made on n-Si and n-Si/PP electrodes in the presence of the ferrocene only, and in the presence of ferrocene/ferrocenium. The Mott-Schottky plots obtained from C-V data are shown in Figure 66. The flat band potential of bare n-Si in the absence of ferrocenium is ≈ -0.5 V, similar to that of n-Si in pure electrolyte. When the electrode is coated with a PP film, the flat band potential shifts to ≈+0.2 V. The shift in V_{fb} occurs because the electrochemical potential of PP adjusts to that of the solution. The Si/PP interface now determines the Helmholtz potential at the semiconductor surface. Upon electrochemical generation of the oxidised form of the redox couple, V_{fb} of bare Si shifts to ≈+0.10 V since electron extraction from semiconductor surface states by ferrocenium is now possible. When a PP film is present, V_{fb} moves slightly positive in accordence with the change in electrochemical potential of PP.

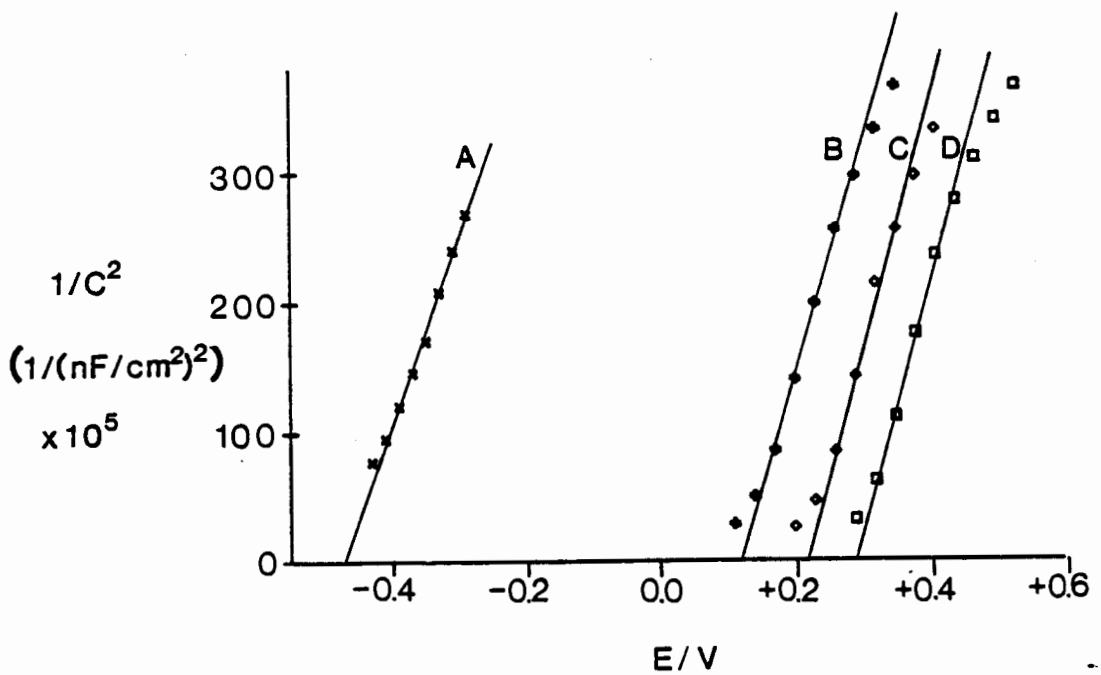

Figure 66. Mott-Schottky plots for n-Si (a&b) and n-Si/PP (c&d) electrodes in the presence of ferrocene/ferrocenium (10 mM): a&c) $E_{solution}$ =+0.16 V, b&d) $E_{solution}$=+0.36 V. Electrolyte, 0.1 M TEAP/CH_3CN; frequency, 5 KHz.

The electrochemical data pertaining to Si and Si/PP electrodes in non-aqueous media can be explained by the presence of silicon surface states. In the case of n-Si/PP electrodes, it is suggested that oxidised PP is capable of extracting electronic charge from Si surface states, thus developing a positive charge on the n-Si surface (with respect to the bare surface). As the electrochemical potential of the polymer is made increasingly positive, the probability of electron extraction is greater. The slope of the V_{fb} vs. E_{pp} plot (Figure 59) is less than unity indicating that the PP film causes a change in both the surface state charge and the degree of band bending.

A similar interpretation is given for p-Si/PP electrodes. In this case, two mechanisms leading to band edge unpinning are evident: A) When the occupied energy levels of the PP film lie above those of p-Si surface states, electron injection from PP to the surface states occurs, resulting in the raising of the flat band potential to more negative potentials. B) When E_{pp} is below the energy associated with surface states, electron extraction from the latter occurs, decreasing the negative charge at the Si/PP interface. The energy barrier between E_{pp} and the Si valence band energy decreases as E_{pp} is made more positive, and the p-Si/PP interface correspondingly changes from rectifying to ohmic. Quasi-ohmic behaviour of p-Si/PP electrodes in non-aqueous media has been previously reported[165]. C-V experiments show that the flat band potential of p-Si shifts by 500 mV for a 600 mV change in E_{pp}, indicating that substantial Fermi level pinning is present. Measurement of the open circuit photovoltage as a function of E_{pp} were consistent with values predicted by the relation $V_{ph} = |V_{fb} - E_{pp}|$.

The change in semiconductor energy levels as a result in changes of E_{pp} are schematically illustrated in Figure 67. It is interesting to note that for solid state systems, a large rectifying barrier is produced at the n-Si/PP interface, and ohmic contacts are formed at the p-Si/PP interface

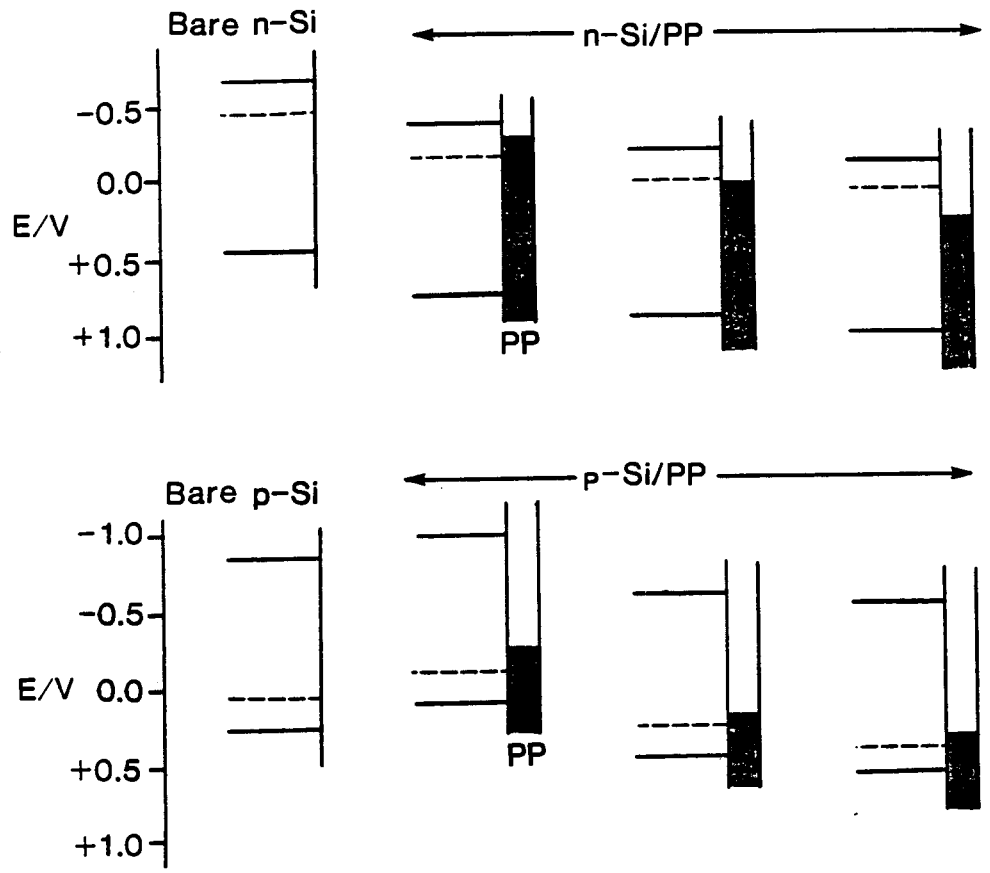

Figure 67. Schematic representation of band edge unpinning at Si/PP interfaces. The semiconductor flat band case is chosen for simplicity.

[198,203]. PEC systems differ from their solid state anologues in that the former allow the development of a Helmholtz potential at the semiconductor-electrolyte interface.

The condition of the semiconductor surface has a pronounced effect on the charge transfer kinetics occurring at the solid/electrolyte interface. Surface modifications are therefore, of great importance. Several reports indicate that the presence of underlying layers of Pt between the semiconductor surface and the PP film retards the peeling of the polymer from the electrode. The effect of an underlying Pt layer on the cyclic voltammetry of Si/PP electrodes is shown in Figure 68. The voltammograms show a clear potential shift in a negative direction. The change in surface potential is confirmed by flat band potential measurements. V_{fb} for n-Si/Pt and p-Si/Pt electrodes were ≈-0.7 and ≈-0.3 V respectively (Figure 69). The Pt layer did not improve the photovoltages generated by Si/PP electrodes, in fact, the values were significantly lower than those obtained in the absence of Pt. It appears that Pt induces additional surface states, thus enabling a greater quantity of charge to reside at the semiconductor surface.

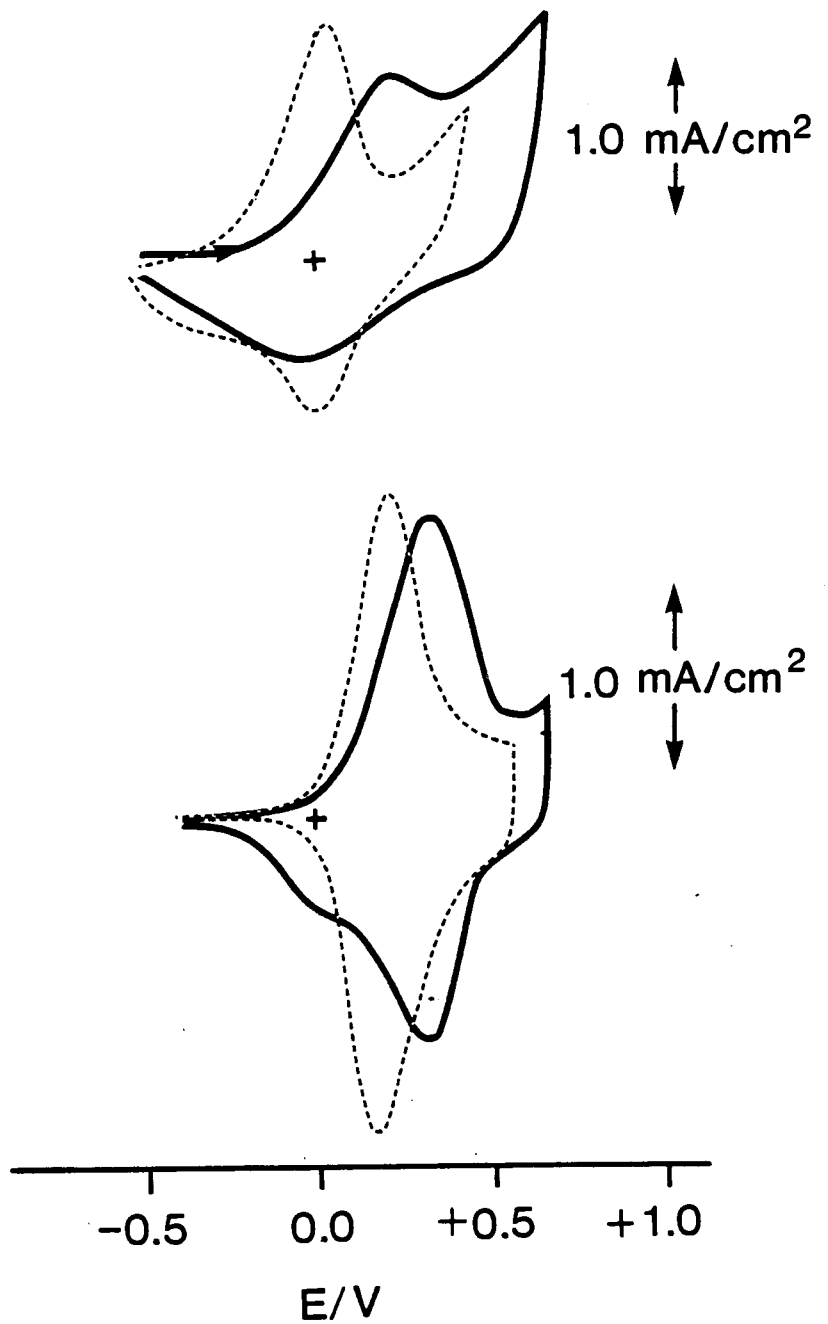

Figure 68. Cyclic voltammetry of Si/PP (——) and Si/Pt/PP (----) electrodes: Top) n-Si, Bottom) p-Si. Electrolyte, 0.1 M TEAP/CH_3CN; scan rate, 50 mV/s; illumination intensity, 80 mW/cm^2.

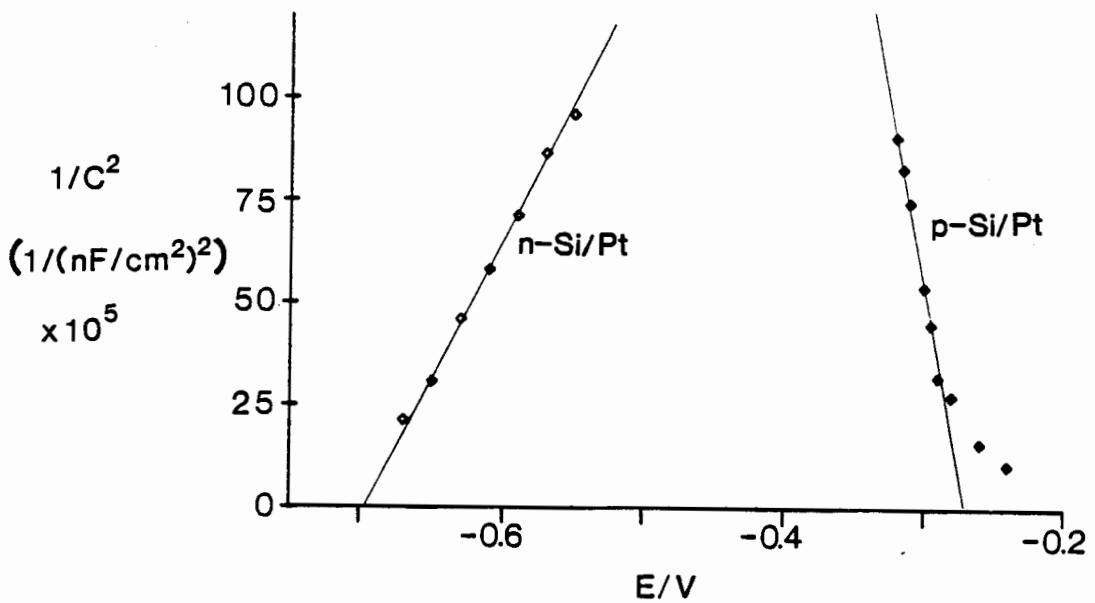

Figure 69. Mott-Schottky plots for Si/Pt electrodes in 0.1 M TEAP/CH_3CN. Frequency, 5 KHz.

IV.4. CONCLUSION

Band edge unpinning of n- and p-type Si in CH_3CN is clearly evident in the presence of a PP film, a redox couple, or both. The phenomena is a result of facile electron transfer between PP and surface states located within the Si band gap region. PP undergoes rapid equilibration with the ferrocene redox couple in solution and thus facilitates electron transfer between the Si electrode and the solution species.

This insight into the energetics of electron transfer between PP coated semiconductors and redox species in solution is important in the design of conducting polymer based PEC cells.

CHAPTER V

ELECTROCATALYTIC ACTIVITY OF POLYPYRROLE FILMS INCORPORATING Pt MICROPARTICLES

V.1. INTRODUCTION

There is considerable academic and technological interest in the deposition of metal particles onto polymer films[204,205]. A common deposition technique involves the electroreduction of a metal salt, such as $PtCl_6^{2-}$ [206]:

$$PtCl_6^{2-} + 4e^- \text{ ---> } Pt^0 + 6Cl^- \qquad (72)$$

In the case of redox polymer films, the redox couple can mediate the reduction of the metal salt. The locus of electrochemical reaction is governed by the diffusion of electrons through the film, the rate of electrochemical reaction, the diffusion and permeation of the metal salt through the solution, and through the film. In the two extreme cases, metal is deposited on the polymer film surface, or on the electrode surface.

A number of reports concerning the electrocatalytic properties of these films have appeared. It is found that the metal particulates act as catalytic sites for multi-electron transfer processes and thus, differ from the majority of catalytic redox polymers.

Wrighton and coworkers utilised viologen and cobaltocene redox polymer films incorporating noble metal catalysts to improve H_2 evolution kinetics at p-type silicon photocathodes [29,30,153,207]. In another system, Pt microparticles and $Ru(NH_3)_6^{3+}$ ions were incorporated into Nafion films with the intention of improving the reaction kinetics of O_2 reduction[208]. In a

similar manner to the previous example, the redox couple mediates electronic charge between the electrode substrate and the metallic catalyst. The current densities observed are however, quite low due to the poor redox conductivity of these films.

Thin films of electro-inactive polymers, such as poly(vinylacetic acid) and poly(vinylpyridine), have also been used as hosts for Pt microparticles [209-211]. These films are found to be catalytic towards H_2 evolution and O_2 reduction. Presumably, sufficient contact between the metal particles, and between metal particles and the electrode surface, is obtained to sustain the large current densities that are observed.

Organic conducting polymers are attractive materials for hosting metallic particulates since electronic charge can readily flow through the film. However, these films become insulators at negative potentials. One group overcame this problem by electrodepositing Ag in the polymer matrix[212,213]. Ag aggregates located along the polymer fibres enhance the conductivity of the latter at negative potentials. H_2 evolution was observed in acid medium at potentials where the film should have been insulating.

The motivation behind incorporating metallic particles into porous matrices, is to increase the specific area of these materials and thus, improve catalytic efficiency. In studying these films a number of factors must be taken into account including the effect of diffusion and permeation of solution species, catalyst loading and catalyst dispersion. The objective of this research was to investigate the electrocatalytic properties of conductive polymer/metal catalyst films, and to examine the effect of varying the distribution and loading of the catalyst in the polymer matrix. For this purpose, conductive PP films containing a controlled dispersion of Pt were fabricated. The quantity and dispersion of catalyst was evaluated using chronocoulometry and Auger electron spectroscopy. The electroactivity of

these films, towards the O_2 reduction reaction, was studied using RDE voltammetry. The scheme for electrocatalysis is illustrated in Figure 70.

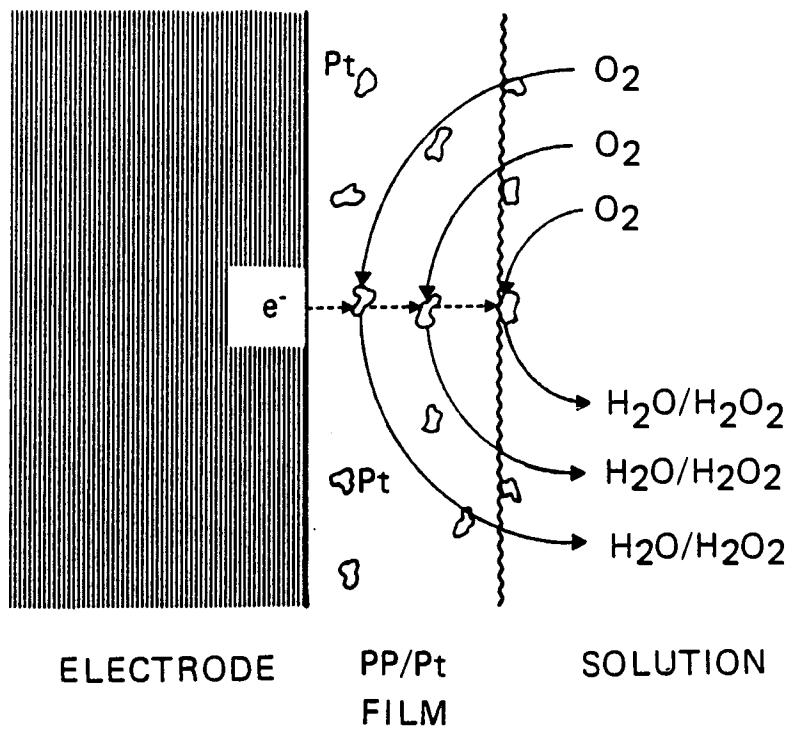

Figure 70. Schematic illustration of mediated O_2 reduction at PP/Pt films.

V.2. EXPERIMENTAL

V.2.1. CHEMICALS

Pyrrole was distilled under reduced pressure in a spinning band column and stored over molecular sieve, type 4A. Potassium ferrocyanide (BDH) and potassium hexachloroplatinate (IV) (Johnson Matthey) were used as received.

V.2.2. PREPARATION OF POLYMER FILMS

PP films were prepared on glassy carbon (GC) and tin oxide coated glass from an aqueous solution of 0.1 M pyrrole and 0.1 M KCl. Films were grown using using a constant current density (71.2 mA/cm^2). The thickness of the film was estimated using the procedure described in Section III.2.2..

Various procedures were used to fabricate PP/Pt microstructures on electrodes. The electrode type, and preparation procedure, are classified below:

Type I electrodes were prepared by the electrodeposition of Pt on bare electrodes from aqueous solutions of 1 mM K_2PtCl_6 and 0.05 M KCl at -0.2 V (SCE). The current density during platinisation was typically 0.2 mA/cm^2. Pt loadings were calculated from the cathodic charge passed.

Type II electrodes were prepared by the deposition of Pt onto a preformed PP film. Conditions were the same as above.

Type III electrodes were prepared by immersing a pre-reduced PP film into a 10 mM K_2PtCl_6 solution. The electrode was removed, rinsed and placed in 0.1M KCl. The free standing potential of the film, E_1, was monitored with respect to a SCE. The film was then reduced by a potential step to -0.5 V. The cathodic charge passed, Q_{red}, allows determination of the Pt loading.

Typically, one deposition cycle provided a Pt loading of: 1.0 $\mu g/cm^2$ for 0.08 μm films; 2.4 $\mu g/cm^2$ for 0.16 μm films; 5.3 $\mu g/cm^2$ for 0.4 μm films; and 10.9 $\mu g/cm^2$ for 0.8 μm films. Pt loadings were increased by repeating the deposition process. These electrodes were prepared in a glove box, under an argon atmosphere, to prevent air oxidation of reduced PP films.

Type IV electrodes were prepared by immersing an <u>oxidised</u> PP film into a $PtCl_6^{2-}$ solution for a period of time. The cathodic charge required to completely reduce the film, Q_{red}, at standing potential, E_1, was recorded. The quantity of charge associated with reduction of $PtCl_6^{2-}$ is obtained from $Q_{red}-Q_{ox}$, where Q_{ox} is the charge passed when a PP film at rest potential, E_1, is completely reduced in 0.1 M KCl for subsequent potential steps. One deposition cycle typically produced a Pt loading of 0.8 $\mu g/cm^2$ for a 0.16 μm film.

The above electrodes were used for electrochemical study, and their composition analysed by Auger Electron Spectroscopy (AES). In addition to these, several other electrode structures were prepared for AES analysis only. These electrodes were used to validate the AES depth profiling technique for monitoring dispersions of Pt in PP/Pt films. Their preparation are described below:

Type V electrodes were prepared by the same method as for type III electrodes with the variation of leaving the coated electrode in 0.1 M KCl for two hours following immersion in $PtCl_6^{2-}$ solution. One deposition cycle for a 0.16 μm film produced a Pt loading of 2.3 $\mu g/cm^2$.

Type VI electrodes were prepared by the electrodeposition of Pt onto a preformed PP film followed by the subsequent deposition of a second PP film. The quantities of material applied were:- inner PP film =0.16 μm; Pt loading =13.1 $\mu g/cm^2$; outer PP film =0.08 μm.

Type VII electrodes were prepared by electroplating platinum (13 $\mu g/cm^2$)

onto bare electrode, followed by deposition of a PP film (0.16 μm) and application of K_2PtCl_6 salt residue by droplet evaporation.

Type VIII electrodes were prepared by the electro-deposition of PP/$Fe(CN)_6^{3-}$ films from a) 0.05 M pyrrole, 0.1 M $K_3Fe(CN)_6$ for Γ_{Fe} vs. PP film thickness studies. b) 0.1 M pyrrole, 0.01 M $K_3Fe(CN)_6$, 0.01 M KCl for AES studies. The quantity of $Fe(CN)_6^{3-}$ incorporated in the PP film, Γ, was determined from the area under a voltammetric wave associated with the reduction of $Fe(CN)_6^{3-}$. Films formed for AES analysis were 0.16 μm thick and had a $Fe(CN)_6^{3-}$ coverage of 0.6×10^{-8} mol/cm^2.

The terminology used to describe PP/Pt films for the remainder of the text is of the form (electrode type, film thickness in μm, Pt loading in μg/cm^2) e.g. a film described as II(0.16)13.0 is a type II electrode, has a film thickness of 0.16 μm and has a Pt loading of 13.0 μg/cm^2.

V.2.3. AUGER ELECTRON SPECTROSCOPY

Auger Electron Spectroscopy (AES) was performed using a Perkin-Elmer 595 Scanning Auger microprobe. This technique was used extensively to determine elemental distributions in PP/Pt films. A surface area of 6.4×10^3 μm^2 was analysed using a 3 KeV electron beam and a beam current of 0.1-0.2 μA. Elements were indentified from their characteristic Auger signals: Pt (64 and 1967 ev); Cl (181 eV); C (272 eV); N (379 eV); Sn (413 eV); O (503 eV), Fe (703 eV). Depth profile analysis were performed by sputtering the polymer film with a 3 KeV Ar^+ ion beam. The rate of sputtering did vary from sample to sample.

PP/Pt films were formed on tin oxide coated glass and allowed the PP/electrode substrate interface to be easily distinguished by depth profile analysis. Due to the weak signal produced by Pt, depth profiles of Pt were

composed by physical measurement of the individual spectra (64 eV) as a function of sputter time. The much weaker 1967 eV Pt signal was used for confirming the presence or absence of Pt.

Quantitative analyses were performed by relating the Pt signal obtained from PP/Pt films to the signal obtained from pure Pt under the same conditions. Back scattered electron effects and the variation of inelastic mean free paths of Auger electrons in the polymer matrix, and pure Pt, were taken into account using standard empirical relations (see Section I.1.3.2). The beam current varied between samples and thus, relative signal intensities required a proportionality factor since signal intensity is directly proportional to beam current. Comparisons of Pt concentration in PP/Pt films were also obtained by monitoring the C:Pt signal ratios.

V.2.4. ELECTROCHEMISTRY

A PAR Electrochemistry System was used for the preparation of PP/Pt films, and a Pine RDE 4 bipotentiostat and a Hewlett-Packard HPZ046B X-Y recorder used for rotating disk experiments. Electrochemical studies were performed using a three compartment cell with a Pt counter electrode and a saturated calomel reference electrode (SCE).

PP/Pt films for electrochemical study were formed on a rotating ring-disk electrode (RRDE) (Pine Instruments) incorporating a glassy carbon disk (0.126 cm^2) and a Pt ring (0.126 cm^2). Before PP deposition, the electrode surface was polished using 1 μm diamand paste, rinsed and finally sonicated in deionised water for 5 minutes. PP/Pt films were studied in aqueous solutions of pH 2.0, 6.0, 10.0 and 12.0, in the presence (O_2 saturated), and absence (N_2 purged), of dissolved oxygen. Solutions of pH 6.0 and 10.0 were buffered, while solutions of pH 2.0 and 12.0 were obtained by titration with

H_2SO_4 and KOH solutions respectively. The temperature of the electrolyte was maintained at 25 °C. Detailed rotating electrode studies were perfomed using O_2 saturated solutions adjusted to pH 12.0 with KOH. The effect of PP film thickness, Pt loading and Pt distribution on the catalytic current density was investigated using electrodes I, II, III and IV. Errors of uncertainty for limted current densities were typically 1-1.5 % at the lowest rotation rate used ($\omega^{1/2}$ = 2.80 [rad/s]$^{1/2}$) and increased with rotation rate (e.g. 4.5-5.0 % at ($\omega^{1/2}$ = 6.47 [rad/s]$^{1/2}$)

V.3. RESULTS AND DISCUSSION

V.3.1. CHARACTERISATION OF PP/Pt FILMS

V.3.1.1. PP FILM THICKNESS

The thickness of PP films was estimated from the coulombic charge associated with film formation and film reduction. The ratio of $Q_{form}:Q_{ox}$ indicates that 8 pyrrole rings are charge stabilised by one Cl^- ion. The molecular weight of the repeating unit (plus dopant) is thus 69.3 g/mol. Table 8 shows the data from which the film thickness , d, can be calculated.

Table 8 Coulombic assay of PP films

	1	2	3	4
Q_{tot} (mC/cm^2)	35.60	71.20	170.80	356.00
Q_{ox} (mC/cm^2)	1.52	4.08	10.48	21.60
Q_{form} (mC/cm^2)	34.08	67.12	167.52	334.40
d (μm)	0.08	0.16	0.40	0.80

V.3.1.2. COULOMETRY AND SPECTROPHOTOMETRY

Deposition of Pt in type II electrodes is simply achieved by the electrochemical reduction of $PtCl_6^{2-}$. However, for type III electrodes the mechanism is not completely electrochemical: Figure 71 shows the spectrophotometric behaviour of PP films on tin oxide coated glass. The reduced and oxidised forms are distinctly different. The spectrum for a reduced film immersed in $PtCl_6^{2-}$ solution for 5 min., rinsed and placed in

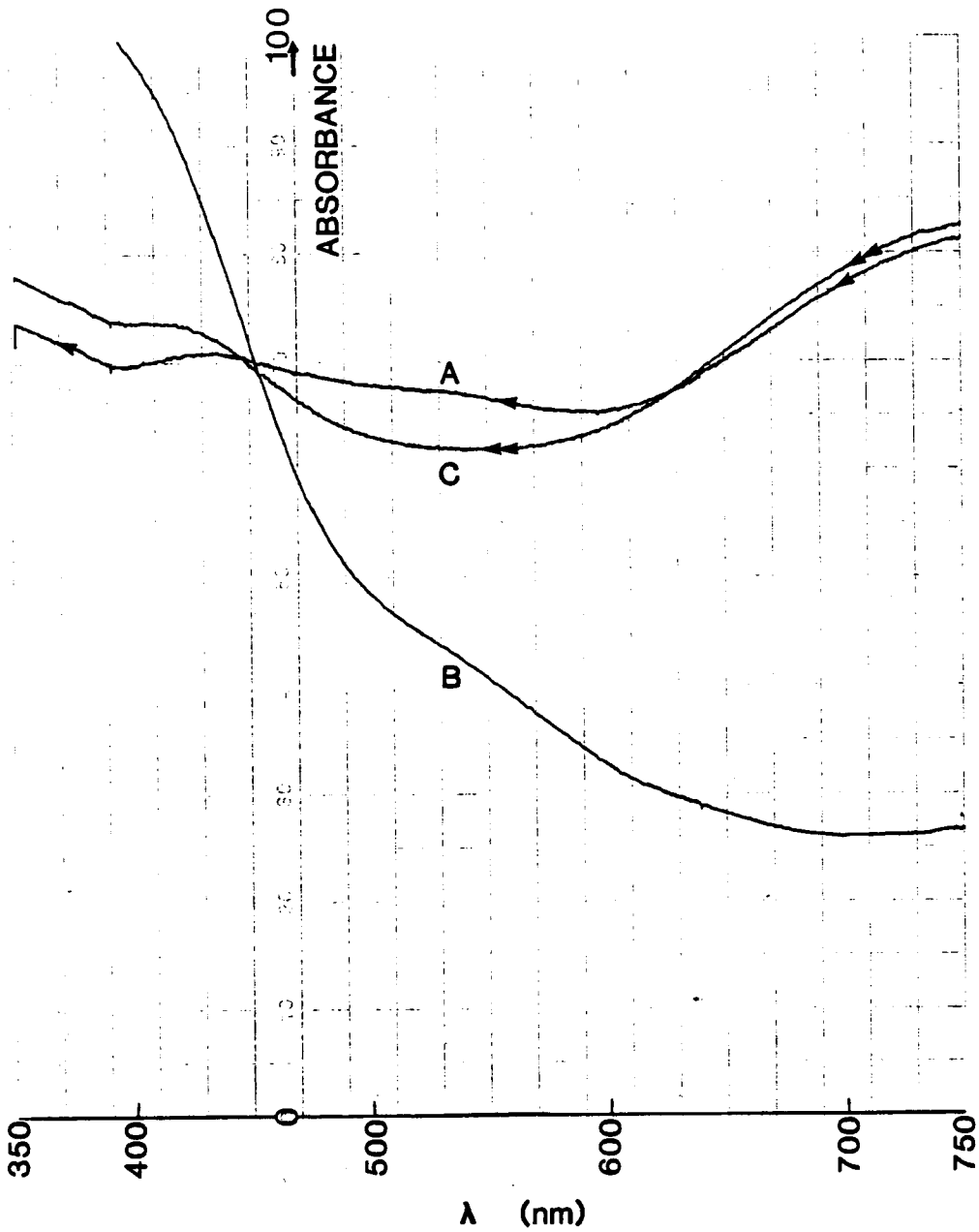

Figure 71. Absorption spectra of PP films (0.16 μm) in deionised water: A) Electrochemically oxidised, B) Electrochemically reduced, C) After (B) has been immersed in 1mM K_2PtCl_6 for several min.

deionised water, is similar to that recorded for the electrochemically oxidised film. The behaviour is consistent with the predicted mechanism:

$$(PP)_x^{red} + nPtCl_6^{2-} \text{ ---> } Pt^0\text{-}(PP)_x^{ox}(Cl^-)_y + (6n-y)Cl^- \qquad (73)$$

A fresh PP/Pt film, when transferred to 0.1 M KCl and electrochemically reduced, produced a cathodic charge which was 25-30% greater than the charge observed for subsequent potential steps. A similar increase was observed when pre-oxidised PP films were immersed in $PtCl_6^{2-}$ solutions followed by reduction in 0.1 M KCl (type IV). However, when an electrode prepared by method III was left in 0.1 M KCl for several hours prior to reduction (type V electrode), little difference in cathodic charge was observed between the first reductive step and subsequent oxidative-reductive steps. It is concluded that type III electrodes contain Pt microparticles due to A) chemical reduction of $PtCl_6^{2-}$ by the pre-reduced PP film, B) electrochemical reduction of $PtCl_6^{2-}$ trapped within the polymer matrix.

The accuracy of the AES technique for characterising PP films was investigated by obtaining quantitative and qualitative AES information for films of known composition. For this purpose electrodes of type VIII were prepared. The surface coverage of $Fe(CN)_6^{3-}$ incorporated in PP films is shown in Figure 72 as a function of charge passed during polymerisation. The linear correlation indicates that $Fe(CN)_6^{3-}$ is incorporated homogeneously through the film.

V.3.1.3. AES

Figure 73 shows a typical elemental survey using AES. The Pt, Cl, C and N signals can be clearly identified. When the film is sputtered away the signals decrease into the baseline and new signals, corresponding to SnO_2,

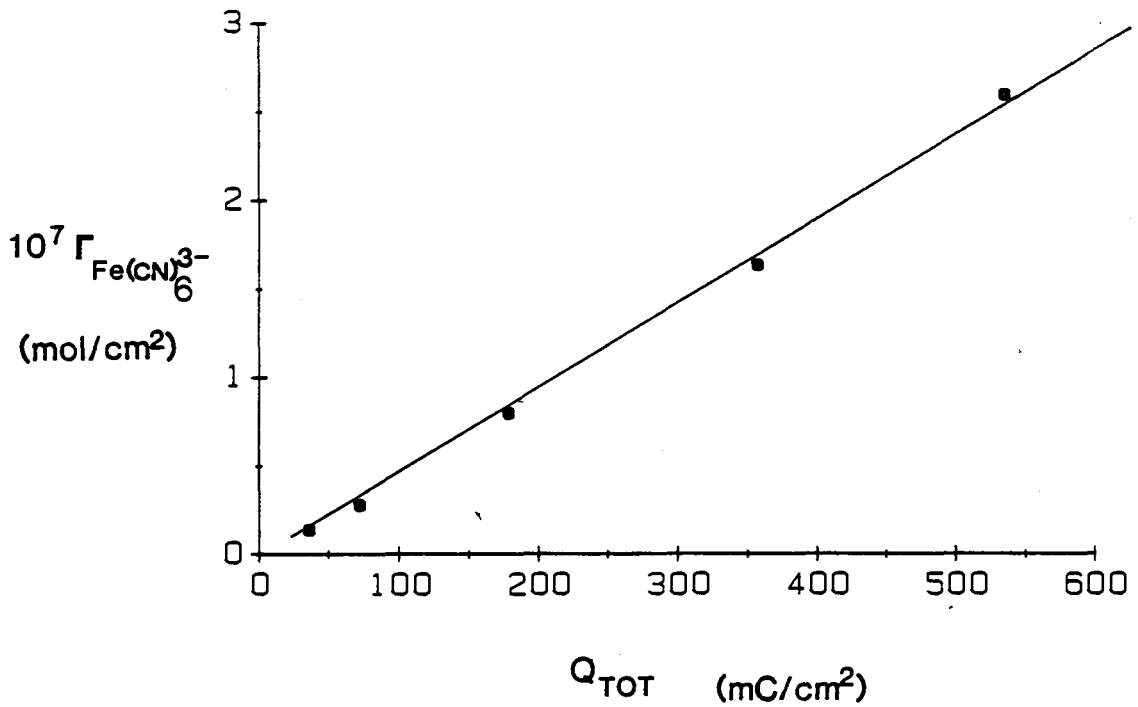

Figure 72. Surface coverage of $Fe(CN)_6^{3-}$ incorporated in PP vs. number of coulombs passed during polymerisation.

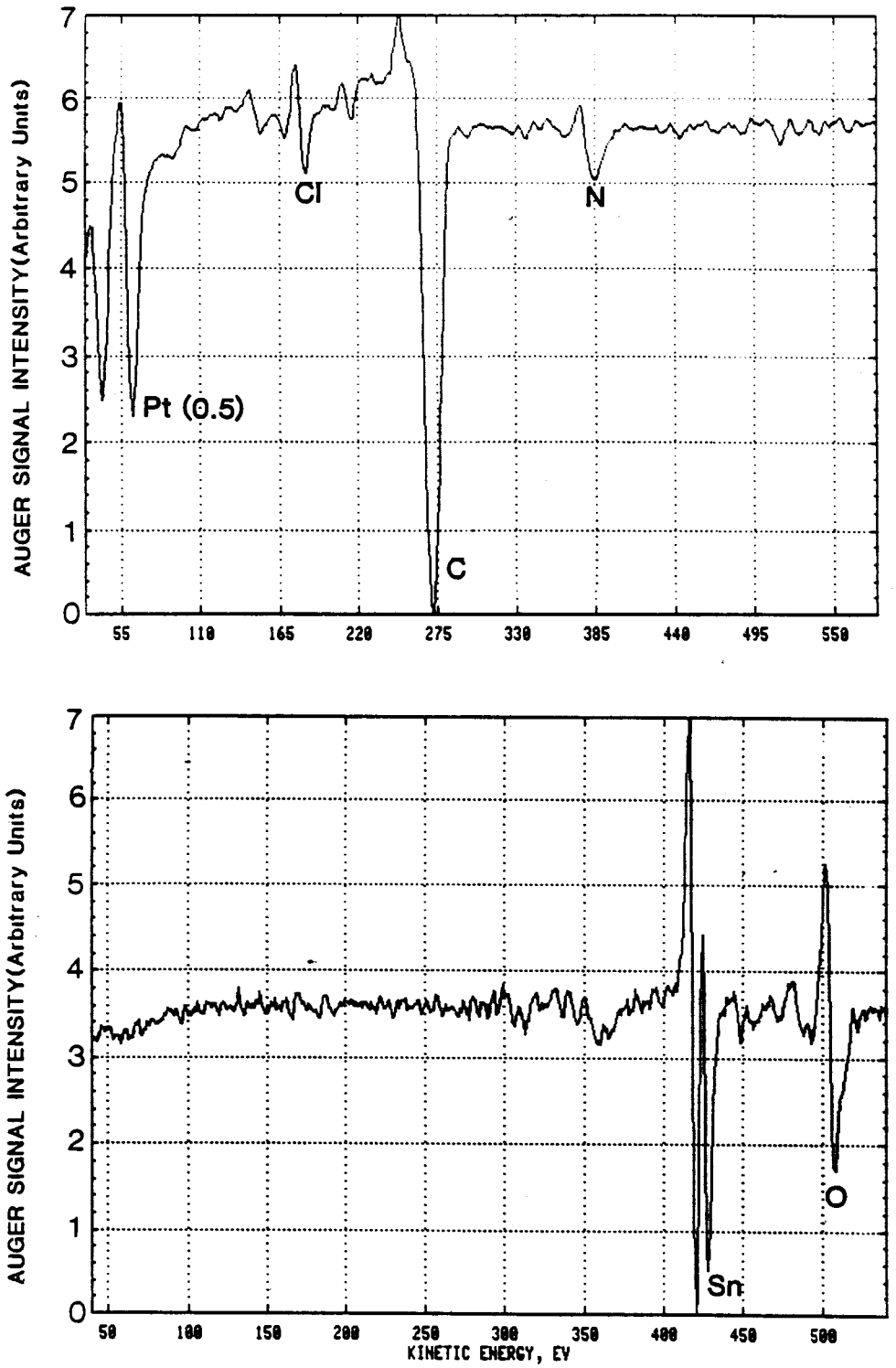

Figure 73. AES elemental survey of electrode III(0.16)13.3 before (top) and after (bottom) sputtering.

appear.

The depth profile analyses of electrodes VI, VII and VIII are shown in Figure 74. The observed elemental profiles are as expected thus employing the AES technique for monitoring Pt dispersions in PP films is justified.

A typical depth profile of type II electrodes is shown in figure 75. From the profile it is evident that Pt resides at the PP/air interface. This indicates that electrochemical reduction of $PtCl_6^{2-}$ at PP coated electrodes occurs at the outer surface of the film, i.e. at the PP/electrolyte interface. Depth profiles for films III, IV and V are shown in Figures 76 and 77. Profiles for type III electrodes indicate that these films possess regions of concentrated and homogeneous Pt. As Pt loading is increased (Figs. 75b, 75c & 76a) the concentration of Pt increases, at both the PP/air interface, and through the film. The distribution of Pt in various PP films, based on the above analyses, are schematically illustrated in Figure 78.

Information on Pt distribution can be obtained by observing the C:Pt signal ratio. Comparing this ratio for films III(0.8)13.0 and III(0.16)13.3 (Figs. 75a & 75b), one finds that the concentration of Pt in the body of the film is diluted by a factor of 5 for a corresponding 5x increase in film thickness.

The C:Pt ratios, in the homogeneous region of the film, for electrodes III(0.16)2.8, IV(0.16)1.7 and V(0.16)2.3 (Figs. 76a, b & c) are approximately 2.0, 3.2 and 9 respectively. These comparisons indicate that for electrodes of type III, Pt is incorporated at the PP/solution interface mainly by the PP^{red}-$PtCl_6^{2-}$ reaction, and is deposited through the bulk of the film mainly by the electrochemical reduction of retained $PtCl_6^{2-}$. These results reinforce the conclusions drawn from coulometric experiments.

Quantitative evaluations were made using the following inelastic mean free path estimates and calculated backscattered electron factors: Pt in PP-

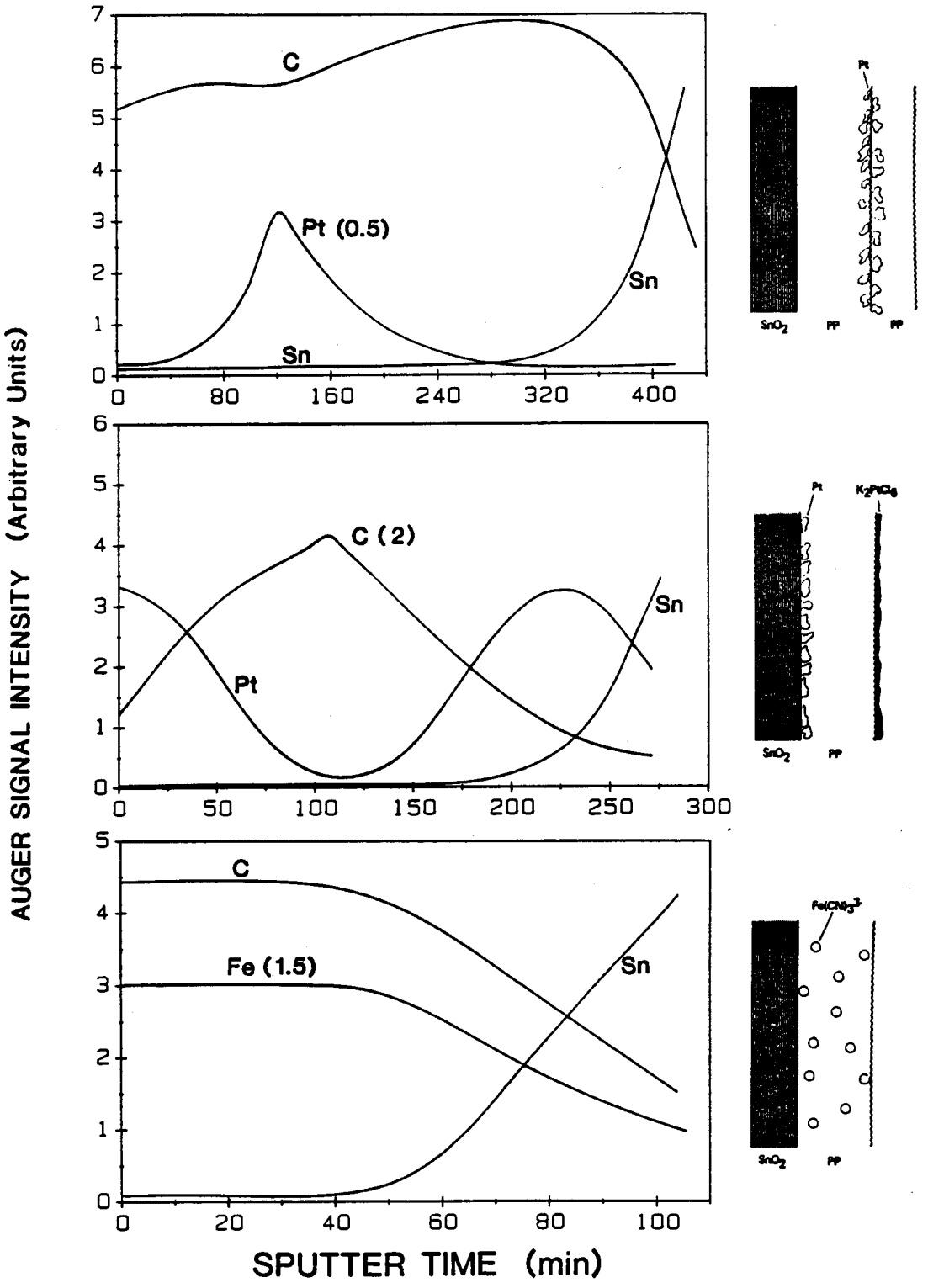

Figure 74. Depth profile analyses and composition of electrodes TOP) VI, MIDDLE) VII, BOTTOM) VIII.

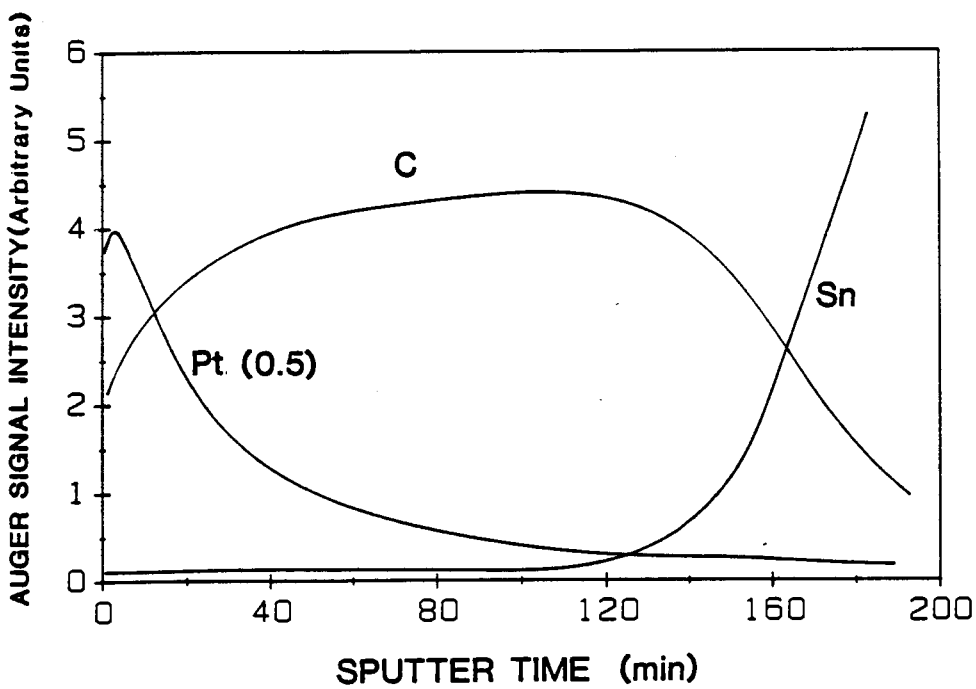

Figure 75. Depth profile analysis of electrode II(0.16)13.1.

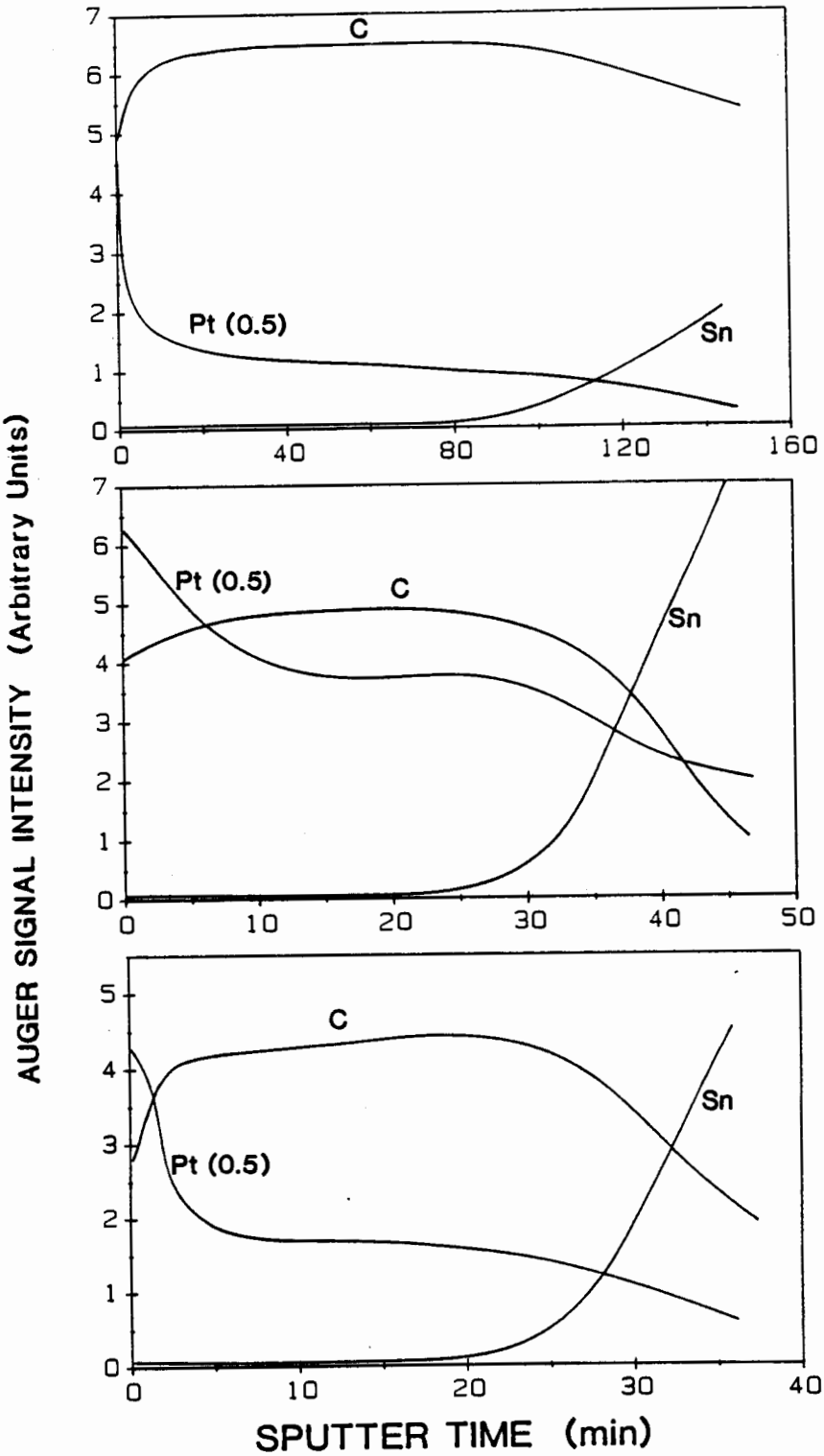

Figure 76. Depth profile analyses of PP/Pt electrodes: TOP) III(0.8)13.0, MIDDLE) III(0.16)13.3, BOTTOM) III(0.16)5.4.

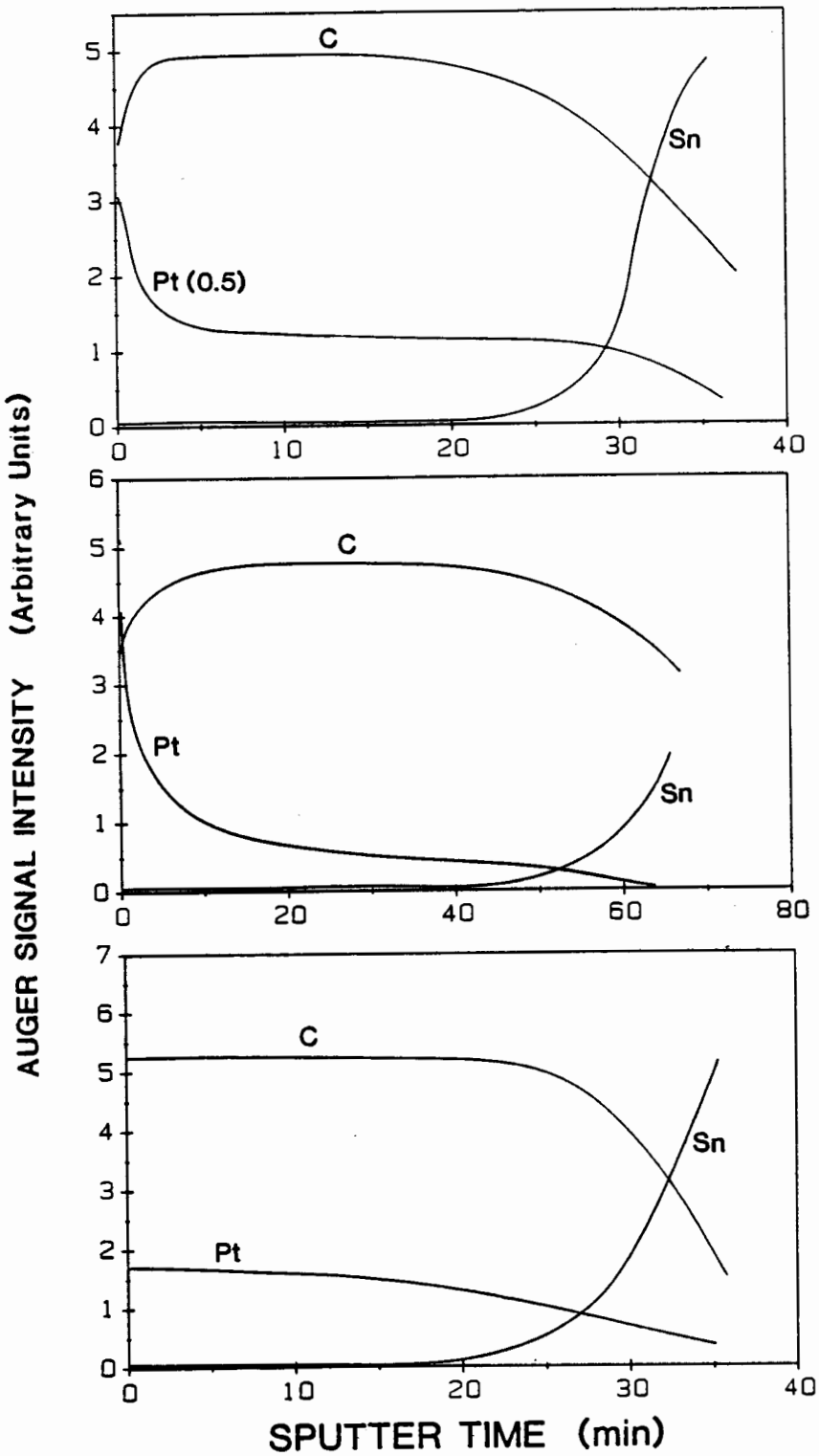

Figure 77. Depth profile analyses of PP/Pt electrodes: TOP) III(0.16) 2.8, MIDDLE) V(0.16)2.3, BOTTOM) IV(0.16)1.7.

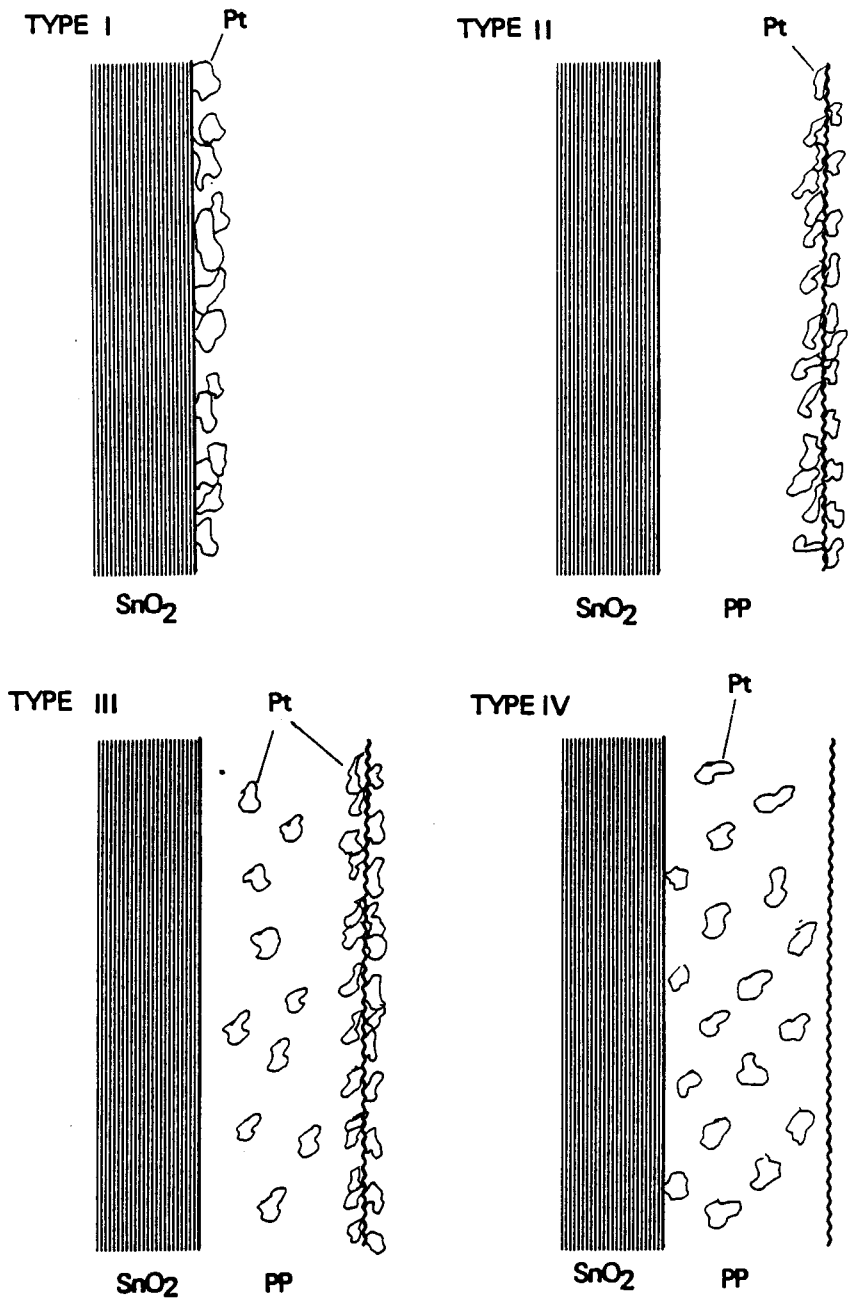

Figure 78. Schematic illustration of the various catalytic films prepared.

1.444 nm & 0.703 respectively; elemental Pt- 2.342 nm & 0.467 ; Fe in PP- 1.127 nm & 2.31 ; elemental Fe- 1.682 nm & 1.43.

A complete homogeneous distribution of incorporated species was obtained only for electrodes IV and VIII. The concentration of $Fe(CN)_6^{3-}$ in film VIII was determined to be 1.3 x 10^{-3} mol/cm^3 by AES, and 0.6 x 10^{-3} mol/cm^3 by cyclic voltammetry. The Pt loading of electrode IV(0.16)1.7 (i.e. Pt loading = 0.11 g/cm^3) was determined to be 0.33 g/cm^3 by AES. AES analysis gave quantitative results that were 2-3 times larger than anticipated. Reasons for this may be 2-fold, 1) estimation of the film thickness, from which electrochemical results were based, may be smaller than anticipated, 2) the back scattering effect of the Auger electrons may be larger than calculated.

The concentration of Pt in the homogeneous regions of electrodes III(0.8)13.0, III(0.16)13.3, III(0.16)5.2, III(0.16)2.8 and V(0.16)2.3 were determined by AES to be approximately 0.4, 1.23, 1.07, 0.61 and 0.2 g/cm^3 respectively. Again the AES calculations were larger than anticipated but their relative values were consistent with the observed C:Pt signal ratios.

V.3.2. ELECTROCATALYTIC PROPERTIES OF PP/Pt FILMS

V.3.2.1. EFFECT OF pH

The electrochemical behaviour of thin PP films in the absence of dissolved oxygen are shown in Figure 79. Incorporating Pt in the film does not dramatically alter the redox behaviour of PP although additional charge transfer, probably due to H^+ adsorption and desorption, is observed at negative potentials. In a solution containing only KOH (pH 12.0) the cathodic and anodic peaks shift 500-600 mV.

The cyclic voltammetry of various electrodes in solutions saturated with

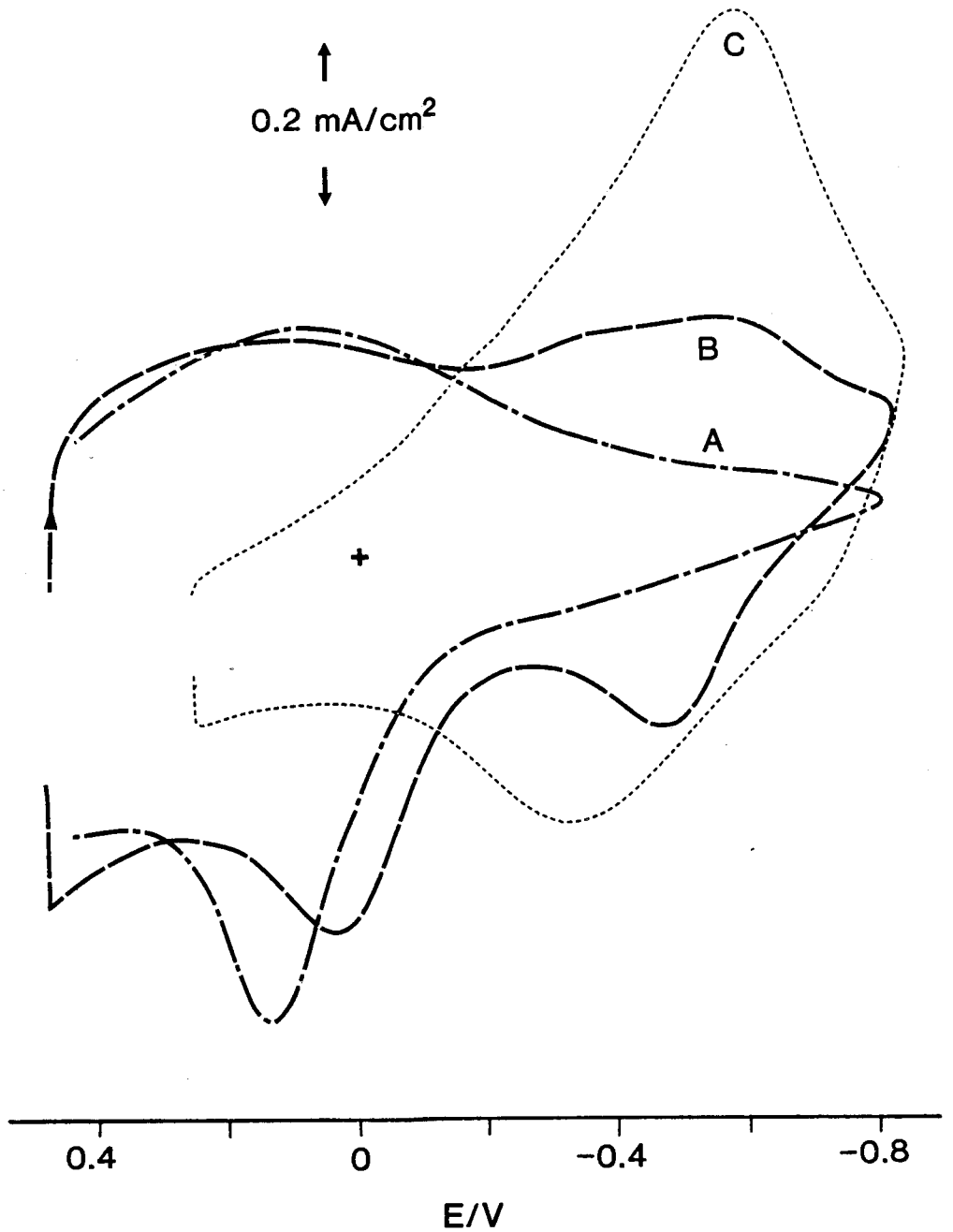

Figure 79. Cyclic voltammetry of PP films (0.16 μm): A) PP only in 0.1 M KCl, B) Electrode III(0.16)13.3 in 0.1 M KCl, C) PP only in KOH solution, pH 12.0. Scan rate, 50 mV/s.

O_2 are shown in Figure 80 at different pH. The variation in cathodic peak potential between PP/Pt films and bare GC are tabulated in Table 9.

The difference in cathodic peak potential between PP/Pt films and bare GC clearly ilustrates the electrocatalytic nature of the former. The variation of peak potential with pH reflects the mechanism of O_2 reduction. At glassy carbon O_2 is reduced predominantly by the 2-electron pathway. This mechanism is more efficient in alkali media and thus, the reaction overpotential decreases at GC electrodes as pH increases. Conversly, with Pt, an efficient 4-electron pathway catalyst, the overpotential is increased with increase in pH since the rate of electron transfer via this mechanism is slower in alkaline media.

Table 9. Cathodic peak potential for O_2 reduction

	E/V (SCE)			
pH	2.0	6.0	10.0	12.0
Bare GC	-0.83	-0.83	-0.74	-0.63
III(0.16)13.1	+0.19	+0.04	-0.13	-0.20

The above analysis is consistent with the H_2O_2/H_2O ratios observed by RRDE experiments (Table 10).

Table 10. % H_2O_2 produced at the GC and PP/Pt electrodes

pH	2.0	6.0	10.0	12.0
Bare GC	< 1%	< 1%	≈ 52%	≈ 100%
III(0.16)13.1	< 1%	< 1%	≈ 8%	≈ 1%

One of the difficulties encountered in studying the O_2 reaction at these films was the narrow potential range for which the reaction could be

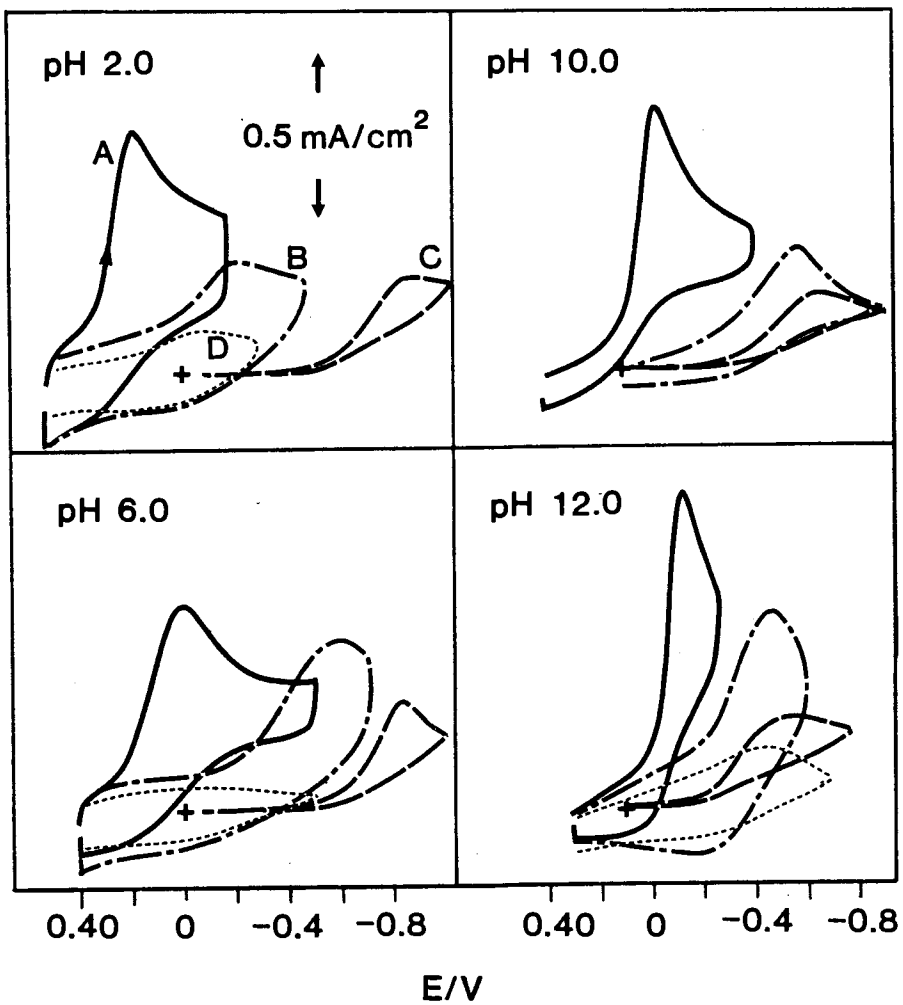

Figure 80. Cyclic voltammetry of PP & PP/Pt electrodes in O_2 saturated solutions of varying pH: A) Electrode II(0.16)13.1, B) PP only (0.16 μm), C) Bare GC, D) PP film in the absence of O_2. Scan rate, 20 mV/s.

observed. This is due to the nature of PP and slow O_2 reaction kinetics. In order to observe limiting current plateaux at fast electrode rotation rates (or high current densities) one has to apply increasingly negative potentials. Inevitably PP is reduced and becomes insulating before a plateau is formed. Thus, studies were limited to slow rotation rates and low current densities. The limiting current obtained from the RDE i-V waves were estimated according to the procedure in Figure 81.

V.3.2. EFFECT OF Pt LOADING AND FILM THICKNESS

The effect of Pt loading on the i-V behaviour for O_2 reduction at electrodes I, II, III and IV are shown in Figure 82. For electrodes with low Pt loadings the overpotential is decreased in the order IV < III < II < I. However, the situation is reversed with larger Pt loadings. The corresponding Levich plots for these electrodes are shown in Figure 83. All Levich plots yield non-zero intercepts. This is expected since the $i_L=0$ when $\omega=0$ relation predicted from the Levich equation, is not strictly correct: At low rotation rates natural convection contributes significantly to the forced convection[214]. Nevertheless, plotting several i_L vs. $\omega^{1/2}$ points produces a slope for which the gradient is independent of the $\omega=0$ contribution.

GC electrodes electroplated with Pt (I) yield linear Levich plots. Their gradients reflect the effective Pt area of deposited Pt. Thus, with Pt loadings of $< \approx 13\ \mu g/cm^2$ the effective area is smaller than that corresponding to a bare Pt electrode of the same geometric area. Similar results are obtained with type II electrodes. Type III electrodes show a large deviation from linearity especially at low Pt coverages. With larger coverages the plots show more linearity and have gradients similar to that

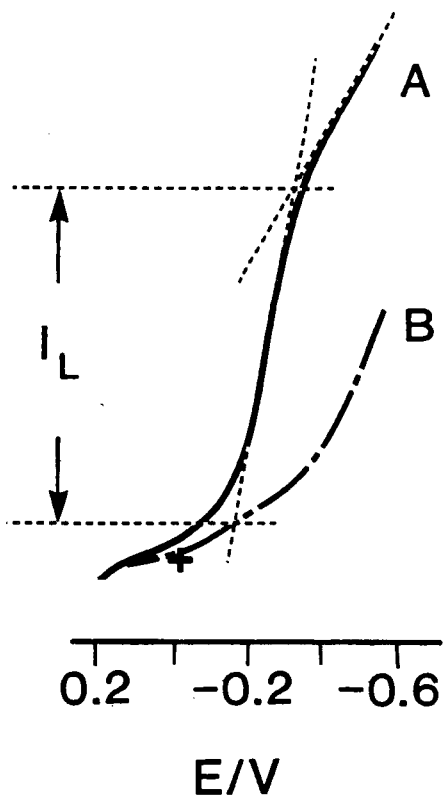

Figure 81. Illustration of how i_L is obtained from the rising plateau of a RDE voltammogram. A) & B) are the voltammograms for a PP film with and without incorporated Pt respectively. pH 12.0; O_2 saturated; scan rate, 20 mV/s; rotation rate, 100 rpm.

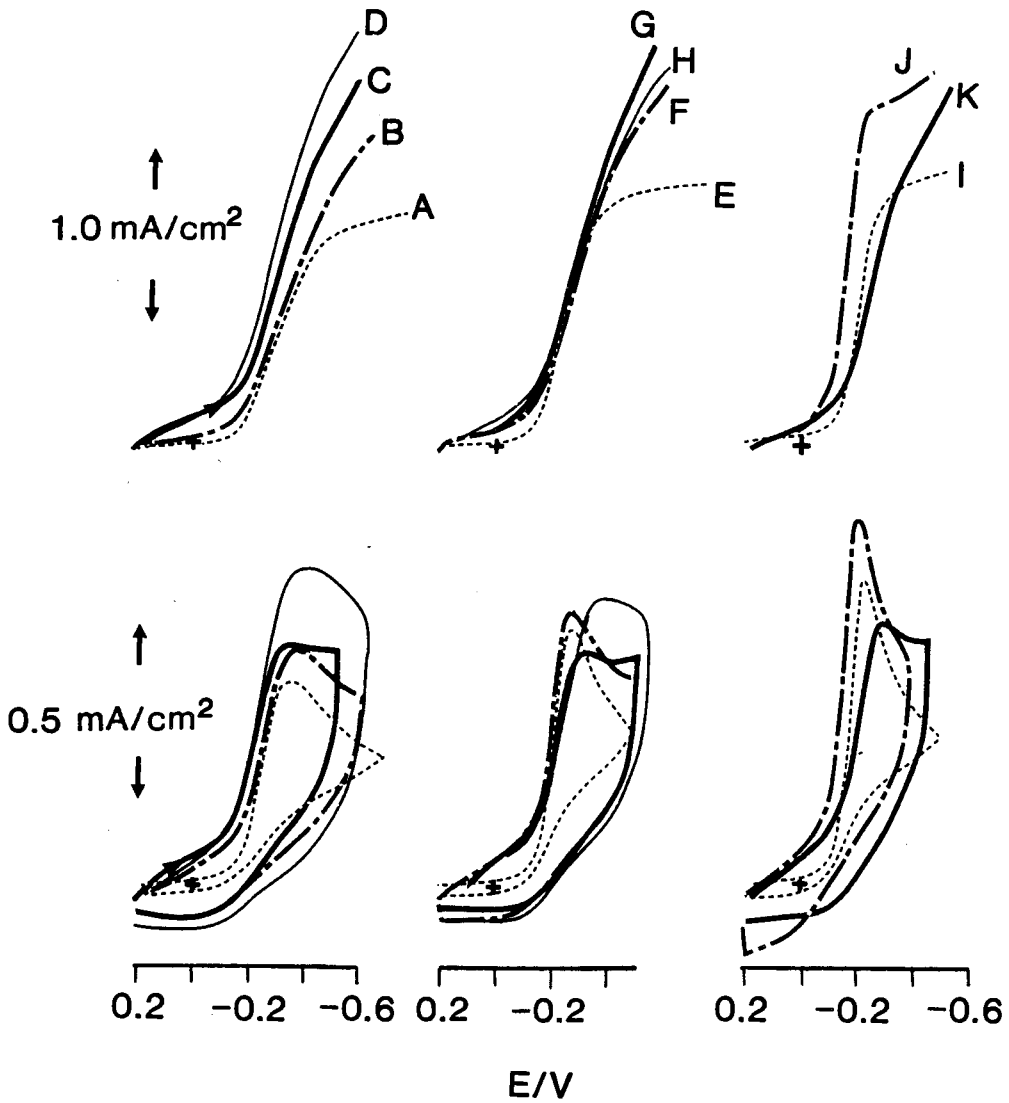

Figure 82. RDE voltammograms of electrodes I, II, III and IV: constant film thickness, varying Pt loading. A) I(-)2.8, B) II(0.16)3.5, C) III(0.16)2.7, D) IV(0.16)1.7, E) I(-)7.0, F) II(0.16)6.1, G) III(0.16)5.5, H) IV(0.16)5.5, I) I(-)13.1, J) II(0.16)13.1, K) III(0.16)13.3. pH 12.0; O_2 saturated; scan rate, 20 mV/s; rotation rate, 100 rpm.

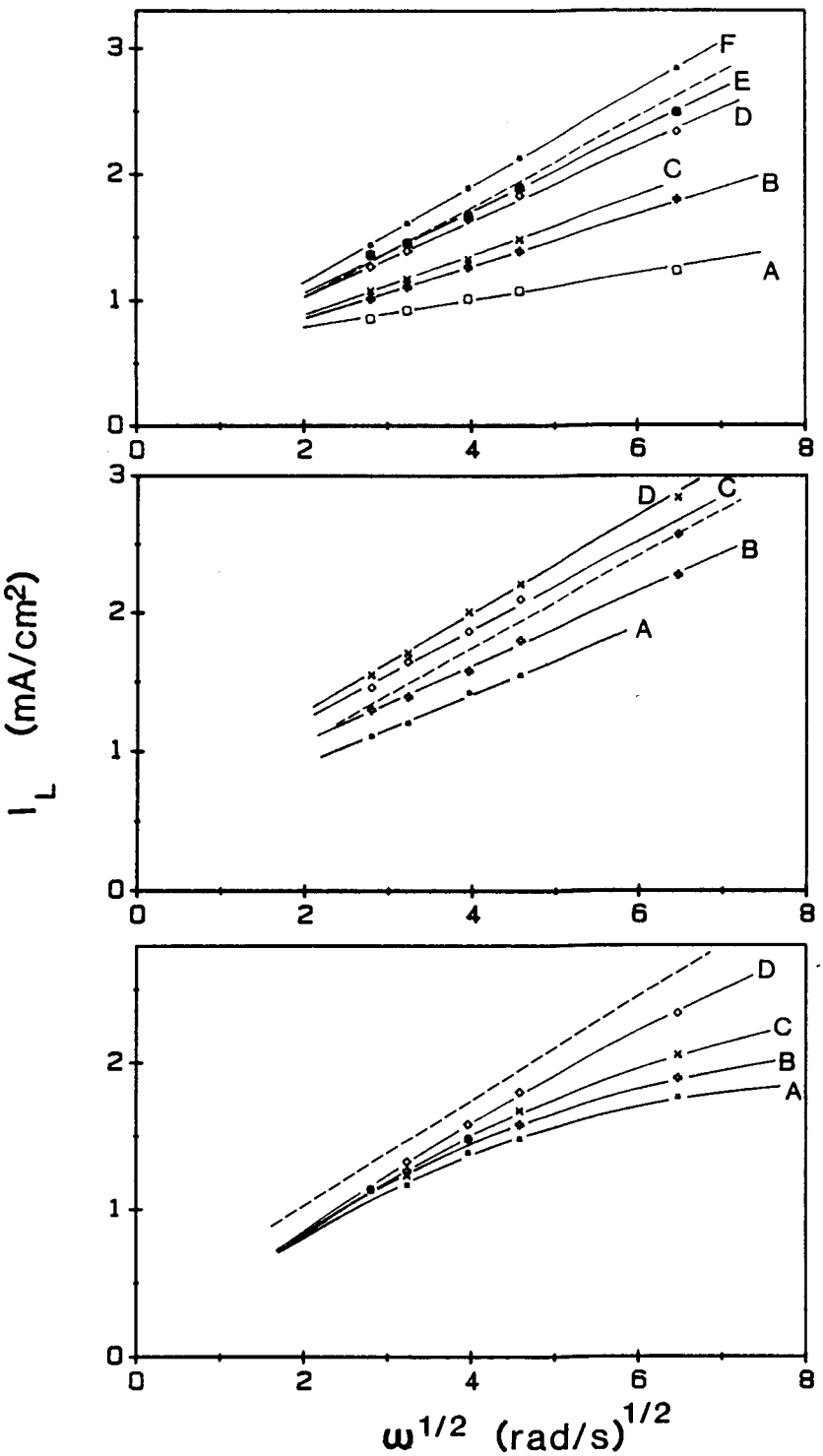

Figure 83. Levich plots for electrodes I, II and III: constant film thickness (0.16 μm), varying Pt loading. TOP) Type I electrodes, Pt loading (μg/cm^2): A) 0.8, B) 1.6, C) 2.8, D) 7.0, E) 13.1, F) 26.2 MIDDLE) Type II electrodes, Pt loading (μg/cm^2): A) 3.5, B) 6.1, C) 13.1, D) 26.2 BOTTOM) Type III electrodes, Pt loading (μg/cm^2): A) 2.8, B) 5.4, C) 13.3, D) 27.8. Dashed line represents bare Pt; pH 12.0; O_2 saturated.

for bare Pt. Levich plots for type IV electrodes were not obtained due to the lack of a convincing plateau region.

The effect of Pt loading is more easily observed when thicker films are used. Figure 84 shows the i-V data and corresponding Levich plots for electrodes of type III coated with 0.8 μm PP films and variable Pt loading. Again, one observes non-linear Levich plots, particularly with low Pt coverages where i_L is almost constant with rotation rate.

Figure 85 show i-V curves and Levich plots for electrodes II and III when one maintains a constant Pt loading ($\approx$13 $\mu g/cm^2$) and varies the film thickness (0.08-0.8 μm). Levich plots for type III electrodes tend towards a constant current as film thickness is increased. Levich plots for type II electrodes have gradients similar to that for bare Pt.

In these catalytic films, the rate constant for electron transfer and the rate of charge propagation through the film is extremely large, much larger than the rates observed for redox catalysts. However, the i-V data and resulting Levich plots for these catalytic systems indicate that the rate of substrate permeation through the film can play a major role in determining the catalytic current density. The O_2 reaction at electrodes I and II, for which Pt is localised at the GC/solution and PP/solution interface respectively, yield limiting currents which are affected by solution hydrodynamics only. Exceptions are found when the Pt loading is low, and the effective area of deposited Pt is less than the geometric area of the electrode. For PP films containing homogeneously dispersed Pt, electrodes III and IV, the finite rate of O_2 permeation is evident. When thick films, or low Pt coverages, are employed O_2 molecules must diffuse through large film distances in order to maintain a current flux equal to the flux of O_2 transported from bulk solution to the film/solution interface. When the demands on the O_2 permeation cannot be met, then non-linear Levich plots are

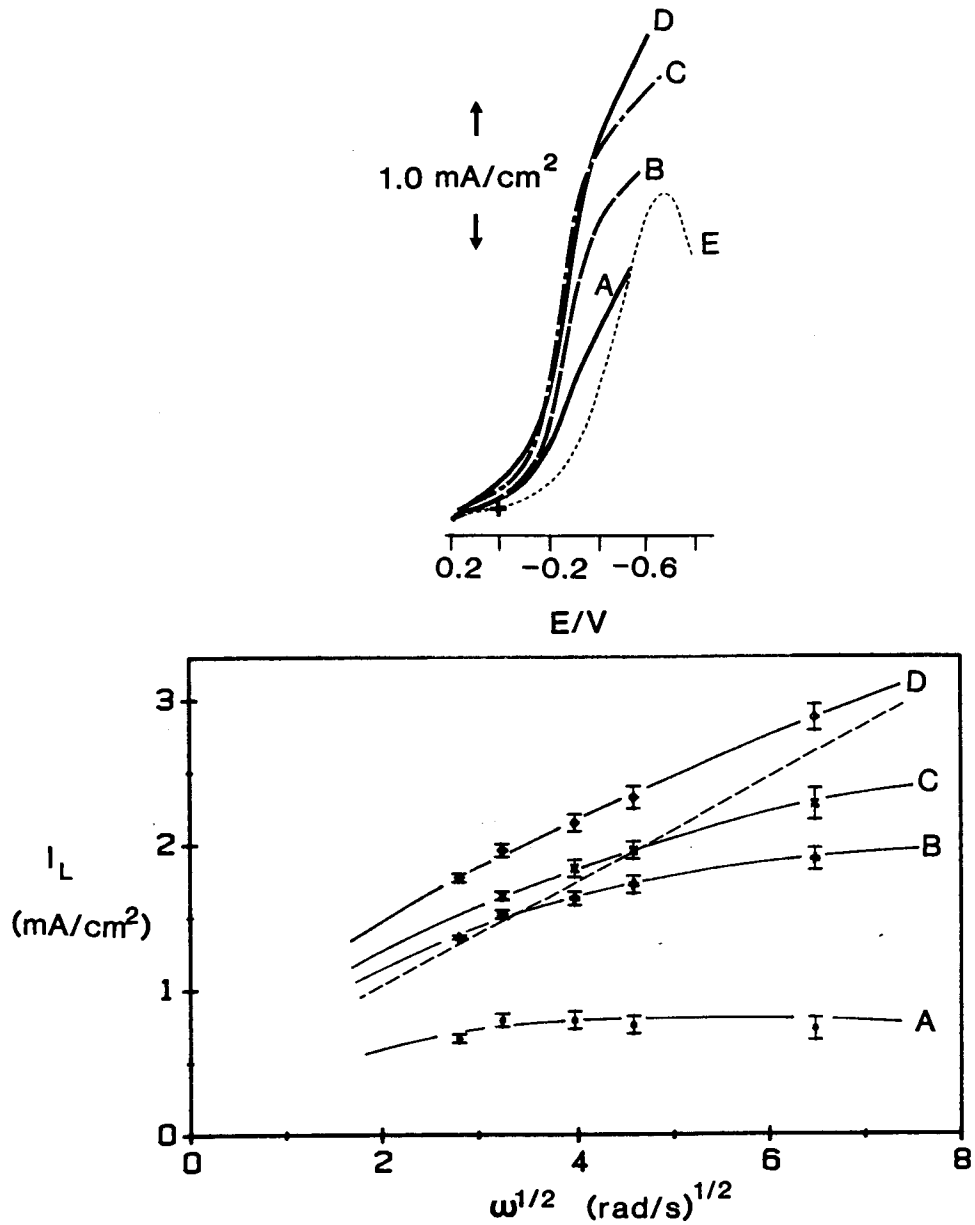

Figure 84. RDE voltammograms and corresponding Levich plots for electrodes III: constant film thickness (0.8 μm), varying Pt loading ($\mu g/cm^2$). A) 9.1, B) 15.5, C) 22.8, D) 31.5, E) PP only. pH 12.0; O_2 saturated, scan rate, 50 mV/s; rotation rate, 100 rpm. Dashed line on the Levich plot represents bare Pt.

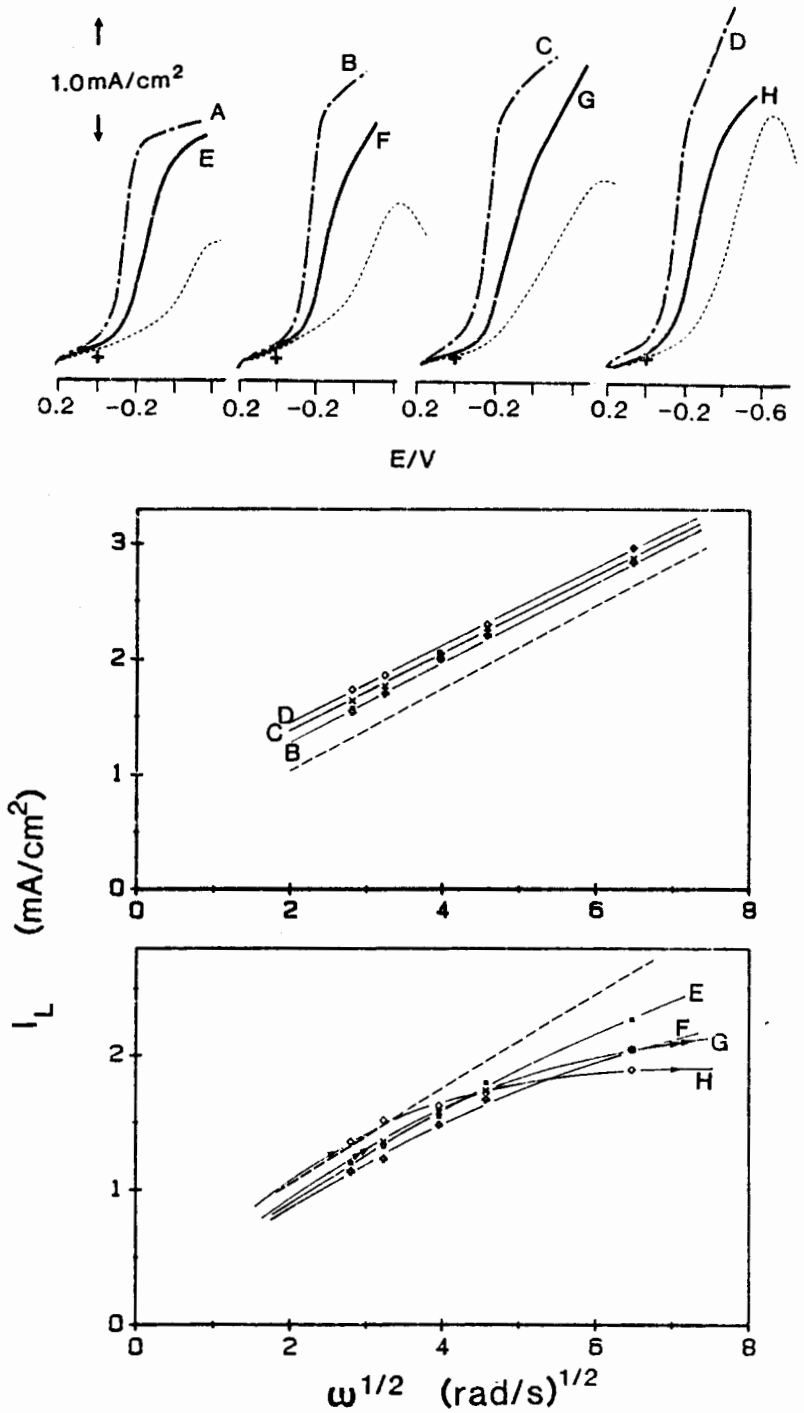

Figure 85. RDE voltammograms and corresponding Levich plots for electrodes II and III: constant Pt loading (≈13 $\mu g/cm^2$), varying film thickness. A-D represent type II electrodes and E-H represent type III electrodes for film thicknesses of 0.08, 0.16, 0.4 and 0.8 μm respectively. The dashed curves on the i-V data represent PP films before Pt deposition while the dashed line on the Levich plot represents bare Pt. pH 12.0; O_2 saturated, scan rate, 50 mV/s, rotation rate, 100 rpm

observed. As Pt concentration is increased, by either increasing the Pt loading or decreasing film thickness, then O_2 has only to diffuse through smaller distances in the film since larger current densities can be obtained from thinner regions at the PP/solution interface.

Conducting polymer films containing particulates, while possessing rapid electron transfer and electron propagation kinetics, are inefficient 3-dimensional catalyst systems due to poor polymer porosity. It may be feasibe to improve the porosity of the polymer matrix, and thus the rate of permeation of solution species, by chemical attachment of bulky groups (e.g. sulphonate substituents) to strategic points in the molecule[193]. Such groups cause polymers to swell in aqueous media by introducing hydrophillic character into the macromolecule, in addition to the steric effects imposed by the substituent. Alternatively, the polymer can be polymerised in a porous membrane, with subsequent dissolution of the membrane, to yield highly permeable polymer films[215,216].

V.4. CONCLUSION

The incorporation of Pt in PP can be controlled by a number of film forming techniques, as clarified by AES. The distribution of Pt can be made homogeneous through the film, or localised at specified regions.

Conductive polymer films incorporating noble metal particulates have a number of qualities which make them attractive for electrocatalysis. Such qualities include facile electron transport to active sites and rapid rates of multi-electron transfer between catalytic sites and solution species.

PP/Pt films are catalytic towards O_2 reduction within a narrow potential window. RDE studies using films of various film thickness and Pt loading indicate that the catalytic current density obtained for films containing homogeneously dispersed Pt are strongly dependent on the rate of O_2 permeation. Thus, the advantage of dispersing Pt in PP, over simply depositing Pt on a flat electrode, is offset by poor substrate permeation. More efficient use of embedded catalyst may perhaps be observed by enhancing film porosity.

REFERENCES

1. R. W. Murray, Chemically Modified Electrodes, "Electroanalytical Chemistry", Vol. 13, Ed. A. J. Bard, Marcel Dekker, New York, 1984.

2. R. W. Murray, Acc. Chem. Res., 13 (1980) 135.

3. R. W. Murray, Ann. Rev. Mater. Sci., 14 (1984) 145.

4. K. D. Snell and A. G. Keenan, J. Chem. Soc., Chem. Soc. Rev., (1979) 259.

5. W. J. Albery and A. R. Hillman, Chem. Soc. Ann. Rep. Progr. Chem., Sec. C, **78** (1982) 377.

6. R. F. Lane and A. T. Hubbard, J. Phys. Chem., **77** (1973) 1401.

7 R. F. Lane and A. T. Hubbard, J. Phys. Chem., **77** (1973) 1411

8. P. R. Moses, L. Weir and R. W. Murray, Anal. Chem., **47** (1975) 1882.

9. A. Merz and A. J. Bard, J. Am. Chem. Soc., **100** (1978) 3222.

10. L. L. Miller and M. R. Van De Mark, J. Electroanal. Chem., **100** (1978) 3223.

11. M. S. Wrighton, R. G. Austin, A. B. Bocarsly, J. M. Bolts and O. Hass, J. Electroanal. Chem., **87** (1978) 429.

12. P. Daum, J. R. Lenhard, D. Rolison and R. W. Murray, J. Am. Chem. Soc., **102** (1980) 4649.

13. R. J. Nowak, F. A. Schultz, M. Umana, R. Lam and R. W. Murray, Anal. Chem., **52** (1980) 315.

14. N. Oyama and F. C. Anson, J. Electrochem. Soc., **127** (1980) 247.

15. A. F. Diaz, K. K. Kanazawa and G. P. Gardini, J. Chem. Soc. Commun., (1979) 635.

16. A. F. Diaz, Chem. Scr., **17** (1981) 145.

17. G. Tourillon and F. Garnier, J. Electroanal. Chem., **135** (1982) 173.

18. R. J. Waltman, A. F. Diaz and J. Bargon, J. Phys. Chem., **88** (1984) 4343.

19. J. Bargon, S. Mohmand and R. J. Waltman, IBM J. Res. Dev., **27** (1983) 330.

20. R. W. Murray, Phil. Trans. R. Soc. Lond., **A 302** (1981) 253

21. J. Zak and T. Kuwana, J. Electroanal. Chem., **150** (1983) 645.

22. J. M. Bolts, A. B. Bocarsly, M. C. Palazzotto, E. G. Walton, N. S. Lewis and M. S. Wrighton, J. Am. Chem. Soc., **101** (1979) 1378.

23. M. S. Wrighton, Acc. Chem. Res., **12** (1979) 303.

24. R. N. Noufi, D. Tench and L. F. Warren, J. Electrochem. Soc., **128** (1981) 2596.

25. A. J. Frank, Mol. Cryst. Liq. Cryst., **83** (1982) 341.

26. P. G. Pickup, C. R. Leidner, P. R. Denisevich and R. W. Murray, J. Electroanal. Chem., **164** (1984) 39.

27. C. R. Leidner, P. R. Denisevich, K. W. William and R. W. Murray, J. Electroanal. Chem., **164** (1984) 63.

28. A. J. Frank and K. Honda, J. Phys. Chem., **86** (1982) 1933.

29. R. N. Dominey, N. S. Lewis, J. A. Bruce, D. C. Bookbinder and M. S. Wrighton, J. Am. Chem. Soc., **104** (1982) 467.

30. J. A. Bruce, T. Murashl and M. S. Wrighton, J. Phys. Chem., **86** (1982) 1552.

31. P. G. Pickup and R. W. Murray, J. Am. Chem. Soc., **105** (1983) 4510.

32. P. Burgmayer and R. W. Murray, J. Am. Chem. Soc., **104** (1982) 6139.

33. H. S. White, G. P. Kittlesen and M. S. Wrighton, J. Am. Chem. Soc., **106** (1984) 5375.

34. K. W. William and R. W. Murray, J. Electroanal. Chem., 133 (1982) 211.

35. P. Burgmayer and R. W. Murray, J. Phys. Chem., **88** (1984) 2515.

36. P. J. Nigrey, A. G. MacDiarmid and A. J. Heeger, Mol. Cryst. Liq. Cryst., **83** (1982) 309.

37. R. J. Waltman, A. F. Diaz and J. Bargon, J. Electrochem. Soc., 131 (1984) 1452.

38. B. Zinger and L. L. Miller, J. Am. Chem. Soc., **106** (1984) 309.

39. R. L. Blankespoor and L. L. Miller, J.C.S. Chem. Comm., (1985) 397.

40. T. Shimidzu, A. Ohtani, T. Iyoda and K. Honda, J. Chem. Soc. Commun., (1986) 1415.

41. M. Okano, A. Fujishima and K. Honda, J. Electroanal. Chem., **185** (1985) 393.

42. P. M. Hoang, S, Holdcroft and B. L. Funt, J. Electrochem. Soc., 132 (1985) 2129.

43. S, Holdcroft and B. L. Funt, J. Electroanal. Chem., in press.

44. S. Piekarski and R. N. Adams, "Physical methods of Chemistry, Part IIA, Electrochemical Methods", Vol. 1, Eds. A. Weissberger and B. W. Rossiter, Wiley, New York, 1981.

45. J. E. B. Randles, Trans. Faraday Soc., 44 (1948) 327.

46. R. S. Nicholson and I. Shain, Anal. Chem., 36 (1964) 706.

47. F. G. Cottrell, Z. Physik. Chem., 42 (1902) 385.

48. W. J. Albery and M. L. Hitchman, "Ring-Disk Electrodes", Oxford University Press, London, 1971.

49. W. Nernst, Z. Physik. Chem., 47 (1904) 52.

50. V. G. Levich, "Physicochemical Hydrodynamics", Prentice-Hall, Englewood Cliffs, N.J., 1962.

51. E. Laviron, J. Electroanal. Chem., 100 (1979) 263.

52. F. B. Kaufman, A. H. Schroeder, E. M. Engler, S. R. Kramer and J. Q. Chambers, J. Am. Chem. Soc., 102 (1980) 483.

53. E. Laviron, J. Electroanal. Chem., 112 (1980) 1.

54. C. P. Andrieux and J. M. Savéant, J. Electroanal. Chem., 111 (1980) 377.

55. P. J. Peerce and A. J. Bard, J. Electroanal. Chem., 114 (1980) 89.

56. E. Laviron, L. Roullier and C. Degrand, J. Electroanal. Chem., 112 (1980) 11.

57. A. J. Bard and L. R. Faulkner, "Electrochemical Methods. Fundamentals and Applications", Wiley, New York, 1980, p. 129.

58. C. P. Andrieux, J. M. Dumas-Bouchiat and J. M. Savéant, J. Electroanal. Chem., 131 (1982) 1.

59. C. P. Andrieux and J. M. Savéant, J. Electroanal. Chem., 134 (1982) 163.

60. C. P. Andrieux and J. M. Savéant, J. Electroanal. Chem., 142 (1982) 1.

61. F. C. Anson, J. M. Savéant and K. Shigehara, J. Phys. Chem., 87 (1983) 214.

62. C. P. Andrieux and J. M. Savéant, J. Electroanal. Chem., 171 (1984) 65.

63. F. B. Kaufman and E. M. Engler, J. Am. Chem. Soc., 101 (1979) 547.

64. W. J. Albery, A. W. Foulds, K. J. Hall and A. R. Hillman, J. Electrochem. Soc., 127 (1980) 654.

65. W. R. Heinman, F. M. Hawkridge and H. N. Blount, "Electroanalytical Chemistry", Vol. 13, Ed. A. J. Bard, Marcel Dekker, New York, 1984.

66. D. Briggs and M. P. Seah, "Practical Surface Analysis by Auger and X-ray Photoelectron Spectroscopy", Wiley, New York, 1983.

67. C. C. Chang, Surf. Sci., **25** (1971) 53.

68. P. W. Palmberg, G. E. Riach, R. E. Weber and N. C. MacDonald, "Handbook of Auger Electron Spectroscopy", Physical Electronics, Perkin-Elmer Corp., Eden Prairie, MN, 1972.

69. S. Mroczkowski and D. Lichtman, Surf. Sci., **127** (1983) 119.

70. M. P. Seah and W. A. Dench, Surf. Int. Anal., 1 (1979) 2.

71. S. R. Morrison, "Electrochemistry at Semiconductor and Oxidised Metal Electrodes", Plenum Press, New York, 1980.

72. A. J. Nozik, Annu. Rev. Phys. Chem., **29** (1978) 189.

73. A. Heller and B. Miller, Electrochimica Acta., **25** (1980) 29.

74. K. Kalyanasundaram and M. Grätzel, Photochem. Photobiol., **40** (1984) 807.

75. M. S. Wrighton, Pure & Appl. Chem., **57** (1985) 57.

76. A. J. Nozik, 3rd Int. Conf. Photochem. Cons. Sol. Energy, Ed. J. S. Connolly, Academic Press, 1981, Chapter 10.

77. A. J. Bard, A. B. Bocarsly, F.-R. Fan, E. G. Walton and M. S. Wrighton, J. Am. Chem. Soc., **102** (1980) 3671.

78. Y. V. Pleskov and Y. Y. Gurevich, " Modern aspects of Electrochemistry", Vol. 16, Eds. B. E. Conway, E. White and J. O'M. Bockris, Plenum Press, New York, 1985, Chapter 5.

79. P. Daum and R. W. M. Murray, J. Phys. Chem., **85** (1981) 389.

80. N. Oyama and F. C. Anson, Inorg. Chem., **20** (1981) 518.

81. L. L. Miller and M. R. van de Mark, J. Am. Chem. Soc., **100** (1978) 639.

82. A. H. Schroeder, F. B. Kaufman, V. Patel and E. M. Engler, J. Electroanal. Chem., 113 (1985) 193.

83. A. H. Schroeder and F. B. Kaufman, J. Electroanal. Chem., **113** (1980) 209.

84. K. Itaya and A. J. Bard, Anal. Chem., **100** (1978) 1487.

85. N. Oyama and F. C. Anson, J. Am. Chem. Soc., 101 (1979) 739.

86. F. C. Anson, J. Phys. Chem., **84** (1980) 3336.

87. I. Rubinstein and A. J. Bard, J. Am. Chem. Soc., **102** (1980) 6641.

88. H. D. Abruna, P. R. Denisevich, M. Umana, T. J. Meyer and R. W. Murray, J. Am. Chem. Soc., **103** (1981) 1.

89. J. R. Hollahan and A. T. Bell, Eds., "Techniques and Applications of Plasma Chemistry", Wiley, New York, 1974.

90. L. R. Faulkner and M. Majda, J. Electroanal. Chem., **137** (1982) 149.

91. W. J. Albery, M. G. Boutelle, P. Colby and A. R. Hillman, J. Electroanal. Chem., **133** (1982) 135.

92. K. A. Macor and T. G. Spiro, J. Am. Chem. Soc., **105** (1983) 5601.

93. M.-C. Pham and J.-E. Dubois, J. Electroanal. Chem., **199** (1986) 153.

94. P. R. Denisevich, K. W. William and R. W. Murray, J. Am. Chem. Soc., **103** (1981) 4727.

95. P. R. Denisevich, H. D. Abruna, C. R. Leidner, T. J. Meyer and R. W. Murray, J. Am. Chem. Soc., **104** (1982) 2153.

96. T. Ikeda, C. R. Leidner and R. W. Murray, J. Electroanal. Chem., **138** (1982) 343.

97. P. Daum and R. W. Murray, J. Electroanal. Chem., **103** (1979) 289.

98. J. B. Kerr, L. L. Miller and M. R. Van De Mark, J. Am. Chem. Soc., **102** (1980) 3383.

99. K. W. William, R. D. Rocklin, R. Nowak, K. Kuo, F. A. Schultz and R. W. Murray, J. Am. Chem. Soc., **102** (1980) 7629.

100. N. Oyama and F. C. Anson, J. Am. Chem. Soc., **101** (1979) 3450.

101. N. Oyama and F. C. Anson, J. Electrochem. Soc., **127** (1980) 640.

102. M. F. Dautartas and J. F. Evans, J. Electroanal. Chem., **109** (1980) 301.

103. S. Nakahama and R. W. Murray, J. Electroanal. Chem., **158** (1982) 303.

104. D. A. Buttry and F. C. Anson, J. Electroanal. Chem., **130** (1981) 333.

105. H. S. White, J. Leddy and A. J. Bard, J. Am. Chem. Soc., **104** (1982) 4811.

106. C. R. Martin, I. Rubinstein and A. J. Bard, J. Am. Chem. Soc., **104** (1982) 4817.

107. J. S. Facci, R. H. Schmehl and R. W. Murray, J. Am. Chem. Soc., **104** (1982) 4959.

108. K. Stutts and R. M. Wightman, Anal. Chem., **55** (1983) 1576.

109. K. Kuo and R. W. Murray, J. Electroanal. Chem., **131** (1982) 37.

110. J. F. Evans, T. Kuwana, M. T. Henne and G. P. Roger, J. Electroanal. Chem., **80** (1977) 409.

111. J. Facci and R. W. Murray, Anal. Chem., **54** (1982) 772.

112. J. B. Kerr and L. L. Miller, J. Electroanal. Chem., **101** (1979) 263.

113. R. D. Rocklin and R. W. Murray, J. Phys. Chem., **85** (1981) 2104.

114. C. Degrand and L. L. Miller, J. Am. Chem. Soc., **102** (1980) 5728.

115. C. D. Ellis, J. A. Gilbert, W. R. Murphy, Jr., T. J. Meyer, J. Am. Chem. Soc., **105** (1983) 4842.

116. G. J. Samuels and T. J. Meyer, J. Am. Chem. Soc., **103** (1981) 307.

117. P. Pickup, K. Kuo and R. W. Murray, J. Electrochem. Soc., **130** (1983) 2205.

118. R. H. Schmehl and R. W. Murray, J. Electroanal. Chem., **152** (1983) 97.

119. N. Oyama and F. C. Anson, Anal. Chem., **52** (1980) 1192.

120. F. C. Anson, Y.-M. Tsou and J. M. Savéant, J. Electroanal. Chem., **178** (1984) 113.

121. F. C. Anson, J. M. Savéant and K. Shigerhara, J. Electroanal. Chem., **145** (1983) 423.

122. J. Facci and R. W. Murray, J. Phys. Chem., **85** (1981) 2870.

123. T. Ikeda, C. R. Leidner and R. W. Murray, J. Am. Chem. Soc., **103** (1981) 7422.

124. K. Shigerhara, N. Oyama and F. C. Anson, Inorg. Chem., **20** (1981) 518.

125. N. Oyama, T. Shimomura, K. Shigerhara and F. C. Anson, J. Electroanal. Chem., **112** (1980) 271.

126. F. C. Anson, T. Ohsaka and J. M. Savéant, J. Am. Chem. Soc., **105** (1983) 4883.

127. E. T. Turner Jones, J. Electrochem. Soc., **132** (1985) 245C.

128. A. Bettelheim, R. J. H. Chan and T. Kuwana, J. Electroanal. Chem., **110** (1980) 93.

129. H. Beret, H. Binder, G. Sandstede and G. G. Scherer, J. Electroanal. Chem., **117** (1981) 29.

130. J. Zagel, P. Bindra and E. Yeager, J. Electrochem. Soc., **127** (1980) 1506.

131. E. Yeager, J. Electrochem. Soc., **128** (1981) 160C.

132. R. Durand, Jr., and F. C. Anson, J. Electroanal. Chem., **132** (1982) 273.

133. E. Yeager, Electrochimica Acta., **29** (1984) 1527.

134. F. Van Den Brink, W. Visscher and E. Barendrecht, J. Electroanal. Chem., **172** (1984) 301.

135. F. C. Anson, C.-L. Ni and J. M. Savéant, J. Am. Chem. Soc., **107** (1985) 3442.

136. J. P. Collman, M. Marrocco, P. Denisevich, C. Koval and F. C. Anson, J. Electroanal. Chem., **101** (1979) 117.

137. J. P. Collman, P. Denisevich, T. Konai, M. Marrocco, C. Koval and F. C. Anson, J. Am. Chem. Soc., **102** (1980) 6027.

138. H.-Y. Liu, I. Abdamuhdi, C. K. Chang and F. C. Anson, J. Phys. Chem., **89** (1985) 665.

139. W. F. Schumb and C. N. Satterfield, "Hydrogen Peroxide", Reinhold, New York, 1955.

140. G. S. Calabrese, R. M. Buchanan and M. S. Wrighton, J. Am. Chem. Soc., **104** (1982) 5786.

141. G. S. Calabrese, R. M. Buchanan and M. S. Wrighton, J. Am. Chem. Soc., **105** (1983) 5594.

142. C. Degrand, J. Electroanal. Chem., **169** (1984) 259.

143. N. Oyama, N. Okl, H. Ohno, Y. Ohnuki, H. Matsuda and E. Tsuchida, J. Phys. Chem., **87** (1983) 3642.

144. K. Itaya, N. Shoji and I. Uchida, J. Am. Chem. Soc., **106** (1984) 3423.

145. O. Ikeda, K. Okabayashi and H. Tamura, Chem. Lett., (1983) 1821.

146. C.-W. Lee, H. B. Gray, F. C. Anson and B. G. Malmström, J. Electroanal. Chem., **172** (1984) 289.

147. N. S. Lewis, A. B. Bocarsly and M. S. Wrighton, J. Phys. Chem., **84** (1980) 2030.

148. K. Shigehara and F. C. Anson, J. Electroanal. Chem., **132** (1982) 107.

149. A. Fujishima and K. Honda, Nature, **238** (1982) 37.

150. M. S. Wrighton, R. G. Austin, A. B. Bocarsly, J. M. Bolts, O. Haas, K. D. Klegg, L. Nadjo and M. C. Palozzotto, J. Am. Chem. Soc., **100** (1978) 1602.

151. M. S. Wrighton, J. M. Bolts, A. B. Bocarsly, M. C. Palozzotto and E. G. Walton, J. Vac. Sci. Technol., **15** (1978) 1429.

152. M. D. Rosenblum and N. S. Lewis, J. Phys. Chem., **88** (1984) 3103.

153. D. J. Harrison and M. S. Wrighton, J. Phys. Chem., **88** (1984) 3932.

154. B. L. Funt and P. M. Hoang, J. Electroanal. Chem., **154** (1983) 229.

155. B. L. Funt and P. M. Hoang, J. Electrochem. Soc., 131 (1984) 2295.

156. D. T. Sawyer and J. L. Roberts, Jr., J. Electroanal. Chem., 12 (1966) 90.

157. J. Q. Chambers, "The Chemistry of the Quinoid Compound", Ed. S. Patai, Wiley, Chichester, 1974, Chapter 14.

158. T. Nagaoka and S. Okazaki, J. Phys. Chem., **89** (1985) 2340.

159. H. J. Byker, V. E. Wood and A. E. Austin, J. Electrochem. Soc., **129** (1982) 1982.

160. J. N. Chazalviel and T. B. Truong, J. Electroanal. Chem., 114 (1980) 299.

161. D. Laser and A. J. Bard, J. Phys. Chem., **80** (1976) 459.

162. G. Nagasubramanian, B. L. Wheeler, F.-R. F. Fan and A. J. Bard, J. Electrochem. Soc., **129** (1982) 1742.

163. B. Keita, I. Kawenoki, J. Kossanyi, D. Garreau and L. Nadjo, J. Electroanal. Chem., **145** (1983) 293.

164. J. A. Turner, J. Manassen and A. J. Nozik, Appl. Phys. Lett., **37** (1980) 488.

165. G. Nagasubramanian, S. DiStefano and J. Moacanin, J. Electrochem. Soc., **133** (1985) 305.

166. J. N. Chazalviel and T. B. Truong, J. Am. Chem. Soc., **103** (1981) 7447.

167. D. T. Sawyer and M. J. Gibian, Tetrahedron, **35** (1979) 1471.

168. T. A. Skotheim, Ed., "Handbook of Conducting Polymers", Vol. 1&2, Marcel Dekker, New York, 1986.

169. R. J. Waltman and J. Bargon, Can. J. Chem., **64** (1986) 76.

170. S. Miyauchi, Int. Pol. Sci. Tech., 12 (1985) T/49.

171. A. F. Diaz and I. Castillo, J.C.S. Chem. Comm., (1980) 397.

172. E. M. Genies, G. Bidan and A. F. Diaz, J. Electroanal. Chem., **149** (1983) 101.

173. E. M. Genies and J. M. Pernaut, Synth. Met., **10** (1984) 117.

174. M. Salmon, A. F. Diaz, A. J. Logan, M. Krounbi and J. Bargon, Mol. Cryst. Liq. Cryst., **83** (1982) 265.

175. A. F. Diaz and K. K. Kanazawa, "Extended Linear Chain Compounds", Ed. J. S. Miller, Plenum Press, New York, 1983, 417.

176. B. L. Funt and S. V. Lowen, Synth. Met., **11** (1985) 129.

177. M. Barak, " Comprehensive Treatise of Electrochemistry", Vol. 3, Plenum Press, New York, 1981.

178. P. J. Nigrey, D. MacInnes, D. P. Nairns, A. G. MacDiarmid and A. J. Heeger, J. Electrochem. Soc., **128** (1981) 165.

179. D. MacInnes, M. A. Druy, P. J. Nigrey, D. P. Nairns, A. G. MacDiarmid and A. J. Heeger, J.C.S. Chem. Comm., (1981) 317.

180. K. Kaneto, M. R. Maxfield, D. P. Nairns, A. G. MacDiarmid and A. J. Heeger, J.Chem .Soc., Faraday Trans. 1, **78** (1982) 3417.

181. P. J. Nigrey, A. G. MacDiarmid and A. J. Heeger, Mol. Cryst. Liq. Cryst., **83** (1982) 309.

182. R. L. Elsenbaumer, L. W. Shacklette, J. M. Sowa, R. R. Chance, D. M. Ivory, G. G. Miller and R. H. Baughman, Polym. Prepr. Am. Chem. Soc. Div. Polym. Chem., **23** (1982) 132.

183. G. C. Farrington, B. Scrosati, D. Frydrych and J. DeNuzzio, J. Electrochem. Soc., 131 (1984) 7.

184. A. G. MacDiarmid, J. C. Chiang, M. Halpern, W. S. Huang, S. L. Mu, N. L. D. Somarsiri, W. Wu and S. Yaniger, Mol. Cryst. Liq. Cryst., 121 (1985) 173.

185. K. Kaneto, K. Yoshino Y. Inuishi, Jpn. J. of Appl. Phys., **22** (1983) L567.

186. K. Kaneto, K. Yoshino Y. Inuishi, Jpn. J. of Appl. Phys., **24** (1985) L107.

187. T. C. Chung, J. H. Kaufman, A. J. Heeger and F. Wudl, Phys. Rev. B, **30** (1984) 702.

188. B. J. Feldman, P. Burgmayer and R. W. Murray, J. Am. Chem. Soc., **107** (1985) 872.

189. A. Mohammadi, O. Inganäs and I. Lundström, J. Electrochem. Soc., **133** (1986) 947.

190. N. Mermilliod, J. Tanguy and F. Petiot, J. Electrochem. Soc., 133 (1986) 1073.

191. J. O'M. Bockris and A. R. Reddy, "Modern Electrochemistry", Vol. 2, Plenum Press, New york, 1970, Chapter 11.

192. G. Bidan, A. Deronzier and J. C. Moutet, J.C.S. Chem. Comm., (1984) 1185.

193. P. Audebert, G. Bidan and M. Lapkowski, J.C.S. Chem. Comm., (1986) 887.

194. A. B. Bocarsly, D. C. Bookbinder, R. N. Dominey, N. S. Lewis and M. S. Wrighton, J. Am. Chem. Soc., **102** (1980) 3683.

195. B. Keita, I. Kawanoki, J. Kossanyi and 1. Nadjo, J. Electroanal. Chem., 145 (1983) 311.

196. F.-R. F. Fan, B. L. Wheeler, A. J. Bard and R. N. Noufi, J. Electrochem. Soc., 128 (1981) 2042.

197. T. A. Skotheim, L.-G. Petersson, O. Inganäs, and I. Lundström, J. Electrochem. Soc., 129 (1980) 1737.

198. T. A. Skotheim, O. Inganäs, J. Prejza and I. Lundström, Mol. Cryst. Liq. Cryst., 83 (1982) 329.

199. T. A. Skotheim and O. Inganäs, Mol. Cryst. Liq. Cryst., 121 (1985) 289.

200. R. N. Noufi, Appl. Phys. Comm., 3 (1983) 33.

201. R. E. Malpas and B. R. Rushby, J. Electroanal. Chem., 157 (1983) 387.

202. R. A. Bull, F.-R. F. Fan, and A. J. Bard, J. Electrochem. Soc., 129 (1982) 1009.

203. T. A. Skotheim, O. Inganäs, and I. Lundström, J. Appl. Phys., 54 (1983) 3636.

204. P.G. Pickup, K. N. Kuo amd R. W. Murray, J. Electrochem. Soc., 130 (1983) 2205.

205. G. K. Chandler and D. Pletcher, J. Appl. Electrochem., 16 (1986) 62.

206. A. T. Hubbard and F. C. Anson, Anal. Chem., 38 (1966) 13.

207. R. A. Simon, T. A. Mallouk, K. A. Daube and M. S. Wrighton, Inorg. Chem., 24 (1985) 3119.

208. H.-Y. Liu and F. C. Anson, J. Electroanal. Chem., 158 (1983) 181.

209. W. H. Kao and T. Kuwana, J. Am. Chem. Soc., 106 (1984) 473.

210. D. E. Weisshaar and T. Kuwana, J. Electroanal. Chem., 163 (1984) 395.

211. D. E. Bartek, B. Kazee, K. Shimazu and T. Kuwana, Anal. Chem., 58 (1986) 2756.

212. G. Tourillon and F. Garnier, J. Phys. Chem., 88 (1984) 5281.

213. G. Tourillon and F. Garnier, Mol. Cryst. Liq. Cryst., 121 (1985) 305.

214. R. N. Adams, "Electrochemistry at Solid Electrodes", Marcel Dekker, New York, 1969, p. 90.

215. R. M. Penner and C. R. Martin, J. Electrochem. Soc., 133 (1986) 887.

216. C. R. Martin, ACS Meeting, Anaheim, California, 1986.